Mechanisms of ventricular arrhythmogenesis in the age dependent Pgc-1β $^{-/-}$ model of mitochondrial dysfunction.

Shiraz Ahmad

Jesus College, University of Cambridge

This dissertation is submitted for the degree of Doctor of Philosophy

Date of Submission: May 2019

DECLARATIONS

This dissertation is the result of my own work and includes nothing which is the outcome of work done in collaboration except as declared in the Preface and specified in the text. It is not substantially the same as any that I have submitted, or, is being concurrently submitted for a degree or diploma or other qualification at the University of Cambridge or any other University or similar institution except as declared in the Preface and specified in the text. I further state that no substantial part of my dissertation has already been submitted, or, is being concurrently submitted for any such degree, diploma or other qualification at the University of Cambridge or any other University or similar institution except as declared in the Preface and specified in the text. It does not exceed the prescribed word limit for the relevant Degree Committee.

SUMMARY - Mechanisms of ventricular arrhythmogenesis in the age dependent Pgc-1β$^{-/-}$ model of mitochondrial dysfunction.

Sudden cardiac death is a leading cause of mortality worldwide. Ventricular arrhythmias, both ventricular tachycardia and ventricular fibrillation, are the primary arrhythmias that lead to sudden cardiac death. A large proportion of ventricular arrhythmias are ischaemic in origin. However, increasing clinical and experimental evidence links metabolic disease, mitochondrial dysfunction and ageing as independent risk factors for arrhythmogenesis beyond the risk they confer to coronary artery disease. To date, researchers have focused upon investigation of monogenic ion channel disorders as well circumscribed diseases to investigate the principles of arrhythmogenesis. This has given insight into the basic theories of arrhythmogenesis as well as the tools needed to dissect them. In this study, we use *Pgc-1β$^{-/-}$* mice as a murine model of mitochondrial dysfunction, to further investigate the link between mitochondrial and energetic insufficiency and arrhythmias.

The study uses electrocardiographic data to characterise the phenotype at the whole animal level, revealing significant age related abnormalities in ventricular activation and abnormal nodal tissue phenotypes. Single cell action potential characteristics in intact Langendorff perfused whole hearts were then used both in programmed electrical stimulation studies and at incrementally paced steady states to investigate the electrophysiological characteristics that give rise to arrhythmia. These experiments revealed a significant deficit in maximal rate of depolarisation and consequent effects on conduction wavelengths, accompanied by instabilities in activation characteristics as evidenced by the presence of electrical alternans. Finally, patch-clamp studies are performed to confirm the hypotheses of the earlier experiments and their effect on cellular currents in a physiological environment which show a physiological deficit in sodium current density. At all stages care was taken to perform experiments in the least disruptive manner, maintaining as much physiological relevance as

possible. The series of experiments reveal that not only is mitochondrial dysfunction related to arrhythmias in an age dependant manner, but that it leads to altered sodium current density with a plausible role of Ca^{2+} as a central mediator of this, allowing future studies to build on this.

Dr Shiraz Ahmad

LIST OF PUBLICATIONS

FIRST AUTHOR ORIGINAL RESEARCH ARTICLES

1. ***Ahmad S*, Valli H*,*** *Salvage SC, Grace AA, Jeevaratnam K, Huang CL.* Age-dependent electrocardiographic changes in Pgc-1β deficient murine hearts. **Clin Exp Pharmacol Physiol. 2018 Feb; 45(2): 174-186.**
2. ***Shiraz Ahmad****, Haseeb Valli, Karan R. Chadda, James Cranley, Kamalan Jeevaratnam and Christopher L.-H. Huang.* Ventricular pro-arrhythmic phenotype, arrhythmic substrate, ageing and mitochondrial dysfunction in peroxisome proliferator activated receptor-γ coactivator-1β deficient (Pgc-1$\beta^{-/-}$) murine hearts. **Mech Ageing Dev. 2018 Jul; 173: 92-103**.
3. ***Shiraz Ahmad,*** *Haseeb Valli, Charlotte Edling, Andrew A. Grace, Kamalan Jeevaratnam and Christopher L-H Huang.* Effects of ageing on pro-arrhythmic ventricular phenotypes in incrementally paced murine Pgc-1β $^{-/-}$ hearts. **European Journal of Physiology/Pflugers Arch. 2017 Dec; 469(12):1579-1590.**
4. ***Shiraz Ahmad****, Haseeb Valli, Robert Smyth, Anita Y. Jiang, Kamalan Jeevaratnam Hugh R. Matthews and Christopher L.-H. Huang.* Reduced cardiomyocyte Na^+ current in the age-dependent murine Pgc-1$\beta^{-/-}$ model of ventricular arrhythmia. **J. Cell Physiol. 2018 Aug 26 (epub ahead of print)**.
5. ***Valli H*, Ahmad S*,*** *Sriharan S, Dean LD, Grace AA, Jeevaratnam K, Matthews HR, Huang CL. Epac-induced ryanodine receptor type 2 activation inhibits sodium currents in atrial and ventricular murine cardiomyocytes.* **Clin Exp Pharmacol Physiol. 2018 Mar;45(3):278-292**

***joint first author**

ORIGINAL RESEARCH ARTICLES ARISING IN COLLABORATION WITH OTHERS

1. *Karan R. Chadda,* ***Shiraz Ahmad,*** *Haseeb Valli, Ingrid den Uijl, Ali BAK Al-Hadithi, Samantha C. Salvage, Andrew A. Grace, Christopher L.-H. Huang & Kamalan*

Jeevaratnam. The effects of ageing and adrenergic challenge on electrocardiographic phenotypes in a murine model of long QT syndrome type 3. **Nature Sci Rep. 2017 Sep 11;7(1):11070.**

2. Ning, F, Luo, L, **Ahmad, S**, Valli, H, Jeevaratnam, K, Wang, T, Guzadhur, L, Yang, D, Fraser, JA, Huang, CL-H et al (2016) *The RyR2-P2328S mutation downregulates Na(v)1.5 producing arrhythmic substrate in murine ventricles* **Pflugers Archiv-European Journal of Physiology, 468 (4). pp. 655-665.**
3. Valli H, Ahmad S, Chadda KR, Al-Hadithi ABAK, Grace AA, Jeevaratnam K, Huang CL. *Age-dependent atrial arrhythmic phenotype secondary to mitochondrial dysfunction in Pgc-1β deficient murine hearts.* **Mech Ageing Dev. 2017 Oct;167:30-45.**
4. Haseeb Valli, **Shiraz Ahmad**, Anita Y.Jiang, Robert Smyth, Kamalan Jeevaratnam, Hugh R.Matthews, Christopher L.-H.Huang. *Cardiomyocyte ionic currents in intact young and aged murine Pgc-1β$^{-/-}$ atrial preparations.* **Mech Ageing Dev. 2018 Jan; 169:1-9**
5. Haseeb Valli, **Shiraz Ahmad**, James A Fraser, Kamalan Jeevaratnam and Christopher L-H Huang. *Pro-arrhythmic atrial phenotypes in incrementally paced murine Pgc1β$^{-/-}$ hearts: effects of age.* **Exp Physiol. 2017 Dec 1; 102(12): 1619–1634.**
6. Matthews HR, Tan SRX, Shoesmith JA, **Ahmad S**, Valli H, Jeevaratnam K, Huang CL. *Sodium current inhibition following stimulation of exchange protein directly activated by cyclic-3',5'-Adenine Monophosphate (EPAC) in murine skeletal muscle.* **Nature Sci Rep. 2019; 9: 1927.**
7. Karan R Chadda, Ibrahim T Fazmin, **Shiraz Ahmad**, Haseeb Valli, Charlotte E Edling, Christopher L-H Huang, Kamalan Jeevaratnam. *Arrhythmogenic mechanisms of obstructive sleep apnea in heart failure patients.* **Sleep. 2018 Sep; 41(9): zsy136**
8. Karan R. Chadda, Charlotte E. Edling, Haseeb Valli, **Shiraz Ahmad**, Christopher L.-H. Huang, and Kamalan Jeevaratnam. *Gene and protein expression profile of selected molecular targets mediating electrophysiological function in PGC1α deficient murine atria.* **Int J Mol Sci. 2018 Nov; 19(11): 3450.**

ACKNOWLEDGEMENTS

I would like to thank the Medical Research Council, as a recipient of an MRC Clinical Training Fellowship, whose funding has allowed me to complete my research. My sincere and heartfelt thanks must go to Professor Chris Huang, whose supervision and guidance has been immensely valuable throughout my PhD, from conception through experimental design and manuscript revision. He has shown true academic excellence, dedication and personal integrity in ensuring the success of my work. His mentorship will always be instrumental to my work, for the years I have spent with his supervision has imbued me with skills and a way of working for which I am indebted. I would also like to give my thanks to Dr Andrew Grace, who has provided me with the administrative support and framework to navigate research as a clinician.

I would also like to extend my deep appreciation to the members of Huang group, whose support, discussion and collaboration has been instrumental in the day to day machinations of productive research. In particular I would like to thank Dr. Samantha Salvage, Dr Haseeb Valli and Dr Kamalan Jeevaratnam whose close collaboration and friendship allowed my research to flourish. I would like to acknowledge Dr Hugh Matthews's work in developing the loose patch clamp technique allowing exciting new research questions to be answered, and Dr James Fraser for help with microelectrode electrode experiments. Mr Paul Frost and Ms Vicky Johnson's technical assistance in equipment and hardware was always a source of comfort during what may otherwise have been disastrous moments. Finally I would like to thank my family, who have supported me through these years and are always a pillar of support.

CONTENTS

LIST OF FIGURES

LIST OF TABLES

ABBREVIATIONS

$(dV/dt)_{max}$ – maximal rate of depolarisation

AF – Atrial fibrillation

ANOVA – Analysis of variance

AP – Action potential

APD – Action potential duration

APD_{90} – Action potential duration at 90% repolarisation

ATP – Adenosine triphosphate

AUC – Area under the curve

AV – Atrioventricular

AVN – Atrioventricular node

BCL – Basic cycle length

Ca^{2+} - Calcium ion

CABG – Coronary artery bypass graft

DNA – Deoxyribonucleic acid

ERP – Effective refractory period

K^{+} - Potassium ion

MANOVA – Multivariate analysis of variance

MAP – Monophasic action potential

ME – microelectrode

MI – Myocardial infarction

mtDNA – mitochondrial DNA

Na^+ - Sodium ion

PGC-1 - Peroxisome proliferator-activated receptor-γ coactivator 1

RMP – Resting membrane potential.

RyR2 – Ryanodine receptor 2

ROS – reactive oxygen species

SAN – Sinoatrial node

SCD - Sudden Cardiac Death

SR – Sarcoplasmic reticulum/reticular

V_m – cell membrane potential

VF – Ventricular fibrillation

VT – ventricular tachycardia

WT – Wild type

1. INTRODUCTION

1.1 EPIDEMIOLOGY OF VENTRICULAR ARRHYTHMIAS AND SUDDEN CARDIAC DEATH

Cardiovascular disease is the leading worldwide cause of mortality. Approximately half of such cases are attributable to sudden cardiac death (SCD) (Go et al., 2013). Cardiovascular disease is responsible for approximately for 17 million deaths per year and sudden cardiac death accounts for 15-25% of these deaths (Mendis SPP and B, 2011; Hayashi et al., 2015). Sudden cardiac death has been defined as sudden death due to a primary cardiac cause identified either at autopsy, or when a potentially fatal cardiac condition (congenital or acquired) was known to be present during life. Sudden cardiac arrest has a very high mortality, with an average 7% survival rate (NICE, 2014). It encompasses sudden death when no obvious extra-cardiac causes have been found by post-mortem examination for which an arrhythmic event is the likely cause of death (Priori et al., n.d.; Zipes et al., 2006) . Ventricular arrhythmias are thus the most common precipitant of sudden cardiac death (Koplan and Stevenson, 2007) of which the commonest presenting rhythm to paramedical staff is ventricular fibrillation (VF). However this is often thought to have been preceded by ventricular tachycardia (VT) (Turakhia and Tseng, 2007).

In most patients, cardiac arrhythmias are the result of underlying ischaemic heart disease (Behr et al., 2003). In a small but significant proportion (around 4%) the sudden cardiac death is of unknown cause (Tung et al., 1994). This proportion is higher in patients under the age of 40, representing almost 15% of resuscitation attempts (Viskin and Belhassen, 1990). Sudden cardiac death and ventricular arrhythmias therefore represent important clinical problems in human health.

1.2 THE ACTION POTENTIAL AND ELECTROPHYSIOLOGICAL BASIS OF ARRHYTHMIAS

Cardiac arrhythmias fundamentally result from disruptions in the normally coordinated sequence of ion channel activation and inactivation underlying cardiac action potential (AP) excitation and its propagation. Ion channel characteristics, their influence over AP generation and propagation, and related major recent discoveries of sarcolemmal, sarcoplasmic reticular, (SR) and cytosolic biomolecules have been described. These molecules are involved in both surface membrane excitation and intracellular signalling (Fig. 1-1). The latter is crucial to the voltage and metabolically sensitive mechanisms mediated by the surface membrane ionic channels. These mechanisms underlie the generation of the automaticity underlying normal (or abnormal) pacing of cardiac activity, the interacting sequence of membrane depolarisation, plateau formation, and recovery, and the propagation of these processes in atrioventricular (AV) nodal and purkinje tissue, as well as ventricular (Figure 1-1C) and atrial cardiomyocytes (Figure 1-1D) (Huang, 2017 a).

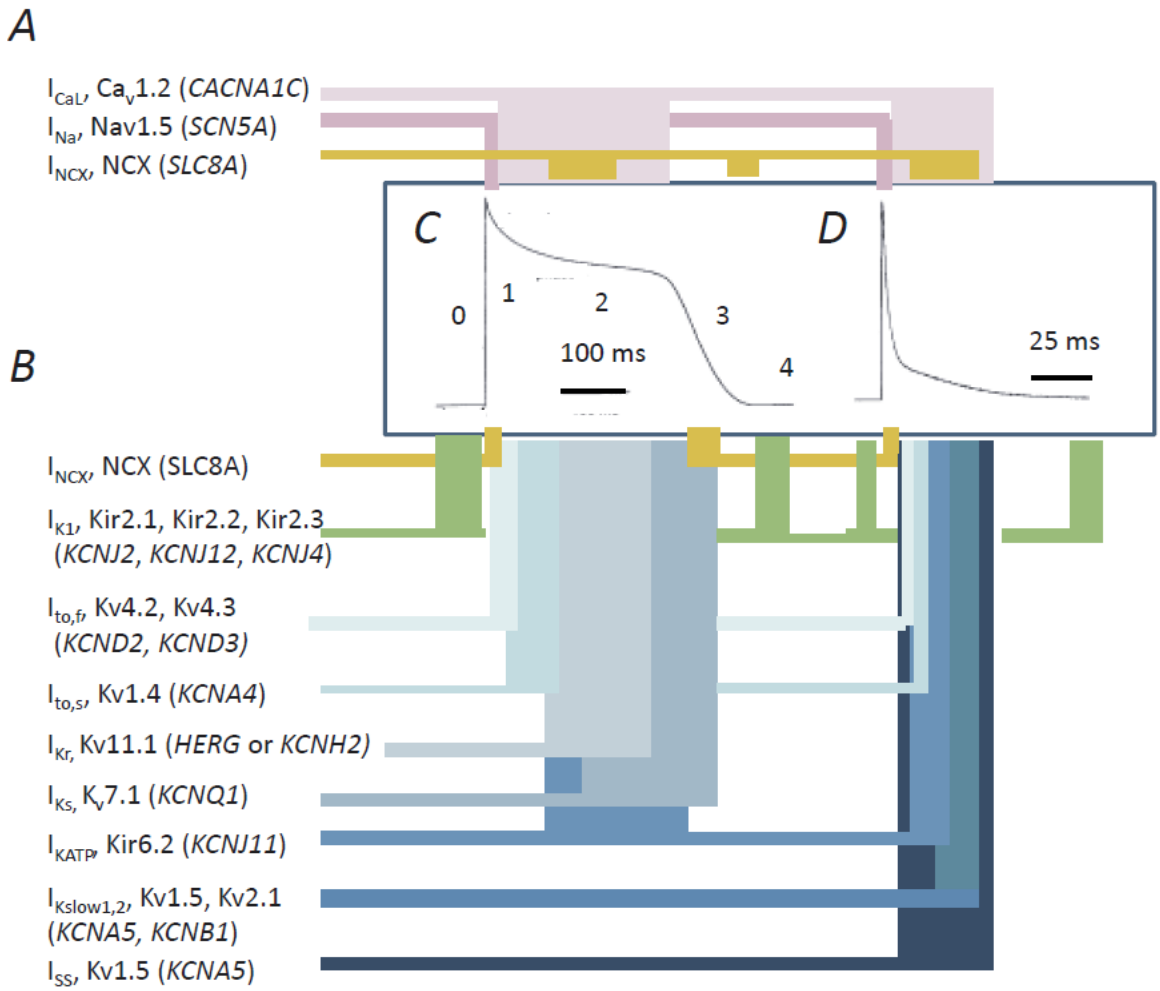

Figure 1-1: The Cardiac Action Potential and Ionic Currents. *Ionic currents involved in plateau generation (A) depolarisation and repolarisation (B) in a ventricular cardiomyocyte (C) and atrial cardiomyocyte (D). The phase of the action potential during which particular ionic current is flowing is highlighted, as well as the channel name and the gene transcript in parentheses. Adapted from* (Huang, 2017 b).

The AP waveform characteristic of cardiac electrophysiological activity consists of a rapid depolarisation (phase 0), an early repolarisation (phase 1), brief atrial and prolonged ventricular plateau (phase 2) and late repolarisation phases (phase 3) ending in electrical diastole (phase 4). AP initiation depends on Na^+ or Ca^{2+} channel activation and its propagation. Ca^{2+} channel activation also contributes to the AP plateau. AP repolarisation (thereby restoring the background resting potential) is driven by a range of K^+ channels (Nerbonne and Kass, 2005; Huang, 2017 a). An effective refractory period (ERP) follows such activity. This may

be modulated either by Na^+ channel inhibition delaying the point at which a critical proportion of Na^+ channels has recovered, or by AP prolongation. The leading edge of the resulting AP propagation wave is followed by regions of myocardium refractory to electrical re-activation. This cyclical pattern of spatial and temporal electrophysiological activity forms a coherent wave of excitation propagating through often anisotropic electrical connections between successive tissues (Figure 1-2); the sino-atrial, atrial, AVN, purkinje and endocardial and epicardial ventricular cardiomyocytes are successively activated, with detailed AP waveforms varying with cell type.

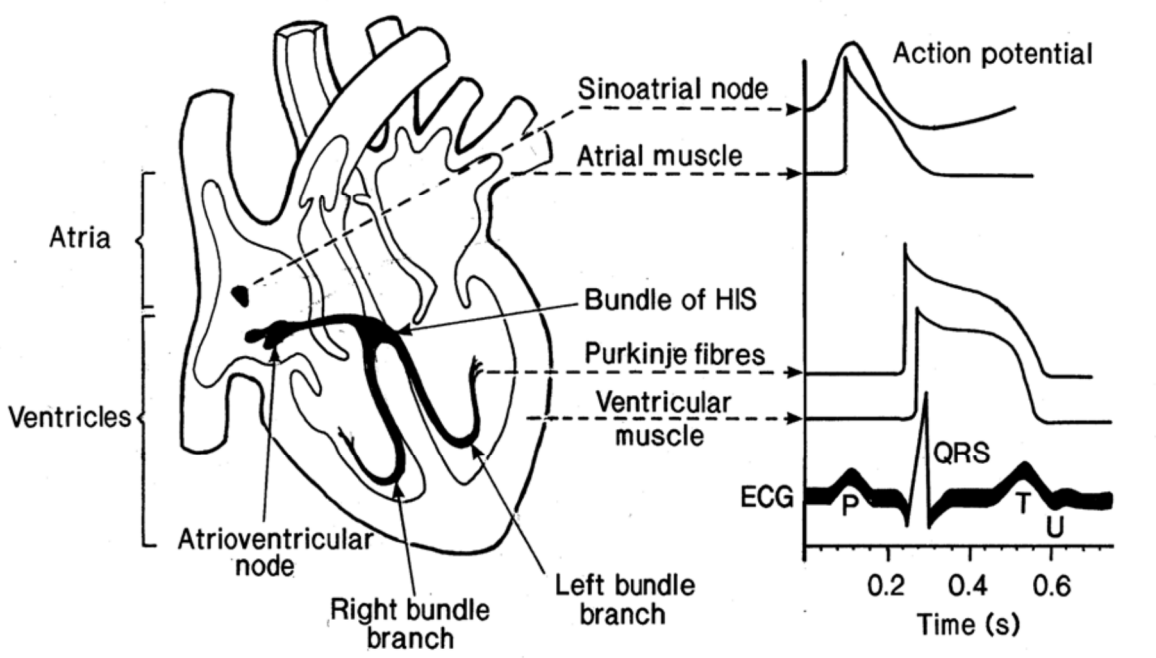

Figure 1-2: The conduction pathway.

Pacemaker and specialized conductile regions of the mammalian heart (left) and their characteristic action potential and the overall electrocardiogram waveform (right). Adapted from (Cranefield and Hoffman, 1968).

Thus atrial cells show shorter APs than ventricular cells, reflecting larger repolarising, transient outward voltage dependent and acetylcholine-sensitive K^+ currents (Kléber and Rudy, 2004; Amin et al., 2010; King et al., 2013 a)

These voltage changes initiate mechanical contraction of the cardiomyocytes by a process known as excitation-contraction coupling. In turn these voltage dependent changes are reciprocally modified by the excitation-contraction coupling processes that they trigger. Excitation-contraction coupling begins with an extracellular Ca^{2+} influx through transverse tubular membrane Ca^{2+} channels during phase 2 of the AP plateau. The resulting local elevations in cytosolic [Ca^{2+}] trigger a ryanodine receptor (RyR2) mediated SR Ca^{2+} release. The consequent elevation in cytosolic $[Ca^{2+}]_i$, drives the Ca^{2+}-troponin binding that initiates mechanical activation. Sarcolemmal and SR Ca^{2+}-ATPase activity as well as surface sarcolemmal Na^+/Ca^{2+} exchange then restore $[Ca^{2+}]_i$ to its ~100 nM baseline level resulting in contractile relaxation ending the activity cycle (Bers, 2001, 2002). Baseline surface and intracellular transmembrane ion gradients driving these processes are then restored by the Na^+-K^+ ATPase and Ca^{2+}-ATPase pumps and other carriers, resetting the effects of this excitable and contractile activity. The overall energetic cost is defrayed by mitochondrial generation of cellular ATP (Brown and O'Rourke, 2010). The inward Na^+ current generated at the outset of the action potential drives local circuit currents. These excite hitherto quiescent regions of membrane, resulting in propagation of the excitation through successive cardiac chambers and regions within these chambers. Finally, following AP recovery, an automaticity property mediated by a spontaneous diastolic, phase 4, depolarisation takes the membrane potential in SAN and AVN cells to the threshold for generation of a subsequent AP. This initiates the electrophysiological events underlying the subsequent heart beat (Mangoni and Nargeot, 2008).

1.3 GENETICALLY MODIFIED MURINE MODELS

The cardiac AP and its propagation is therefore intimately dependant on the array of ionic channels and molecules that are involved in the cardiac AP. Disruption of these molecular functions may lead to disordered excitation or propagation of APs. Previous studies have examined the roles of these individual channels in cardiac arrhythmogenesis. They have often employed models with monogenic modifications or pharmacological manipulations directed at specific channels providing valuable insights into the contributions of particular channels to

arrhythmic events (Huang, 2017 a). Mice provide genetic systems that are readily manipulated, providing a system where the cardiac effects of specific ion channel modifications can be studied and used to model the corresponding human conditions.

Importantly, the basic structure of the heart is preserved across all mammalian species. Both mouse and human hearts work within a dual circulation. There are left and right circulations with the ventricular chambers being structurally homologous. Murine atria do not form a single continuous structure with the ventricles as they do in humans; rather they are structured as two leaflets above the ventricle. (Figure 1-3). Nevertheless, they share similar conduction systems particularly regarding their nodal tissues and His-Purkinje system (Rentschler et al., 2001).

Mouse and human hearts do differ considerably in size. The small size of the murine heart initially led to speculation that it was incapable of sustaining and developing cardiac arrhythmias (Garrey, 1914). Later studies have proven this view incorrect and atrial as well as ventricular arrhythmias are well characterised in WT animals as well as a diverse array of genetically modified murine models (Sabir et al., 2007 a; Killeen et al., 2008 a; Dautova et al., 2009; Matthews et al., 2013 a; Salvage et al., 2015; Ning et al., 2016 a). Although, there are a number of important electrophysiological differences that exist between the two species, the major electrophysiological differences between murine and human cardiac electrophysiology concern the repolarisation currents (Huang, 2017 a).

The cardiac action potential in the mouse lacks a well-defined plateau region and is consequently shorter than the human AP (Killeen et al., 2008 a). Thus the transient outward current, I_{to}, is the major repolarising current, while IK_s and IK_r appear to have a reduced role. This contrasts with the situation in human cardiomyocytes, where the slow and rapid components of the latter two currents are the major repolarising currents (Grant, 2009; Huang, 2017 a). In contrast, hearts in both species share a rapid I_{Na}-mediated depolarisation phase.

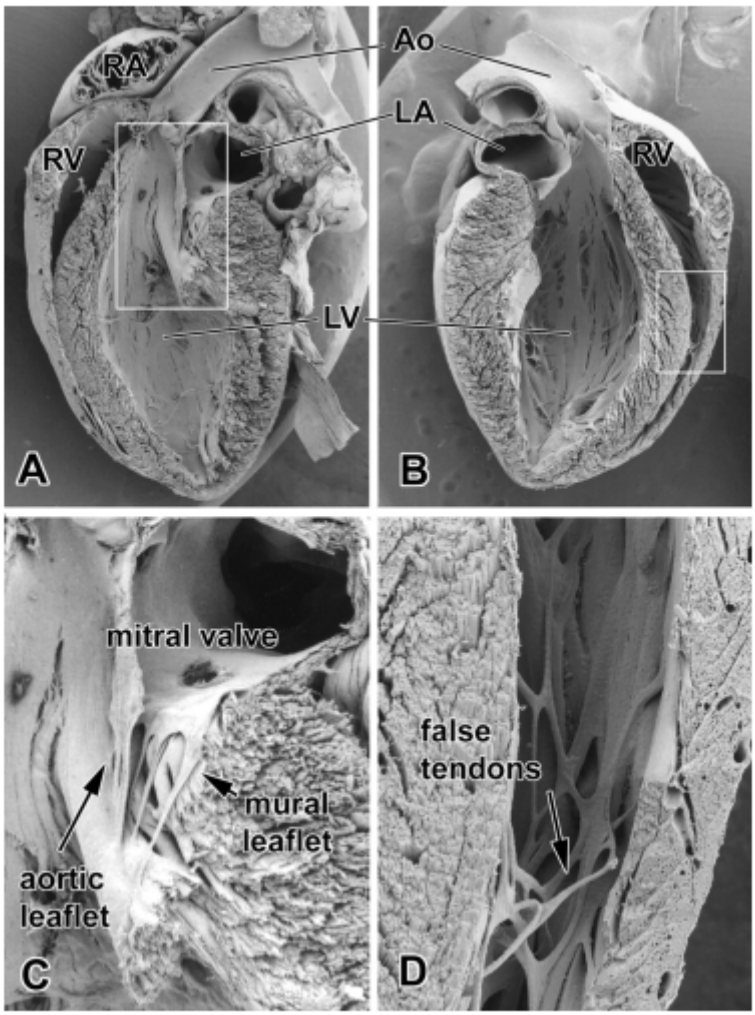

Figure 1-3: Cross section of the mouse heart.

Mouse and human hearts show a marked structural homology, although in mouse hearts the left atrium (LA) and right atrium (RA) are positioned as leaflets just above the right and left ventricles (RV and LV) (A and B). The main ventricular chambers and the other supporting structures such as the valves (C), tendons (D), arteries and veins are similar to that of humans (Wessels and Sedmera, 2003).

Thus, the fidelity and translation of findings from murine models to human models is empirically more likely in processes that affect depolarisation. Both human and mouse hearts are able to demonstrate AP duration heterogeneity which leads to important tissue level electrophysiological phenomenon such as repolarization gradients; both transmural and apico-basal, as well as the development of arrhythmias when these gradients are altered (Knollmann et al., 2001 a; Killeen et al., 2008 b).

The similar electrophysiological properties has contributed to the widespread use of the mouse as an electrophysiological model for a myriad of different cardiac arrhythmic syndromes. The ease of genetic manipulation of the mouse genome and the development of

knock-outs and knock-ins has been used to isolate and dissect the role of particular proteins in arrhythmogenesis. Presently, the use of genetically modified mouse models in such cases has helped elucidate and provide important mechanistic insights and therapeutic strategies for genetically linked disorders. In cardiac arrhythmia research, genetically modified mice have become one of the main species studied which has helped our understanding of arrhythmogenesis.

Studies in $Na_V1.5$ haplo-insufficient murine *Scn5a*$^{+/-}$ hearts have implicated loss of Na^+ channel function and accelerated age-related fibrotic changes in compromising AP conduction velocities. This accentuates tissue-level re-entrant circuit formation, ultimately resulting in the generation of the ventricular arrhythmic substrate present in the Brugada Syndrome (Jeevaratnam et al., 2011, 2012; Martin et al., 2012 b; Huang, 2017 b). Further studies in variants with abnormal Na^+ or K^+ channel properties have explored disruptions in the repolarisation process, associated with long QT syndromes. Finally, studies using variants involving intracellular ion channel function, particularly the RyR2-Ca^{2+} release channel have examined the relationship between alterations in Ca^{2+} homeostasis and the surface electrical changes.

1.4 The Surface Electrocardiogram

The electrical activity of the heart is readily recorded from the body surface. This is now done using recording electrodes placed in standard positions originally defined by Einthoven in his work on the first clinically applicable electrocardiogram (ECG) (Einthoven W, 1903). The ECG is a fundamental tool in the analysis of cardiac elelctrophysiology, both in normal and diseased states, and still in routine use in clinical practice today. Its characteristics can give important information about abnormal rhythms caused by damage to the conductive tissue or by imbalance in the body's electrolytes (Van Mieghem et al., 2004).

The normal human ECG is composed of a P wave, a QRS complex and a T wave (Figure 1-4). The P wave represents the depolarisation of the atria, whereas the QRS complex is generated by potentials when the ventricles depolarise and is seen on the ECG as the QRS complex. The QRS complex comprises of three deflections - the Q wave (first negative deflection preceding the R wave), R wave (first positive deflection) and S deflection (negative wave following an R wave), each corresponding to distinct electrical activity occurring in the heart at a given point in time.

After ventricular depolarisation, the large ventricular mass undergoes repolarisation and this is reflected by an upright deflection on the surface ECG known as the T wave. The atria, by contrast, do not have sufficient mass to cause a detectable perturbation by their repolarisation at the sampling frequency and standard gain settings on the human surface ECG in clinical practice. Atrial repolarisation is also masked by the much larger depolarisation of the QRS complex. Left and right atrial depolarisation are not usually seen as discrete components in the standard clinical human ECG though they may be delineated in other ECGs such as stress ECGs used in clinical practice.

Also notable within the surface human ECG are isoelectric periods, the most prominent of which is known as the PR segment. This corresponds to the time for conduction from the atria to the atrioventricular node (AVN) (Surawicz et al., 2008). The ST segment represents the phase 2 plateau

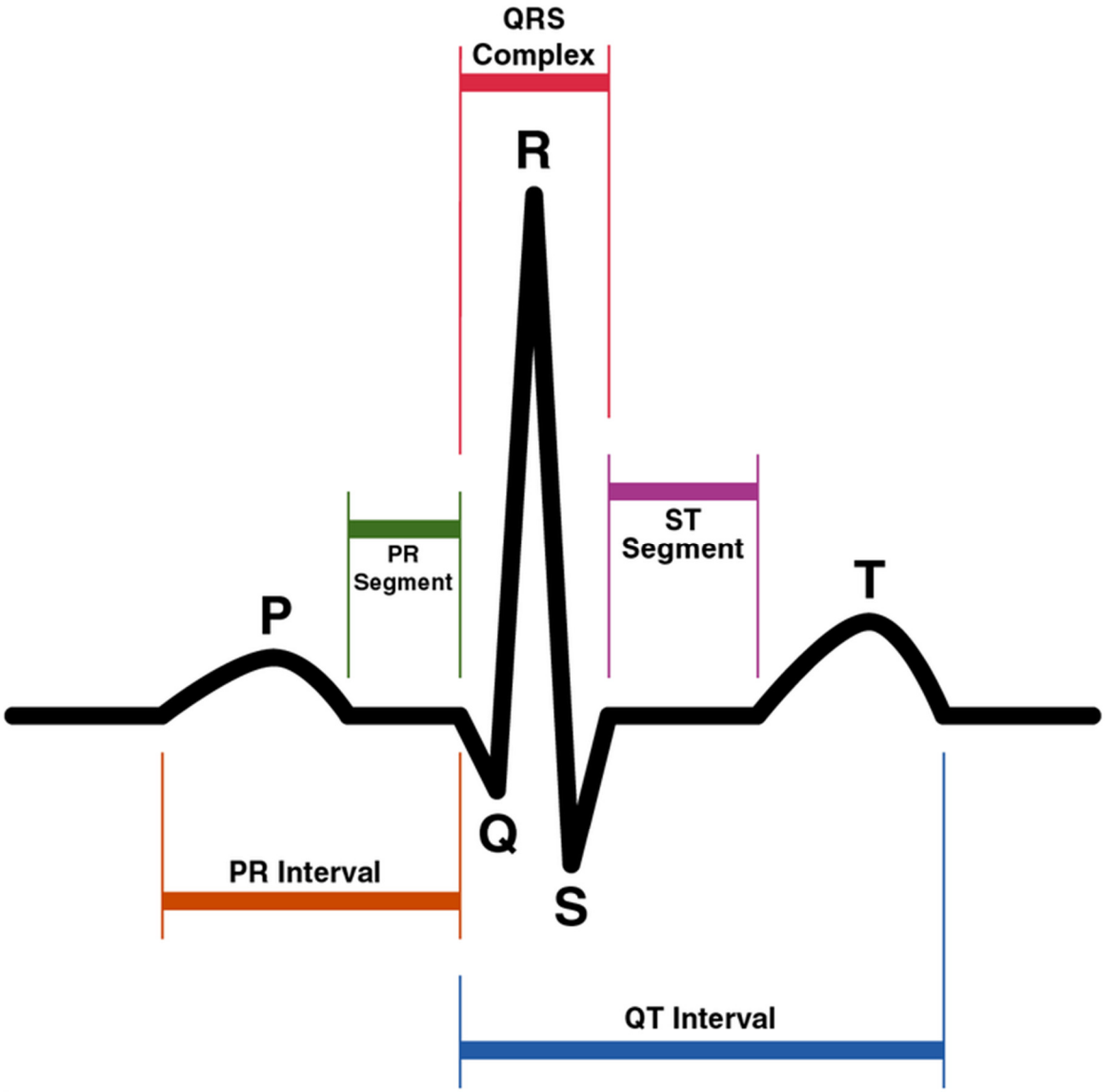

Figure 1-4: The human surface ECG:

Labelled are the P wave representing atrial depolarization, the isoelectric PR segment representing time to AV conduction, the QRS complex representing the ventricular depolarization, the ST segment representing the phase 2 plateau period and the T wave representing the ventricular repolarisation. Displaying the major deflections of the human surface ECG and the description of the varying intervals. Also labelled are the PR interval and QT interval, two frequently measured intervals in clinical practice.

period of the human AP (Surawicz et al., 2008). Changes in the duration of the waves or the intervals between them often represent a pathological process in cardiac conduction.

Physiological age related variations in the surface ECG are accepted in clinical practice. In paediatric patients, with the removal of the placental circulation leading to the functional closure of the foramen ovale, the paediatric heart undergoes significant change. The left ventricle to right ventricle ratio (LV/RV ratio), an indicator of their respective free wall thicknesses, has been reported to change to 1.5:1from 0.8:1 and slowly to the adult ratio of 2.5:1 (Tipple, 1999), while there is a steady reduction in heart rate attributed to an increase in vagal tone (O'Connor et al., 2008). As the cardiac muscle mass is less in children than in adults, the AV conduction assessed by PR interval, and ventricular depolarisation duration assessed by QRS duration, is shorter in children (O'Connor et al., 2008).

The murine surface ECG has a number of important homologies to the human ECG used in clinical practice as well as some important differences. Firstly the P wave (Figure 1-5) is bifid with two discernible waves present representing the left and right atrial depolarisation; this is something that is also seen in the normal human ECG, though not routinely in clinical practice due to the sampling rate employed in clinical ECGs (Surawicz et al., 2008). The QRS complex is conserved but instead of terminating at an isoelectric ST segment is followed almost immediately by two further waves representing the repolarisation phase of the ventricles – the R' wave and the C wave (Figure 1-5). The definitions of the relevant intervals from the human surface ECG thus have direct murine correlates – the PR interval, QRS complex (now including up to the peak of the R' wave) and QT interval all have homologous murine interval equivalents. However there is no isoelectric ST segment. Finally, the RR interval represents the interval from the peak of the R wave from one R wave to the peak of the subsequent R wave.

Typical physiological values for all these intervals have not been extensively investigated in the mouse heart, apart from the RR interval and the QT interval – these have been found to vary between 60-200ms for the RR interval and around 40-60ms for the QT interval (Jeevaratnam et al., 2010; Boukens et al., 2014). Similar studies on different mouse strains are consistent with this, with typical values for the QRS duration around 10-12ms and the PR interval between 35-60ms (Jeevaratnam et al., 2010; Boukens et al., 2014; Chadda et al., 2017).

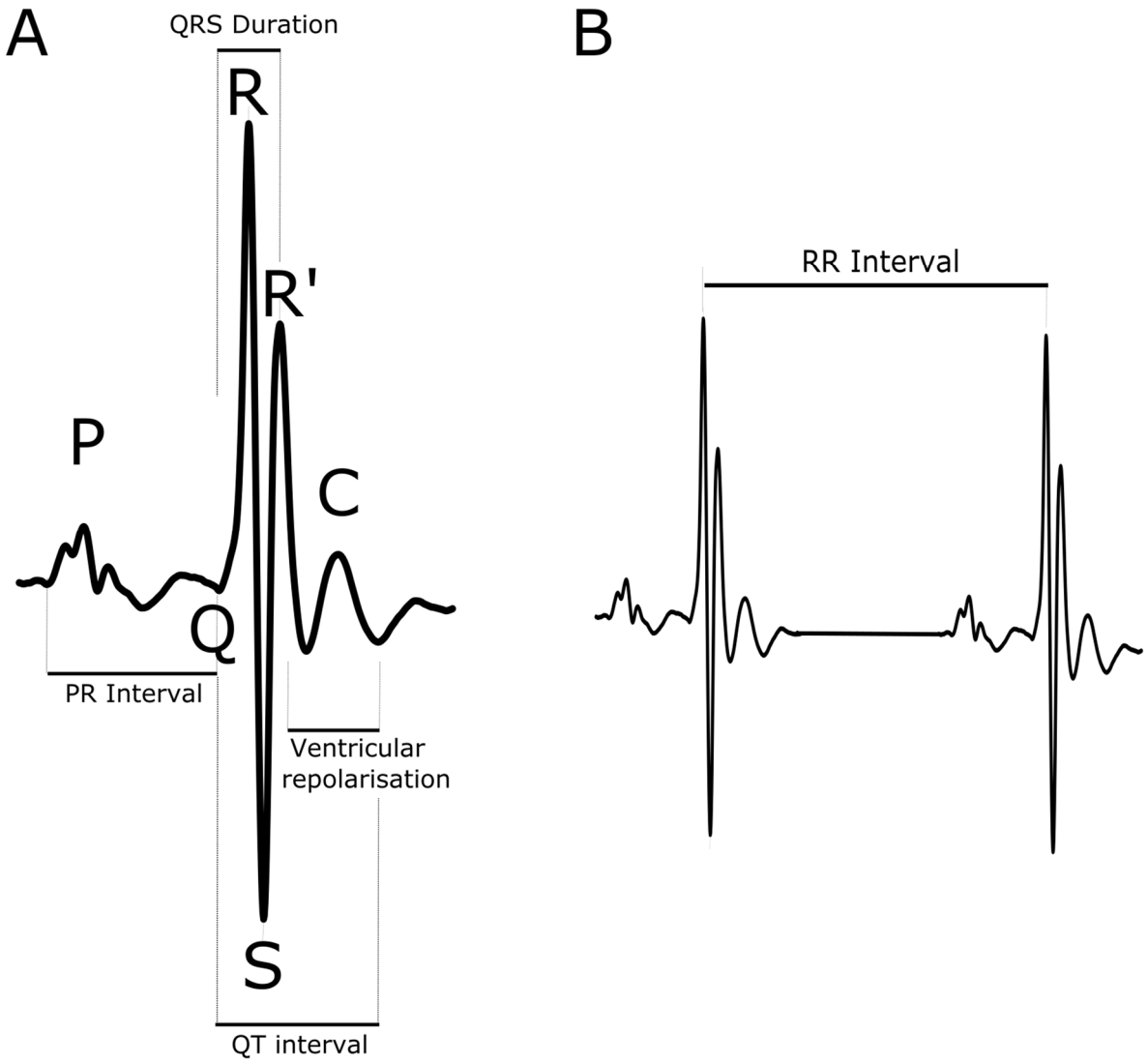

Figure 1-5: The murine ECG:

A: *Typical ECG and definition of deflections used in quantitative analysis including the P-wave; Q wave/start of QRS complex; R wave peak; S wave; R' deflection (not present on human ECG); C wave (not present on human ECG); There is no direct correspondence to an* isoelectric *ST segment as in a human ECG though the period between the QRS complex and the beginning of the ventricular repolarisation represents the same phases in the murine AP. The murine equivalent of the T wave encompasses both the R' wave and the C wave. The corrected QT interval, QT_c is taken as the interval from C to H and corrected for RR intervals (Mitchell et al., 1998).* ***B****: Two successive murine ECG complexes and the RR interval. The shorter the RR interval the greater the heart rate.*

1.5 MITOCHONDRIAL DYSFUNCTION IS ASSOCIATED WITH AGEING, METABOLIC DISEASE AND CARDIAC FAILURE.

Monogenic ion channel defects account for a relatively small proportion of SCD in the clinical setting. A growing body of epidemiological evidence links ageing and the common metabolic/age related conditions of obesity, diabetes mellitus and heart failure (Kucharska-Newton et al., 2010; Hookana et al., 2011; Yeung et al., 2012) to mitochondrial dysfunction. Such disorders are a growing problem in human populations especially in developed nations. These conditions constitute risk factors for SCD independent of any underlying coronary artery disease (Yeung et al., 2012; Adabag et al., 2015).

The link between ageing, metabolic disease and mitochondrial dysfunction is corroborated with evidence at the physiological level (Larsson, 2010). Ageing is associated with mitochondrial DNA (mtDNA) damage and respiratory chain deficiency is a consequence of clonal expansion of these mutations in human mitochondria (Ademowo et al., 2017; Krishnan et al., 2007; Trifunovic and Larsson, 2008). Human cardiomyocytes isolated at autopsy show defects of cytochrome-c-oxidase, the terminal enzyme of the respiratory chain which occur with increasing frequency with age (Muller-Hocker, 1989). Similar features are also observed in other mammalian species: deterioration of respiratory chain function secondary to age-associated mtDNA damage is observed in mouse (Piko et al., 1988), rat (Wanagat et al., 2001), and rhesus monkey (Schwarze et al., 1995) models (Larsson, 2010). Furthermore, in a murine model of premature ageing, somatic mtDNA mutations were found with increasing frequency (Larsson, 2010; Trifunovic et al., 2004). Thus, there is a strong experimental and observational evidence supporting the link between increased age and mitochondrial dysfunction.

A similar link also exists for metabolic dysfunction and mitochondrial deficiency at the physiological level, as evidenced by complex I electron transport chain (ETC) abnormalities and decreased state 3 respiration in cardiac mitochondria in metabolic disease states. This has

been shown in human tissue taken from diabetic patients during coronary artery bypass graft surgery (Schrauwen-Hinderling et al., 2016). Similarly, high-fat-diet fed obese mice showed increased mitochondrial dysfunction, also associated with a defect in complex 1 functioning (Wang et al., 2015). Therefore, in common with increased age, there is evidence to support a link between metabolic disorders and mitochondrial dysfunction.

Finally, there is also a strong link between cardiac failure and mitochondrial and metabolic dysfunction. Indeed the paradigm of the failing heart as an energetically starved heart has evidence accumulated over many years of scientific study. Cardiac tissue has a high energetic demand, and produces more than 90% of its demand from mitochondrial respiration. The importance of energy sufficiency in cardiac function is evidenced by the fact that mitochondria occupy around 30% of cardiomyocyte volume. Mitochondria also exhibit ordered structural specialisations such as spatial arrangement in rows between myofilaments such that a constant diffusion distance exists between mitochondria and the core of myofilaments. The energy balance in the heart is finely tuned – during maximal exercise the organ uses more than 90% of its oxidative capacity, demonstrating that there is no excess energy production capacity (Mootha et al., 1997).

It is now known that the energy metabolism in cardiomyocytes from failing hearts show remodelling of energetic pathways whereby key enzymes and regulators in metabolic pathways such as the phosphotransferase reactions, the glycolytic pathway, the mitochondrial Krebs cycle and the electron transport chain itself have altered expression levels or are dysregulated (Ingwall, 2009). This results in progressive loss of cytosolic [ATP]. In the failing human myocardium and in hearts of animal models of severe failure, [ATP] is ∼30% lower than in normal myocardium (Neubauer, 2007). Key metabolic compounds such as AMP and Cr serve as energy sensors, and determine the metabolic remodelling that takes place often through changes in phosphorylation state among other chemical modifications of proteins for short term preservation of ATP (Dyck and Lopaschuk, 2006). In uncompensated hypertrophy and in other forms of heart failure, flux through the creatinine kinase (CK)

pathway and oxidation of fatty acids (which occurs in mitochondria) are both lower (Osorio et al., 2002; Stanley et al., 2005; Sorokina et al., 2007; O'Donnell et al., 2008) and glucose utilisation is not sufficient to compensate for overall decreases in the capacity for ATP supply leading to decreased ATP availability (Luptak et al., 2005; Neglia et al., 2007).

In the early stages of heart failure, human studies have shown that fatty acid oxidation is largely intact or even slightly increased. However in the latter stages, there is a marked downregulation of the fatty acid oxidation pathways in mitochondria (Sack et al., 1996; Osorio et al., 2002; Lei et al., 2004). Importantly, inadequate intracellular oxygen availability does not seem to be a limiting factor of oxygen consumption (Gong et al., 2003) implicating peak O_2 utilization being limited by maximal oxidative ATP synthetic capacity or by the maximal capacities of the ATPases to utilize ATP. Failing hearts also show greater inefficiency in utilising oxygen for ATP generation in mitochondria; decreased ADP/O ratio has been observed that is reflected in a 14% decrease in efficiency of the failing hearts (Murray et al., 2008). Decreased activity of the respiratory chain and the Krebs cycle is correlated with reduced cardiac function in human and experimental studies of heart failure (Jarreta et al., 2000; Ning et al., 2000).

The link between metabolic and mitochondrial insufficiency and heart failure is underscored by the fact that inborn errors of fatty acid metabolism (such as acyl-coA dehydrogenase deficiency) are associated with cardiomyopathy in humans. Targeted gene knockouts in mouse models recapitulates these findings giving further weight to a link between metabolic dysfunction and heart failure (Exil et al., 2003; Abdurrachim et al., 2015). We can therefore see that the exploration of mitochondrial function is key to examining its role in a wide range of linked pathologies.

1.6 CARDIAC ARRHYTHMIAS ARE ASSOCIATED WITH AGEING, METABOLIC DISEASE, CARDIAC FAILURE

Just as ageing, metabolic disease and cardiac failure are each associated with mitochondrial dysfunction (see section 1.4) each of these disorders are in turn linked to cardiac arrhythmia. There is also a more indirect link between mitochondrial dysfunction itself and cardiac arrhythmias at the clinical and experimental level. Mitochondria from patients with chronic atrial fibrillation, the most common cardiac arrhythmia, show structural abnormalities, increased DNA damage and impaired function (Ad et al., 2005; Bukowska et al., 2008; Lin et al., 2003; Tsuboi et al., 2001; Valli et al., 2017a). Additionally, fatal ventricular arrhythmias are a feature of inherited mitochondrial disorders such as Kearns-Sayre syndrome (Kabunga et al., 2015; Valli et al., 2017b). Both acute and chronic mitochondrial dysfunction promote cardiac arrhythmogenesis in animal models (see review (Akar and O'Rourke, 2011)). Acute, ischaemic-reperfusion-induced mitochondrial impairment results in VF in guinea pigs which can be abolished by pharmacological manipulations of mitochondrial membrane potential (Akar et al., 2005; Brown et al., 2010; Valli et al., 2017b). Furthermore, in goat and dog models of AF, abnormal structure and function of mitochondria have been observed (Ausma et al., 1997; Morillo et al., 1995; Valli et al., 2017a). Thus, mitochondrial dysfunction is an interesting setting in which to study arrhythmogenesis.

Second, growing clinical and epidemiological evidence links these conditions (ageing, metabolic dysfunction and heart failure) to cardiac arrhythmias (Kucharska-Newton et al., 2010; Hookana et al., 2011; Yeung et al., 2012). This is reflected in the increasing trend in the incidence and prevalence of atrial fibrillation for which 60% of the increase has been attributable to metabolic factors. (Miyasaka et al., 2006; Valli et al., 2017b). Diabetes mellitus, obesity, physical inactivity, and metabolic syndrome have all been associated with increased risk of developing AF (Mozaffarian et al., 2008; Nichols et al., 2009; Tedrow et al., 2010; Valli et al., 2017b; Watanabe et al., 2008). Metabolic disorders also predispose to ventricular arrhythmias, which have been identified as a common presentation in patients with inherited

fatty acid oxidation disorders (Bonnet et al., 1999). In middle aged individuals who do not smoke, obesity increases the risk of SCD. An increased risk of SCD is also seen in diabetic patients compared to non-diabetic patients post myocardial infarction (Yeung et al., 2012).

Ageing itself is also associated with an increased incidence of cardiac rhythm disturbances including both pathological bradycardic rhythms as well as atrial and ventricular tachy-arrhythmias (Go et al., 2001; Deo and Albert, 2012; Bradshaw et al., 2014), though the underlying mechanisms remain unclear. Thus, the risk of cardiac rhythm abnormalities accumulates with age. Defects of the cardiac conduction system leading to heart block are known to be an age related disease process (Lenegre, 1964; Lev, 1964). Incidences of atrial and fatal ventricular arrhythmias increase with age over time, with the prevalence of atrial fibrillation rising rapidly from around 4% of individuals aged 60 to 70 years of age to nearly 20% of individuals aged over 80 (Zoni-Berisso et al., 2014). There is a similar age dependant risk of ventricular arrhythmias, with the annual incidence of sudden cardiac death 8 times higher in 75 year olds compared to people aged 50 years (Deo and Albert, 2012). Age dependant trends are also seen with inherited arrhythmic syndromes; the number of symptomatic patients with the Brugada syndrome increases dramatically with age (Gourraud et al., 2017), despite the defect being present since birth.

Finally, the link between heart failure syndromes and fatal and non-fatal ventricular arrhythmias has long been established (Chakko et al., 1989) . These are an important cause of mortality in heart failure. In severe congestive heart failure, ventricular arrhythmias (including non-sustained VT) are observed in up to 85% of patients (Singh et al., 1997). The establishment of implantable cardioverter defibrillators (ICDs) as a proven heart failure therapy in both primary and secondary prevention (Investigators, 1997; Moss et al., 2002; Bardy et al., 2005) emphasises the close link between heart failure and fatal ventricular arrhythmias.

1.7 THE PGC SYSTEM AS A REGULATOR OF MITOCHONDRIAL FUNCTION

We have seen how ageing, metabolic dysfunction and cardiac failure are each associated with mitochondrial dysfunction and how these three disorders are also associated with cardiac arrhythmias. Taken together these experimental and clinical findings converge upon a central role for mitochondrial dysfunction in cardiac arrhythmogenesis (Figure 1-6).

Mitochondria have been implicated in modulating cytosolic Ca^{2+} in cardiomyocytes (Lukyanenko et al., 2009) and so it is plausible that mitochondrial dysfunction will alter spatial and temporal properties of calcium handling at the cellular level, leading to the necessary ion concentration changes for a pro arrhythmic phenotype. In addition, the development of an age related pro-arrhythmic electrophysiological phenotype in various models has also been linked to cellular changes in calcium handling (Hatch et al., 2011; Yang et al., 2015) such as a decrease in the amplitude of the systolic Ca^{2+} transient and in some cases a decrease in peak L-type Ca^{2+} current (Feridooni et al., 2015).

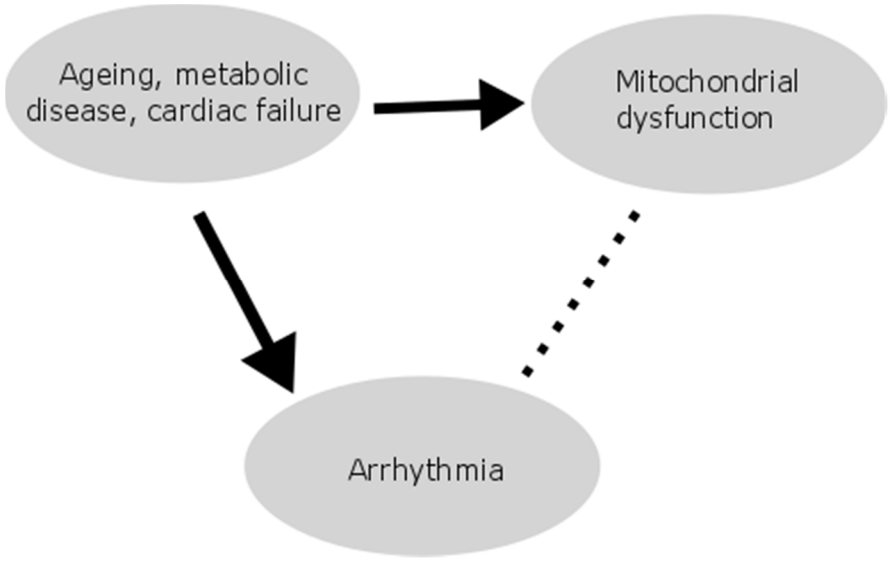

Figure 1-6: The relationship of ageing, metabolic disease and cardiac failure with mitochondrial dysfunction and cardiac arrhythmia based on current evidence. *The dashed line represents a link where the evidence is less substantial.*

With ageing, the rate of sarco/endoplasmic reticulum Ca^{2+}-ATPase (SERCA)-mediated Ca^{2+} removal is reduced (Jiang et al., 1993) and the properties of SR Ca^{2+} release in terms of Ca^{2+} sparks are altered (Jiang et al., 1993). These changes are also correlated with reductions in the peak tension developed in cardiac tissue with advancing age, especially at higher heart rates (Lim et al., 1999) Other studies showed that the maximum rate of tension development (+ dT/dt) and maximum rate of relaxation (− dT/dt) are slowed with age (Jiang et al., 1993; Lim et al., 1999).

Chronic mitochondrial dysfunction in cardiomyocytes would then be expected to lead to cumulative, age related changes, which may be evidenced by abnormal calcium handling. Studies of such dysfunction have been expedited through targeting the PGC system as this is known to act as a central mitochondrial regulator. This has been permitted through the use of genetically modified murine models. The *Pgc*-1 gene family consists of three members: *Pgc-1α*, *Pgc-1β*, and *Pgc-1-related coactivator* (PRC) (Villena, 2015). A recent review (Villena, 2015) describes the mechanism of action of PGC-1 coactivators in detail. The expression patterns of *Pgc-1α* and *Pgc-1β* are similar. Both show high expression levels in tissues with high energy requirements and mitochondrial content such as the heart, skeletal muscle, kidney and brown adipose tissue (BAT) (Villena, 2015).

The PGC-1 proteins regulate mitochondrial mass, function and cellular metabolism, upregulating expression of nuclear and mitochondrial genes involved in fatty acid β–oxidation, the tricarboxylic acid cycle and electron transport (Arany et al., 2005) (Figure 1-7). In particular, PGC-1α and PGC-1β are highly expressed in oxidative tissues such as the heart, serving to co-ordinate mitochondrial activity with upstream cellular signals (Sonoda et al., 2007). PGC-1 family members operate to match increased energy demands during prolonged stimuli such as exercise or fasting, to the expression levels of catabolic enzymes. This is achieved by an increase in the activity of transcription factors, which themselves are regulated by transcriptional coactivators, of which PGC-1 coactivators are a subset (Villena, 2015). PGC-

1 coactivators thus link cellular energy stores with external stressors, matching mitochondrial activity with energy demands (Figure 1-8).

Thus, PGC-1 forms a nexus for a range of metabolic pathways within the cardiomyocyte, central to the heart's ability to meet energetic demands. Their expression is down-regulated in obesity, insulin resistance, heart failure and type II diabetes mellitus and is accompanied with an associated mitochondrial dysfunction (Dillon et al., 2012). Mice deficient in *both Pgc-1α* and *Pgc-1β* develop a perinatal, lethal, low cardiac output state and conduction disease (Lai et al., 2008). In contrast, both *Pgc-1α*$^{-/-}$ and *Pgc*-1*β*$^{-/-}$ hearts show normal baseline function (Arany et al., 2005; Lelliott et al., 2006), with *Pgc*-1*β*$^{-/-}$ hearts displaying abnormal electrophysiological responses to adrenergic challenge. Together with its normal baseline contractile function these features make *Pgc-1β*$^{-/-}$ models attractive to investigating pro-arrhythmic effects of *chronic* mitochondrial dysfunction.

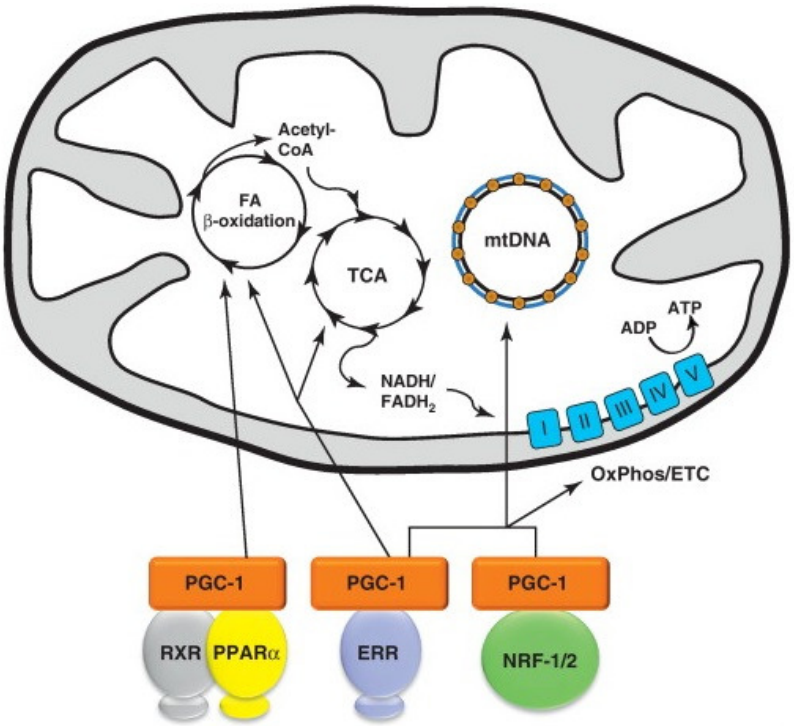

Figure 1-7: Control of mitochondrial biogenesis by the PGC-1 signaling.

Interaction between PGC-1 and specific transcription factors orchestrates the major functions of mitochondria, including fatty acid β-oxidation, the tricarboxylic acid cycle (TCA), mtDNA replication and oxidative phosphorylation, and the electron transport chain (OxPhos/ETC), in addition to biogenesis of this organelle. PPARα interacts with its binding partner, the retinoid X receptor (RXR), to control the expression of many fatty acid β-oxidation enzymes. NRF-1 and NRF-2 contribute to the maintenance of mtDNA and the expression of multiple components of the ETC. ERR members regulate the expression of virtually all functions of the mitochondria including those shown here. Adapted from (Scarpulla et al., 2012)

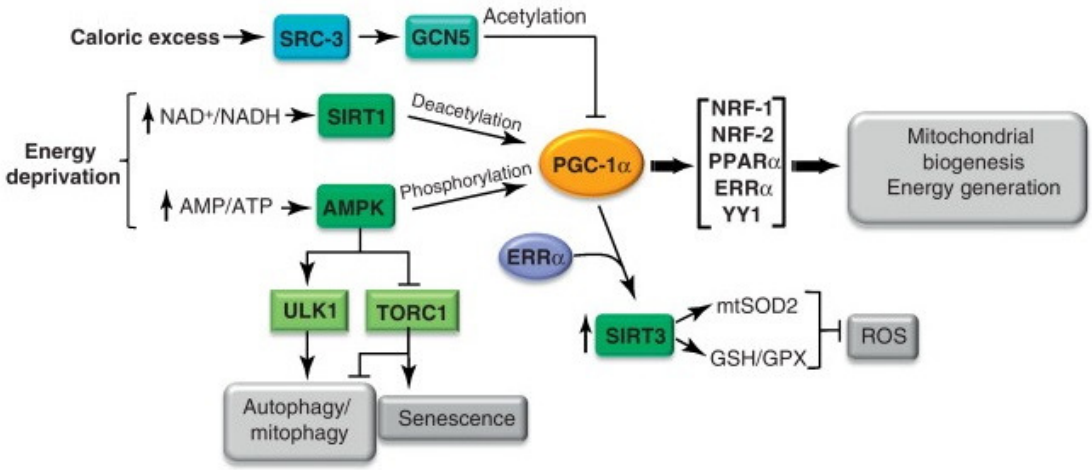

Figure 1-8: Integration of energy-generating and antioxidant pathways by PGC-1 signalling.

PGC-1α is activated via post-transcriptional phosphorylation by AMPK or by deacetylation via SIRT1 in response to nutrient deprivation. Induction or activation of the coactivator can enhance mitochondrial biogenesis and oxidative function through the coactivation of multiple transcription factors involved in respiratory gene expression. PGC-1α activation may also promote an antioxidant environment by coactivating ERRα to induce SIRT3, a mitochondrial sirtuin that has been implicated in reactive oxygen species (ROS) detoxification. In addition, AMPK promotes autophagy through direct phosphorylation of ULK1 or via suppression of the TORC1 kinase complex. Inhibition of the TORC1 pathway also has been shown to have a negative effect on senescence. Increased autophagy, enhanced ROS detoxification, and inhibition of TORC1, are all associated with health and longevity. Under conditions of caloric excess, SRC-3 induces GCN5, which inactivates PGC-1α through acetylation. Adapted from (Scarpulla et al., 2012)

Despite their similar expression patterns, the functions of *Pgc-1α* and *Pgc-1β* differ. *Pgc-1α* appears to have a more dynamic function, as its expression is upregulated by physiological stimuli such as fasting, exercise and cold temperatures in the liver, skeletal muscle and BAT, respectively. *Pgc-1β* expression does not appear to be altered by these stimuli. Thus, it is assumed that *Pgc-1α* works to adapt tissues to conditions of high energy demand whereas the role of *Pgc-1β* relates mainly to the maintenance of basal mitochondrial function (Villena, 2015).

Both *Pgc-1α*$^{-/-}$ and *Pgc-1β*$^{-/-}$ mice demonstrate mitochondrial dysfunction. However, *Pgc-1α*$^{-/-}$ mice demonstrate further cardiac phenotypes including cardiac pump failure. *Pgc-1β*$^{-/-}$ mice

display an electrophysiological phenotype in the absence of pump failure, and are thus an attractive model for the study of arrhythmias in a setting of chronic mitochondrial dysfunction (Lelliott et al., 2006). This model has recently been introduced to study biochemical (Gurung et al., 2011; Lelliott et al., 2006) and electrophysiological (Ahmad et al., 2017b; Valli et al., 2017a; Valli et al., 2017b) sequelae of chronic mitochondrial dysfunction and energetic deficiency.

Pgc-1β$^{-/-}$ mice show mitochondrial dysfunction and accompanying energetic deficiency. They show a reduction in cardiac mitochondrial volume fraction, along with decreased expression of ETC genes (Lelliott et al., 2006). *Pgc-1β*$^{-/-}$ and wild-type (WT) heart mitochondria are similarly packed between myofibres, and there are no changes in density of mitochondrial cristae within mitochondria (Lelliott et al., 2006), suggesting that the internal mitochondrial structure is unchanged in *Pgc-1β*$^{-/-}$ hearts (Lelliott et al., 2006). This is a plausible explanation of why the knockout of *Pgc-1β* alone causes only minor effects on the function of cardiac mitochondria (Lelliott et al., 2006; Sonoda et al., 2007; Villena, 2015). Indeed, defects in mitochondrial function seen in *Pgc-1β*$^{-/-}$ mice are partly abrogated by up-regulation of *Pgc-1α* (Lelliott et al., 2006).

Electrophysiological studies on *Pgc-1β* knockout in murine hearts have yet to be studied in detail. Resting heart rate and left ventricular contractility are similar between *Pgc-1β*$^{-/-}$ and WT but on dobutamine injection, the chronotropic response in *Pgc-1β*$^{-/-}$ mice is blunted compared to WT mice (Lelliott et al., 2006). *Pgc-1β*$^{-/-}$ mice also demonstrate increased cardiac arrhythmogenicity during in-vivo isoprenaline challenge or programmed electrical stimulation (PES) in Langendorff-perfused murine hearts (Gurung et al., 2011). However, the detailed electrophysiological phenotype of the *Pgc-1β* knockout mouse and how age impacts on its development has thus far not been studied.

1.8 OBJECTIVES OF THE THESIS

The present project is directed at investigating the relationship between chronic energetic deficiency, ageing and cardiac arrhythmias in a murine model (Figure 1-9). The study will accordingly focus on *Pgc-1β*$^{-/-}$ mice as the adopted model, as it does not display cardiac pump failure unlike other mitochondrial lesions. The hypothesis is that while ageing, metabolic disease and cardiac failure are linked to both cardiac arrhythmias and mitochondrial dysfunction (see section 1.4 and section 1.5 respectively) mitochondrial dysfunction and cardiac arrhythmias are themselves intimately linked (Figure 1-9). The objective of the study is to demonstrate whether a primary mitochondrial lesion can lead to susceptibility to arrhythmia and if this susceptibility is age dependent. As arrhythmias are a tissue level/whole organ phenomenon, the experimental design preserves cellular and tissue level architecture as much as possible. The study will first characterize the electrocardiographic and tissue level electrophysiological features of *Pgc-1β* ablation and the effect of age on these. This allows the study to explore the study question while preserving cellular and tissue and organ level architecture as much as possible. The focus on electrocardiographic characteristics in the first part of the study allows the determination of whether there are spontaneous ventricular arrhythmias or not and gives indications as to cellular level changes that may be found – these are then explored in the subsequent experiments included in the thesis.

As well as the primary objective to determine if there are statistically more arrhythmias in the *Pgc-1β*$^{-/-}$ mice and whether this propensity to arrhythmia (if it exists) is age dependent, the study aims to explore a number of other secondary objectives. Importantly, the study aims to explore and characterize the electrophysiological instabilities that may be present in *Pgc-1β* ablated hearts through standard electrophysiological protocols employed widely in clinical practice and research and analyze whether they correspond to known arrhythmic theories. These include S1S2 and restitution studies that, importantly, utilize a technique that allows for intracellular recordings. This technique is used for the first time in the literature. This again permits interrogation of the system to see whether it is pro-arrhythmic, as well as analysis of

protocols that can help elucidate the underlying arrhythmic mechanisms. The novel micro-electrode technique also permits additional measurements of membrane potentials and correlates of sodium channel density that give important indications of cellular level ion channel changes. These are then be explored in the final phase of the study with a loose patch clamping technique to assess ionic currents in an intact whole tissue preparation. This gives further corroborating evidence to the cellular electrophysiological changes elucidated previously. Together, the study engages the question of the electrophysiological characterization of mitochondrial deficiency at the whole organ, tissue and single cell level.

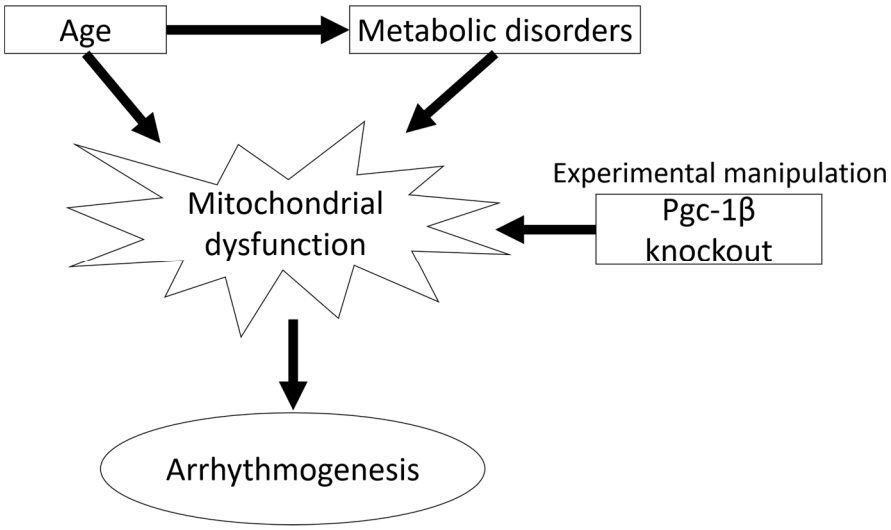

Figure 1-9: Postulated relationship between metabolic disorders, age, mitochondrial dysfunction and cardiac arrhythmias.

Age and metabolic disorders, themselves age-dependent, lead to mitochondrial dysfunction which in turn predisposes to arrhythmogenesis. In the present study, the experimental model used to investigate the effects of mitochondrial dysfunction on arrhythmogenesis was Pgc-1β knockout mice.

2. MATERIALS AND METHODS

2.1 EXPERIMENTAL ANIMALS

This research has been regulated under the Animals (Scientific Procedures) Act 1986 Amendment Regulations 2012 following ethical review by the University of Cambridge Animal Welfare and Ethical Review Body (AWERB). Age-matched homozygote *Pgc-1β*$^{-/-}$ and WT inbred C57/B6 mice were studied. *Pgc-1β*$^{-/-}$ mice were generated using a triple LoxP targeting vector as previously described (Lelliott et al., 2006). Heterozygous triple LoxP mice crossed with ROSA26-Cre mice generated heterozygous *Pgc-1β*$^{-/-}$ mice, which were further bred to generate homozygous *Pgc-1β*$^{-/-}$ mice. This body of work was completed prior to the initiation of the study (Gurung et al., 2011 a). Mice were bred on a C57/B6 background to avoid possible strain-related confounds. The young WT and young *Pgc-1β*$^{-/-}$ groups consisted of mice aged between 3-4 months; animals aged greater than 12 months were used for the aged WT and aged *Pgc-1β*$^{-/-}$ groups. Mice were housed in plastic cages maintained at 21 ± 1^{o}C, subjected to 12 hour dark/light cycles, and had unconstrained access to water, sterile rodent chow (RM3 Maintenance Diet, SDS, Witham, Essex, UK), bedding and environmental stimuli.

2.2 ECG STUDIES

2.2.1 ELECTROCARDIOGRAPHY

Mice were anaesthetised with tribromoethanol (avertin: 2,2,2 trimethylethanol, Sigma-Aldrich, Poole UK) administered into the intra-peritoneal space with a 27G hypodermic needle. Young and aged, WT (n = 5 and 8) and *Pgc-1β*$^{-/-}$ (n = 9 and 6) animals were used. They were then weighed, placed supine on a warmed (37°C) platform, and their limbs secured with adhesive tape to minimise movement artefact and enable correct lead positioning. Three 2-

mm diameter electrodes (MLA1204; ADInstruments, Colorado Springs, CO, USA) placed in the right forelimb, left forelimb and left hindlimb respectively enabled lead I and lead II ECG recordings. The electrodes were connected to a 4-channel NL844 pre-amplifier whose outputs were then led through 4-channel NL820 isolator and NL135 low-pass filter units (set at a 1.0-kHz cut-off and with a 50-Hz notch) within a NL900D chassis and power supply (Neurolog-Digitimer, Hertfordshire, UK). To reduce electrical noise, all recordings were carried out within a grounded Faraday cage. Signals were sampled at 5 kHz and analogue-to-digital conversion employed a CED 1401c interface (Cambridge Electronic Design, Cambridge, UK). This then conveyed the signal to a computer for display and recording using Spike II software (Cambridge Electronic Design).

ECG recordings commenced immediately following electrode attachment in anaesthetised animals. These were continued for 5 minutes to permit preparations to reach a steady state, and for a further 5 min to obtain traces for quantitative analysis. Dobutamine hydrochloride, a β_1 adrenoreceptor agonist used to stimulate cardiac adrenergic responses in clinical practice, was then administered into the intraperitoneal space (3 mg/kg; Sigma Aldrich, Poole UK)**.** ECG recording was then continued until a new steady state was reached. A further 5 min recording period provided traces for quantitative ECG analysis following pharmacological challenge.

2.2.2 DIGITAL SIGNAL PROCESSING

All analysis employed custom-written software in the open-source R programming language. Data was imported into the R program. An infinite impulse response (IIR) high pass Butterworth filter of order 2 was designed and the signal passed through to eliminate baseline drift. The signal was filtered in both forward and reverse directions to negate effects of any phase shift. A low-pass Savitzky-Golay algorithm was then applied. R peak fiducial points were identified with a peak-finding algorithm used to detect QRS complexes. An iterative process determined the signal envelope and an adaptive threshold was used to identify time points in the signal that were greater than threshold in the continuous ECG signal. QRS complex timing positions were determined; peaks on a more substantive upward or downward trend were disregarded in favour of the peak with the larger absolute value. If multiple peaks were

detected within 2 ms the peaks were analysed again and the larger maximum value taken as the correct peak, and the smaller peak discarded. In addition, all detections were visually verified. P waves were analyzed independently of QRS complexes by deleting the QRS complexes and subsequent isolation of the P wave parameters. This analysis thus made no assumption of QRS complexes being preceded by P waves. Analysis was performed on 300 second periods of ECG data immediately prior to and following administration of dobutamine hydrochloride. The effect of dobutamine was judged from observed ECG parameter changes. Figure 1-5A and Figure 3-1 depict typical murine ECG recordings with parameters calculated based upon this archetypal signal. Intervals were corrected for heart rate using the formula previously described (Mitchell et al., 1998).

2.3 WHOLE HEART LANGENDORFF PREPARATIONS

All chemical agents were purchased from Sigma-Aldrich (Poole, UK) except where otherwise indicated. Mice were first anticoagulated with 200 IU heparin sodium administered into the intra-peritoneal space with a 27G hypodermic needle. After a 10 min interval, mice were killed by cervical dislocation (Schedule 1: UK Animals (Scientific Procedures) Act (1986)), a sternotomy performed, and the hearts were rapidly excised and submerged in ice-cold KH solution. No recovery, anaesthetic or surgical procedures were required.

The aorta was then cannulated with a modified 21G hypodermic needle, secured with a 5-0 braided silk suture and retrogradely perfused with Krebs-Henseleit (KH) solution warmed to 37^{o}C by a water jacket heat-exchange coil (model C-85A, Techne, Cambridge, UK) at a constant rate of 2.05 ml min^{-1} by a peristaltic pump (MINIPULS3, Gilson, Luton, UK) through 200 µm and 5 µm Millipore filters (Millipore, Watford, UK). The KH buffer was made with NaCl (119 mM), $NaHCO_3$ (25 mM), KCl (4 mM), $MgCl_2$ (1 mM), KH_2PO_4 (1.2 mM), $CaCl_2$ (1.8 mM), glucose (10 mM) and sodium pyruvate (1.8 mM), bubbled with 95% O_2/5% CO_2 (British Oxygen Company, Manchester, UK) to achieve a pH of 7.4 preventing $CaCO_3$ precipitation and matching the 7.3–7.4 pH of mouse plasma. Following commencement of perfusion,

preparations were only further studied if they demonstrated sustained intrinsic activity with a basic cycle length (BCL) <200 ms and 1:1 atrioventricular conduction (AV) for 10 minutes. Hearts meeting these criteria were then perfused with 150 ml KH solution containing 20 µM blebbistatin after which perfusion with plain KH solution continued through to the conclusion of the experiment. The blebbistatin (20 µM, Selleckchem, Houston, USA) was used to electromechanically uncouple the heart during the microelectrode studies and permit stable cardiomyocyte impalement (Fedorov et al., 2007).

2.3.1 Electrophysiological recordings

Simultaneous microelectrode and electrocardiograph (ECG) studies were performed in a Faraday cage incorporating a modified horizontal Langendorff perfusion system, a light microscope (objective ×5, eyepiece ×5, W. Watson and Sons Limited, London, UK), custom-built head stage and a warmed tissue holding chamber. All equipment was electrically isolated. The stimulating and recording electrodes were positioned relative to the heart using two precision micromanipulators (Prior Scientific Instruments, Cambs, UK). Hearts were paced using a bipolar platinum-coated stimulating electrode (NuMed, New York, USA) positioned against the lateral surface of the right ventricle, connected to a DS2A-Mk.II stimulator (Digitimer, Welwyn Garden City, Herts., UK) delivering a voltage that was twice the diastolic excitation threshold plus 0.5 mV.

Whole heart volume conducted ECGs were recorded simultaneously with intracellular recordings to distinguish between local cellular and generalised organ level events. Two unipolar ECG leads were immersed into the warmed bath and placed adjacent to the right and left ventricles. Signals were amplified using model NL104A amplifiers (NeuroLog; Digitimer, Hertfordshire, UK), filtered with model NL125/126 filters, set to a bandwidth of 5 – 500 Hz, and the analogue signal digitised using a model 1401 interface (Cambridge Electronic Design). Sharp microelectrodes for intracellular recordings were drawn from borosilicate glass pipettes (OD 1.2 mm, ID 0.69 mm, Harvard Apparatus, Cambridge, UK) using a homebuilt microelectrode puller, and filled with 3 M KCl (tip resistance 15 – 25 MΩ). The microelectrode

was mounted onto a right-angled microelectrode holder containing a Ag/AgCl tip and connected to a high-input impedance direct-current microelectrode amplifier system (University of Cambridge, Cambridge, UK). Measurements of intracellular voltage were made relative to that of the Ag/AgCl reference electrode. An impalement was accepted for further recording if it resulted in an abrupt appearance of a resting membrane potential (RMP) between -65 mV and -90 mV, with APs that were normal in waveform and had an amplitude >75 mV. Impalements were restricted to the proximal left ventricle to avoid confounds of regional differences in AP characteristics. Hearts were first studied under conditions of regular pacing at a frequency of 8 Hz.

2.3.2 Pacing protocols

Hearts were stimulated at two times the threshold voltage plus 0.5 mV. Hearts underwent two pacing protocols. The electrophysiological properties of the whole heart langendorff preparation were interrogated using a number of different protocols. The S1S2 protocol is a programmed electrical stimulation (PES) protocol consisting of drive trains of eight paced (S1) beats at a BCL of 125 ms followed by a single extra stimulus (S2) every ninth beat. The initial S1-S2 coupling interval was 89 ms, reducing by 1 ms every subsequent cycle. The protocol was terminated when the ventricular effective refractory period (ERP) was reached, defined as the final S1-S2 coupling interval at which the S2 stimulus successfully triggered an AP, or sustained arrhythmia was observed. Incremental pacing protocols began at a 130 ms basic cycle length (BCL) before being decremented by 5 ms for each subsequent cycle of 100 stimulations. This cycle was repeated until the heart showed entry into 2:1 block or arrhythmia.

2.4 Quantification of AP parameters and arrhythmic incidence

AP amplitude was measured from the RMP to the peak voltage attained. The time from AP peak to repolarisation to 90% of baseline was taken as the action potential duration (APD_{90}). AP latencies were measured as the time intervening between the stimulus delivery and the

AP peak. The maximum rate of depolarisation $(dV/dt)_{max}$ was obtained from the first differential of the intracellular AP waveform. The incidence of abnormal rhythms was quantified from the PES protocol as follows: an isolated non-triggered AP following an S2 beat was termed an ectopic beat, and two successive non-triggered beats were termed a couplet. Episodes of ventricular tachycardia were categorised as non-sustained ventricular tachycardia (NSVT) if the episode consisted of ≥3 consecutive non-triggered beats but lasting <30 s; episodes lasting for >30 s were categorised as sustained VT.

2.5 Quantification of cardiac fibrosis

The degree of fibrotic change was assessed as previously described (Jeevaratnam et al., 2011). Briefly, following cardiectomy hearts were flushed with KH buffer, then perfused with 4% buffered formalin for 5 minutes, followed by storage in formalin overnight. After fixation, gross transverse sections of 7 µm thickness were cut and subjected to routine tissue processing, paraffin embedding and staining with picrosirius red. Sections were subsequently viewed, magnified and images digitally acquired using the Nano Zoomer 2.0 Digital Pathology system (Hamamatsu, Hertfordshire, UK). For quantification of fibrosis, a custom made 17 cm × 30 cm morphometric grid was superimposed on each photomicrograph, and each corresponding 0.2 mm × 0.2 mm area of tissue within the grid was assessed first for the presence or absence of cardiac tissue, and then for presence of fibrosis. The degree of fibrosis was expressed as the proportion of squares containing cardiac tissue that displayed evidence of fibrosis. The assessment was conducted independently by two investigators who were blinded to the animal identification, and their results were assessed for consistency by applying an inter-class correlation coefficient analysis (ICC), which can be interpreted as follows: 0 – 0.2 indicates poor agreement; 0.3 – 0.4 indicates fair agreement; 0.5 – 0.6 indicates moderate agreement; 0.7 – 0.8 indicates strong agreement; and >0.8 indicates almost perfect agreement.

2.6 LOOSE PATCH CLAMP EXPERIMENTS

2.6.1 VENTRICULAR PREPARATIONS

Hearts were excised and mounted on the Langendorff perfusion system as described previously. Hearts were then perfused with 75 ml of a KH solution to which 10 mM 2,3-butanedione monoxime (BDM) and 10 µM blebbistatin (Cayman Chemical Company, Ann Arbor, Michigan, USA) were added to give a KH-BDM/blebbistatin solution to achieve electromechanical uncoupling. The heart was then immediately placed in ice-cold KH-BDM/blebbistatin solution for dissection of the right ventricle from the rest of the heart. The right ventricle was then mounted on Sylgard (Dow Chemical Company, Staines, UK) and placed in a temperature monitored experimental chamber filled with filtered KH buffer solution at 27 ^{o}C.

2.6.2 PIPETTE MANUFACTURE

Pipettes, pulled from borosilicate glass capillaries (GC150-10 Harvard Apparatus, Cambourne, Cambridge, UK) using a Brown-Flaming microelectrode puller (model P-97, Sutter Instrument Co. Novato, CA, USA) were mounted under a microscope with 250× magnification and a calibrated eyepiece graticule for fracturing using a diamond knife. This applied a transverse force to the distal tip of the pipette, giving a fracture perpendicular to the pipette shaft. Selected pipettes were then fire-polished under visual guidance at 400× magnification using an electrically heated nichrome filament. Finally the pipette tips were bent so they made a ~45^{o} angle with the pipette shaft. When mounted at an angle on the recording amplifier headstage they could then be made to approach the membrane vertically. Maximum internal pipette tip diameters, measured at 1000× magnification, were 28-32 µm following polishing.

2.6.2 LOOSE PATCH CLAMP RECORDINGS

The distal ends of the pipette were filled with KH solution, and then mounted onto a pipette holder incorporating an Ag/AgCl half-cell connected to the headstage. This lowered the pipette onto the membrane surface. Gentle suction was then applied through an air-filled line

connecting the pipette holder and a syringe. This resulted in seal formation with a membrane patch. Figure 6-1 illustrates (A) the recording layout and (B) the equivalent circuit resulting from apposing the loose patch clamp electrode to the membrane surface. Voltage-clamp steps were applied under computer control. Owing to its relatively low seal resistances, the loose patch clamp results in larger leakage currents compared to those associated with conventional patch clamping. Most of the leakage current, series resistance errors and displacement currents through the pipette capacitance were compensated for using a custom-built amplifier (Stühmer et al., 1983). Residual leakage and capacitative currents were then corrected by using reference records obtained from subsequent P/4 control protocols that applied voltage steps with amplitudes scaled down by a factor of 4 in a direction opposite to those of the test steps as previously described (Almers et al., 1983 a; b). Each established patch was then subject to a complete set of pulse procedures examining either inward or outward current activation, which could be accomplished within 30 s making effects arising from prolonged changes in the patch such as bleb formation unlikely (Milton and Caldwell, 1990).

The loose patch clamp controls the voltage at the extracellular surface of the membrane within the seal in an intact cardiomyocyte. Accordingly, positive and negative voltage steps applied through the pipette respectively hyperpolarise and depolarise the membrane potential relative to the cardiomyocyte resting membrane potential (RMP). Voltage steps are therefore described in terms of the alterations they produce relative to the RMP, following the convention in earlier studies that introduced this technique (Almers et al., 1983 a; b). Current-voltage curves display current densities ($pA/\mu m^2$) obtained by normalizing the observed currents (nA) to the cross sectional area (πa^2) of the pipette tip, radius a. Inactivation curves plotted maximum current densities normalized to the maximum current densities obtained at the most polarised holding potentials. Curve-fitting was performed using the open source R programming language.

2.7 STATISTICAL ANALYSIS

2.7.1 ECG DATA

Statistical analysis used the R programming language. Data sets were first tested for normality with the Shapiro-Wilk test before statistical analysis using two way factorial multivariate analysis of variance, i.e. MANOVA with Pillai trace. The data sets analysed were the steady state heart rates, P wave durations, PR intervals, activation parameters of QR, QS and QR' durations, recovery parameters of RT_c, $R'T_c$ and ST_c durations, as well as the QT_c interval. Each of these were measured from ECG records of young and aged, WT and *Pgc-1β*$^{-/-}$ mice respectively, both before and following dobutamine challenge. The initial MANOVA tests examined each parameter for significant effects of age, genotype or interactive effects of age and genotype either prior to or following dobutamine challenge. Where MANOVA testing indicated existence of significant differences prior to dobutamine administration, further ANOVA analyses were conducted on pre-drug parameters testing for effects of genotype, age of interacting effects of the two. The presence of significant effects then prompted pairwise Tukey honest significant difference testing of differences between pairs of individual parameters. Similarly, where significant differences were indicated post-dobutamine, a similar procedure of significance testing was performed examining for significant effects post drug challenge. Peak heart rates that were obtained following dobutamine challenge, were analysed by a two way factorial ANOVA: there was no meaningful peak heart rate pre-dobutamine. These were then also followed by post hoc Tukey tests for differences between individual parameters if prompted by the significance levels. An ANCOVA analysis was also performed for correlation of heart rates pre and post dobutamine administration.

A $p < 0.05$ following Bonferroni correction where appropriate was considered to indicate a significant difference. Murine ECGs which demonstrated P wave dissociation in the analysis period were discarded for P wave dependent parameter analysis. All diagrams were produced with the R-grammar of graphics package.

2.7.2 Analysis of action potential data

Measures of arrhythmia duration included the number of beats during an episode of non-sustained (NSVT) or sustained ventricular tachycardia (VT), and the duration in seconds of the respective episode. Alternans was defined as beat to beat changes in the value of a parameter such that the direction of the change oscillates for at least ten successive action potentials.

The data was analysed with a custom-written programme using the python programming language and all statistical analysis performed in the R programming language (R Core Team, 2015). Data are expressed as means ± standard errors of the mean (SEM). Differences between experimental groups in AP parameters and degrees of fibrosis were compared using a two-way analysis of variance (ANOVA) testing for significant effects of genotype, ageing, and an interaction between the two. Where the *F*-ratio yielded a significant result, post-hoc Tukey honesty significant difference testing was performed. ANCOVA analysis was used to model the effect of genotype on heart rate while controlling for co-variate effects of pre-drug heart rates. Analysis of the S2 AP parameter curves was confirmed with a linear mixed effects analysis of the relationship using R (R Core Team, 2012) and lme4 (Bates et al., 2015). Categorical variables describing the incidence of arrhythmia were compared using a chi-squared test.

Both were analysed with a multivariate negative binomial regression model. Risk factors and confounders were included in the multivariate analysis based on the regression analysis of each variable individually. Each variable could only be added to the multivariate model if it showed a significant effect in the simple univariate analysis. In all cases a $p < 0.05$ was taken to be significant, with application of Bonferroni correction where appropriate.

2.7.2 Analysis of Loose Patch Clamp Data

Statistical analysis of results applied two-way analysis of variance (ANOVA) to the experimental groups of young and aged, WT and *Pgc-1β*$^{-/-}$ preparations to test for significant differences arising from independent or interacting effects of age and/or genotype on fitted parameters. The presence of such differences was then explored by pairwise tests for differences using Tukey's honestly significant difference testing.

3. AGE DEPENDENT ELECTROCARDIOGRAPHIC CHANGES IN *Pgc-1β* DEFICIENT MURINE HEARTS

3.1 INTRODUCTION

Murine electrocardiography (ECG) and analysis of ECG waveforms have proven useful in investigating electrophysiological changes associated with cardiac disease (Goldbarg et al., 1968). Murine ECGs differ in their sinus rates and action potential waveforms (Figure 1-4, Figure 1-5 and Figure 3-1) (Danik et al., 2002; Boukens et al., 2014) as compared to human ECGs, but nevertheless can be used to clarify alterations in heart rate, its variability, and timings in the cardiac excitation sequence. Thus, their P waves, and PR, QRS and QT intervals, continue to reflect atrial and ventricular, depolarisation and repolarisation whose alterations could reflect potentially pro-arrhythmic electrophysiological changes. Alterations in murine ECG waveforms have thus proven useful in studying murine models for the Brugada syndrome (Jeevaratnam et al., 2010; Martin et al., 2010), long QT syndrome type 3 (Wu et al., 2012) and catecholaminergic polymorphic ventricular tachycardia (Zhang et al., 2011).

The present study investigates ECG changes associated with the energetic dysfunction occurring with *Pgc-1β* ablation. As the underlying chronic mitochondrial lesions likely exert cumulative phenotypic effects with advancing age, we studied both young and aged, WT and genetically modified animals both at baseline and following adrenergic stress. This provided additional insights into possible interactions between genotype and ageing.

3.2 RESULTS

There were no significant differences in weights between different experimental groups, whether stratified by age or genotype. Aged *Pgc-1β*$^{-/-}$ mice had a mean weight of 35.49 ± 1.44 g compared to 35.57 ± 1.13 g for aged wild type (WT) mice. Young *Pgc-1β*$^{-/-}$ and WT mice had mean weights of 31.30 ± 1.56 g and 35.31 ± 2.26 g respectively. The complete ECG records confirmed sinus rhythm as the predominant rhythm (Figure 3-2A) with ECG complexes including clearly identifiable deflections as reported on earlier occasions (Mitchell et al., 1998) (Figure 3-1). Two mice, both aged *Pgc-1β*$^{-/-}$, showed multiple ectopic beats (Figure 3-2B) (Table 3-1). ST segment depression, defined in mice as the segment of the ECG signal representing ventricular repolarisation (Figure 1-5-A) having values abnormally depressed below the isoelectric baseline, was also analysed for. This initial analysis confirmed that ST segment changes that might signal acute ischaemic change never occurred prior to dobutamine challenge.

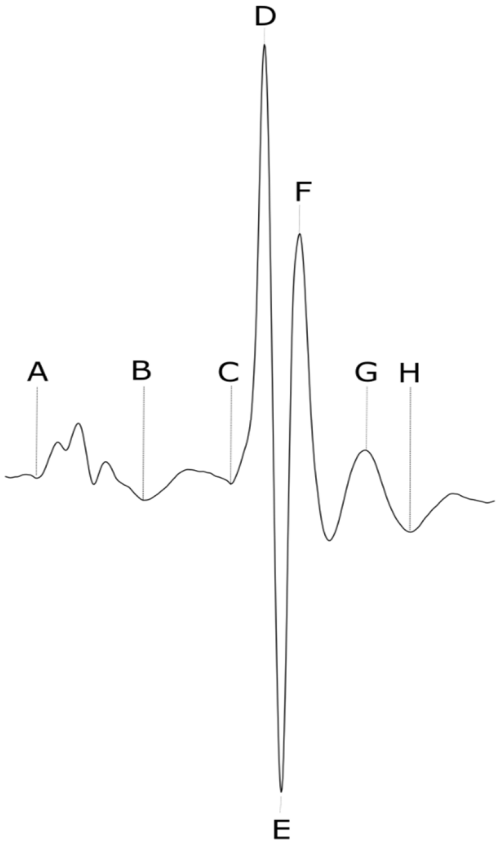

Figure 3-1: The murine ECG.

Typical ECG and definition of deflections used in quantitative analysis (A) start of P-wave; (B) End of P-wave; (C) Q wave/start of QRS complex; (D) R wave peak; (E) S wave; (F) peak of R' deflection; (G) C wave; (H) End of C wave. The corrected QT interval, QT_c is taken as the interval from C to H and corrected for RR intervals (Mitchell et al., 1998)

ST segment depression occurred in a small number of both WT and *Pgc-1β*$^{-/-}$ aged mice following such challenge (Figure 3-1D and 3-1E).

Table 3-1: *Incidence of particular electrocardiographic features in the experimental groups.*

		WT		*Pgc-1β*$^{-/-}$	
		Young	Aged	Young	Aged
(A)	Ischaemic change				
	Ischaemic changes present	0	2	0	2
	Ischaemic changes absent	5	6	9	4
(B)	Arrhythmic ECG patterns				
	Sinus Rhythm only	5	4	8	3
	Isorhythmic AV dissociation	0	4	1	3
	Ectopic beats	0	0	0	1

Electrocardiographic records obtained at baseline prior to pharmacological intervention in young WT (n = 5), aged WT (n = 8), young Pgc-1β$^{-/-}$ (n = 9) and aged Pgc-1β$^{-/-}$ (n = 6)

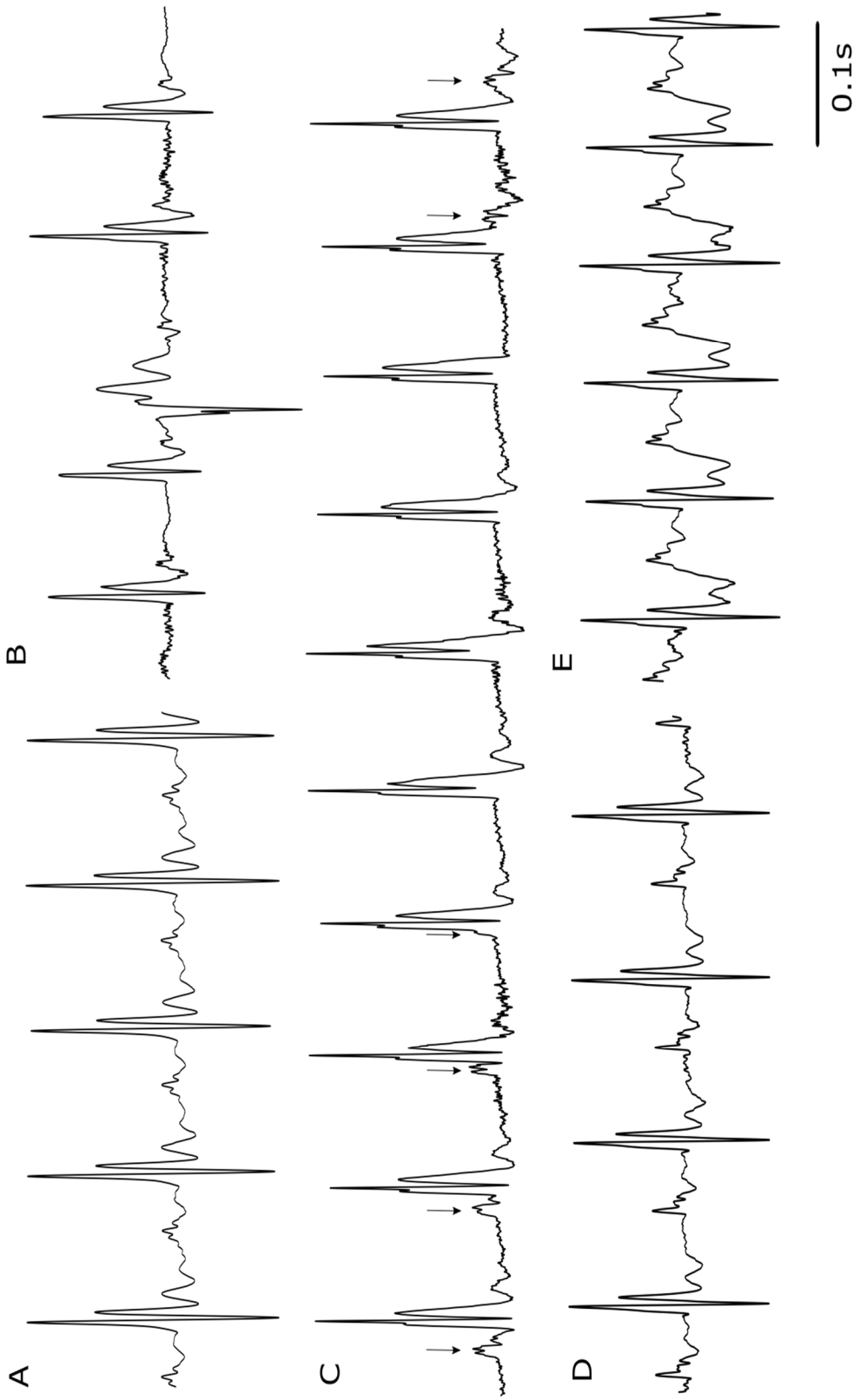

Figure 3-2: *Typical ECG records from Pgc-1β$^{-/-}$ hearts*

(A) normal sinus rhythm from a typical WT mouse; (B) ectopic beat; (C) atrioventricular (AV) dissociation; records obtained from the same mouse - arrows indicate timings of P-waves (D) pre-dobutamine and (E) following dobutamine challenge with ECG showing ST depression

3.2.1 PGC-1B$^{-/-}$ HEARTS DISPLAY IMPAIRED HEART RATE RESPONSES

Chronotropic incompetence is an established clinical feature of cardiac failure, although it can also occur in association with other cardiac pathology. It has been variably defined, but is commonly identified as a failure to reach an arbitrary percentage of the predicted maximum heart rate following sympathetic challenge, ranging from 70 – 85 % (Brubaker and Kitzman, 2011). A previous study had reported an impaired chronotropic response in isolated ex-vivo *Pgc-1β$^{-/-}$* hearts challenged with dobutamine. These findings had not been statistically significant at a 10 ng/kg/min infusion rate and depended on single heart rate recordings at each, predefined, time point (Lelliott et al., 2006). The present experiments systematically analysed steady-state parameters over 5-min recording periods before and following dobutamine challenge in intact animals.

Figure 3-3 shows typical heart rate profiles at baseline and in response to dobutamine for each experimental group. As there is no algorithm predicting normal murine heart rates at different ages as there is with humans, we assessed the chronotropic responses to dobutamine challenge using two different parameters: (1) peak heart rate attained after dobutamine administration and (2) mean heart rate observed post dobutamine administration. Figure 3-4 plots mean heart rates observed before dobutamine challenge against results obtained following dobutamine challenge for each individual animal. *Pgc-1β$^{-/-}$* animals displayed a tendency to slower basal heart rates under both conditions. A Pearson product-moment correlation coefficient assessing the co-variance between mean heart rates before and following dobutamine challenge demonstrated a positive association between variables, ($r=0.692$, $p < 0.0001$). Lower resting heart rates thus correlated with lower heart rates after dobutamine challenge. Further ANCOVA analysis yielded a significant association of the heart rate after dobutamine challenge with both the pre-dobutamine heart rate ($F = 33.4$, $p < 0.01$) and with the experimental group the animal came from, ($F = 4.34$, $p = 0.016$), suggesting that the relationship of heart rate to dobutamine exposure is significantly affected by genotype, with *Pgc-1β$^{-/-}$* mice have lower heart rates than their WT counterparts. However there were

no significant interacting effects of experimental group with the pre-dobutamine heart rate ($p = 0.36$).

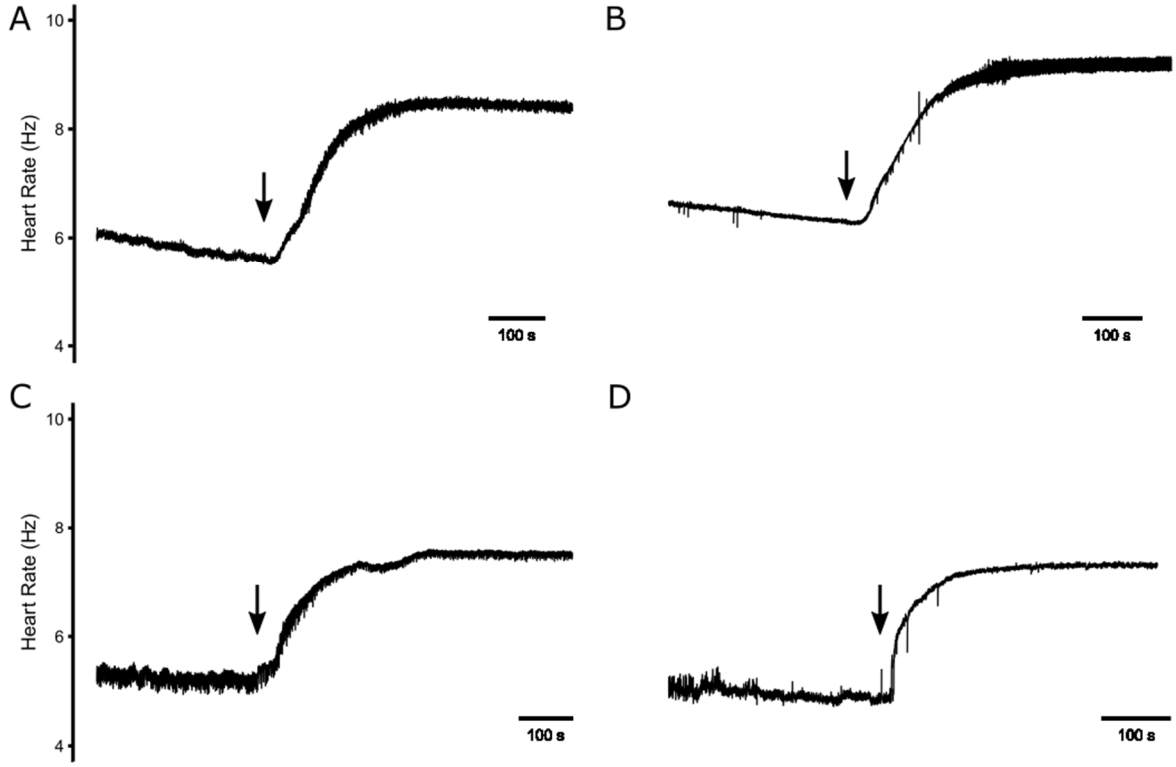

Figure 3-3: Heart rate response to dobutamine challenge. *Traces plotting heart rate response curves before and following dobutamine challenge in a (A) young WT, (B) aged WT; (C) young Pgc-1β$^{-/-}$ and (D) aged Pgc-1β$^{-/-}$ mouse*

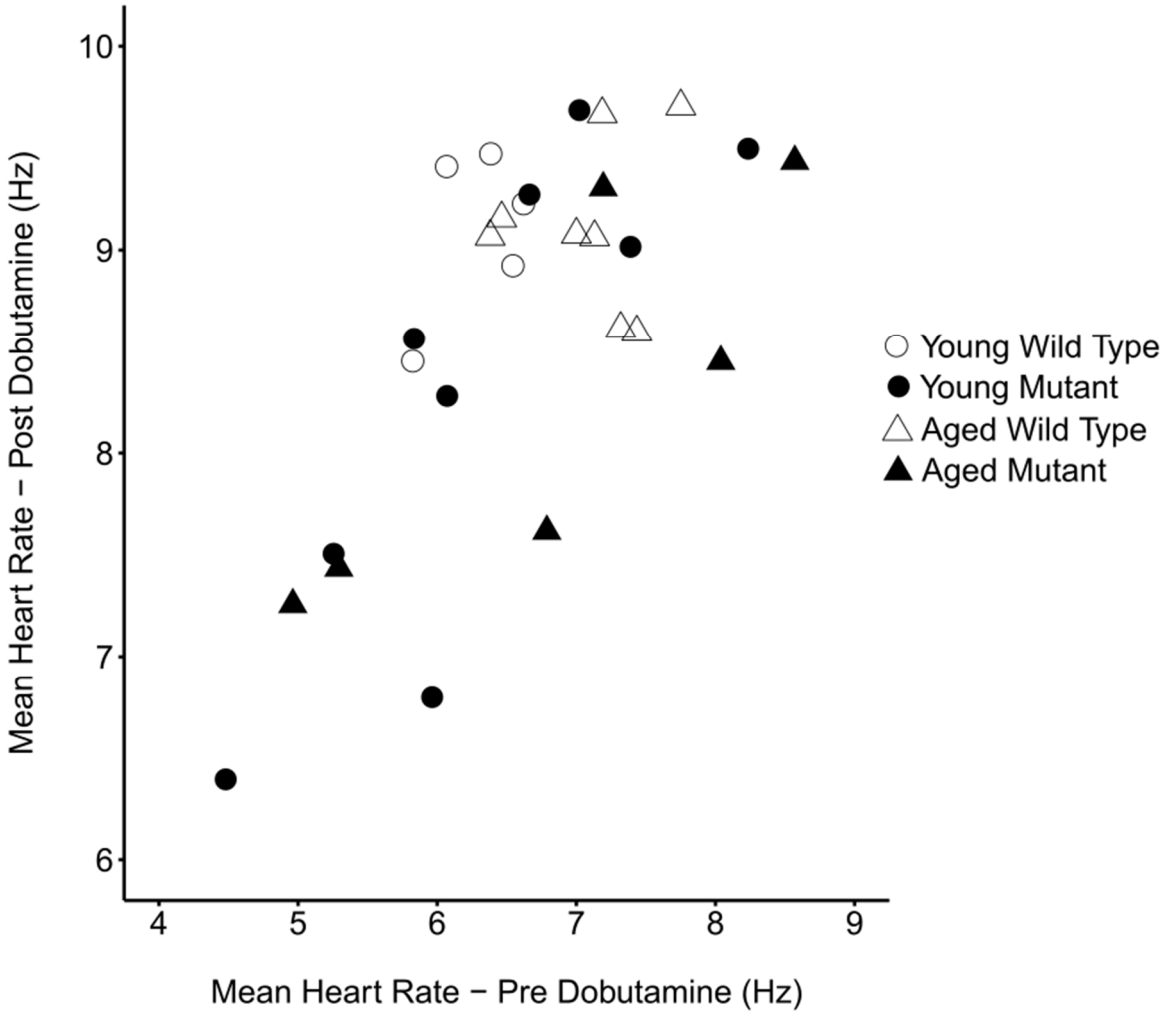

Figure 3-4: *Correlations between heart rates observed pre- vs post-dobutamine challenge in Pgc-1β$^{-/-}$ and WT hearts. Young WT (n = 5), aged WT (n = 8), young Pgc-1β$^{-/-}$ (n = 9) and aged Pgc-1β$^{-/-}$ (n = 6)*

MANOVA demonstrated significant effects of genotype (p = 0.022) and age (p = 0.048) on *steady state* heart rates. Post hoc Tukey tests demonstrated that genotype and age neither exerted independent nor interacting effects upon baseline steady state heart rates. In contrast, genotype exerted independent effects, with the *Pgc-1β$^{-/-}$* mutation reducing heart rates observed following dobutamine challenge (*Pgc-1β$^{-/-}$* 8.30 ± 0.28 Hz, n=15; WT: 9.11 ± 0.11 Hz, n = 13; p = 0.021) (Figure 3-5). In contrast, there were no significant effects of either

age or interactions between age and genotype. Similarly, ANOVA demonstrated independent significant effects of genotype (p = 0.011) but no significant effects of age or interactive effects between genotype and age on maximum heart rates attained after dobutamine challenge. Thus, post-hoc tests demonstrated lower peak heart rates in *Pgc-1β*$^{-/-}$ than WT mice (mean peak heart rate 8.47 ± 0.28 vs 9.53 ± 0.21 Hz, p = 0.0084, n = 13 vs 15 respectively).

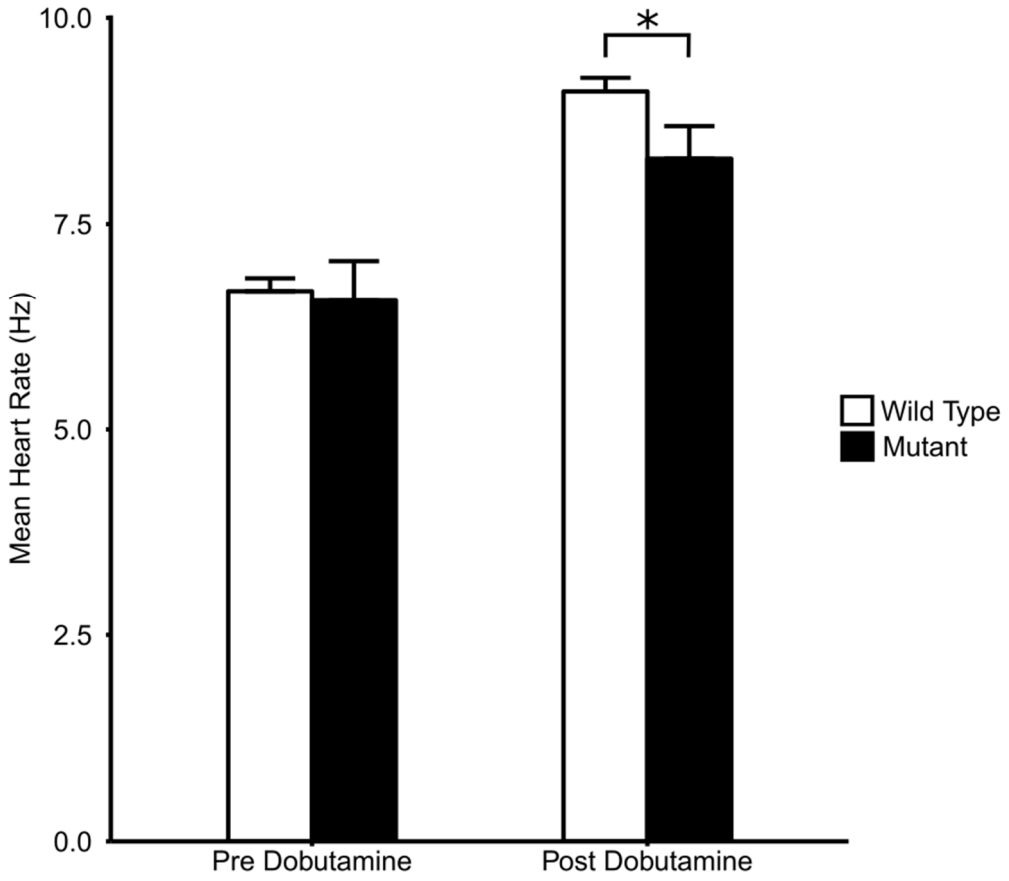

Figure 3-5: Mean steady state heart rates *in the 5 minute analysis window before and after dobutamine administration in WT (n = 13) and Pgc-1β*$^{-/-}$ *mice (n = 15). Asterix denotes a significant difference between the groups with ANOVA testing, p = 0.021.*

Heart rate variabilities, reflecting autonomic influences on the heart, are known to be related to adverse mortality risk, were expectedly altered within each experimental group following dobutamine challenge. However, the respective findings obtained before or following dobutamine did not vary between experimental groups. This was reflected in Poincare plots constructed for each mouse (Fig. 3-6A, B), exemplified in pre- (A) and post-dobutamine (B),

young (a,b) and aged (c,d), WT (a,c) and *Pgc-1β*$^{-/-}$ mice (b,d). The dispersion of these points was quantified by the standard deviation of the ΔRR interval before (Fig. 3-6C) and following dobutamine challenge (Fig. 3-6D).

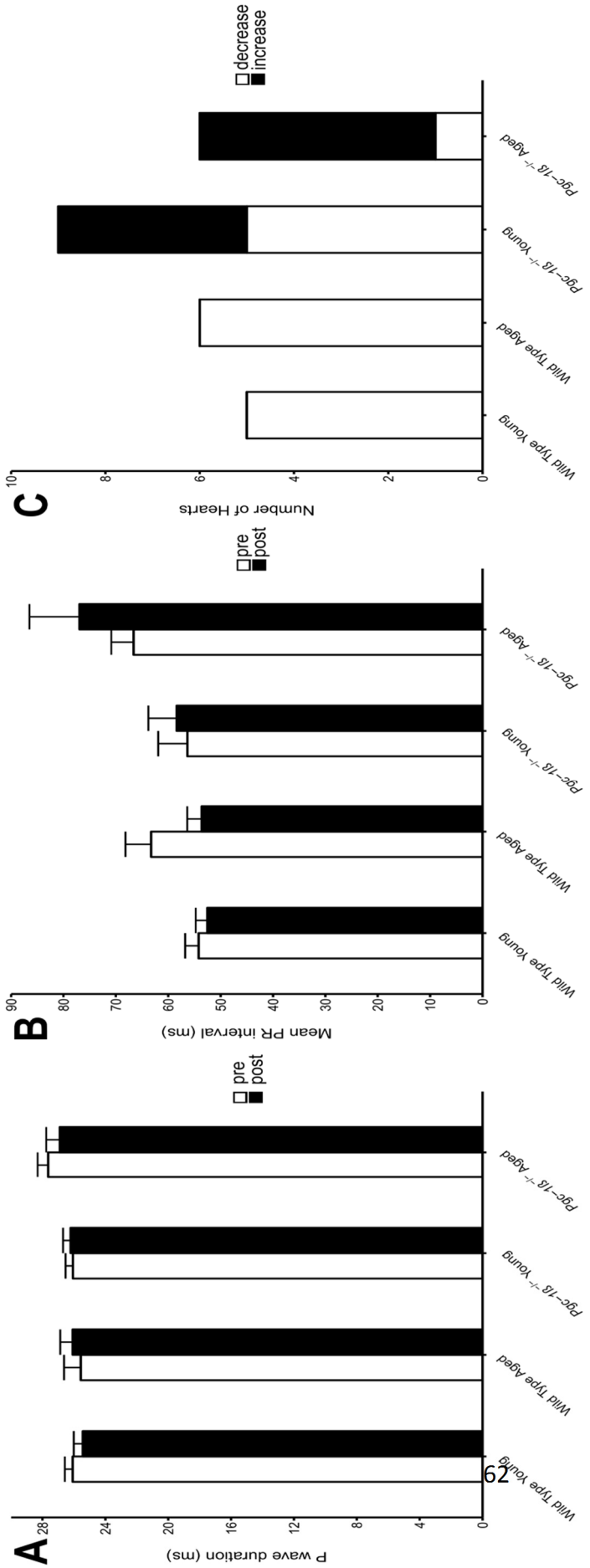

Figure 3-6: Sino-atrial and AV nodal electrocardiographic parameters.

Plots of P wave duration both pre (white bars) and post dobutamine (black bars) in the various experimental groups (A); mean PR interval pre (white bars) and post dobutamine (black bars) in the various experimental groups (B); and the number of hearts showing either an increase or decrease in PR interval after dobutamine administration dobutamine in the various experimental groups (C). There were no significant differences between groups by MANOVA analysis for P wave duration (A) or mean PR interval (B) (p = 0.39 and p = 0.47 respectively; young WT (n = 5), aged WT (n = 8), young Pgc-1β$^{-/-}$ (n = 9) and aged Pgc-1β$^{-/-}$ (n = 6))

ANOVA demonstrated no significant differences in such dispersions before or after dobutamine addition between different experimental groups. These results attribute the present findings to the existence of a sino-atrial node (SAN) defect as opposed to autonomic dysfunction in *Pgc-1β*$^{-/-}$ mice.

3.2.3 Age-related SA node disease in WT and Pgc-1β$^{-/-}$ murine hearts

Although sinus rhythm was the prevailing rhythm in all groups, both WT and *Pgc-1β*$^{-/-}$ mice demonstrated intermittent episodes of isorhythmic AV dissociation (Massumi and Ali, 1970) during the recording period. Isorhythmic AV dissociation is defined by a cardiac rhythm in which there is no fixed association between the P waves and the ventricular complex though each still occurs in a 1:1 ratio. These episodes predominantly occurred in aged animals, affecting 3/6 aged WT mice and 4/8 aged *Pgc-1β*$^{-/-}$ mice, but in only one young *Pgc-1β*$^{-/-}$ and none of the young WT mice (Table 3-1). They most frequently occurred immediately following dobutamine challenge, whilst RR intervals were decreasing from their baseline, pre-treatment values. During these episodes, RR intervals were shorter than their corresponding PP intervals, but the ventricular complexes remained identical to those observed during sinus rhythm. The latter suggests a supraventricular (likely junctional) pacemaker focus driving such activity (Figure 3-2C).

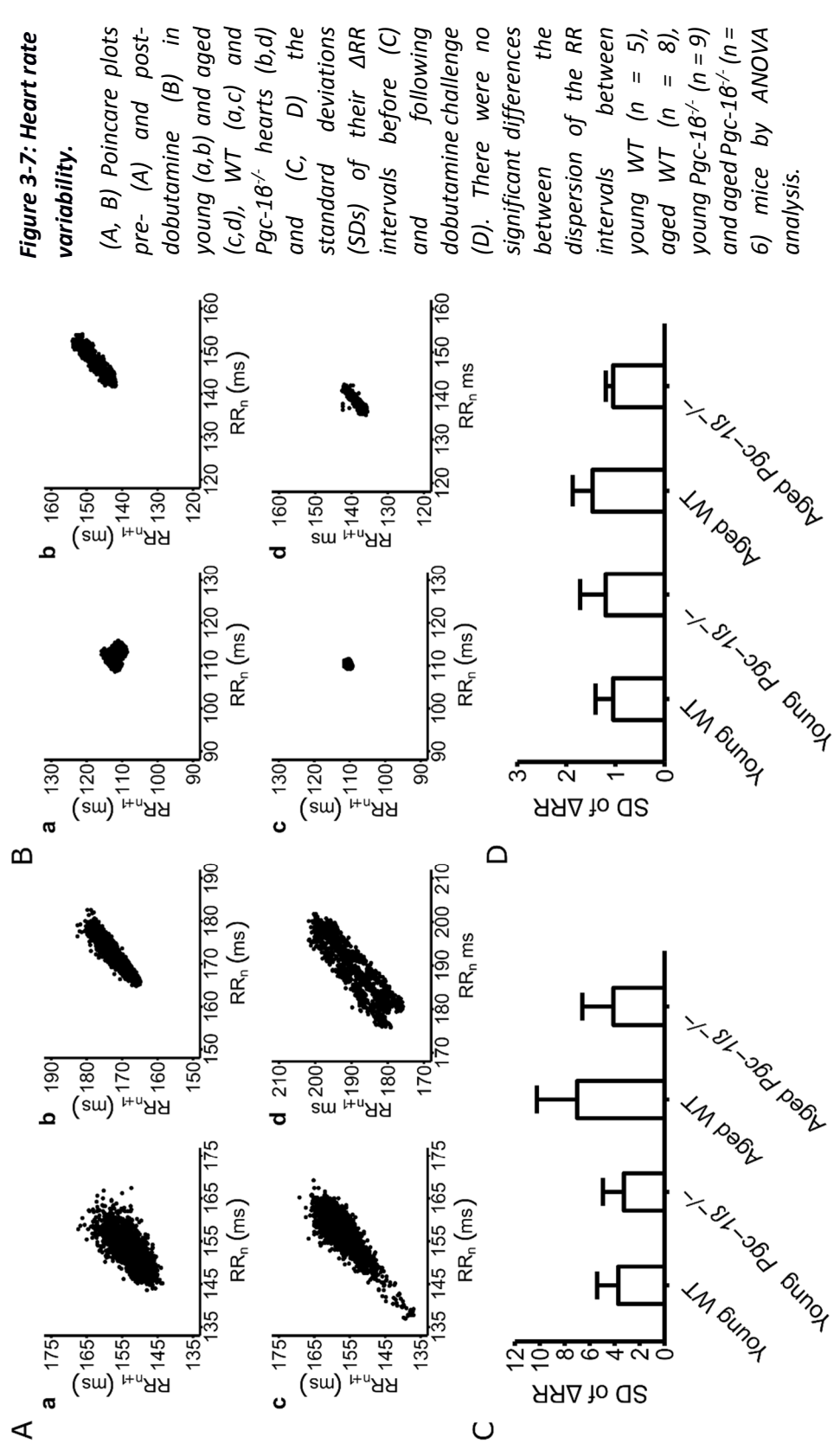

Figure 3-7: Heart rate variability.

(A, B) Poincare plots pre- (A) and post-dobutamine (B) in young (a,b) and aged (c,d), WT (a,c) and Pgc-1β$^{-/-}$ hearts (b,d) and (C, D) the standard deviations (SDs) of their ΔRR intervals before (C) and following dobutamine challenge (D). There were no significant differences between the dispersion of the RR intervals between young WT (n = 5), aged WT (n = 8), young Pgc-1β$^{-/-}$ (n = 9) and aged Pgc-1β$^{-/-}$ (n = 6) mice by ANOVA analysis.

3.2.4 PGC-1B-/- HEARTS DISPLAY PARADOXICAL ATRIOVENTRICULAR NODE FUNCTION

MANOVA analysis indicated that P-wave durations were not affected by either independent or interacting effects of age or genotype, whether before or following dobutamine challenge (Fig 3-2A). In contrast, two alteration patterns of altered PR interval reflecting atrioventricular node (AVN) function were observed with dobutamine administration. These took the form of either positive or negative dromotropic effects of dobutamine appearing as increases or decreases in PR interval (Figure 3-6C; Figure 3-8),

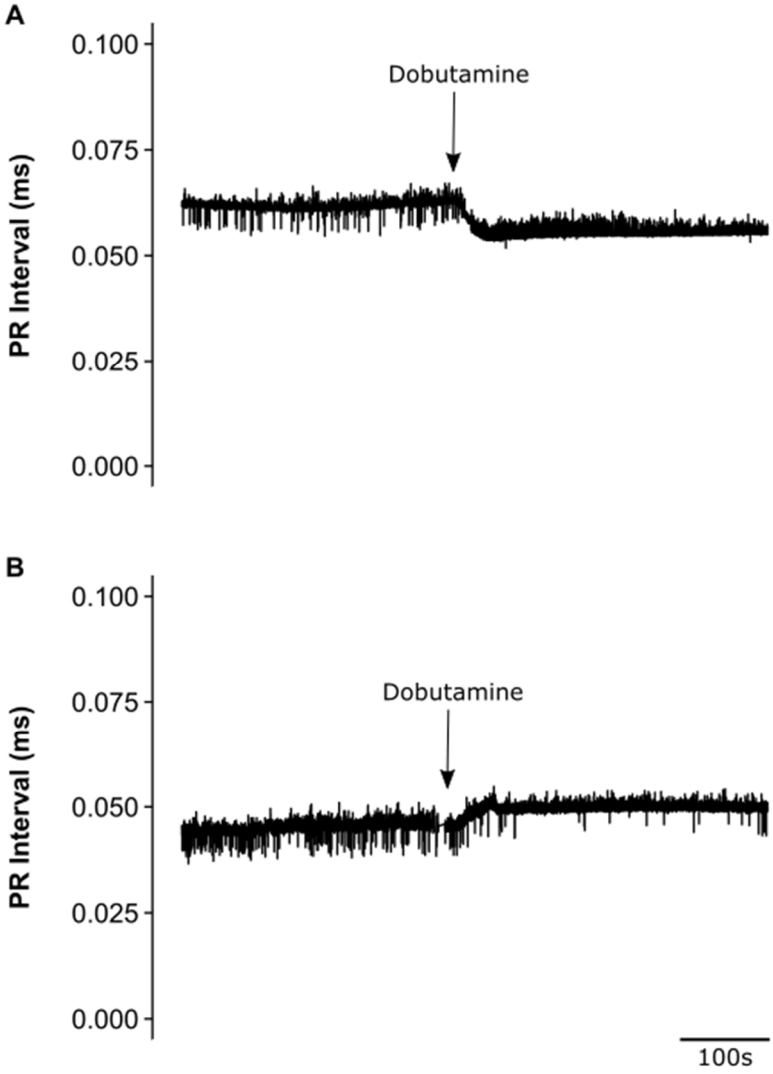

Figure 3-8: PR intervals *reflecting paradoxical AV dysfunction before and following dobutamine challenge in (A) young WT and (B) aged Pgc-1β-/- mouse*

taking place despite unchanged P-wave durations that were similar between experimental groups suggesting a continued normal atrial conduction (Figure 3-6A).

MANOVA indicated that neither age nor genotype affected PR interval whether before or following dobutamine challenge (Figure 3-6B). Nevertheless, the alteration in PR interval following dobutamine challenge demonstrated differing responses from WT and *Pgc-1β*$^{-/-}$ mice. All young (5 of 5) and aged (6 of 6) WT mice showed decreased PR intervals following dobutamine challenge. In contrast, the PR interval decreased in 5 of 9 and increased in the remaining four young *Pgc-1β*$^{-/-}$ mice. In aged *Pgc-1β*$^{-/-}$ mice the result was even more marked with only one mouse showing the expected positive dromotropic effect with dobutamine administration and 5 of 6 mice showing a paradoxical negative dromotropic effect in response to dobutamine. In addition to the SAN dysfunction seen with the *Pgc-1β* knockout there was compromised AVN conduction in a subset of mutant hearts, an effect exacerbated by increasing age.

The presence of AVN dysfunction in mutant mice which also demonstrated impaired heart rate responses led us to examine whether paradoxical AV node dysfunction underlies or is associated with the blunted chronotropic responses. Such a comparison demonstrated that *Pgc-1β*$^{-/-}$ animals with a normal AVN response showed a mean heart rate of 9.10 ± 0.22 Hz (n = 6) following dobutamine challenge. In contrast, *Pgc-1β*$^{-/-}$ animals with a paradoxical AVN response to dobutamine showed a heart rate of 7.77 ± 0.34 Hz (n = 9). A two-tailed student t test confirmed that the difference was significant (p = 0.0061). Thus these findings suggest that the *Pgc-1β*$^{-/-}$ mutation is associated only with significantly altered AV nodal function in a subset of mutant mice, and that the presence of AV nodal dysfunction itself may be a marker for impaired heart rate responses.

3.2.5 Aged Pgc-1β$^{-/-}$ *hearts display slowed ventricular activation*

Ventricular activation is a synchronised, sequential process, whose onset is easily detected as the beginning of the Q wave deflection (Figure 3-1). Ventricular recovery is considered to

begin at a timepoint between the S wave trough, and the beginning of the R' peak. Examination of three independent ECG indicators, of QR, QS and QR' durations, of ventricular activation, suggested interacting effects of age and genotype upon its duration (Figure 3-9).

MANOVA demonstrated that genotype and age, whilst not exerting independent effects, showed interacting effects upon all the three parameters of QR ($p = 0.032$), QS ($p = 0.040$) and QR' duration ($p = 0.039$). This was also the case with QR, QS, but not QR' (QR: $p = 0.029$; QS: $p = 0.029$; QR': $p = 0.086$) prior to dobutamine challenge and with all three parameters following (QR: $p = 0.016$; QS: $p = 0.022$; QR': $p = 0.026$) dobutamine challenge. Post hoc Tukey tests then demonstrated that prior to dobutamine administration, QR durations were longer in aged *Pgc-1β*$^{-/-}$ than aged WT ($p = 0.030$), with indications of such differences in aged compared to young *Pgc-1β*$^{-/-}$ mice ($p = 0.059$). QS intervals were longer in aged *Pgc-1β*$^{-/-}$ than either young *Pgc-1β*$^{-/-}$ ($p = 0.040$) or aged WT mice ($p = 0.024$). Following dobutamine administration, QR durations were longer in aged *Pgc-1β*$^{-/-}$ than either aged WT ($p = 0.035$) or young *Pgc-1β*$^{-/-}$ ($p = 0.030$). QS durations were longer in aged *Pgc-1β*$^{-/-}$ than either young *Pgc-1β*$^{-/-}$ ($p = 0.035$) or aged WT mice ($p = 0.026$). QR' durations were longer in aged *Pgc-1β*$^{-/-}$ mice than either aged WT ($p = 0.039$) or young *Pgc-1β*$^{-/-}$ mice ($p = 0.017$).

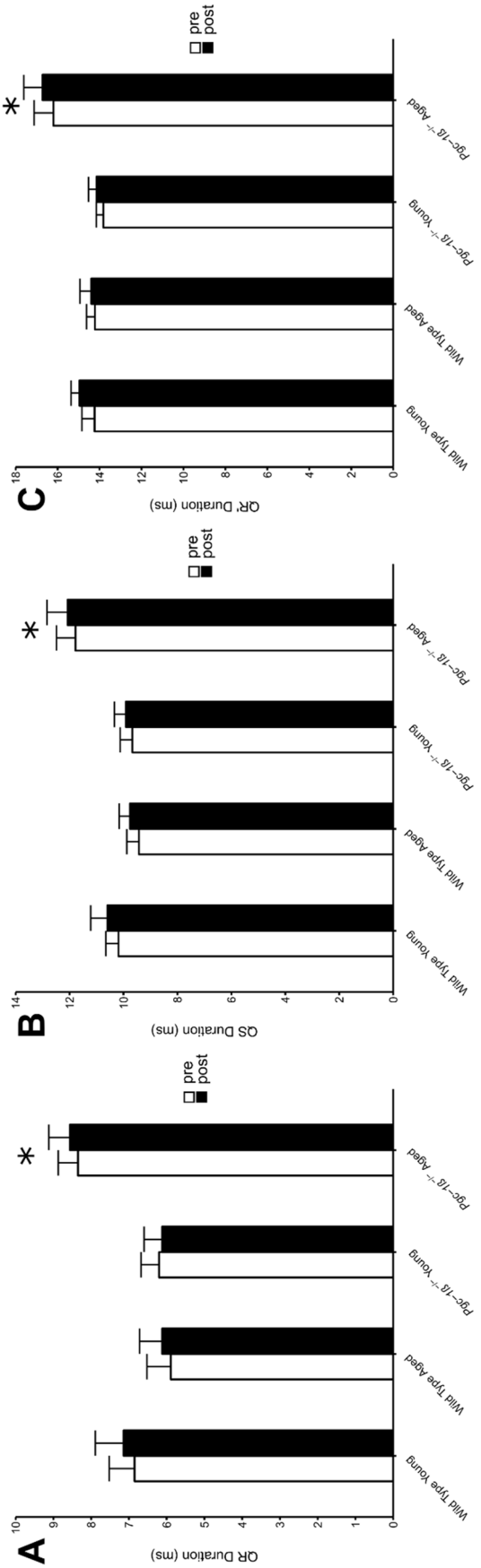

Figure 3-9: Electrocardiographic ventricular activation

Plots of QR interval both pre (white bars) and post dobutamine (black bars) in the various experimental groups (A); Plots of QS interval pre (white bars) and post dobutamine (black bars) in the various experimental groups (B); Plots of QR' interval pre (white bars) and post dobutamine (black bars) in the various experimental groups. The asterix (*) symbol denotes that there is a significant difference between the asterixed groups by MANOVA, post hoc ANOVA and tukey HSD testing ($p < 0.05$). QR and QS durations in aged Pgc-1β$^{-/-}$ mice were significantly different before dobutamine exposure ($p = 0.029$, $p = 0.029$ respectively; $n = 6$) compared to young WT ($n = 5$), aged WT ($n = 8$) and young Pgc-1β$^{-/-}$ ($n = 9$) mice. QR, QS and QR' durations were significantly different in aged Pgc-1β$^{-/-}$ mice ($p = 0.016$, $p = 0.022$, $p = 0.026$ respectively; $n = 6$) post dobutamine challenge compared to young WT ($n = 5$), aged WT ($n = 8$) and young Pgc-1β$^{-/-}$ ($n = 9$) mice.

3.2.6 PGC-1B-/- HEARTS SHOW SHORTENED VENTRICULAR RECOVERY TIMES AFTER ADRENERGIC CHALLENGE

Age and genotype exerted contrasting effects on ventricular recovery times. Genotype affected all three measures of recovery (RT_c, $R'T_c$ and ST_c durations; p = 0.0098, p = 0.0014 and p = 0.0029 respectively) (Figure 3-10). In contrast, age did not significantly affect any of these recovery parameters, nor were there any interactive effects of age and genotype. Post hoc testing showed that (for all parameters) the difference lay in findings obtained post dobutamine challenge; there were no differences due to age, genotype or their interaction prior to dobutamine administration. Following dobutamine administration all three parameters showed a marked effect of genotype (p = 0.015, p = 0.021 and p = 0.0067 respectively) but no other effects. Post hoc Tukey tests showed that *Pgc-1β-/-* showed significantly shorter RT_c, $R'T_c$ and ST_c intervals than WT mice (p = 0.0053, p = 0.018 and p = 0.0080 respectively). Thus, all three recovery parameters were highly concordant confirming that the *Pgc-1β* ablation significantly shortened ventricular recovery parameters (Figure 3-10).

3.2.7 EMERGENCE OF A SHORT-QT PHENOTYPE IN PGC-1B-/- ANIMALS

The QT_c interval (QT interval corrected for RR interval) has traditionally been used as a marker for repolarisation abnormalities in that the electrocardiographic phenotype is usually caused by a defect in ventricular recovery. However, it is more accurate to describe the QT_c interval as a parameter that describes the combined durations of both activation and recovery i.e. the duration of ventricular excitation. The onset of ventricular activation is represented by the Q wave deflection; the C wave trough was taken to represent the end of ventricular recovery and hence used for calculation of the QT interval in the present study (Figure 3-1). Genotype, but neither age (p= 0.083) nor interactions between age and genotype (p = 0.075), significantly affected QT_c interval (p = 0.0071) (Figure 3-11). ANOVA indicated no differences between groups at baseline. Following dobutamine challenge, genotype (p = 0.032), but not age affected QT_c interval. Post hoc Tukey HSD tests revealed that, following dobutamine

administration, young *Pgc-1β*$^{-/-}$ had shorter QT_c intervals than both young WT ($p = 0.026$) and aged WT mice ($p = 0.041$). There was also a trend towards young *Pgc-1β*$^{-/-}$ mice having shorter QT_c intervals than aged *Pgc-1β*$^{-/-}$ mice ($p = 0.094$). Thus, *Pgc-1β*$^{-/-}$ mice had shorter QT_c intervals than their WT counterparts with most of the effect arising from shortening of the QT_c intervals in young *Pgc-1β* $^{-/-}$ mice.

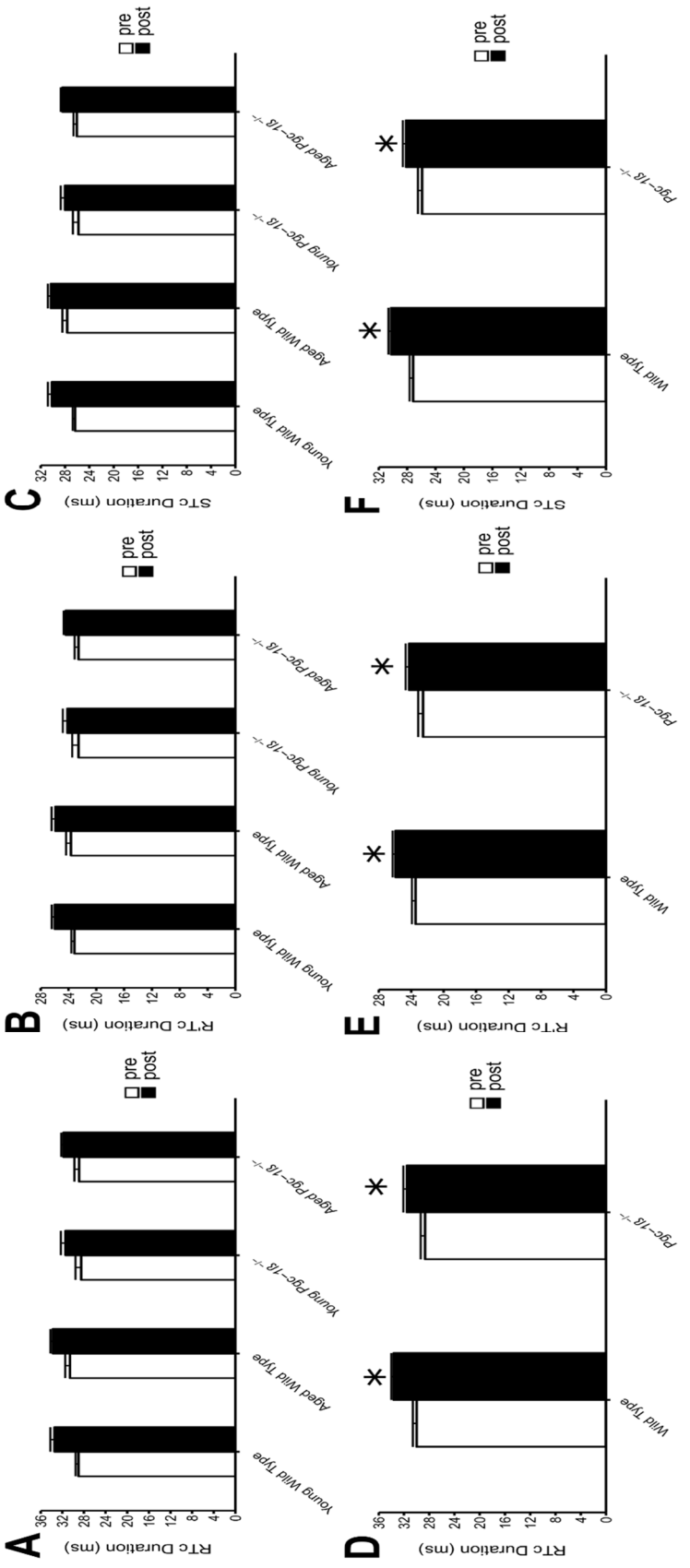

Figure 3-10: Electrocardiographic ventricular recovery intervals

Electrocardiographic measurements made of RT_c durations in both pre (white bars) and post dobutamine (black bars), panel (A), $R'T_c$ durations both pre (white bars) and post dobutamine (black bars) in panel (B) and ST_c durations before and following dobutamine challenge panel (C) in young WT (n = 5), aged WT (n = 8), young Pgc-1β$^{-/-}$ (n = 8) and aged Pgc-1β$^{-/-}$ (n = 5) mice. One young and one aged Pgc-1β$^{-/-}$ mouse were excluded as these showed paradoxical dromotropic effects that lead to prolonged PR intervals and P waves that interfered with determinations of the end ventricular recovery to give the following n values stated. Panel (C), (D) and (E) display the RTc, R'Tc and STc intervals grouped by genotype (WT (n = 13), Pgc-1β$^{-/-}$ (n= 13)). The asterix (*) symbol denotes that there is a significant difference between the paired asterixed groups by MANOVA analysis, followed by post hoc tukey HSD testing ($p < 0.05$)

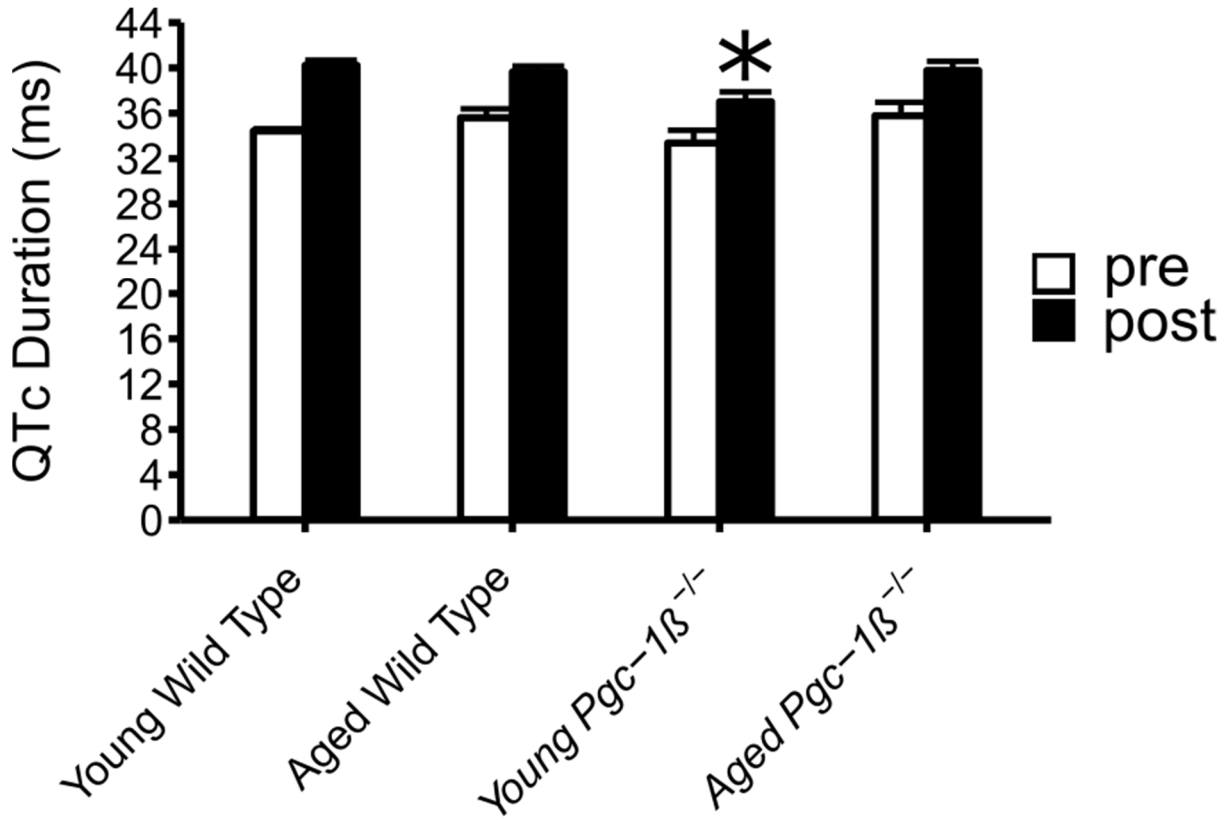

Figure 3-11: Electrocardiographic measurement of QTc durations

Electrographic measurements made of QT_c durations before and following dobutamine challenge in young WT (n = 5), aged WT (n = 8), young Pgc-1β$^{-/-}$ (n = 8) and aged Pgc-1β$^{-/-}$ (n = 5) mice. One young and one aged Pgc-1β$^{-/-}$ mouse were excluded as these showed paradoxical dromotropic effects that lead to prolonged PR intervals and P waves that interfered with determinations of the end ventricular recovery to give the following n values stated. The asterix denotes a significant difference (p < 0.05) between young Pgc-1β$^{-/-}$ post dobutamine and young and aged WT mice in post hoc tukey HSD analysis. Please see text for detailed statistical breakdown.

3.3 DISCUSSION

The ECG yields much prescient and strategic clinical electrophysiological information as a primary investigational tool. Its experimental application has demonstrated valuable insights into electrophysiological abnormalities in murine hearts modelling clinical arrhythmic conditions. Cellular energetic dysfunction following metabolic disturbances is increasingly recognised as an important factor in the aetiology of such atrial and ventricular arrhythmias. Destabilisation of inner mitochondrial membrane potentials results in approximately 10-fold increases in reactive oxygen species production (Liu et al., 2010 a), in turn affecting maximum Na^+ (Liu et al., 2010 a) and K^+ current (Wang et al., 2004), sarcolemmal K_{ATP} channel function, Na^+ and L-type Ca^{2+} channel inactivation kinetics and late Na^+ current. They also affect ryanodine receptor function which in turn affects surface membrane excitability and intracellular Ca^{2+} homeostasis (Terentyev et al., 2008; Brown and O'Rourke, 2010; Bovo et al., 2012). Mitochondria are also the main cardiomyocyte ATP source and ATP/ADP depletion increases sarcolemmal ATP-sensitive K^+ channel ($sarcK_{ATP}$) open probabilities affecting action potential duration (APD), effective refractory period (ERP) and heterogenous current sinks potentially causing current-load mismatch (Akar and O'Rourke, 2011). These cellular mechanisms could in turn potentially give rise to potentially pro-arrhythmic effects on cell-cell coupling (Smyth et al., 2010), AP conduction (Liu et al., 2010 a) and AP repolarisation (Wang et al., 2004). There may also be an appearance of alternans and Ca^{2+} mediated triggering phenomena (Terentyev et al., 2008). The *Pgc-1β*$^{-/-}$ genetic modification has thus been associated with altered ion channel function and ventricular arrhythmias in Langendorff-perfused heart preparations (Gurung et al., 2011 b).

ECG alterations accompanying the associated mitochondrial dysfunction were therefore investigated in intact anaesthetised *Pgc-1β*$^{-/-}$ mice murine hearts lacking the transcriptional coactivator PGC-1β. The present study yielded electrophysiological features associated with *Pgc-1β* ablation in the in vivo system with intact autonomic innervation and normal cardiac mechanical function, building upon earlier reports from the cellular studies (Gurung et al.,

2011 b) and ex-vivo hearts (Lelliott et al., 2006). The pharmacological manoeuvres involving dobutamine challenge in the latter studies would largely involve β1-adrenergic receptor activity, whereas the present in vivo studies could potentially further involve β2-adrenergic receptor mediated extracardiac changes, which in the clinical setting are also known to influence arrhythmic risk.

The present experiments characterised the intervals separating specific ECG waveform components more closely than did previous studies. Quantitative statistical analysis of these steady state parameters then employed two way factorial MANOVA testing for interacting and non-interacting effects of age and genotype before and after dobutamine challenge. The presence of significant differences then prompted further, two way factorial ANOVA to ascertain whether the difference occurred before or following dobutamine application. Finally, appropriate Tukey HSD tests assessed for particular differences between individual parameters. Peak heart rates following dobutamine challenge were analysed by themselves by a two way factorial ANOVA followed by post hoc Tukey tests.

The ECG analysis demonstrated a range of age-dependent abnormalities associated with the *Pgc-1β*$^{-/-}$ genotype. The predominant ECG pattern in both young and aged, WT and *Pgc-1β*$^{-/-}$ mice was one of sinus rhythm. Any ischaemic ECG changes observed were associated with age but were not specific to *Pgc-1β*$^{-/-}$ or WT genotypes, suggesting that there was no underlying difference in vascular (as opposed to primary cardiomyocyte) function between the two groups. However, we demonstrated for the first time blunted chronotropic responses to dobutamine challenge in an intact *Pgc-1β*$^{-/-}$ mammalian system despite heart rate variabilities suggesting unchanged autonomic backgrounds. Previous reports had hinted at compromised heart rate responses in ex-vivo Langendorff perfused *Pgc-1β*$^{-/-}$ hearts following dobutamine challenge (Lelliott et al., 2006). These results together suggest that the impaired heart rate response of *Pgc-1β*$^{-/-}$ hearts does not reflect generalised autonomic dysfunction but rather alterations in the intrinsic myocardial response to dobutamine. Ageing did not affect this chronotropic response, implicating the mutation as opposed to background deterioration of maximal heart rate with age.

Aged mice, independent of genotype, also showed episodes of isorhythmic AV dissociation with dobutamine challenge. During these episodes regular ventricular responses were seen, with normal, narrow QRS complexes despite the absence of a fixed PR interval, even when P wave complexes were buried within the ventricular signal. These findings suggest that the murine SAN is vulnerable to degenerative changes with age, with appearances of supraventricular, most likely junctional, pacemaker foci intermittently dictating the ventricular rate. The anatomical level of block that produce the AVN abnormalities seen could theoretically be at the level of the AVN, intra-hisian (within the his-purkinje system), or infra-hisian (distal to the his-purkinje AVN system). A narrow ventricular complex is most compatible with an AV nodal or intra-His problem, though a wide QRS complex certainly may occur with A-V nodal or intra-His disease in the presence of coexistent bundle branch block or conduction delay. Thus the only way to delineate the level of block is through an intracardiac multielectrode recording from the SAN, AVN and infra-hisian cardiac sites so that the level of block can be determined. This represents a limitation of the current analysis as though a relatively narrow complex QRS with a lengthened AV delay is suggestive but not diagnostic of an intranodal pathology.

Pgc-1β$^{-/-}$ ablation also appeared to cause a more generalised defect also affecting the AVN. A significant proportion of *Pgc-1β*$^{-/-}$, particularly aged, mutants, demonstrated an abnormal negatively dromotropic response to dobutamine challenge, suggesting progressive deterioration in AVN function in *Pgc-1β*$^{-/-}$ hearts with age. Furthermore, mice showing this abnormal AVN function showed more pronounced blunting in their chronotropic response to dobutamine, relating an AVN dysfunction to the chronotropic deficit observed here.

Pathological bradycardic rhythms secondary to cardiac conduction system disease are known to occur with ageing, often necessitating permanent pacemaker implantation. Progressive fibrotic change is a recognised feature of cardiac ageing in both animal (Jeevaratnam et al., 2012, 2016) and human studies (Gazoti Debessa et al., 2001). Fibrotic change could directly

disrupt gap junction function, increasing tissue resistance (Xie et al., 2009), or increase fibroblast-cardiomyocyte coupling, increasing effective membrane capacitance (Chilton et al., 2007). More recent studies indeed implicate abnormal gap junction function in both SAN and AVN disease (Jones et al., 2004; Nisbet et al., 2016). Interestingly, oxidative stress, associated with mitochondrial impairment increases transforming growth factor (TGF)-β activity (Sullivan et al., 2008 a), in turn implicated in such age-related myocardial fibrosis (Davies et al., 2014). Conversely augmented mitochondrial anti-oxidant capacity protects against features of cardiac ageing including fibrotic change (Dai et al., 2009). Mitochondrial dysfunction could also impair gap junction function through elevating intracellular [Ca^{2+}] or altering connexin phosphorylation through oxidative stress (Sovari et al., 2013). Finally, the range of ionic currents including RyR2 channel function (Bhuiyan et al., 2007) involved in SAN and AVN activity, are potentially modifiable by mitochondrial dysfunction. Isolated cardiomyocytes from *Pgc-1β*$^{-/-}$ hearts have previously been reported to display altered diastolic Ca^{2+} transients in keeping with abnormal *RyR2* function (Gurung et al., 2011 b).

ECG deflections related to ventricular activation and recovery confirmed previous reports that murine ECGs lack well-defined ST segments (Danik et al., 2002; Zhang et al., 2014). The murine ECG shows an R' wave deflection not seen in the human ECG. This is followed by a further but variably reported deflection which has not been systematically identified or formally correlated with particular action potential components. This variability may be attributed to the greater rostro-caudal anatomical alignment of the mouse heart in the thoracic cavity and variations in limb positioning during experimental recording between reports, with consequent variations in the effective positioning of the centre of the Einthoven triangle relative to the heart. Thus, although we also identified C waves, small changes in lead positioning could lead to its apparent disappearance in one or both ECG leads. This may account for the controversy concerning its inconsistent appearance (Danik et al., 2002).

The onset of ventricular recovery in the murine ECG has been considered to occur from time points ranging from the S wave nadir to the R' peak. A number of authors have suggested that the late component of the R' wave or the R' wave in totality is in fact part of ventricular

repolarisation (Goldbarg et al., 1968; Boukens et al., 2014; Zhang et al., 2014). Others suggested that inclusion of the R' wave may lead to systematic overestimation of ventricular activation, while its exclusion in genetically modified mouse models, such as that of the Brugada syndrome, which displays slowed conduction, may lead to underestimation of ventricular activation times (Boukens et al., 2014).

We accordingly explored a set of related recovery parameters that utilised both the S wave nadir and peak of the R' wave as cut-off separating ventricular activation and recovery phases. Each parameter is likely to capture activation and recovery in different areas of myocardium, reflecting the non-simultaneous nature of electrical activity in the myocardium. This increased the robustness of our analysis and permitted us to assess the possibility of early repolarisation in our genetic model. The statistical analysis of the different parameters of recovery and activation were highly concordant. *Pgc-1β*$^{-/-}$ hearts showed a prolongation of all such measures of ventricular activation with age whether before or following adrenergic stress, in an absence of independent effects of age or genotype. These findings parallel the reduced conduction velocities reported in other arrhythmic genetic models. These had accompanied either fibrotic change or reduced Na^+ currents resulting from Nav1.5 deficiency in *Scn5a*$^{+/-}$ (Jeevaratnam et al., 2011, 2012, 2016) and *Scn5a*$^{+/\Delta KPQ}$ (Wu et al., 2012), or secondary to Ca^{2+} handling abnormalities in *RyR2-P2328S* hearts (King et al., 2013 b; Zhang et al., 2014; Ning et al., 2016 a). These findings are also compatible with reports that mitochondrial abnormalities could alter I_K and therefore result in current-load mismatch (Akar and O'Rourke, 2011; Kabunga et al., 2015).

Pgc-1β$^{-/-}$ hearts also showed shorter recovery parameters than WT after dobutamine administration, without effects of age whether acting independently or interacting with genotype. Such shortened repolarisation intervals have also been implicated in arrhythmic risk. Human short QT syndrome is diagnosed using the J point to T peak interval that may represent the interval between the end of the ventricular complex to the peak of the repolarisation wave (Gollob et al., 2011). Short QT syndrome has been traced to HERG and other K^+ channel mutations and more recently, Ca^{2+} channel function (Antzelevitch et al.,

2007). The present findings are thus consistent with alterations in K^+ conductance properties or Ca^{2+} handling properties in the *Pgc-1β*$^{-/-}$ system that would also modify current-load matching (Gurung et al., 2011 a). These changes appeared to result in shortened QT_c intervals for mutant mice with adrenergic stress. Although the mechanisms underlying these changes remain unclear, increased expression of *Kcna5* was reported in the latter study and may contribute to the increased K^+ conductance. Additionally, the opening and K^+ conductance of the sarcK_{ATP} is linked to rising cellular ADP levels, therefore correlating its activity to cellular metabolic status. Its activity is known to reduce the action potential duration and is thought to contribute to increased arrhythmic risk (Billman, 2008). Oxidative stress is also known to enhance sarcK_{ATP} activity; however the cellular mechanism are yet to be established but may occur through depletion of cellular ATP. Nevertheless, the effects of ROS upon sarcK_{ATP} activity could be attenuated through inhibition of protein kinase C, protein kinase G and calcium-calmodulin kinase II but not protein kinase A, providing some insights into the pathways involved (Yan et al., 2009).

Finally, these findings prompted us to measure QT_c intervals reflecting the total activation times of the ventricular myocardium. *Pgc-1β*$^{-/-}$ mice showed shorter QT_c intervals than their WT counterparts. The majority of this effect seemed to be due to young mutant mice, though this was not significant. This is in contrast to the shortened repolarisation parameters in both young and aged *Pgc-1β*$^{-/-}$. This likely reflects the additional, prolonged, depolarisation parameters in aged *Pgc-1β*$^{-/-}$ mice, offsetting to some degree the shortening in the repolarisation parameters.

The experiments presented here utilise sample sizes that could be criticised for being too small; however, they are consistent with the sample sizes in previous ECG studies of murine models (Salama and London, 2007; Jeevaratnam et al., 2010; Boukens et al., 2014; Chadda et al., 2017), and were constructed to be adequately powered to detect differences of the order of magnitude seen in previous studies of genetically modified mice. The limited exploration of the murine ECG and its analysis in previous studies also limits the interpretation of the findings in this study - there is an absence of accepted 'normal' or physiological values for the

majority of ECG parameters and intervals measured. Thus while the statistical methods presented can gauge differences between groups, it is not possible at this time to comment on many if not all of the absolute values of the intervals found and whether these are concordant with expected WT values or not.

The use of volatile anaesthetic compounds for the study also presents another limitation – it is known that many volatile anaesthetic affect the murine ECG and alter ventricular recovery parameters, in particular the QT_c (Loushin, 2005). However, the study employed a standardised protocol for anaesthesia and assessing the depth of anaesthesia to ensure this affect was present across all experimental groups equally as much as was feasible. It is not however known if volatile anaesthetics would differentially affect ECG parameters in mitochondrial dysfunction; this empirically seems unlikely though cannot be absolutely ruled out. The choice of anaesthetic, avertin, was also deliberate as it is known to be among the anaesthetic agents with the least cardiovascular and in particular electrophysiological effects (Hart et al., 2001; Pachon et al., 2015).

An alternative technique using telemetry with surgical implantation of ECG telemetry could be used and would avoid the known cardiac effects of volatile anaesthetics. However telemetry has its own drawbacks including lower sampling rates, increased noise (which is particularly important for the P wave features which have a low signal to noise ratio) and being unable to control for activity levels of a mouse which may lead to rapid changes in heart rates and ECG intervals making analysis problematic.

With these considerations in mind, the conclusions of this section of the study point to a range of electrocardiographic abnormalities associated with the *Pgc-1β*$^{-/-}$ genotype and those features particularly vulnerable to advanced age. Thus, *Pgc-1β*$^{-/-}$ mice show reduced sino-atrial response to dobutamine, paradoxical atrioventricular nodal function increasing in prevalence with age, slowed ventricular activation with ageing and shortened recovery parameters after dobutamine challenge.

4. VENTRICULAR PRO-ARRHYTHMIC PHENOTYPE, ARRHYTHMIC SUBSTRATE AND AGEING IN *Pgc-1β*$^{-/-}$ HEARTS

4.1 Introduction

The previous chapter explored the ECG changes associated with chronic mitochondrial dysfunction in the *Pgc-1β*$^{-/-}$ model. However, relatively few studies have investigated the electrophysiological consequences of the cellular changes of mitochondrial dysfunction and their implications for arrhythmic triggering or arrhythmic substrate at the level of *intact Pgc-1β*$^{-/-}$ hearts.

The present experiments characterize the electrophysiological changes underlying arrhythmic substrates and how these progress with age in *Pgc-1β*$^{-/-}$ hearts modelling chronic mitochondrial dysfunction. They compared four groups of intact, young and aged, wild type (WT) and genetically modified, Langendorff-perfused *Pgc-1β*$^{-/-}$ hearts. Triggering events provoking arrhythmia in the presence of substrate were mimicked by S2 stimuli interposed at differing intervals following regular S1 pacing trains similar to protocols established on earlier occasions (Thomas et al., 2007 a, 2008). Direct intracellular determinations of resting membrane potentials (RMPs), AP amplitudes and latencies, and maximum rates of AP depolarization, $(dV/dt)_{max,}$ in cardiomyocytes in situ ensured unperturbed intracellular conditions, particularly of Ca^{2+} homeostasis. *Pgc-1β*$^{-/-}$ as opposed to WT genotypes were implicated in decreased $(dV/dt)_{max}$ and increased AP latencies in the absence and in the presence of effects of age respectively. The latter segregation prompted explorations demonstrating distinct dependences of AP latency on $(dV/dt)_{max}$ in young and aged WT hearts but a single such dependence in both *Pgc-1β*$^{-/-}$ groups approximating the functions observed

in aged WT. The difference could be accounted for effects on AP latency of increases in fibrotic change arising from both *Pgc-1β*$^{-/-}$ genotype and ageing. Predictions of arrhythmic substrate from wavelengths derived from these AP activation and recovery terms, paralleled the relative incidences of arrhythmia in *Pgc-1β*$^{-/-}$ and WT hearts.

4.2 RESULTS

The experiments involved simultaneous ECG recordings in intact hearts and intracellular microelectrode recordings from ventricular cardiomyocytes in situ. The intracellular recordings employed microelectrode impalement sites confined to the proximal region of the left ventricle and consistent stimulating electrode positioning between hearts, minimising variabilities in distance between stimulating and recording electrode sites. They explored and characterised effects of the *Pgc-1β*$^{-/-}$ genotype and ageing upon arrhythmic properties at the organ level in Langendorff-perfused murine hearts during both regular pacing and programmed electrical stimulation (PES). These findings were then correlated with cellular electrophysiological quantifications of action potential (AP) activation and propagation, as well as recovery characteristics, and morphometric assessments of age-related structural change, features previously implicated in arrhythmic substrate.

The intracellular recordings confirmed fully polarised resting membrane potentials (RMPs) in all groups studied (young WT (n = 27): -79.0 ± 1.5 mV; aged WT (n = 27): -79.0 ± 1.5 mV; young *Pgc-1β*$^{-/}$ (n = 37)$^{-}$*:* -75.0 ± 1.5 mV; aged *Pgc-1β*$^{-/-}$ (n = 29): -80.0 ± 1.5 mV; all values rounded to the nearest 0.5mV) with slightly more polarized RMPs in young *Pgc-1β*$^{-/-}$ compared to each of the remaining groups ($p < 0.05$ in each case). AP amplitudes (young WT (n = 27): 83.0 ± 1.0 mV; aged WT (n = 27): 88.0 ± 1.5 mV; young *Pgc-1β*$^{-/}$ (n = 37)$^{-}$*:* 80.0 ± 1.0 mV; aged *Pgc-1β*$^{-/-}$ (n = 29): 81.0 ± 1.0 mV; all values rounded to the nearest 0.5mV), were slightly greater in aged WT than in each of the remaining experimental groups ($p < 0.05$ in each case). Nevertheless, comparisons of RMPs and AP amplitudes confirmed AP overshoots were positive as expected

from recordings from viable ventricular cardiomyocytes.

4.2.1 PGC-1B$^{-/-}$ *VENTRICLES DEVELOP ARRHYTHMIC PHENOTYPES*

The occurrence of spontaneous arrhythmic events were first quantified during regular 8 Hz pacing resembling normal resting heart rates. Arrhythmic substrate (i.e an electrophysiological state of the myocardium that is pro-arrhythmic) was thereafter assessed by applying extrasystolic S2 stimuli in a programmed electrical stimulation (PES) protocol. Figure 4-1 shows typical ECG (upper trace in each panel) and intracellular AP recordings (lower trace in each panel) obtained during such regular 8 Hz pacing (A) and PES (B) from a young WT ventricle. The PES protocol comprised cycles of eight S1 beats at a baseline BCL (basic cycle length, i.e the unit of time between two stimuli) of 125 ms followed by an extra stimulus (S2) every ninth beat. The initial S1-S2 coupling interval was 89 ms, decrementing by 1 ms with each cycle. Differences in arrhythmic propensity were quantified from occurrences or otherwise of both spontaneous and provoked arrhythmic events, and the S1-S2 intervals at which the latter took place. None of the hearts in any of the experimental groups showed spontaneous arrhythmic events during the regular 8 Hz pacing. In contrast, the PES protocols elicited a range of abnormal rhythms, exemplified in Figure 4-2 for an aged *Pgc-1β*$^{-/-}$ ventricle. These included single (A) or pairs (couplets) of successive ectopic beats (B), non-sustained (C) and sustained ventricular tachycardia (D).

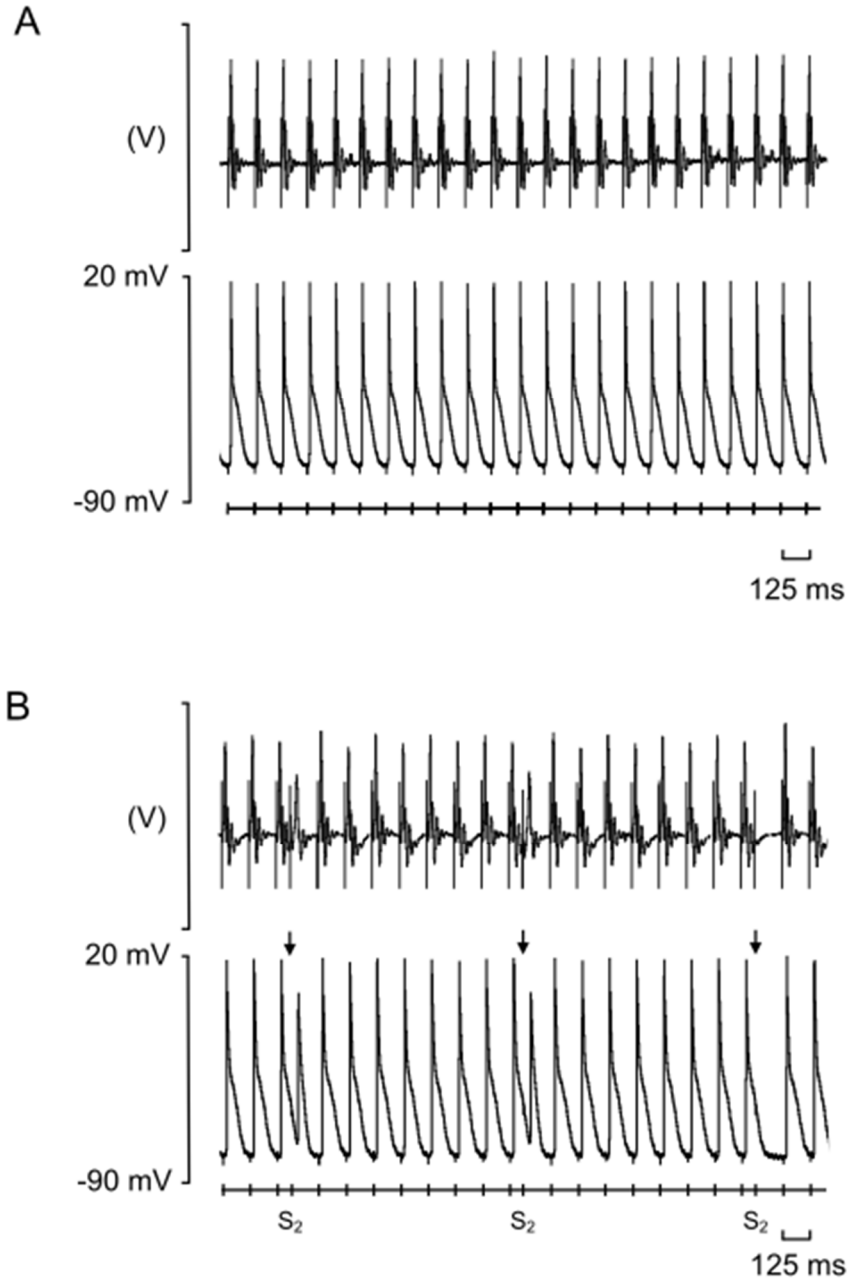

Figure 4-1: Typical electrocardiographic and intracellular action potential recordings. *Typical electrocardiographic (ECG) (upper panel in each) and simultaneous intracellular action potential (AP) recordings (lower panel in each) obtained during 8 Hz pacing (A) and programmed electrical stimulation (PES) (B), recorded from a young wild type (WT) heart. The timings of stimulus delivery are given in the bar beneath the AP recordings, and corresponding stimulation artefacts can be seen on the ECG and AP traces, preceding the respective complexes. In panel (B), arrows indicate the imposition of S2 extrastimuli. The first two S2 stimuli trigger APs, whereas the third S2 stimulus fails to elicit a response, thus representing a refractory outcome.*

Table 4-1 summarises frequencies with which these different categories of abnormal rhythms occurred stratified by experimental group. Young *Pgc-1β*$^{-/-}$ ventricles demonstrated greater incidences of rhythm disturbances than other experimental groups, particularly in the form of non-sustained ventricular tachycardia (NSVT) ($p < 0.001$). Young WT ventricles demonstrated few abnormal rhythms of any description; all the NSVT episodes observed occurred in the same heart.

Aged *Pgc-1β*$^{-/-}$ displayed fewer individual episodes of abnormal rhythms than young *Pgc-1β*$^{-/-}$ hearts, and a similar number as aged WT hearts. However arrhythmias in the aged *Pgc-1β*$^{-/-}$ group appeared to be associated with the greatest risk of major cardiac events. The durations of the VT episodes, whether non-sustained or sustained, were influenced by interacting effects of age and genotype with the VT episodes in aged *Pgc-1β*$^{-/-}$ hearts significantly longer in duration than in the other groups ($p < 0.05$). Aged *Pgc-1β*$^{-/-}$ hearts were also the only experimental group showing sustained VT episodes. Thus an S2 beat could trigger an episodes of a short and self-terminating run of NSVT in a young *Pgc-1β*$^{-/-}$ heart, with subsequent S2 beats triggering further short-lived episodes. In contrast, an episode of VT in an aged *Pgc-1β*$^{-/-}$ ventricle was more likely to be prolonged thereby precluding subsequent S2 beats from triggering further episodes.

Finally, Figure 4-3 compares incidences of NSVT and sustained VT in young (A, C) and aged (B, D) WT (A, B) and *Pgc-1β*$^{-/-}$ hearts (C, D), sorted by the S1S2 coupling interval at which the episodes took place. Both young and aged *Pgc-1β*$^{-/-}$ hearts showed arrhythmic phenomena over more extensive ranges of S1-S2 coupling intervals than the young and aged WT hearts.

Table 4-1: *Summary of arrhythmic events according to experimental group.*

Experimental Group	Numbers that developed NSVT or VT (n / total)	Ectopic Beats	Couplets	NSVT	Sustained VT	Duration of VT Episode	
		Mean number of beats (± SEM)	Mean number of couplets (± SEM)	Mean number of episodes (± SEM)	Mean number of episodes (± SEM)	No. of Beats (mean ± SEM)	Time (s) (mean ± SEM)
Young Wild Type	1 / 31	0	0.03 (± 0.03)	0.26 (± 0.26)	0	4.13 ± 0.74	0.022 ± 0.004
Aged Wild Type	4 / 29	0	0.03 (± 0.03)	0.89 (± 0.47)	0	5.96 ± 0.66	0.032 ± 0.004
Young *Pgc-1β*$^{-/-}$	7 / 37	0.09 (± 0.04)	1 (± 0.48)	1.70 (± 0.80)*	0	6.81 ± 2.00	0.041 ± 0.016
Aged *Pgc-1β*$^{-/-}$	6 / 29	0.14 (± 0.10)	0.10 (± 0.30)	0.72 (± 0.43)	0.07 (± 0.05)	103.57 ± 64.32*	7.835 ± 3.765*

Symbols denote significant differences of the labelled value from corresponding measurements in the other experimental groups based on post hoc Tukey HSD analysis. These post hoc-tests were performed if the *F* value from two-way ANOVA was significant. Single asterix denotes significance at $p < 0.05$ comparison made to other groups. Aged *Pgc-1β*$^{-/-}$ mice had significantly longer duration of VT episodes both by number of beats ($p = 0.016$) and by time ($p = 0.021$) compared to other groups.

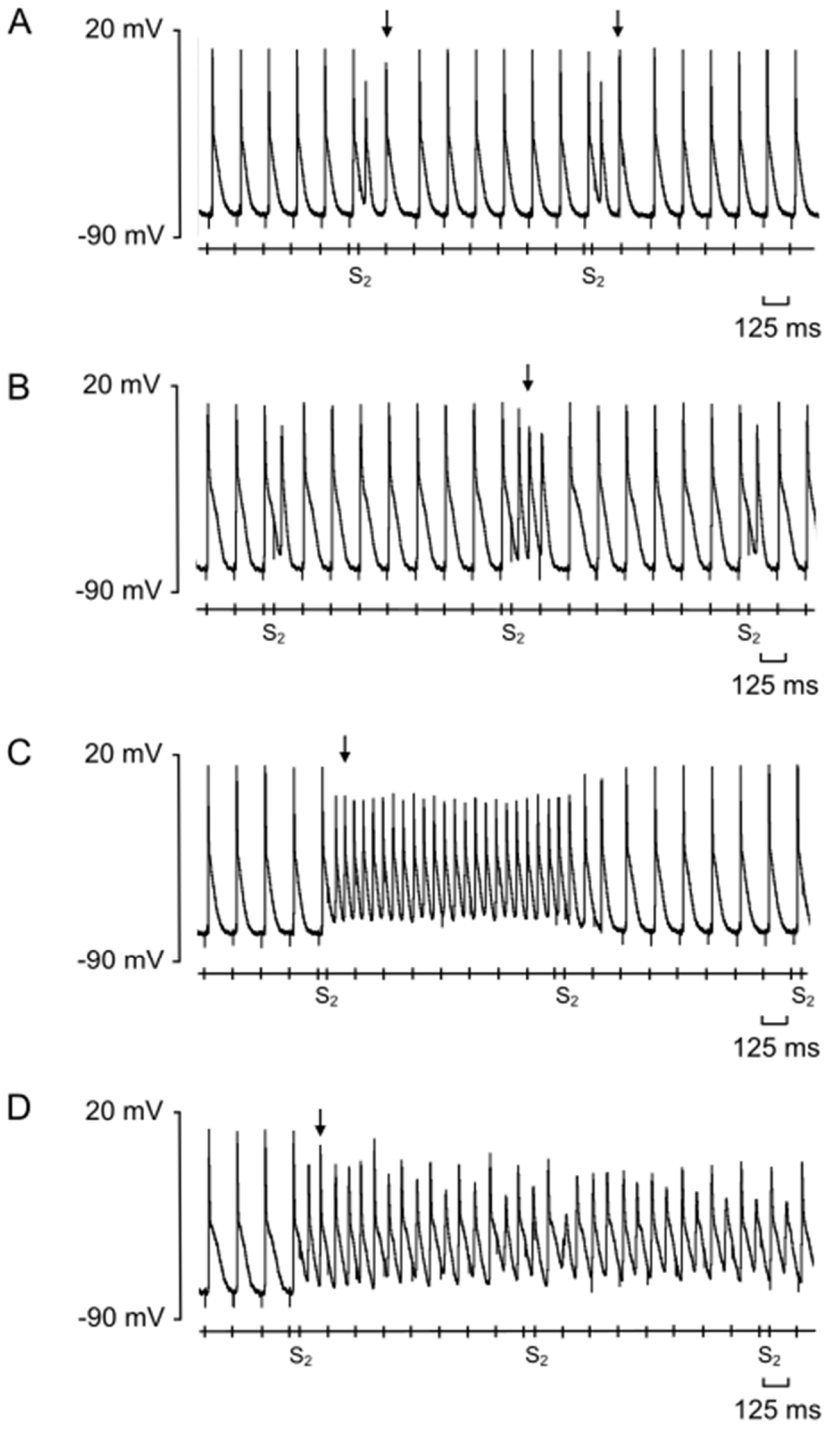

Figure 4-2: Typical AP recordings of different abnormal rhythms observed during programmed electrical stimulation *(PES) in an aged Pgc-1β*$^{-/-}$ *heart following an extrasystolic S2 stimulus. These were classified as an individual ectopic beat (A), a couplet of two successive ectopic beats (B), non-sustained ventricular tachycardia (NSVT) (C) and sustained ventricular tachycardia (D). The timings of stimulus delivery are given in the bar beneath the AP recordings and arrows indicate the onset of the abnormal rhythm.*

4.2.2 Altered AP parameters in Pgc-1β$^{-/-}$ *ventricles during regular pacing*

Parameters corresponding to AP initiation, propagation and recovery were next examined (by intracellular cardiomyocyte recordings) under conditions of regular 8 Hz pacing for differences between groups, in order to correlate these with the arrhythmic phenotypes delineated above (Table 4-2). *Pgc-1β* ablation independently altered both AP activation and recovery properties in directions compatible with pro-arrhythmic defects in an absence of effects of ageing whether independently, or interacting with genotype. Thus, maximum AP upstroke velocities, $(dV/dt)_{max}$, were reduced in *Pgc-1β*$^{-/-}$ compared to WT ventricles ($F = 31.606$, $p < 0.001$), without effects of age ($F = 1.973$, $p > 0.05$) or interacting effects of age and genotype ($F = 0.904$, $p > 0.05$). Post hoc tests confirmed lower $(dV/dt)_{max}$ in both young and aged, *Pgc-1β*$^{-/-}$ group than either WT group. Assessments of AP conduction similarly demonstrated longer AP latencies between stimulus delivery and the AP peak, in *Pgc-1β*$^{-/-}$ than WT ventricles ($F = 11.458$, $p < 0.001$) without effects of age ($F = 0.494$, $p > 0.05$) or interactions between age and genotype ($F = 0.744$, $p > 0.05$). However, post hoc analysis demonstrated shorter AP latencies in young WT than both young ($p < 0.05$) and aged *Pgc-1β*$^{-/-}$ ($p < 0.05$) ventricles, but no differences between aged WT ventricles and the remaining groups.

Of recovery characteristics, AP durations at 90%, 70% and 50% repolarisation, APD_{90}, APD_{70} and APD_{50} respectively, were indistinguishable between groups. Finally, ventricular effective refractory periods (ERPs) were evaluated from the PES protocol as the shortest S1-S2 coupling interval at which an S2 stimulus successfully triggered a ventricular beat. *Pgc-1β*$^{-/-}$ ventricles showed shorter ERPs than WT ($F = 13.508$, $p < 0.001$) without effects of either age ($F = 0.208$, $p > 0.05$) or interactions between age and genotype ($F = 0.391$, $p > 0.05$). Post hoc Tukey tests demonstrated shorter ERPs in both young ($p < 0.05$) and aged *Pgc-1β*$^{-/-}$ ($p < 0.05$) compared to aged WT ventricles.

Table 4-2: *Action potential properties in WT and Pgc-1β*$^{-/-}$ *hearts during regular 8 Hz pacing.*

Experimental Group (n)	$(dV/dt)_{max}$ (V s^{-1})	AP latency (ms)	APD_{90} Duration (ms)	APD_{70} Duration (ms)	APD_{50} Duration (ms)	Effective Refractory Period (ms)
Young Wild Type (27)	156.08 (± 6.00)$^{***, \dagger}$	9.70 (± 0.32)$^{*, \dagger}$	51.01 (± 1.47)	27.51 (± 1.29)	7.27 (± 0.64)	57.15 (± 1.92)
Aged Wild Type (27)	158.14 (± 5.45)$^{\ddagger\ddagger\ddagger, \alpha}$	10.92 (± 0.35)	51.24 (± 1.68)	26.08 (± 1.57)	7.63 (± 0.63)	59.92 (± 2.20)$^{*, \dagger}$
Young *Pgc-1β*$^{-/-}$ (37)	119.23 (± 5.49)$^{***, \ddagger\ddagger\ddagger}$	12.85 (± 0.77)*	47.31 (± 2.12)	23.58 (± 1.67)	8.69 (± 1.00)	51.54 (± 1.74)*
Aged *Pgc-1β*$^{-/-}$ (29)	132.21 (± 5.73)$^{\dagger, \alpha}$	12.79 (± 1.09)†	53.14 (± 1.60)	28.19 (± 1.47)	8.27 (± 0.54)	51.25 (± 2.42)†

All values are given as mean (± SEM). Symbols denote significant differences on post hoc analysis between pairs of experimental groups with the same symbol. These post-hoc tests were performed if the *F* value from two-way ANOVA was significant. Single, double and triple symbols denote $p < 0.05$, $p < 0.01$ and $p < 0.001$ respectively.

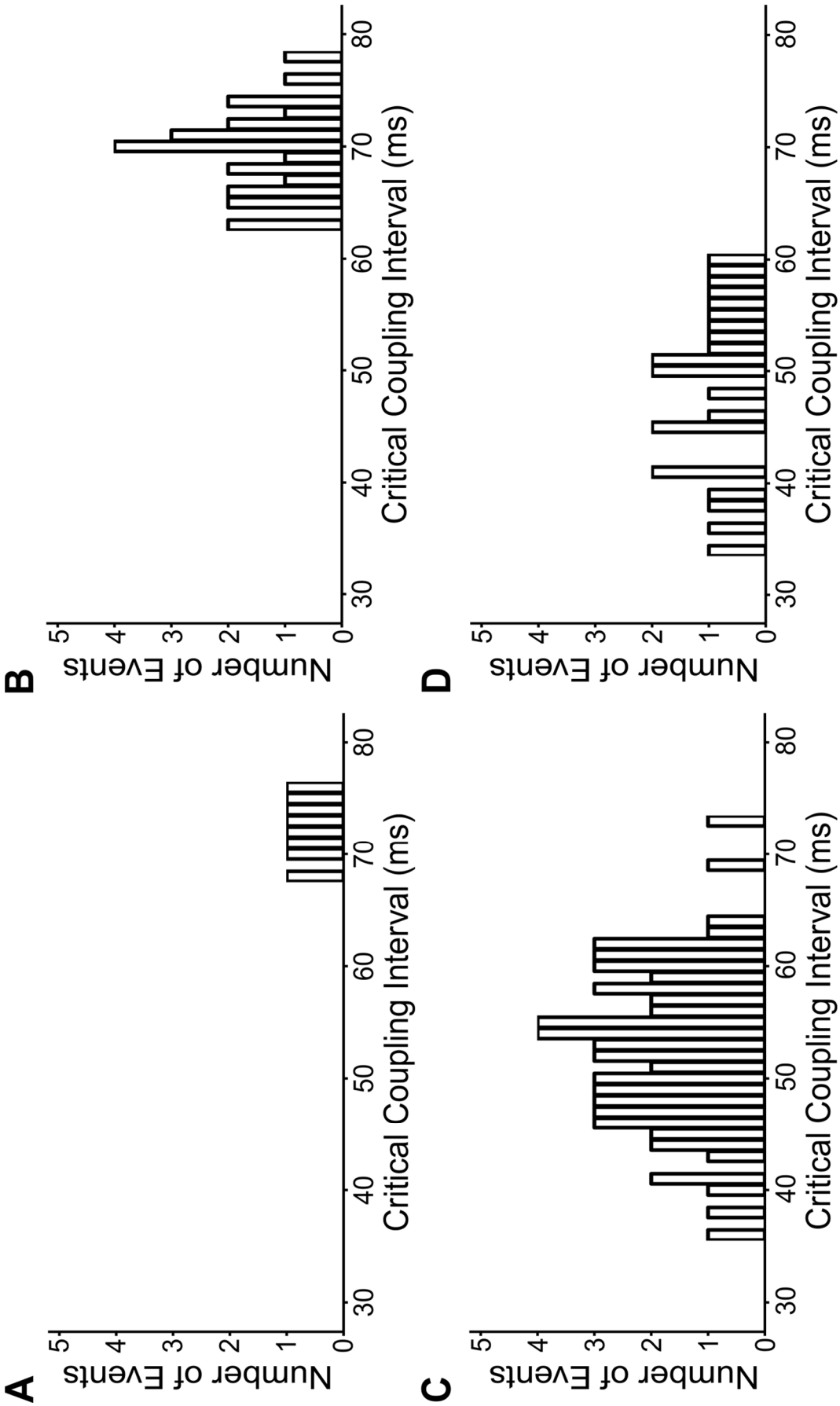

Figure 4-3: Occurrences of episodes of non-sustained ventricular tachycardia or sustained tachycardia recording during PES protocols *in (A) young WT (n = 27), (B) aged WT (n = 27), (C) young Pgc-1β*$^{-/-}$ *(n = 37) and (D) aged Pgc-1β*$^{-/-}$ *hearts (n = 29), stratified according to the S1-S2 coupling interval (critical coupling interval) that provoked the arrhythmia.*

4.2.3 Altered AP parameters in Pgc-1β$^{-/-}$ *ventricles subjected to extrasystolic stimuli*

Whereas regular 8 Hz pacing permitted evaluation of electrophysiological properties under conditions resembling resting heart rates, a PES protocol explored the presence or absence of an arrhythmic substrate. The PES protocol utilised transient perturbations, in the form of isolated S2 extra stimuli mimicking ectopic APs, that are thought to act as arrhythmic triggers. PES protocols gave APs triggered by S2 stimuli over the range of S1-S2 coupling intervals explored. There were variations in $(dV/dt)_{max}$ and of AP latency which showed contrasting dependences upon genotype and age, despite invariant dependences of APD_{90} with coupling interval.

Thus, plots of $(dV/dt)_{max}$ against S1-S2 coupling interval (Figure 4-4A(i)) confirmed lower $(dV/dt)_{max}$ values in *Pgc-1β*$^{-/-}$ compared to WT ventricles ($F = 30.167$, $p < 0.001$) at the long coupling intervals early in the PES protocol. There were no effects of age or interactions of age and genotype. A second statistical analysis was also performed to confirm these results. Using R and lme4 (R Core Team, 2012) a linear mixed effects regression analysis of the relationship between $(dV/dt)_{max}$ and genotype and age was performed. As fixed effects, genotype and age (with an interaction term) were entered into the model. As random effects, intercepts for each cell impalement and the BCL were set, as well random slopes for the effect. Visual inspection of residual plots did not reveal any obvious deviations from homoscedasticity or normality. P values were obtained by likelihood ratio tests of the full model with the effect in question against the model without the effect in question. Genotype significantly affected $(dV/dt)_{max}$, with the *Pgc-1β* ablation significantly lowering $(dV/dt)_{max}$ by 24.52 V/s ($\chi2$ 6.1082, $p = 0.047$) with no significant effect of age ($\chi2$ 0.66, $p = 0.72$) or significant interaction of age and gentoype together ($\chi2$ 0.27, $p = 0.61$). These statistical tests are concordant with each other and in keeping with those from the regular 8 Hz pacing.

Post hoc testing demonstrated lower $(dV/dt)_{max}$ in each individual *Pgc-1β*$^{-/-}$ group compared

to any WT group (Fig. 4-4A(ii)), but no differences between young and aged ventricles within either group. $(dV/dt)_{max}$ fell with shortening S1-S2 coupling interval preserving their relative magnitudes between experimental groups consistent with progressive reductions in conduction velocity and the increased arrhythmic tendency. The $(dV/dt)_{max}$ values then converged to indistinguishable values whether stratified by genotype ($F = 1.395$, $p > 0.05$) or age ($F = 0.060$, $p > 0.05$) (Fig. 4-4A(ii)).

The corresponding AP latencies (Fig. 4-4B(i)) were longer in *Pgc-1β*$^{-/-}$ than WT ventricles at the longest S1-S2 coupling intervals ($F = 8.633$, $p < 0.01$) without independent effects of age ($F = 0.001$, $p > 0.05$) or interacting effects of age and genotype ($F = 2.689$, $p > 0.05$), consistent with the $(dV/dt)_{max}$ readings. The mixed effect analysis was again concordant, with genotype significantly affecting latency; the *Pgc-1β*$^{-/-}$ mice had an increased latency by 1.2ms ($\chi2$ 7.6013, $p = 0.022$) with no significant effect of age ($\chi2$ 3.1027, $p = 0.21$) or interaction with age and genotype ($\chi2$ 2.7854, $p = 0.095$). However, young *Pgc-1β*$^{-/-}$ showed longer AP latencies than young WT ventricles on post hoc Tukey analysis ($p < 0.05$) though with no further differences. Furthermore, AP latencies increased with falling S1-S2 intervals to varying extents amongst groups. AP latencies at the shortest S1-S2 intervals were affected by interactions between genotype and age ($F = 4.100$, $p < 0.05$). Young WT ventricles here showed shorter AP latencies than the remaining groups (post hoc Tukey tests: young WT *vs.* young *Pgc-1β*$^{-/-}$ $p < 0.01$; young WT *vs.* aged *Pgc-1β*$^{-/-}$: $p < 0.05$; no significant differences in the remaining comparisons). AP latency did not differ between aged WT and either young or aged *Pgc-1β*$^{-/-}$ ventricles. Thus at the shortest S1-S2 coupling intervals the young WT ventricles, which were the least arrhythmic, showed smaller increases in AP latency than any other group including aged WT ventricles.

Finally, similar shortenings of APD_{90} with reductions in S1-S2 coupling intervals (Fig. 4-4C(i)) were observed through all groups, with indistinguishable APD_{90} at both the longest (genotype: $F = 0.004$, $p > 0.05$; age: $F = 0.309$, $p > 0.05$) and shortest S1-S2 intervals (genotype: $F = 2.661$, $p > 0.05$; age: $F = 2.152$, $p > 0.05$) (Fig. 4-4C(ii)). The mixed effects analysis confirmed these

results, with no significant effect of genotype ($\chi2$ 8.8976, p = 0.064) or age ($\chi2$ 7.2975, p = 0.121) or interactions with age and genotype ($\chi2$ 8.3611, p = 0.079) on APD_{90}. Table 4-3 demonstrates that these similarities in action potential recovery extended to the respective values of APD_{50} and APD_{70} at the longest and shortest S1-S2 intervals.

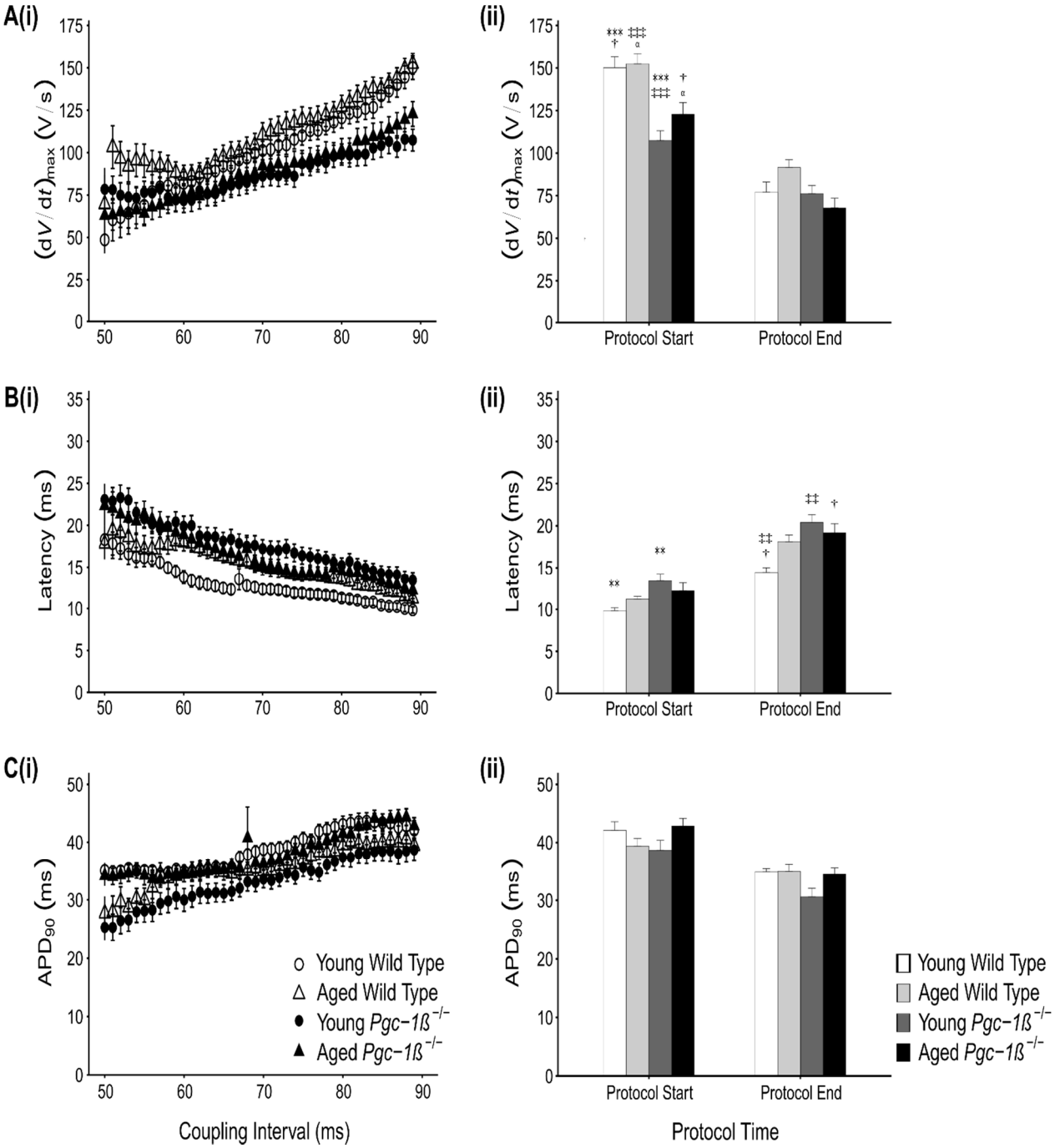

Figure 4-4: Mean AP parameters for S2 triggered APs. *Means ± SEM of maximum action potential upstroke rate, $(dV/dt)_{max}$(A), AP latencies (B) and action potential durations to 90% recovery, APD_{90} (C) for S2 triggered APs in the four experimental groups (young WT (n = 27), aged WT (n = 27), young Pgc-1ß$^{-/-}$ (n = 37) and aged Pgc-1ß$^{-/-}$ hearts (n = 29)), for (i) S1-S2 intervals falling from 89 ms to 50 ms during the PES protocols. Panel (ii) for each provides a comparison of these values at the outset and at the end of the pacing protocol, corresponding to a refractory outcome or the onset of sustained arrhythmia. The symbols denote significant differences between each pair, obtained from post hoc Tukey testing, which was conducted if the ANOVA indicated a significant outcome. Single, double and triple symbols denote p < 0.05, p < 0.01 and p < 0.001 respectively.*

Table 4-3: *Action potential duration time in WT and Pgc-1β*$^{-/-}$ *hearts during programmed stimulation.*

Experimental Group (n)	APD_{50} Duration (ms) Protocol Start	APD_{50} Duration (ms) Protocol End	APD_{70} Duration (ms) Protocol Start	APD_{70} Duration (ms) Protocol End	APD_{90} Duration (ms) Protocol Start	APD_{90} Duration (ms) Protocol End
Young Wild Type (27)	6.51 (± 0.50)	9.98 (± 0.63)	22.56 (± 1.03)	20.63 (± 0.50)	42.11 (± 1.48)	34.86 (± 0.54)
Aged Wild Type (27)	6.78 (± 0.58)	8.98 (± 0.75)	20.00 (± 1.13)	20.42 (± 1.02)	39.38 (± 1.33)	34.95 (± 1.19)
Young *Pgc-1β*$^{-/-}$ (37)	8.73 (± 0.92)	8.15 (± 0.86)	20.19 (± 1.30)	16.93 (± 1.20)	38.67 (± 1.73)	30.60 (± 1.48)
Aged *Pgc-1β*$^{-/-}$ (29)	7.74 (± 0.61)	9.12 (± 0.61)	22.85 (± 0.99)	19.69 (± 0.75)	42.84 (± 1.34)	34.46 (± 1.06)

All values are given as mean (± SEM). Post-hoc tests were performed if the *F* value from two-way ANOVA was significant. There were no significant differences between groups.

4.2.4 Distinct dependences of AP latency upon $(dV/dt)_{max}$ in WT and Pgc-1β$^{-/-}$ ventricles

These detailed differences in the effects of genotype and age upon the dependences of AP latency and $(dV/dt)_{max}$ upon S1-S2 coupling interval prompted investigations of the relationship between these two parameters. Figure 4-5 plots mean (±SEM) latencies of the extrasystolic S2 APs against their corresponding $(dV/dt)_{max}$ values for each experimental group. Both WT and *Pgc-1β*$^{-/-}$ showed AP latencies increasing with falling $(dV/dt)_{max}$ and shortening S1-S2 coupling intervals, consistent with much of this increased AP latency being related to falls in $(dV/dt)_{max}$. However, young and aged WT ventricles generated two separable plots of AP latency against $(dV/dt)_{max}$ (Fig. 4-5A), with aged showed greater AP latencies than young WT ventricles at any given $(dV/dt)_{max}$. In contrast, *both* young and aged *Pgc-1β*$^{-/-}$ ventricles gave similar AP latency - $(dV/dt)_{max}$ plots (Fig. 4-5B), whose values closely resembled those of aged as opposed to young WT.

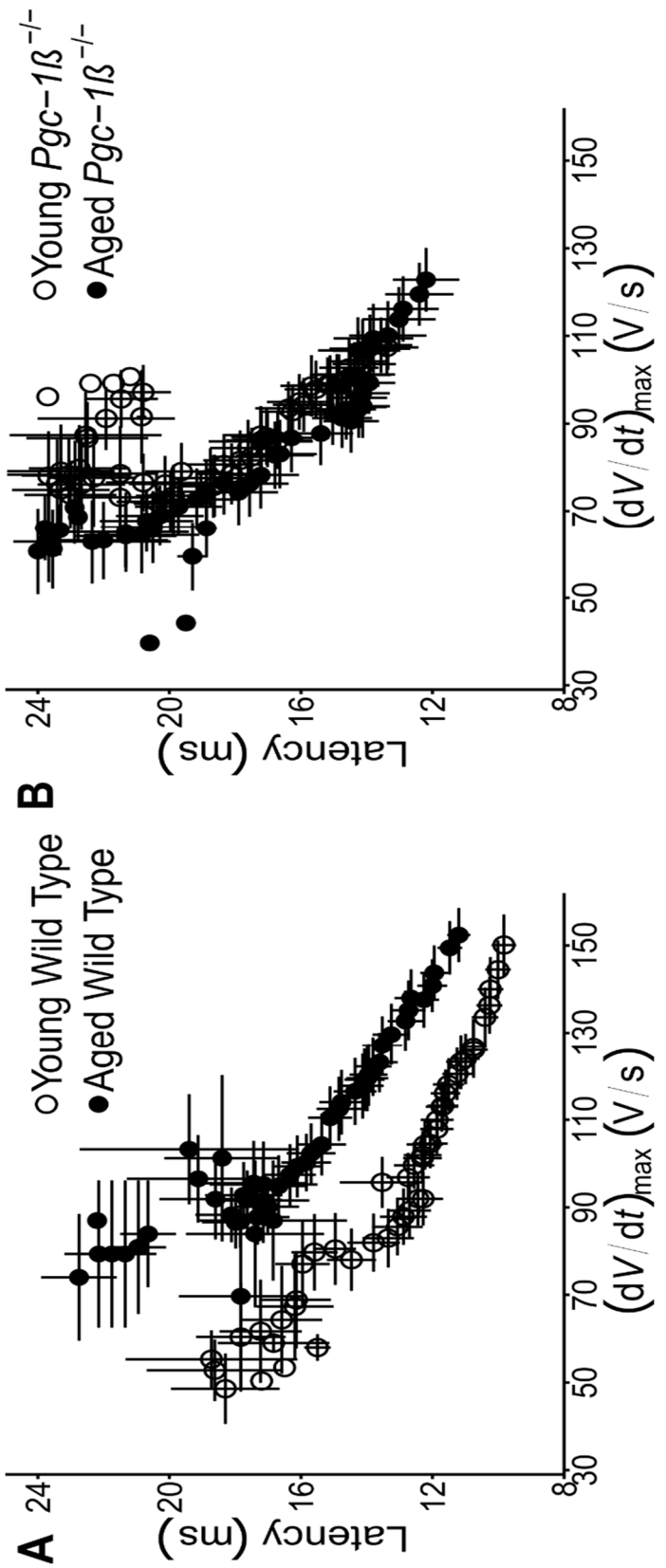

Figure 4-5: Dependences of AP latency upon (dV/dt)$_{max}$ *through the programmed electrical stimulation (PES) protocol compared in (A) young and old WT (n = 27 and n = 27 respectively) and (B) young and aged Pgc-1β$^{-/-}$ hearts (n= 37 and n = 29 respectively).*

4.2.5 Increased fibrotic change with Pgc-1β ablation

Young and aged WT ventricles thus showed distinct dependences of AP latency upon $(dV/dt)_{max}$ whereas both young and aged *Pgc-1β*$^{-/-}$ ventricles showed a single dependence resembling that shown by the aged as opposed to the young WT. $(dV/dt)_{max}$ classically reflects cardiomyocyte membrane depolarisation driven by regenerative inward Na^+ current important in AP conduction (King et al., 2013 c; Zhang et al., 2013). However, AP conduction additionally varies with tissue conductivity properties reflecting gap junction resistances separating successive coupled cardiomyocytes, and their cell membrane capacitances influenced by fibroblast-myocyte fusion (King et al., 2013 a; Davies et al., 2014). Previous reports in murine *Scn5a*$^{+/-}$ hearts had implicated age-dependent fibrotic change and such effects on tissue conductivity in similar pro-arrhythmic alterations in AP conduction (Royer et al., 2005; Jeevaratnam et al., 2011, 2012). The final experiments accordingly made morphometric assessments for fibrotic change amongst the four experimental groups. This was conducted blindly by two independent investigators achieving a high measure of consistency (ICC = 0.94). Figure 4-6 illustrates typical histological sections from young and aged WT and *Pgc-1β*$^{-/-}$ hearts (A), higher power representations of normal and fibrotic tissue (B) and quantifications of this fibrotic change (C). Age and genotype independently increased levels of fibrosis in ventricular tissue ($p < 0.05$ for both), with no evidence of interaction between variables. The differing fibrotic levels in aged vs. young WT ventricles paralleled their differing AP latency - $(dV/dt)_{max}$ association, whereas the similar fibrotic levels in young *Pgc-1β*$^{-/-}$ and aged WT ventricles paralleled their similar AP latency - $(dV/dt)_{max}$ plots.

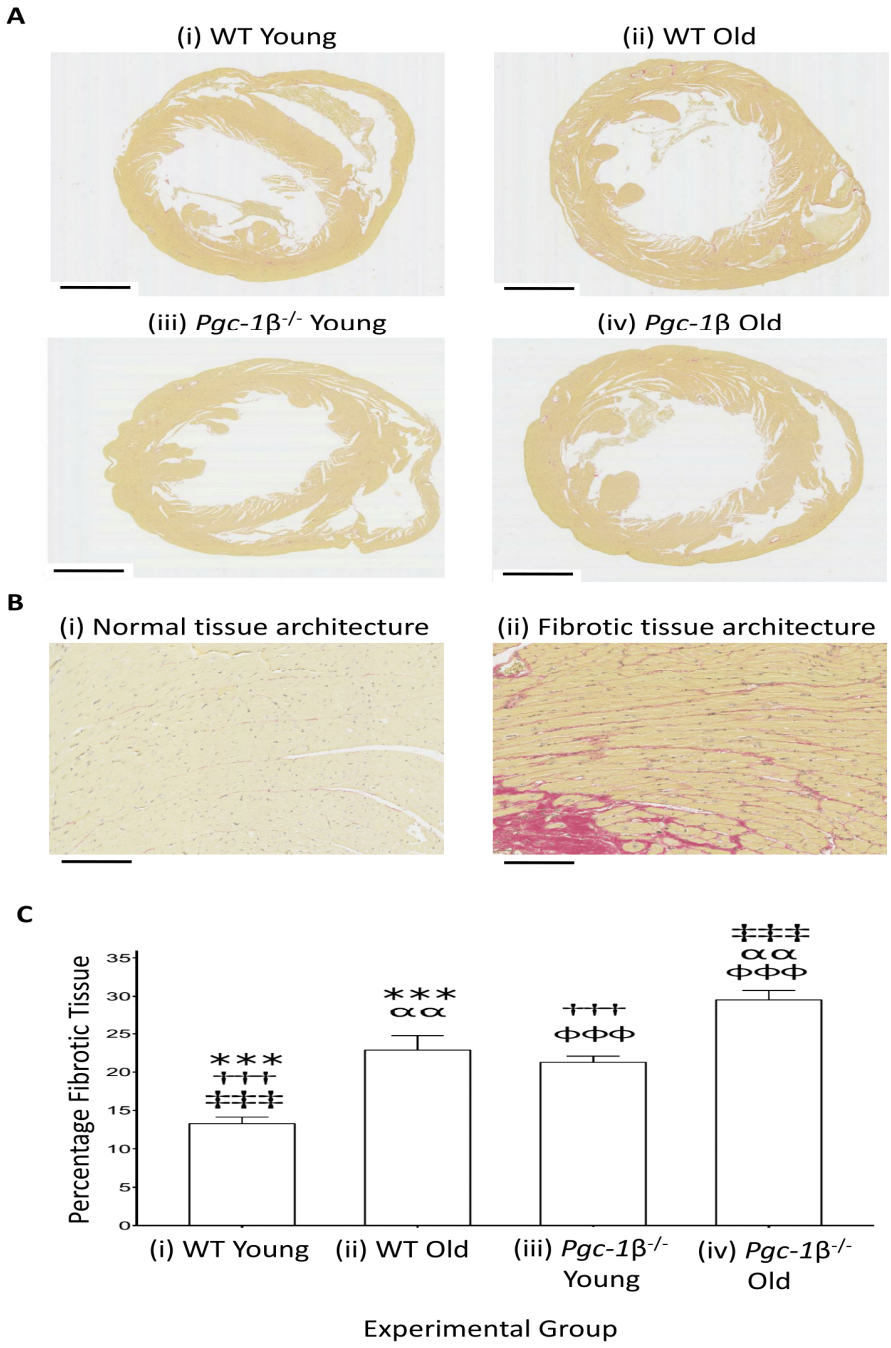

Figure 4-6: Morphological assessment of fibrotic change.

(A) Representative examples of histological samples from young ((i) and (iiii)) and old ((ii) and (iv)), WT ((i) and (ii)) and Pgc1β$^{-/-}$ hearts ((iii) and (iv)) used for morphological assessment of fibrotic change (scale bar 1 mm), with (B) typical higher power appearances to illustrate (i) normal tissue architecture in young WT and (ii) tissue structure showing fibrotic change in aged Pgc-1β$^{-/-}$ ventricles (scale bar 100 µm). (C) The degree of fibrotic change was assessed as the proportion of morphometric squares covering tissue that showed positive evidence of fibrotic change as detected by picrosirius red staining. Numbers of hearts examined: young WT (n = 8), aged WT (n = 8), young Pgc-1β$^{-/-}$ (n = 9), aged Pgc-1β$^{-/-}$ (n = 10). Symbols denote pairs of points showing significant differences from post hoc Tukey testing, where single, double and triple symbols denote p < 0.05, p < 0.01 and p < 0.001 respectively.

4.2.6 Action potential wavelengths and pro-arrhythmic phenotypes in Pgc-1β$^{-/-}$ *ventricles*

Wavelengths made up of AP activation and ERP terms have provided indications of arrhythmic substrate arising from slowed conduction and/or shortened ERP, in earlier experimental analyses of cardiac arrhythmia (Weiss et al., 2005; Matthews et al., 2013 b; Huang, 2017 a). Figure 4-7 summarises such an analysis for the experimental groups studied during the regular pacing (A) and with the extrasystolic S2 stimuli imposed through the different S1-S2 coupling intervals during PES pacing (B). With $(dV/dt)_{max}$ as the activation term (Fig. 4-7A(i) and 4-7B(i)), ANOVA demonstrated shorter wavelengths in *Pgc-1β*$^{-/-}$ compared to WT ventricles ($F = 38.591$, $p < 0.001$) without effects of either age ($F = 1.943$, $p > 0.05$) or interactions between age and genotype ($F = 0.016$, $p > 0.05$). Post hoc analysis revealed significant differences between each WT group compared to either *Pgc-1β*$^{-/-}$ group (young WT *vs.* young *Pgc-1β*$^{-/-}$ $p < 0.001$, young WT *vs.* aged *Pgc-1β*$^{-/-}$ $p < 0.01$, aged WT *vs.* young *Pgc-1β*$^{-/-}$ $p < 0.001$, aged WT *vs.* aged *Pgc-1β*$^{-/-}$ $p < 0.001$). However, there were no significant differences between young or aged groups of the same genotype. This thus accounts for the more marked arrhythmic substrate in both young and aged *Pgc-1β*$^{-/-}$.

With 1/(AP latency) as the activation term, representing wavelength by the ratio ERP/(AP latency) thereby including tissue conductivity changes produced by fibrotic change (Figure 4-7A(ii) and B(ii)), ANOVA similarly associated *Pgc-1β* ablation with shortened wavelengths compared to WT ventricles ($F = 22.766$, $p < 0.001$) with no effect of age ($F = 0.36$, $p > 0.05$) or interaction between age and genotype ($F = 1.872$, $p > 0.05$). However, the post hoc testing revealed longer wavelengths in young WT than either young *Pgc-1β*$^{-/-}$ ($p < 0.001$) or aged *Pgc-1β*$^{-/-}$ ($p < 0.01$) ventricles. However, wavelengths in aged WT, although higher than in young *Pgc-1β*$^{-/-}$ ventricles ($p < 0.05$), were similar to those shown by aged *Pgc-1β*$^{-/-}$ ventricles ($p > 0.05$). Similarly, dependences of wavelength on S1-S2 coupling intervals showed greater wavelengths in young WT ventricles, shortened values in *Pgc-1β*$^{-/-}$ and intermediate measures in aged WT ventricles. Both these findings parallel further findings in Table 4-1 showing that

aged *Pgc-1β*$^{-/-}$ hearts displayed fewer individual episodes of abnormal rhythms compared to young *Pgc-1β*$^{-/-}$ hearts, and a similar number to the aged WT group.

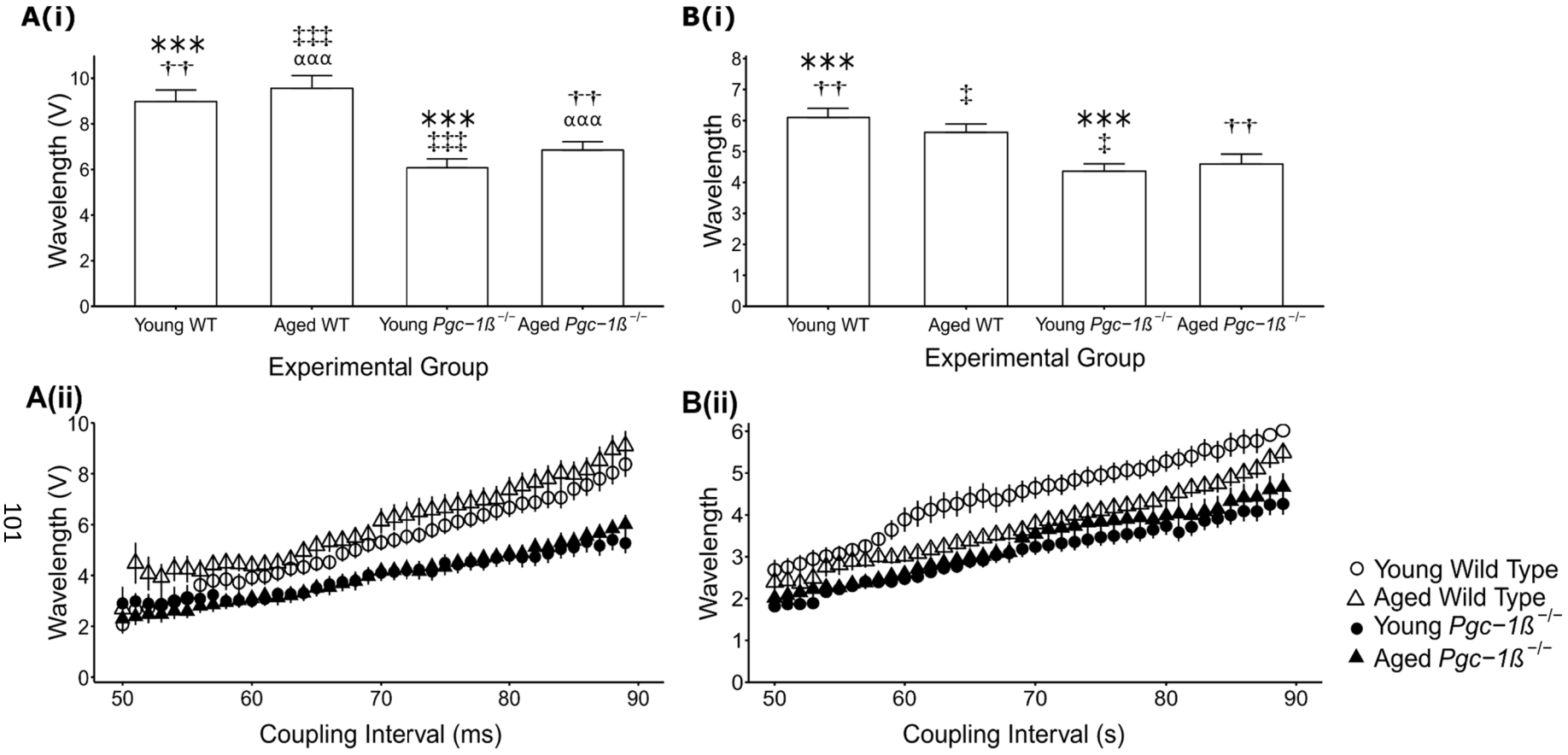

Figure 4-7: AP wavelength assessed using (dV/dt)max and AP latency at different S1-S2 intervals. *Dependences of AP wavelength assessed using $(dV/dt)_{max}$ (A(i) and B(i)) and AP latency (A(ii) and B(ii)) through regular 8 Hz pacing (A) and in response to extrasystolic S2 stimulation at different S1-S2 intervals in the PES protocol (B) in young and aged, WT and Pgc-1ß$^{-/-}$ hearts (n= 27, n = 27, n= 39, n = 29 respectively). Wavelength was calculated as the product of the respective conduction parameter (either $(dV/dt)_{max}$ or AP latency) and the corresponding ERP for that heart. In panels (A(i)) and (A(ii)), symbols denote significant differences between each pair, obtained from post hoc Tukey testing, which was conducted if the ANOVA indicated a significant outcome. Single, double and triple symbols denote p < 0.05, p < 0.01 and p < 0.001 respectively.*

4.3 DISCUSSION

PGC-1β expression is restricted to tissues with high oxidative capacity such as the heart and plays a key role in modulating cellular mitochondrial biogenesis, energy substrate uptake and utilisation (Arany et al., 2005; Lin et al., 2005; Finck and Kelly, 2006). Mice lacking both *Pgc-1β* and the related *Pgc-1α* have significantly reduced mitochondrial content and die at birth due to heart failure (Lai et al., 2008). In contrast isolated deficiency of *Pgc-1β* is not associated with cardiac contractile dysfunction (Lelliott et al., 2006). However cellular studies indicate an increased vulnerability to arrhythmia (Gurung et al., 2011 a). The latter report demonstrated that murine *Pgc-1β*$^{-/-}$ cardiomyocytes also showed irregular and extrasystolic Ca^{2+} signalling patterns and spontaneous Ca^{2+} propagating waves associated with arrhythmic phenotypes in other situations (Balasubramaniam et al., 2004; Goddard et al., 2008 a; Hothi et al., 2008; Gurung et al., 2011 a). The *Pgc-1β* system thus provides a suitable model to investigate the electrophysiological alterations secondary to metabolic impairment.

The present study is the first report investigating the electrophysiological phenotype and associated arrhythmic tendency associated with *Pgc-1β* knockout at the organ as opposed to the cellular level. Sustained arrhythmia likely depends upon interactions between contributions from triggering events and arrhythmic substrate (Huang, 2017 a). We employed a modified Langendorff preparation, enabling simultaneous intracellular recordings from the left ventricular epicardium and volume conducted electrocardiograph monitoring surveying whole heart activity. The arrhythmic vulnerability could therefore be correlated with cellular electrical properties in young and aged WT and *Pgc-1β*$^{-/-}$ hearts during regular 8 Hz pacing and PES protocols. The measurements provided effective refractory periods (ERPs), and parameters related to action potential (AP) initiation, propagation, and recovery. Adoption of intracellular recording methods permitted closer estimates of the activation parameters, $(dV/dt)_{max}$ and AP latency (King et al., 2013 c) than did the monophasic AP recordings, primarily used to determine AP recovery parameters as APD_{90} and ERP measurements, on previous occasions (Thomas et al., 2007 a; b, 2008).

The resulting measurements could also be compared with those obtained by previous electrophysiological studies employing similar methods in other, monogenic, murine systems that characterised arrhythmic phenotypes associated with specific genetic ion channel modifications. These had previously implicated distinct electrophysiological features in arrhythmic substrate and triggering. Reduced maximum rates of depolarisation, $(dV/dt)_{max}$, attributed directly to a loss of Na^+ channel function, were implicated as pro-arrhythmic factors in *Scn5a*$^{+/-}$ hearts through their effects upon AP conduction and therefore latency (Martin et al., 2010, 2012 b). Alterations in cardiomyocyte coupling further limiting AP propagation could arise from connexin Cx40 or Cx43 deficiency (Simon et al., 1998; Royer et al., 2005; Verheule and Kaese, 2013), or tissue morphological changes in the form of fibrosis (Jeevaratnam et al., 2011, 2012). These potentially alter intracellular electrical resistances between cardiomyocytes, with the latter additionally increasing cardiomyocyte-fibroblast fusion (Xie et al., 2009; Davies et al., 2014; Mahoney et al., 2016). Alternatively, compromised AP recovery altering APD_{90} and/or ERP, as might arise from late inward Na^+ current or deficient outward K^+ current, were demonstrated in the pro-arrhythmic *Scn5a*$^{+/\Delta kpq}$ and *Kcne5*$^{-/-}$ systems respectively, particularly where the relative APD_{90} and ERP durations gave rise to potential windows for a generation of re-entrant excitation (Thomas et al., 2007 a; b, 2008). Altered intracellular Ca^{2+} homeostasis was associated with both membrane instabilities in the form of early or delayed after depolarising triggering phenomena (Balasubramaniam et al., 2004; Goddard et al., 2008 a; Hothi et al., 2008), and altered AP $(dV/dt)_{max}$ and conduction attributed to indirect effects upon Na^+ channel function (Zhang et al., 2013; Salvage et al., 2015; Huang, 2017 b).

We here report an arrhythmic phenotype associated with chronic mitochondrial dysfunction that evolves with age, extending earlier cellular studies linking *Pgc-1β* ablation to increased arrhythmic risk (Gurung et al., 2011 a). No arrhythmias were observed in any group during regular pacing at a frequency of 8 Hz. Regular pacing at this rate falls within the murine resting heart range and so would not be expected to trigger arrhythmias. The *Pgc-1β* deficient hearts

are known to have a mild cardiac phenotype in the non-stressed state in keeping with these findings. In contrast, several arrhythmias were observed in *Pgc-1β*$^{-/-}$ hearts during programmed electrical stimulation. Exceptionally few arrhythmias occurred in young WT hearts and the incidence was greater in aged WT hearts reflecting patterns seen in the clinical setting and underlining the impact of age on arrhythmic risk. Mitochondrial dysfunction progresses with age through the accumulation of mutations in mitochondrial DNA and impaired autophagy (Michikawa et al., 1999; Pyo et al., 2013), with this shift in arrhythmic risk possibly being its sequelae. This effect was further emphasised by the even higher incidence of arrhythmia seen in *Pgc-1β* deficient hearts that possess a more pronounced mitochondrial deficit. Here, young *Pgc-1β*$^{-/-}$ hearts had the greatest incidence of arrhythmia of any group. The absolute incidence in aged *Pgc-1β*$^{-/-}$ hearts was lower; however these hearts displayed alterations in the nature of the arrhythmias that would be expected to have the most deleterious features. That is, the duration of arrhythmias occurring in aged *Pgc-1β*$^{-/-}$ hearts were far greater than that in any other group including the young *Pgc-1β*$^{-/-}$ hearts. Thus although the incidence was higher in young *Pgc-1β*$^{-/-}$ hearts, the proportion of time spent in arrhythmia was greatest in aged *Pgc-1β*$^{-/-}$ hearts.

Characterisation of the electrophysiological parameters suggested that the increased vulnerability to arrhythmia in *Pgc-1β*$^{-/-}$ hearts arise primarily through abnormalities in AP initiation and conduction. Both young and aged *Pgc-1β*$^{-/-}$ hearts showed reduced $(dV/dt)_{max}$ values compared to WT hearts during regular pacing. However no difference was observed between young and aged hearts of the same genotype. APs in response to S2 stimuli during the PES protocol displayed a similar segregation between genotypes in terms of $(dV/dt)_{max}$ values at longer S1-S2 intervals. The values of $(dV/dt)_{max}$ fell in all experimental groups whilst preserving their relative magnitudes between groups with shortening S1-S2 coupling interval. However $(dV/dt)_{max}$ values converged at the shortest intervals that represented the greatest electrophysiological stress. Thus *Pgc-1β*$^{-/-}$ hearts displayed compromised $(dV/dt)_{max}$ at modest levels of stress, underpinning their greater vulnerability to arrhythmia through longer periods of the protocol. Values of $(dV/dt)_{max}$ have been shown to correlate with both peak sodium current and conduction velocity in skeletal and cardiac muscle (Hondeghem and Katzung,

1977; Jack et al., 1983; Usher-Smith et al., 2006; Fraser et al., 2011).

Metabolic stress has been previously reported to reduce peak sodium currents in cardiomyocytes (Liu et al., 2009) and this could be reversed with the mitochondrial specific ROS scavenger mitoTEMPO (Liu et al., 2010 b). Additionally, activity of the mammalian voltage-gated Na^+ channel is influenced by cytosolic [Ca^{2+}] through C-terminal IQ- and EF-hand-like motifs sensitive to calmodulin/calmodulin kinase II (Mori et al., 2000). Elevated intracellular [Ca^{2+}] caused reductions in I_{Na} density and $(dV/dt)_{max}$ in cardiomyocytes in vitro (Casini et al., 2009), and in whole hearts either through application of caffeine (Zhang et al., 2009), previously shown to increase diastolic Ca^{2+} release, or mutations associated with diastolic Ca^{2+} release (Glukhov et al., 2013; King et al., 2013 b; Li et al., 2014; Ning et al., 2016 a). Diastolic Ca^{2+} transients have been demonstrated in myocytes from *Pgc-1β*$^{-/-}$ hearts (Gurung et al., 2011 a), thus presenting a further mechanism through which $(dV/dt)_{max}$ may be reduced.

Additionally, slow AP conduction in *Pgc-1β*$^{-/-}$ hearts was also reflected in measurements of AP latencies. These increased with ageing in WT hearts despite similar values of $(dV/dt)_{max}$ in young and aged hearts. In contrast, AP latency times were prolonged in *Pgc-1β*$^{-/-}$ hearts to an even greater degree, with no difference in young and aged hearts. *Pgc-1β*$^{-/-}$ hearts showed longer latencies than WT hearts during both regular pacing and at the longest S1-S2 coupling intervals without effects of age or its interactions with genotype. AP latencies increased with falling S1-S2 intervals preserving their relative magnitudes between groups. However, at the shortest S1-S2 intervals interactive effects of genotype and age appeared to result in significantly shorter AP latencies in young WT hearts than the remaining groups. The latter differences between $(dV/dt)_{max}$ and AP latency properties with PES were explored by comparing dependences of AP latency upon $(dV/dt)_{max}$ between groups. AP latencies consistently increased with falling $(dV/dt)_{max}$ values in APs obtained in response to the extrasystolic S2 stimuli during PES as expected from established relationships between Na^+ currents, $(dV/dt)_{max}$ and conduction velocity (Hunter et al., 1975). However, young and aged

WT hearts displayed two separate plots reflecting consistently greater AP latencies at any given $(dV/dt)_{max}$, in aged compared to young WT. In contrast, both young and aged *Pgc-1β*$^{-/-}$ fell on similar functions that resembled those obtained in aged as opposed to young WT hearts.

The latter differences were tested in terms of suggestions that whereas $(dV/dt)_{max}$ primarily reflects discharge of the cardiomyocyte membrane capacitance by sodium current, AP conduction velocity is further influenced by increases or decreases in tissue resistance and capacitance (Jeevaratnam et al., 2011; King et al., 2013 a). Previous reports had associated such conduction changes with progressive myocardial fibrosis with age in various animal (Eghbali et al., 1989; Orlandi et al., 2004; Lin et al., 2008; Jeevaratnam et al., 2012, 2016) and human studies (Gazoti Debessa et al., 2001). Histological results at least partly confirmed such a hypothesis. Age and genotype then independently resulted in increased ventricular fibrosis ($p < 0.05$ for both), with no evidence of effects of age-genotype interaction. There was thus increased fibrotic change in aged compared to young WT hearts, but also increased fibrotic change in *Pgc-1β*$^{-/-}$ hearts in which fibrotic levels in young *Pgc-1β*$^{-/-}$ hearts reached those shown by aged WT hearts.

These findings at the tissue level fulfil predictions from previous evidence for cellular roles for mitochondrial ROS in fibrotic change (Weiss et al., 1989; Wang et al., 2004; Terentyev et al., 2008; Brown and O'Rourke, 2010; Liu et al., 2010 b; Bovo et al., 2012). Mitochondrial targeted catalase overexpression protected transgenic mice from features of cardiac ageing including myocardial fibrosis (Dai et al., 2009). Conversely, mice lacking mitochondrial sirtuin SIRT3 demonstrated increased mitochondrial ROS production and cardiac fibrosis (Hafner et al., 2010). Finally, TGF-β activity, thought involved in age-related myocardial fibrosis (Brooks and Conrad, 2000; Rosenkranz et al., 2002; Guzadhur et al., 2010; Hao et al., 2011; Davies et al., 2014) is enhanced by oxidative stress (Barcellos-Hoff and Dix, 1996; Sullivan et al., 2008 b). Such fibrotic change could disrupt gap junction function increasing tissue resistance (Xie et al., 2009). It could also increase fibroblast-cardiomyocyte coupling through Cx43 and Cx45, and

the consequent effective membrane capacitances (Camelliti et al., 2004; van Veen et al., 2005; Chilton et al., 2007). The mitochondrial dysfunction in *Pgc-1β*$^{-/-}$ hearts could also potentially directly impair gap junction function through elevating intracellular [Ca^{2+}] (De Mello, 1983) or cause oxidative stress induced alterations in connexion phosphorylation (Sovari et al., 2013).

No differences in APD_{90}, APD_{70}, APD_{50} or APD_{30} were observed between groups. These parameters are in turn surrogates of APD, which is difficult to measure as it approaches the baseline RMP asymptotically. Thus all these parameters may be taken as measuring a corollary of APD, though as the percentage of repolarisation measured shortens, the relative contribution of the various channels in the murine action potential (Figure 1-1) varies, with a greater contribution of the plateau period, Ca^{2+} and I_{to} currents at shorter APD percentages.

Although both young and aged *Pgc-1β*$^{-/-}$ hearts showed shorter effective refractory periods (ERPs) than WT, particularly aged WT hearts. Although ERP shortening is often accompanied by corresponding reductions in APD (Davidenko and Antzelevitch, 1986; Lee et al., 1992), this need not be the case in all circumstances and indeed discordant alterations in APD and ERP have been reported previously (Martin et al., 2011 a). At all events, this ERP shortening would be consistent with increased likelihoods of re-entry in the *Pgc-1β*$^{-/-}$ hearts.

Finally the AP wavelength, expressed as a product of AP activation and recovery terms, has been used as a criterion for pro-arrhythmic tendency. Wavelength has been postulated to be an important parameter in arrhythmic theory. Longer and shorter wavelengths respectively correspond to reduced or increased likelihood of re-entry (Davidenko et al., 1995; Zaitsev et al., 2000; Weiss et al., 2005; Matthews et al., 2013 a; Pandit and Jalife, 2013; Spector, 2013). Shorter wavelengths are presumed to have more pro-arrhythmic potential, as it allows for re-entry of excitation in a circuitous manner; circus movement re-entry occurs when an activation wavefront propagates around an anatomic or functional (e.g. refractory myocardium) obstacle or core, and re-excites the site of origin (Antzelevitch and Burashnikov,

2011). In this type of re-entry, all cells take turns in recovering from excitation so that they are ready to be excited again when the next wavefront arrives. The stability of this kind of re-entrant arrhythmia is determined by the fact that the circuit is longer than the wavelength of the electrical impulse, leaving an excitable gap between head and tail of the circulating wave to allow re-excitation. Shorter wavelengths are thus more pro-arrhythmic as they allow for a longer excitable gap. Cardiac fibrosis may can exacerbate this excitable gap between the head and tail of a circulating wave in a number of ways. Firstly, if the fibrosis is local and dense it can be an anatomical block for a re-entrant circuit to propagate around. Secondly, it may slow conduction velocity by increasing tissue resistivity, disrupt gap junction function and therefore shorten wavelength.

The experimental configuration employed to determine wavelength entailed uncertainty in measuring conduction velocity owing to corresponding uncertainty concerning the path taken by the depolarising wave. The experimental technology to map multiple areas of myocardium simultaneously exists to a limited degree for the surface myocardium/epicardium – however there is no method in existence to map the conduction path in an intra-mural course and this yields a degree of uncertainty over the true conduction path and conduction length between hearts if they contain anatomic heterogeneities which may impact upon the conduction path. Similarly, ERP measurements reflect AP recovery from refractoriness over the entire line of tissue *between* stimulus and recording sites, and any heterogeneities in either ERP or of effective AP conduction along this pathway (Martin et al., 2011 a). Furthermore, in contrast to the *absolute* refractory period, ERP depends upon the value of the effective stimulus intensity at the site of membrane excitation (Duehmke et al., 2012). Nevertheless, the present estimates employed two separate conduction velocity measures of $(dV/dt)_{max}$ and the reciprocal of AP latency and ERPs were obtained under conditions of applied stimuli amplitudes consistently scaled relative to the observed AP thresholds. Wavelengths derived from $(dV/dt)_{max}$ would incorporate electrophysiological properties at the single cell level whereas wavelengths derived from AP latency would further include contributions from cardiomyocyte coupling resulting from tissue fibrosis. Both measures demonstrated lower values in *Pgc-1β*$^{-/-}$ compared to WT hearts but no effects of either age or interactions between

age and genotype. However, in post hoc analysis of wavelengths derived from AP latencies, aged WT hearts showed significantly higher values than young *Pgc-1β*$^{-/-}$ hearts but not aged *Pgc-1β*$^{-/-}$ hearts, accounting for the observed differences in the arrhythmic incidences.

However despite the initial elegance of such a wavelength based theory of arrhythmia, there are a number of gaps that should be highlighted. Firstly, the theory should mean that there is a minimal myocardial volume necessary for arrhythmia – yet structures such as murine atria were long thought not to have sufficient volume for sustained arrhythmia as the wavelength of excitation is in the same order of magnitude as the size of the entire atria. It was thus proposed that there needed to be a critical cardiac mass for sustained arrhythmias (Janse and Rosen, 2006) but this has also been demonstrated to be insufficient to explain arrhythmogenesis (Vaidya et al., 1999). Many studies have shown that murine atria can sustain arrhythmia rendering such analyses oversimplified at best or incorrect at worst (Riley et al., 2012; Huang, 2017 b). Thus it is evident that while wavelength may be part of arrhythmic theory it is not sufficient to explain arrhythmia, not least in small mammals.

Further limitations of the study centre around the use of Langendorff perfused heart studies, which are routinely used in the domain of cardiac electrophysiology. However, it must be borne in mind that despite its widespread adoption, the Langendorff heart has a number of important limitations which do impact upon the study. The Langendorff preparation is designed to emulate a physiological state as far as possible, with a whole intact organ perfused by its natural vasculature through retrograde filling of the coronary arteries. However, the perfusion is not completely physiological – firstly the perfusate is typically a crystalloid solution such as Krebs-Henseleit or Tyrode's solution. Thus the oxygen carrying capacity of such a perfusate is limited compared to blood. The perfusate requires continuous gasification (typically with 95% O_2/5% CO_2 carbogen) to increase oxygen concentration to a point which allows a stable, non-hypoxic, preparation. Despite this, the oxygen carrying capacity is limited, and could potentially compound experiments in which mitochondrial function (which in turn impacts upon oxidative phosphorylation) is being examined. This is mitigated somewhat by

ensuring all experimental hearts are exposed to the same conditions, though does not rule out hearts with mitochondrial dysfunction being more sensitive to such experimental conditions and thus over-estimating the effect of electrophysiological changes attributed to mitochondrial dysfunction .

Conversely, the use of blebbistatin in our experiments reduces the energetic requirements of the heart and in turn oxygen requirements. Again, as the experimental protocol is standardised, the magnitude of the effect could be postulated to be identical across all groups – and would in fact tend to underestimate the magnitude of any arrhythmic effect in mitochondrial dysfunction (i.e *Pgc-1β*$^{-/-}$ mice) in any statistical analysis. The use of blebbistatin itself is widespread in cardiac electrophysiology optical mapping studies with suggestions of minimal electrophysiological effect, importantly having no effect on calcium transients unlike other electromechanical uncouplers (Fedorov et al., 2007; Physiology et al., 2010). However, it cannot be assumed to be completely inert in term of its electrophysiological effect, as a number of studies have postulated that electromechanical feedback is an important factor in arrhythmogenesis (ter Keurs, 2011; Wall et al., 2012). Further, a single study has found that there are electrophysiological changes associated with its use in rabbit hearts (though making it more difficult to provoke arrhythmia) (Brack et al., 2013).

Overall these findings extend initial studies on the *Pgc-1β*$^{-/-}$ model at the cellular level to obtain electrophysiological evidence for increased arrhythmic substrate under conditions of chronic mitochondrial deficiencies. They then attribute this predominantly to decrements in measures of AP conduction, as reflected in $(dV/dt)_{max}$ and AP latency, and demonstrate this is accompanied by increased fibrotic change with age in *Pgc-1β*$^{-/-}$ mice.

5. EFFECTS OF AGEING ON PRO-ARRHYTHMIC VENTRICULAR PHENOTYPES IN INCREMENTALLY PACED MURINE *Pgc-1β*$^{-/-}$ HEARTS

5.1 INTRODUCTION

Previous studies on models of monogenic ion channel disorders have studied action potential (AP) waveforms and their stability in isolated Langendorff-perfused hearts subjected to episodes of regular pacing at progressively decremented basic cycle lengths (BCLs) (Sabir et al., 2007 b; Matthews et al., 2013 c). Monophasic action potential (MAP) recordings provided indications of AP latencies, durations (APDs) and refractory periods. They also provided evidence as to whether alternans in AP characteristics, occurred with decreasing BCLs (Ning et al., 2016 a). Alternans is defined by the alternation of an AP characteristic between successively lower and higher values (for at least ten successive beats in this study – see methods) and has been established as presaging arrhythmia in clinical and experimental situations (Rosenbaum et al., 1994; Gold et al., 2000). These instabilities could be analysed in terms of restitution analyses (Nolasco and Dahlen, 1968), a theoretical construct to assess AP recovery properties through dependences on APDs and diastolic intervals (DI) (Sabir et al., 2008 a, 2010; Matthews et al., 2012). Similarly, AP activation or propagation properties have been assessed through an adaptation of restitution analysis (Martin et al., 2012 a; Huang, 2017 b), by calculation of an AP wavelength parameter and through construction and comparisons of active and resting AP wavelengths (Matthews et al., 2013 c). Together, these separated arrhythmic phenotypes arising from alterations in recovery properties in *Scn5a*$^{+/\Delta KPQ}$ and hypokalaemic hearts (Killeen et al., 2007; Sabir et al., 2007 c) from those attributed to compromised AP activation and conduction in *Scn5a*$^{+/-}$ hearts (Martin et al., 2011 a; b).

The present study extends these analyses to the *Pgc-1* model of mitochondrial dysfunction in an exploration of the electrophysiological consequences of energetic dysfunction. It explores whether the various wavelength characteristics of *Pgc-1β*$^{-/-}$ mice offer further insight into the arrhythmic characteristics seen in earlier chapters, as well as calculation of active and resting wavelength parameters to explore the concordance of these arrhythmic models with the present findings.

5.2 RESULTS

We performed simultaneous electrocardiographic (ECG) whole heart recordings and action potential (AP) measurements from single cardiomyocytes in intact ex-vivo Langendorff-perfused hearts. Each procedure began with a programmed electrical stimulation protocol interposing extrasystolic (S2) stimuli at successively decremented intervals following trains of 8 regular (S1) stimuli applied at a 125 ms basic cycle length (BCL). Overall ventricular electrical activity through the S1S2 protocol was monitored by the ECG recordings. Analysis of these initial recordings yielded ventricular effective refractory periods (VERPs) that indicated the extent to which BCLs could be decreased in the succeeding experiments. A comparison of VERPs in young and aged, WT (57.36 ± 2.06 and 56.3 ± 1.96 ms , (n = 23) and (n = 19) respectively) and *Pgc-1β*$^{-/-}$ hearts (53.99 ± 2.2 and 47.64 ± 1.84 ms (*n* = 21) and (*n* = 25) respectively), demonstrated that *Pgc-1β*$^{-/-}$ hearts showed shorter VERPs than WT hearts (56.88 ± 1.42 vs 50.54 ± 1.48 ms; (n = 42 vs 46); $p < 0.01$), without effects of either age or interactions between age and genotype.

Intracellular microelectrode recordings of cardiomyocyte APs within left ventricular epicardia were then obtained in parallel with ECG recordings of isolated Langendorff hearts during an incremental pacing protocol. Trains of 100 regular stimuli were imposed at BCLs progressively shortened by 5 ms with each successive stimulus train. These examined for the presence of arrhythmic activity and alternans in AP parameters related to their activation or recovery. Figure 5-1 tracks the progress of the experiments through the incremental pacing protocol in

all four groups, using Kaplan-Meier plots of the probability of hearts showing regular 1:1 evoked activity with decreasing BCL. Quantitative analysis was performed for BCLs up to 55 ms, after which insufficient hearts showed regular 1:1 capture for analysis. The BCL at which hearts failed to follow the repetitive pacing and entered 2:1 block reflect their VERP at that particular pacing rate. A log rank test demonstrated that the Kaplan-Meier curves from the different experimental groups (Figure 5-1) showed significant differences from each other ($p < 0.01$). VERPs at the termination of the protocol (young WT: 64.35 ± 2.16 ms, (n = 23); aged WT: 61.84 ± 2.33 ms (n = 19); young *Pgc-1β*$^{-/-}$: 68.33 ± 1.26 ms (n = 21); aged *Pgc-1β*$^{-/-}$ hearts: 61.0 ± 1.83 ms (n = 25)) were obtained from the BCLs achieved just prior to the onset of 2:1 atrioventricular conduction block.

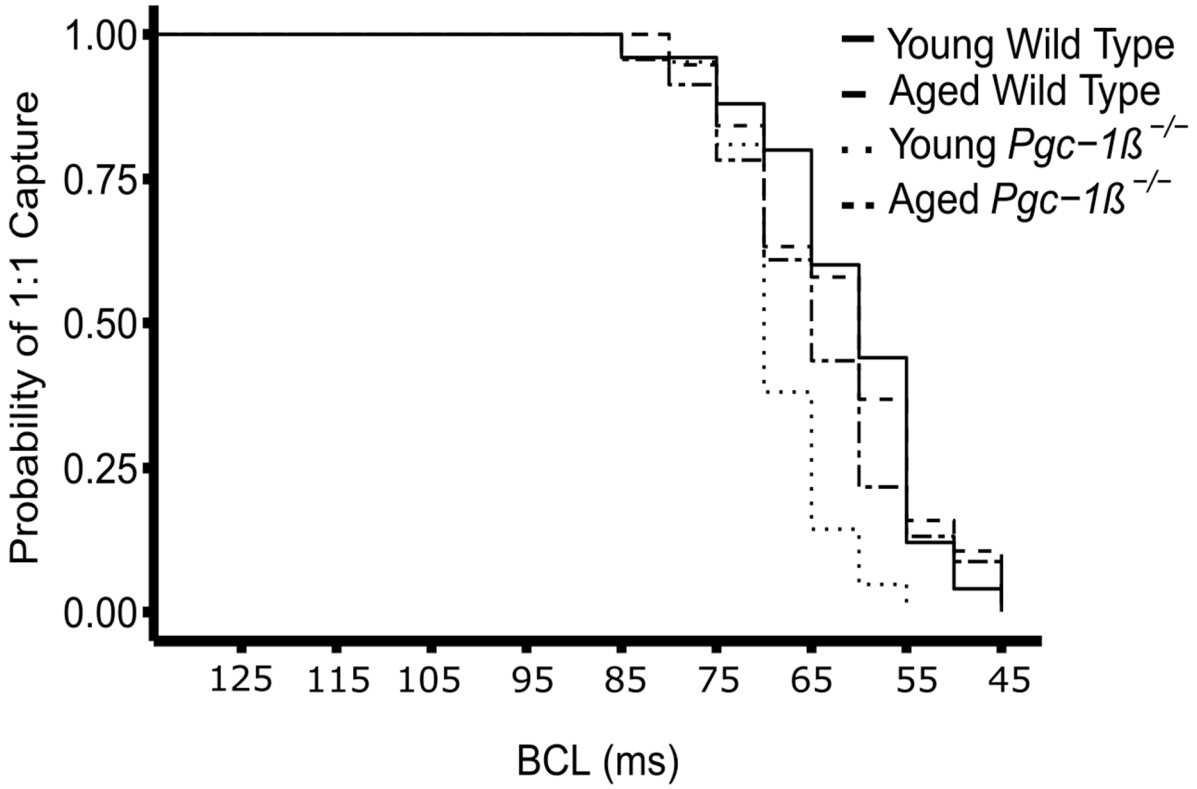

Figure 5-1: Kaplan-Meier plot of 1:1 capture. *Kaplan-Meier plot of the proportion of young and aged WT and Pgc-1β*$^{-/-}$ *hearts showing regular activity with increasing pacing frequency with the progressive fall off at higher pacing frequencies resulting in hearts losing capture and entering either 2:1 conduction block or arrhythmia. Total sample size: young WT (n = 23), aged WT (n = 19), young Pgc-1β*$^{-/-}$ *(n = 21) aged Pgc-1β*$^{-/-}$ *(n = 25).*

5.2.1 AGE-DEPENDENT ARRHYTHMIC PHENOTYPES IN PGC-1B$^{-/-}$ *HEARTS*

Figure 5-2 exemplifies traces of normal, arrhythmic and pro-arrhythmic activity from all four experimental groups obtained in the course of the incremental pacing protocol. Under these experimental conditions, there were no observations of spontaneous early or delayed after-depolarizations. The latter have been reported in other pro-arrhythmic murine systems where they have been implicated in arrhythmic triggering (Balasubramaniam et al., 2004, 2005; Goddard et al., 2008 b). Figure 5-2 compares parallel ECG (i) and intracellular AP recordings (ii) of regular activity at a BCL of 130 ms in ventricles from a young WT mouse (A). Similar simultaneous ECG (i) and intracellular AP recordings (ii) recordings made it possible to detect ectopic beats (B), monomorphic ventricular tachycardia (VT) (C) and torsades de pointes (TdP - an uncommon and distinctive form of polymorphic VT characterized by a gradual change in the amplitude of the ventricular complexes and their twisting around the isoelectric baseline) (D) in aged *Pgc-1β*$^{-/-}$ hearts. The intracellular recordings at expanded time bases made it possible to discern alternans in APD (E) and both maximal AP upstroke rate, $(dV/dt)_{max}$ and APD (F) in *Pgc-1β*$^{-/-}$ hearts.

Table 5-1 quantifies the occurrence of arrhythmic phenomena in cardiomyocytes from which the intracellular records were obtained. Aged *Pgc-1β*$^{-/-}$ hearts showed the highest arrhythmic incidences compared to the remaining groups ($p < 0.05$). The latter groups showed similar, reduced, arrhythmic frequencies. Aged *Pgc-1β*$^{-/-}$ hearts were also the only experimental group that showed ectopic activity, monomorphic VT and polymorphic VT (Fig. 2B, C, D). The incidence of arrhythmias in hearts from young *Pgc-1β*$^{-/-}$ hearts was not distinguishable from their WT counterparts.

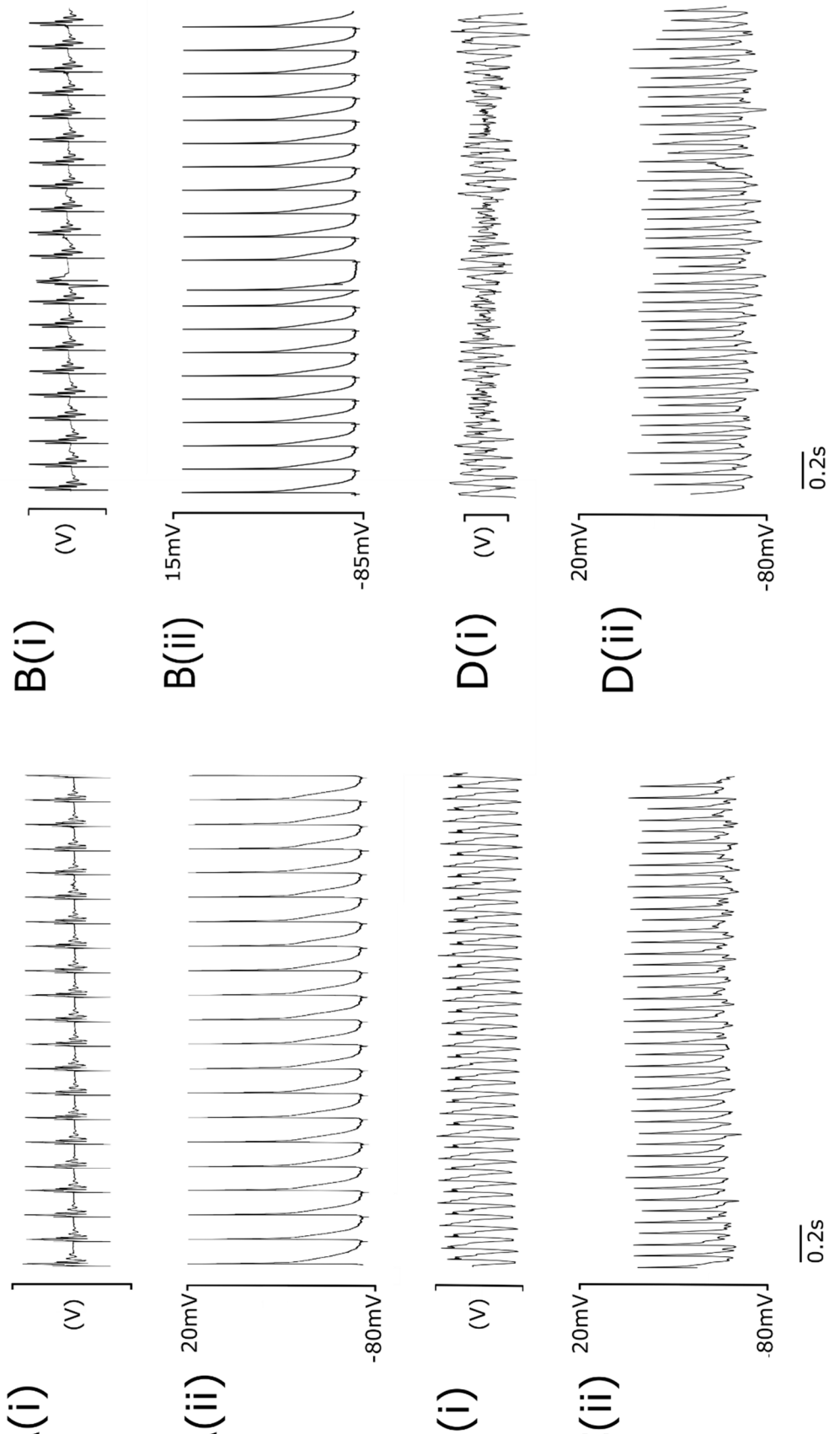

Figure 5-2: Parallel ECG and intracellular AP recordings from incrementally paced hearts.

A–D *Parallel ECG (i) and intracellular AP recordings (ii) of regular activity at a 130 ms BCL in ventricles from a young WT mouse* ***(A)****, an ectopic beat* ***(B)****, monomorphic VT* ***(C)*** *and torsades de pointes (TdP)* ***(D)*** *in aged Pgc-1β* $^{-/-}$ *hearts*

Table 5-1: *Frequency of arrhythmia in the various experimental groups.*

	Arrhythmic	Non Arrhythmic	Total (n)	Percentage Arrhythmic
Young WT	4	19	23	17.4
Aged WT	3	16	19	15.8
Young *Pgc-1β*$^{-/-}$	4	17	21	19.0
Aged *Pgc-1β*$^{-/-}$	12*	13	25	48*

* denotes a significance level of $p < 0.05$ using a fisher exact test

Figure 5-3 exemplifies the different forms of alternans in AP characteristics observed in a typical aged *Pgc-1β*$^{-/-}$ heart. Each panel displays (from top to bottom) AP waveforms, AP latencies, the first derivative, d*V*/d*t,* of the AP waveform, APD_{90} and RMP respectively. This makes it possible to directly visualize alternans in one or more electrophysiological parameters. The panels demonstrate the possible combinations of alternans involving activation or recovery parameters. Thus, the alternans in (A) involves the recovery variable of APD_{90} alone while (B) demonstrates alternans in the activation variables of AP latency and $(dV/dt)_{max}$ alone. In contrast, (C) and (D) exemplify simultaneous alternans involving both activation and recovery variables. They include the extreme situations resulting in alternate high/low latencies (and therefore low/high $(dV/dt)_{max}$) simultaneously associated with high/low APD_{90} (C) or low/high APD_{90} (D). The second case (D) would correspond to the most pro-arrhythmic situation. The bottom control trace shows the (relatively constant) resting potentials through the alternans phenomena.

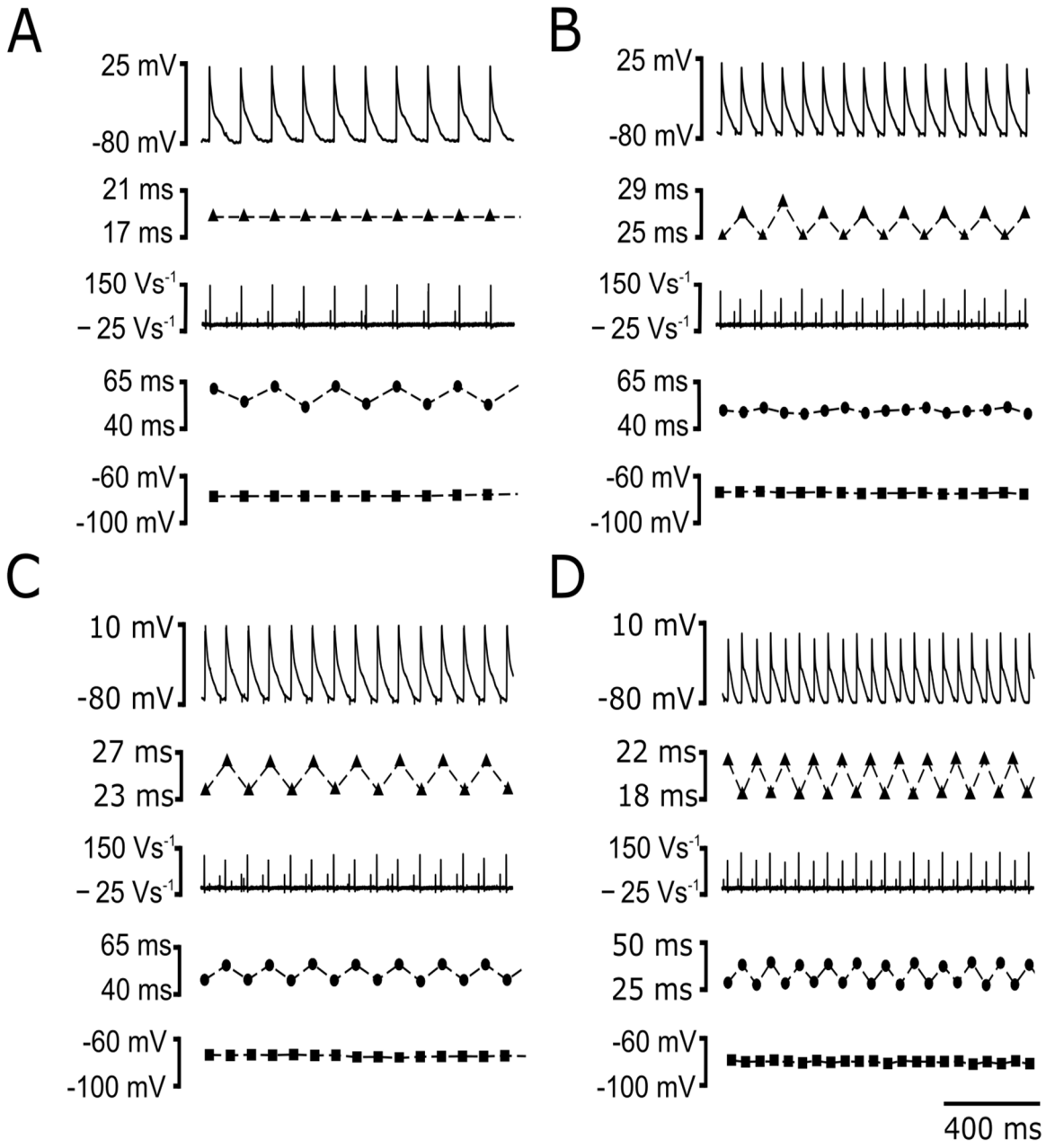

Figure 5-3: Alternans phenomena. *Examples of alternans phenomena comparing records of AP waveform, AP latency, (dV/dt), APD_{90} and RMP respectively in each panel. In (A), alternans exclusively involves the recovery variable APD_{90} while in (B), it involves the activation variables of AP latency and (dV/dt) alone. In (C) and (D), there is simultaneous alternans involving both activation and recovery variables. These include situations in which the alternating action potentials with higher/lower latencies and therefore lower/higher $(dV/dt)_{max}$ show either higher/lower (C) or lower/higher (D) APD_{90}, respectively*

5.2.2 INCREASED FREQUENCIES OF ALTERNANS IN PGC-1B$^{-/-}$ *HEARTS*

The presence of alternans in one or more AP characteristics with variations in BCL is an established marker for the instability presaging development of arrhythmia. We first compared the number of beats showing alternans in maximum AP upstroke rate $(dV/dt)_{max}$ (Fig. 5-4A), AP latency (Fig. 5-4B), AP duration to 90% recovery (APD_{90}) (Fig. 5-4C) and resting membrane potential (RMP) (Fig. 5-4D) in young and aged, WT and *Pgc-1β*$^{-/-}$ hearts through the incremental pacing protocol described above.

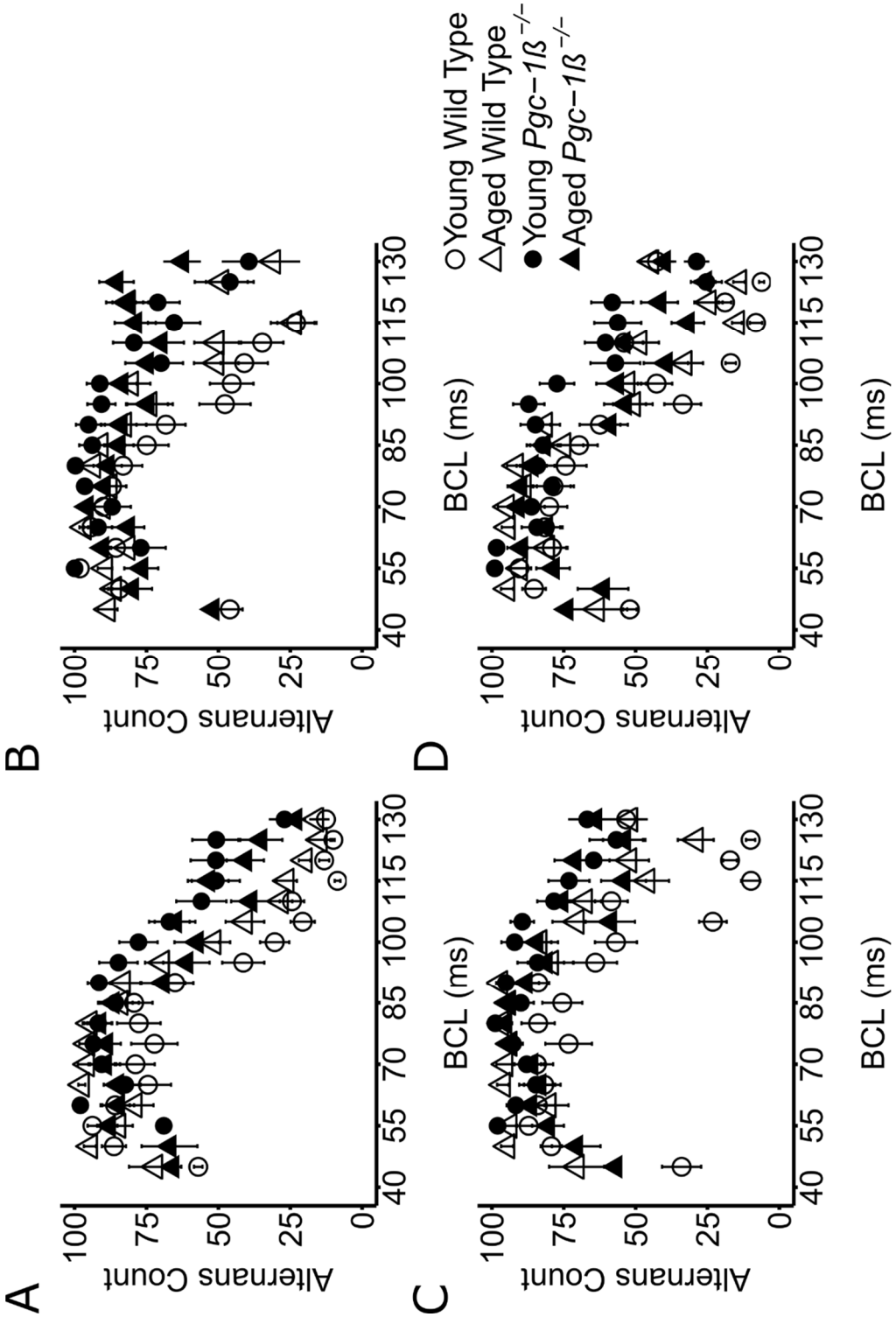

Figure 5-4: Incidence of alternans. *Incidence of alternans out of 100 beats at each BCL in the activation variables of maximum AP upstroke rate $(dV/dt)_{max}$ (a), AP latency (b), and the recovery variables of AP duration to 90% recovery (APD_{90}) (c) and resting membrane potential (RMP) (d) in young and aged, WT and Pgc-1β $^{-/-}$ hearts through the incremental pacing protocol*

Overall incidences of alternans were obtained for each heart by summing the number of beats of alternans at each BCL examined. The results were then compared between experimental groups. *Pgc-1β*$^{-/-}$ hearts showed greater overall incidences of alternans compared to WT hearts in all the parameters $(dV/dt)_{max}$, AP latency, APD_{90} and RMP. Thus, both young and aged *Pgc-1β*$^{-/-}$ hearts displayed an increased tendency to display alternans (Table 5-2).

Table 5-2: *Results of ANOVA comparisons of alternans features in Pgc-1β*$^{-/-}$ *and WT hearts. Values represent number of beats out of 1600 beats.*

	AP parameter	*Pgc-1β*$^{-/-}$	WT	p-value
Overall incidences of alternans (beats)	$(dV/dt)_{max}$	872 ± 42	659 ± 41	$p < 0.0001$
	AP latency	928 ± 49	672 ± 35 ;	$p < 0.001$
	APD_{90}	1089 ± 40	868 ± 46	$p < 0.001$
	RMP	852 ± 42	694 ± 44	$p = 0.01$
Maximum duration of alternans episodes (beats)	$(dV/dt)_{max}$	535 ± 41	404 ± 36	$p < 0.05$
	AP latency	611 ± 46	456 ± 34	$p < 0.01$
	APD_{90}	682 ± 57	509 ± 44	$p < 0.05$
	RMP	417 ± 35	312 ± 32	$p < 0.05$

Secondly, in addition to the above effects of genotype alone, genotype and age exerted interacting effects on the incidence of AP latency alternans ($p < 0.05$) and APD_{90} alternans ($p < 0.05$). Young WT hearts had the lowest incidences of AP latency alternans (575 ± 51 beats) with progressive increases in this incidence through the series: young *Pgc-1β*$^{-/-}$ hearts (785 ± 78 beats), aged WT hearts (790 ± 33 beats) and aged *Pgc-1β*$^{-/-}$ hearts (923 ± 81 beats), with the last group showing the greatest amount of AP latency alternans. Post hoc testing

demonstrated significantly more AP latency alternans in young *Pgc-1β*$^{-/-}$ hearts compared to young WT hearts ($p < 0.01$) and aged *Pgc-1β*$^{-/-}$ hearts compared to young WT hearts ($p < 0.001$). A similar pattern emerged in post hoc testing for APD_{90} alternans: all remaining groups showed significantly more alternans than young WT hearts (young WT vs young *Pgc-1β*$^{-/-}$:726 ± 65 beats vs 1068 ± 53 beats, $p < 0.001$; young WT vs aged WT: 726 ± 65 beats vs 1040 ± 37 beats, $p = 0.001$; young WT vs aged *Pgc-1β*$^{-/-}$: 726 ± 65 beats vs 1107 ± 60 beats; $p < 0.0001$).

5.2.3 Alternans at longer BCLs, with longer episodes, and involving multiple AP parameters in Pgc-1β$^{-/-}$ *hearts*

Fig. 5-4 also displays the distribution of alternans in each parameter across different BCLs for each experimental group. It is apparent that there are greater incidences of alternans at longer BCLs in *Pgc-1β*$^{-/-}$ hearts than WT hearts. This suggests that they have a greater tendency to instability even at lower heart rates. In addition to the absolute burden of alternans described previously, we quantified the number of discrete sequences of alternans per protocol, the maximum duration of alternans as well as the amount of simultaneous alternans between multiple parameters.

First, there were no distinguishable differences in the number of discrete episodes of alternans in $(dV/dt)_{max}$, APD_{90} or RMP between young and aged, *Pgc-1β*$^{-/-}$ and WT hearts. In contrast, aged *Pgc-1β*$^{-/-}$ hearts showed a higher number of discrete runs of AP latency alternans than young WT hearts (11.0 ± 1.24 vs 7.43 ± 0.58 runs of alternans; $p < 0.05$).

Secondly, the maximum duration of individual alternans episodes, whether involving $(dV/dt)_{max}$, AP latency, APD_{90} or RMP, were significantly longer in *Pgc-1β*$^{-/-}$ hearts than in WT hearts. The maximum duration of alternans episodes involving AP latency also showed significant interactive effects of age and genotype ($p < 0.05$). Post hoc testing demonstrated

that young *Pgc-1β*$^{-/-}$ hearts showed longer durations of AP latency alternans than young WT hearts (683 ± 62 beats vs 406 ± 50 beats $p < 0.01$).

Thirdly, alternans simultaneously involving different AP characteristics were observed within the same heart. This could involve situations in which the alternating high/low AP latencies or reduced/increased $(dV/dt)_{max}$ coincided with higher/lower APD_{90} values (Fig. 5-3C), or in the more pro-arrhythmic pattern, occurred out of phase with higher/lower APD_{90} values (Fig. 5-3D). *Pgc-1β*$^{-/-}$ hearts showed more frequent simultaneous $(dV/dt)_{max}$ and APD_{90} alternans compared to WT hearts (72.15 ± 2.22% vs 64.97 ± 3.03% of beats respectively; $p = 0.05$), with similar occurrences of both patterns of alternans. *Pgc-1β*$^{-/-}$ hearts also showed more frequent simultaneous APD_{90} and AP latency alternans (74.03 ± 2.92% vs 65.11 ± 2.61% of beats; $p < 0.05$). In this case a greater number of beats assumed the more pro-arrhythmic pattern (697 ± 58 beats vs 537 ± 43 beats; $p < 0.05$). The incidence of the more pro-arrhythmic pattern of alternans was also significantly affected by interactions between age and genotype ($p < 0.05$). Post-hoc Tukey tests demonstrated that young *Pgc-1β*$^{-/-}$ hearts showed higher incidences of simultaneous alternans than young WT hearts ($p = 0.01$).

Finally, we quantified the amplitude of alternans where this occurred, by calculating the mean differences between successive peak and trough values in each parameter. These findings contrastingly demonstrated no significant variations between groups.

5.2.4 Altered action potential characteristics in young and aged Pgc-1β$^{-/-}$ *hearts*

These differences in electrophysiological stability and pro-arrhythmic tendency were then correlated with differences in AP activation and recovery characteristics over the range of BCLs explored. Fig. 5-5 plots the activation variables of $(dV/dt)_{max}$ (A) and AP latency (B) as well as the recovery variables of APD_{90}, (C) RMP (D), as well as diastolic interval, DI, (given by the time between the action potential peak and the preceding APD_{90}) (E) against BCL in young and

aged, *Pgc-1β*$^{-/-}$ and WT hearts. All data varied monotonically with BCL and so their overall magnitudes could be compared by the areas beneath their curves. Table 5-3 demonstrates that hearts with the *Pgc-1β*$^{-/-}$ genotype have lower $(dV/dt)_{max}$ values and increased AP latencies relative to WT (both $p < 0.001$). However, there were no detectable effects of either ageing or any interaction between genotype and ageing on $(dV/dt)_{max}$. In contrast, neither APD_{90} nor RMPs were influenced by genotype alone. However, APD_{90} was longer in aged *Pgc-1β*$^{-/-}$ hearts than young *Pgc-1β*$^{-/-}$ hearts ($p < 0.05$), and RMP greater in aged than young hearts.

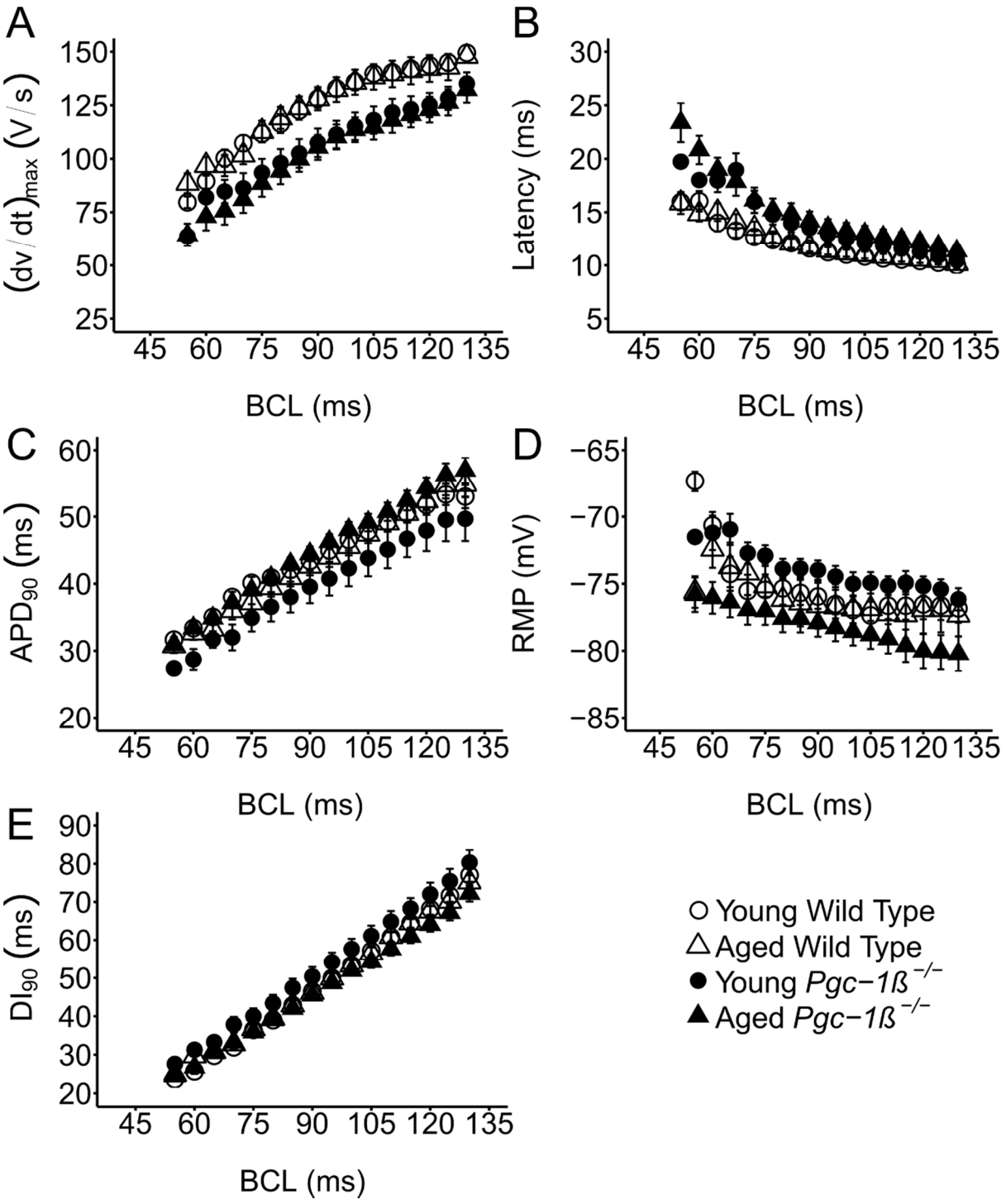

Figure 5-5: Variation of AP parameters with basic cycle length. *Dependence of maximum rate of AP depolarization, $(dV/dt)_{max}$ (a), AP latency (b), APD_{90} (c), RMP (d) and DI (e) on BCL in young and aged, WT and Pgc-1β hearts (n = 23; n = 19; n = 21; n= 25 respectively).*

Table 5-3: *Areas under the curves (AUC) of AP parameter with respect to BCL.*

Parameter	All WT	Young WT	Aged WT	All *Pgc-1β*$^{-/-}$	Young *Pgc-1β*$^{-/-}$	Aged *Pgc-1β*$^{-/-}$	All Young	All Aged
$(dVdt)_{max}$ (mV)	8719.17 ± 241.3***	8644.38 ± 315.86	8809.71 ± 380.44	7202.22 ± 323.25***	7118.87 ± 429.06	7272.23 ± 480.81	7916.3 ± 284.69	7936.14 ± 336.1
APD_{90} (ms^2)	3025.52 ± 77.85	3049.12 ± 111.58	2996.97 ± 109.6	2938.67 ± 101.34	2658.59 ± 153.61†	3173.94 ± 117.74†	2862.73 ± 97.22	3097.52 ± 82.14
DI_{90} (ms^2)	3425.62 ± 86.84	3432.78 ± 85.07	3416.96 ± 165.08	3470.24 ± 110.69	3608.28 ± 174.96	3354.29 ± 140.05	3516.54 ± 94.39	3381.35 ± 105.68
AP Latency (ms^2)	815.11 ± 29.12***	797.85 ± 38.96	836.02 ± 44.48	994.64 ± 54.38***	970.68 ± 80.8	1014.77 ± 74.79	880.33 ± 45.04	937.58 ± 48.1
RMP (mV)	-5214.08 ± 114.15	-5148.33 ± 149.22	-5293.68 ± 178.95	-5144.06 ± 133.21	-4768.19 ± 91.03	-5459.8 ± 215.23	-4966.9 ± 92.91‡	-5388.06 ± 143.66‡

Table represents the overall magnitude of each parameter across the different experimental categories. Values were obtained by calculating the area under the curves for each parameter in each heart and then means and standard errors calculated. Results of statistical tests are shown. Each symbol represents statistical results from ANOVA; *** denote $p < 0.001$ for independent effects of genotype; ‡ denote $p < 0.05$ for independent effects of age; † denote $p < 0.05$ for interacting effects of genotype and age

5.2.5 WAVELENGTH AS THE BASIS FOR ARRHYTHMIC SUBSTRATE

The findings above demonstrate pro-arrhythmic features in aged *Pgc-1β*$^{-/-}$ hearts. Further quantification demonstrated increased alternans in both young and aged *Pgc-1β*$^{-/-}$ hearts. This in turn correlated with altered AP activation characteristics as reflected in $(dV/dt)_{max}$ and AP latency, as opposed to the recovery characteristics, APD_{90} and RMP. The following analyses further tested the hypothesis that activation and not recovery parameters are the primary determinant of arrhythmia in this system.

First, hearts were stratified by arrhythmic and non-arrhythmic phenotypes, regardless of genotype or age. AP parameters observed prior to the onset of either arrhythmia or entry into 2:1 block were then compared. Arrhythmic hearts (n = 20) showed lower $(dV/dt)_{max}$ and longer AP latencies than non-arrhythmic hearts (n = 68) ($(dV/dt)_{max}$: 67.29 ± 6.85 V s^{-1} vs 87.66 ± 3.28 V s^{-1}, $p < 0.05$; AP latencies: 22.25 ± 1.50 ms vs 18.64 ± 0.88 ms, $p < 0.05$ respectively). Diastolic interval (DI_{90}) durations were calculated from the APD_{90} time to the next action potential peak, thus they were consequently altered as expected from the altered AP rise times (27.43 ± 1.53 ms vs. 31.54 ± 1.09 ms; $p < 0.05$). There were no significant differences between their APD_{90} (32.75 ± 1.22 ms and 34.79 ± 0.92 ms) and RMPs (-73.81 ± 1.16 mV vs. -73.60 ± 0.72 mV). These findings implicate AP activation rather than recovery parameters in the initiation of arrhythmia.

Secondly, previous reports have correlated alternans characteristics to arrhythmic tendency in both monogenic murine models as well as in clinical situations. Arrhythmic syndromes primarily attributed to repolarisation abnormalities, exemplified by the murine *Scn5a*$^{+/\Delta KPQ}$ model, were associated with alterations in the relationship between APD_{90} and VERP with varying DI (Sabir et al., 2008 a; Matthews et al., 2010, 2012). In contrast, arrhythmia attributed to altered conduction in *Scn5a*$^{+/-}$ hearts was associated with altered relationships between active AP wavelengths, λ, and BCL (Ning et al., 2016 a) or resting wavelength λ_0 (Matthews et

al., 2013 c). Figure 5-6 illustrates the outcome of analyses testing both assumptions. These demonstrated indistinguishable limiting slopes in restitution plots of APD_{90} against DI_{90} in all four experimental groups (Fig. 5-6A), in opposition to the prediction from the first hypothesis. We then proceeded to determine λ, calculated as the product of conduction velocity represented by 1/(AP latency) and the corresponding VERP at each BCL. This was derived by interpolating values from the VERP obtained during the S1S2 protocol at a BCL of 125 ms and from the VERP obtained from the BCL during incremental pacing prior to loss of 1:1 stimulus capture. Young and aged WT hearts showed similar λ-BCL and λ-λ_0 plots (Fig. 5-6B, C). However, *Pgc-1β*$^{-/-}$ hearts showed lower plateau λ values compared to WT hearts, particular with ageing. This would be consistent with the relative arrhythmic tendencies in the four experimental groups reported here. Further strengthening this hypothesis, the mean wavelengths immediately prior to termination of the protocol into either arrhythmia or 2:1 block were significantly different ($p = 0.01$) at 4.4 ± 0.31 ($n = 20$) for arrhythmic vs 5.4 ± 0.20 ($n = 68$) for non-arrhythmic hearts.

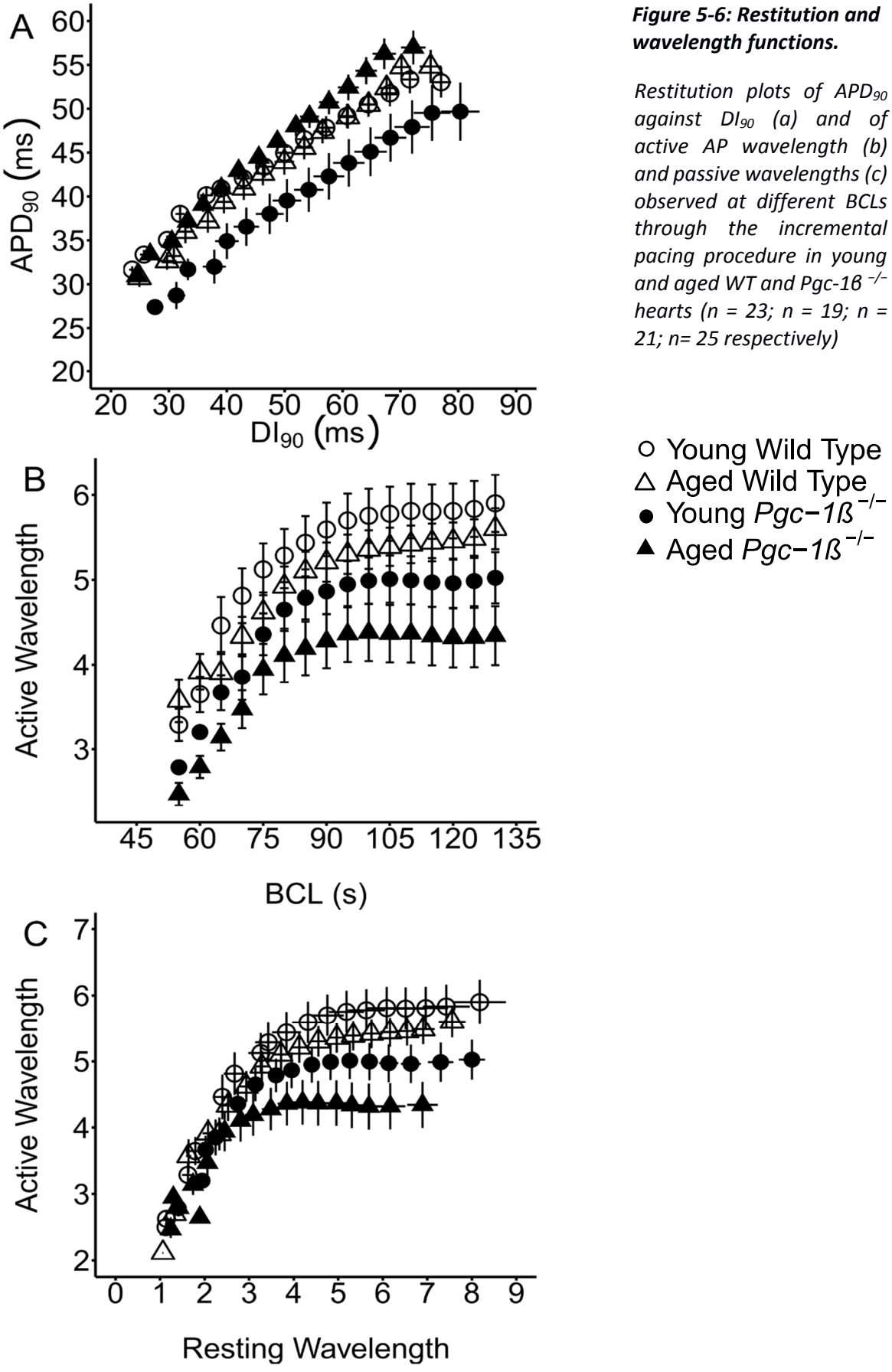

Figure 5-6: Restitution and wavelength functions.

Restitution plots of APD_{90} against DI_{90} (a) and of active AP wavelength (b) and passive wavelengths (c) observed at different BCLs through the incremental pacing procedure in young and aged WT and Pgc-1ß $^{-/-}$ hearts (n = 23; n = 19; n = 21; n= 25 respectively)

5.3 DISCUSSION

The present studies explored arrhythmic and pro-arrhythmic phenotypes and their evolution with age in murine hearts deficient in peroxisome proliferator activated receptor-γ coactivator-1β. PGC-1β upregulates cardiac mitochondrial mass and function, cellular metabolism (Lin et al., 2005; Finck and Kelly, 2006; Zamiri et al., 2014), and expression of nuclear and mitochondrial genes key to the tricarboxylic acid cycle, fatty acid β–oxidation and oxidative phosphorylation (Arany et al., 2005). *Pgc-1β*$^{-/-}$ hearts thus provided models to study effects of mitochondrial impairment on cardiac arrhythmia (Gurung et al., 2011 a). Such energetic dysfunction occurs in a number of common, age-dependent, acute and chronic, clinical situations (Vianna et al., 2006; Sato et al., 2009; Kucharska-Newton et al., 2010; Akar and O'Rourke, 2011) themselves constituting independent risk factors for major ventricular arrhythmias (Yeung et al., 2012; Adabag et al., 2015).

Previous studies had characterized arrhythmic phenotypes in murine models of specific human monogenic channelopathies. These analyses had attributed arrhythmic substrate variously to triggering events resulting in triggered AP firing (Balasubramaniam et al., 2004; Goddard et al., 2008 b), altered recovery from excitation (Killeen et al., 2007; Thomas et al., 2008) or to altered AP activation and propagation (Martin et al., 2012 a; Huang, 2017 b). Protocols imposing regular pacing at progressively incremented steady state heart rates determined the corresponding stability or instability of action potential (AP) characteristics and the onset of alternans (Sabir et al., 2008 a; Matthews et al., 2010, 2012). Alternans, whether involving electrocardiographic T-wave deflections or QT intervals, clinically correlates with eventual breakdown of the stable, normal pattern of electrical activity leading to major arrhythmias (Rosenbaum et al., 1994; Euler, 1999).

The particular experiments described here were prompted by reports that murine *Pgc-1β*$^{-/-}$ cardiomyocytes showed irregular and extrasystolic Ca^{2+} signalling patterns and spontaneous

Ca^{2+} propagating waves but normal APDs (Gurung et al., 2011 a). They thus shared phenotypic similarities with *RyR2*-P2328S/P2328S myocytes modelling the similarly arrhythmic catecholaminergic polymorphic ventricular tachycardia (Goddard et al., 2008 b; Zhang et al., 2013). Recent work had attributed arrhythmic substrate in *RyR2*-P2328S/P2328S hearts following adrenergic challenge to slowed AP conduction reflecting reduced $(dV/dt)_{max}$ (Hunter et al., 1975; Zhang et al., 2013), in turn attributable to reduced Na^+ current (King et al., 2013 b; d). The resulting arrhythmic substrate would have similarities with that shown by Nav1.5-haploinsufficient *Scn5a*$^{+/-}$ hearts (Sheikh et al., 2001; Martin et al., 2012 a; King et al., 2013 a) despite it arising from a primary genetic defect not directly involving Nav1.5 (King et al., 2013 d). Certainly, acute manipulations of Ca^{2+} homeostasis alter membrane excitability in WT skeletal (Usher-Smith et al., 2006) and cardiac muscle (King et al., 2013 b; Li et al., 2017), and murine hearts carrying a primary RyR2-P2328S/P2328S genetic modification (Salvage et al., 2015, 2017; Ning et al., 2016 a). Altered cytosolic Ca^{2+} handling thus proved a potential mechanism modifying Nav1.5 function (Tan et al., 2002; Aiba et al., 2010; Ashpole et al., 2012) or expression (Taouis et al., 1991; Duff et al., 1992; Chiamvimonvat et al., 1995) in *RyR2*-P2328S/P2328S hearts. This could potentially take place through direct Ca^{2+}- Nav1.5 binding at an EF hand motif close to the Nav1.5 carboxy-terminal (Wingo et al., 2004) or indirect Ca^{2+} binding involving an additional 'IQ' domain binding site for Ca^{2+}/CaM in the Nav1.5 C-terminal region (Mori et al., 2000; Wagner et al., 2011; Grandi and Herren, 2014). At the cellular level patch-clamped myocytes show reduced I_{Na} and $(dV/dt)_{max}$ with increased pipette $[Ca^{2+}]$ (Chiamvimonvat et al., 1995; Casini et al., 2009).

We used intact Langendorff-perfused hearts to permit electrophysiological exploration of the arrhythmic and pro-arrhythmic phenotype of *Pgc-1β*$^{-/-}$ hearts at physiological and varied steady-state heart rates. Previous studies in this preparation had employed monophasic action potential recordings (Killeen et al., 2007; Thomas et al., 2008). The present study introduced a combination of intracellular recordings from individual epicardial left ventricular cardiomyocytes and ECG recordings of isolated Langendorff perfused hearts. This permitted determinations of absolute resting membrane potentials (RMPs), AP amplitudes, AP latencies and action potential durations (APD_{90}), and sufficient bandwidth to follow maximum rates of

AP depolarisation $(dV/dt)_{max}$, determinations that are not possible with monophasic action potential recording. The simultaneous ECG recordings made it possible to distinguish arrhythmic and non arrhythmic events at the whole organ or chamber levels. As chronic mitochondrial lesions likely exert cumulative and time-varying phenotypic effects with advancing age, the experiments compared young and aged, *Pgc-1β*$^{-/-}$ and WT animals.

This use of the Langendorrf preparation is therefore subject to a similar set of limitations as discussed previously in Chapter 4. Notably, the use of a crystalloid perfusate and the use of an electromechanical uncoupler is something to be borne in mind when interpreting the results. The Krebs-Henseleit solution used contains glucose and pyruvate as the primary substrate for ATP generation. The heart relies almost entirely on the oxidation of fatty acids as its primary fuel source (Jafri et al., 2001) not glucose or pyruvate. This is potentially problematic as it reflects non-physiological conditions in an experiment designed to explore mitochondrial dysfunction – an organelle intimately involved in fatty acid oxidation. However in an aggressive pacing protocol such as used here the energetic demands of the heart are raised and even in physiological conditions there would be the expectation of glucose utilisation as a metabolic fuel.

The initial experiments applying extrasystolic S2 stimulation following trains of regular 8 Hz stimuli at successively decremented S1S2 intervals revealed significantly shorter effective refractory periods in *Pgc-1β*$^{-/-}$ hearts compared to WT hearts, without effects of age or interactions of age and genotype. The resulting ERPs informed the subsequent incremental protocols, applying sequences of steady stimulation at progressively shortened BCLs. These yielded Kaplan Meir curves following the progress of each experimental group into either 2:1 block or arrhythmia and the corresponding ERP from the BCL beyond which this disruption from 1:1 stimulation took place.

Incremental pacing proved an effective method of assessing for the presence of pro-arrhythmic phenotypes in energetically compromised *Pgc-1β*$^{-/-}$ hearts. The demonstration of a pro-arrhythmic phenotype in aged *Pgc-1β*$^{-/-}$ hearts aligned with epidemiological clinical data suggesting age-dependent arrhythmic risks with metabolic disease. Thus, these incremental protocols first demonstrated that aged, but not young, *Pgc-1β*$^{-/-}$ hearts showed increased incidences of arrhythmic events. These took the form of both sustained and non-sustained monomorphic and polymorphic tachycardias. Early or delayed afterdepolarisation phenomena, previously implicated in arrhythmic triggering processes (Balasubramaniam et al., 2004; Thomas et al., 2007 a) were not observed, making an arrhythmic phenotype dependent on such events less likely.

Secondly, the incremental pacing protocol demonstrated an increased incidence of alternans phenomena in *Pgc-1β*$^{-/-}$ hearts irrespective of age, as compared to WT hearts. These alternations concerned both AP activation ($(dV/dt)_{max}$ and AP latency) and recovery (APD_{90} and RMP) features. These instabilities appeared at lower pacing frequencies in *Pgc-1β*$^{-/-}$ hearts compared to WT hearts. All four groups of mice showed episodes of simultaneous $(dV/dt)_{max}$ and APD_{90} alternans, that were less frequent in young WT compared to aged WT, and young and aged *Pgc-1β*$^{-/-}$ hearts.

APD alternans has been described as occurring due to the instability of voltage kinetics at the tissue level or Ca^{2+} handling dynamics at the cellular level. However, the exact mechanism of cardiac alternans has been difficult to elucidate due to the two-way coupling between voltage and Ca^{2+} handling kinetics. There are two main cellular mechanisms of APD alternans that have been postulated from the experimental evidence and simulation studies. At high pacing rates or under pathological conditions alternans can originate from the kinetics of the membrane voltage, which subsequently causes alternated intracellular Ca^{2+} mainly through voltage-related L-type Ca^{2+} channel (LCC) current (I_{CaL}) (Merchant and Armoundas, 2012; Nivala and Qu, 2012). Secondly, the instability of Ca^{2+} handling dynamics leads to alternated intracellular

Ca^{2+}, which then causes voltage alternans mainly by I_{CaL} and Na^{+}-Ca^{2+} exchange current (I_{NCX}) (Kanaporis and Blatter, 2015) .

As can be seen there is a great deal of uncertainty regarding the primary instigating abnormality that triggers APD alternans. Alternans in activation parameters has never been described before in the literature and this study represents the first to do so. This stems from the difficulty in recording intracellular action potentials from a moving beating preparation and nearly all studies have focused on optical mapping which cannot be used for determination of parameters such as $(dV/dt)_{max}$. Thus the determination of the mechanism of such alternans is currently unknown. Empirically, a number of feedback mechanisms could be involved including Ca^{2+} transients (which are involved in APD alternans) to modulate Na^{+} channel function.

Experimental protocols to dissect the contribution of activation parameter alternans from recovery parameter alternans would likely necessitate a multi-pronged experimental approach, with pharmacological manipulation to abolish Ca^{2+} transients, in conjunction with a voltage clamp method in different experimental pairings to determine if one form of alternans is a bigger contributor to arrhythmogenesis than the other. This approach would be strengthened by the simultaneous use of a computer modelling approach to probe fruitful avenues of exploration and to feed the gathered experimental data into to verify and generate new hypotheses.

Incremental pacing together with quantification of findings from micro-electrode recording methods permitted discrimination of the role of activation variables, measured as $(dV/dt)_{max}$ and AP latency, and the recovery variables of APD_{90} and RMP and their dependence upon BCL in these pro-arrhythmic phenomena. This associated the *Pgc-1β*$^{-/-}$genotype with reduced $(dV/dt)_{max}$ and increased AP, but with no further effects of either ageing or interactions between genotype and ageing. Genotype alone did not influence either APD_{90} or RMP,

although aged *Pgc-1β*$^{-/-}$ hearts showed longer APD_{90} than young *Pgc-1β*$^{-/-}$ hearts, and RMP was greater in aged than young hearts. Finally, stratifications by arrhythmic or non-arrhythmic phenotype (regardless of age or genotype) demonstrated that $(dV/dt)_{max}$ and AP latencies in APs obtained prior to arrhythmia were significantly lower than $(dV/dt)_{max}$ and AP latencies in APs prior to entry into 2:1 block in non-arrhythmic hearts. However, there were no significant differences in APD_{90} and RMP values when stratified by arrhythmic phenotype. These findings therefore attribute the greater frequency of alternans in *Pgc-1β*$^{-/-}$ hearts to alterations in AP activation characteristics.

Fourthly, previous reports have demonstrated that arrhythmic substrate resulting from repolarisation abnormalities as reported in the *Scn5a*$^{+/\Delta KPQ}$ model and hypokalaemic hearts for long QT syndrome give restitution plots of APD_{90} against DI_{90} with distinct gradient properties from those of WT hearts (Sabir et al., 2008 a). However, the present analysis applied to *Pgc-1β*$^{-/-}$ and WT hearts gave loci with indistinguishable limiting slopes.

Finally, a contrasting form of arrhythmic substrate has been attributed to the altered AP conduction occurring in *Scn5a*$^{+/-}$ and *RyR2-P2328S/P2328S* hearts modelling the Brugada Syndrome and catecholaminergic polymorphic ventricular tachycardia respectively. This has been associated with alterations in action potential wavelength, λ, reflected by the product of conduction velocity and effective refractory period (Sabir et al., 2008 a, 2010, Matthews et al., 2010, 2012, 2013 c; Ning et al., 2016 a). The present experiments demonstrated that whereas young and aged WT hearts showed similar λ-BCL and λ-λ_0 plots, young and aged *Pgc-1β*$^{-/-}$ hearts showed progressively reduced maximum λ, an effect more marked in the aged *Pgc-1β*$^{-/-}$ hearts. This finding is an exact parallel of the demonstrations of the presence of arrhythmic phenotypes and of pro-arrhythmic alternans phenomena. It should be remembered however that the wavelength calculations rest upon a number of presumptions not least a reproducible conduction path from the stimulating electrode to the recording microelectrode; this may not be the case and certainly it may be that different hearts have variant anatomical courses of the conduction pathways over different distances. Effort was made to ensure consistent

placement of the stimulating electrode and the recording microelectrode though it is not possible to ensure that the conduction path between the two is identical in all hearts. Further, it is possible that the conduction path changes during the course of an experiment as the BCL is decremented; i.e. some conduction paths might become refractory necessitating an alternate path. The VERP for each pacing frequency have been interpolated between the two measured VERPs at 8hz and at loss of 1:1 capture; there simply exists no data in the literature as to how VERP may be altered with pacing frequency. A linear relationship is the simplest mathematical model to explain the relationship though definitive experimental evidence would be needed to prove this.

However, overall the experimental evidence attributes arrhythmogenesis in *Pgc-1β*$^{-/-}$ hearts to altered $(dV/dt)_{max}$ and activation latency. The present findings thereby also throw light on possible more widespread effects of altered intracellular homeostasis on AP propagation in addition to suggesting electrophysiological mechanisms for the increased arrhythmic risk associated with metabolic disturbance.

6. REDUCED CARDIOMYOCYTE NA^+ CURRENT IN THE AGE DEPENDENT MURINE *Pgc-1β*$^{-/-}$ MODEL OF VENTRICULAR ARRHYTHMIA.

6.1 INTRODUCTION

The present experiments were designed to explore a hypothesis implicating alterations in Na^+ channel function in the age-dependent ventricular pro-arrhythmic *Pgc-1β*$^{-/-}$ phenotype. Application of the loose patch technique (Figure 6-1) permitted a comparison of Na^+ against K^+ currents in ventricular preparations from young and aged, WT and *Pgc-1β*$^{-/-}$ hearts. The loose patch clamp technique apposes an extracellular solution filled electrode against an intact, in situ, cardiomyocyte membrane patch without perturbing its intracellular space thereby preserving in vivo extracellular [Na^+] and intracellular Ca^{2+} homeostatic conditions (Almers et al., 1983 b; Stühmer et al., 1983; King et al., 2013 b). This contrasts with the cardiomyocyte isolation and intracellular Ca^{2+} chelation entailed in conventional whole-cell patch clamp (Lei et al., 2005; Gurung et al., 2011 a; Martin et al., 2012 b). Previous loose patch clamp experiments reversibly manipulating extracellular [Na^+] had identified early inward currents elicited by depolarising steps with Na^+ currents determining the maximum cardiac AP upstroke rate, $(dV/dt)_{max}$, (King et al., 2013 b). The present experiments could thus assess and quantify the activation, inactivation, and recovery from inactivation of inward Na^+ currents attributable to Nav1.5. They then compared these to the corresponding activation and rectification properties of voltage-dependent K^+ currents in the same preparations.

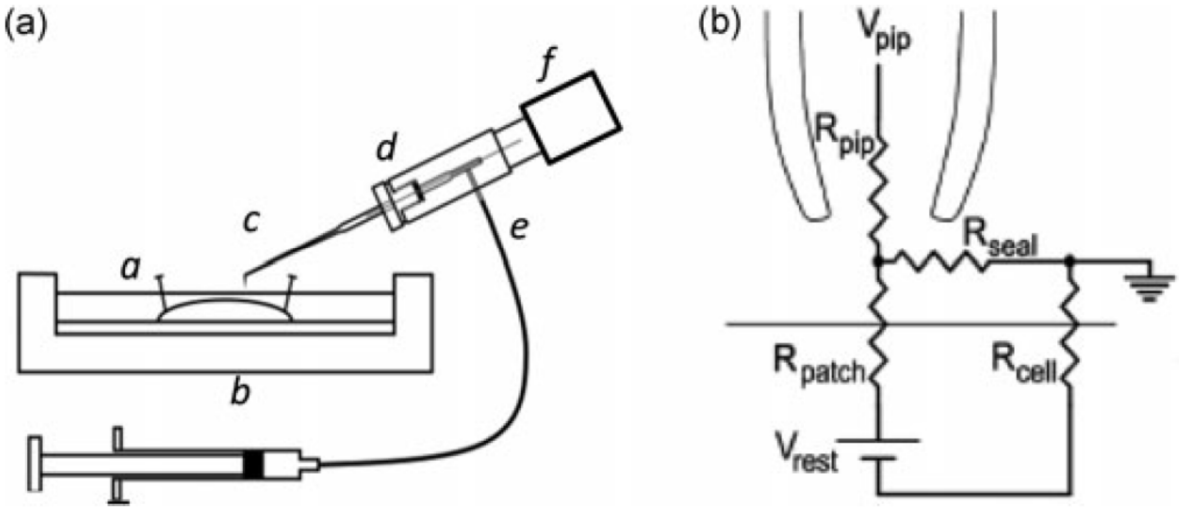

Figure 6-1: Loose patch clamp configuration. *Loose patch clamping of murine ventricular myocytes. (a) Experimental loose patch configuration: (a) mounted muscle preparation under Krebs–Henseleit solution within (b) experimental chamber. (c) Loose patch pipette mounted at 45° to the preparation but bent to permit right-angled contact of pipette tip with the myocyte surface. Pipette held within (d) half-cell chamber in turn connected to (e) air line and suction syringe, and mounted on (f) headstage moved under micromanipulator and upright microscope guidance. (b) Equivalent circuit of loose patch clamp electrode on membrane. Pipette clamped at voltage Vpip. Compensation for the voltage error arising from currents flowing through the series combination of the pipette resistance (Rpip) and the seal resistance (Rseal) achieved using a bridge circuit in the custom-designed loose patch clamp amplifier. As the loose patch technique alters the extracellular potential within the patch relative to RMP, negative and positive voltage excursions in Vpip, respectively, produce hyperpolarising and depolarising voltage steps relative to RMP.RMP: resting membrane potential; Rpatch: patch membrane resistance; Rcell: overall cell membrane resistance*

6.2 RESULTS

6.2.1 CURRENTS REFLECTING VENTRICULAR NA^+ CHANNEL ACTIVATION

Isolated ventricular preparations were used for loose patch clamp recordings. Typical results of Na^+ current activation are shown in Figure 6-2. Comparisons were made between experimental groups that consisted of preparations from young (panels A, C; E, G) and aged (B, D, F, H), wild-type (A, B, E, F) and *Pgc-1β*$^{-/-}$ hearts (C, D, G, H). Displays of the resulting current traces are shown at slow (A-D) timebases illustrating the full time course of the current records. Those at rapid (E-H) timebases show the detailed kinetics of the transient

components of the observed currents. The pulse protocol (Figure 6-2I) used first held the patches at the resting membrane potential (RMP) for 5 ms from the beginning of the 80 ms recording period. A 5 ms prepulse step to V_0 = (RMP - 40 mV) was then applied to remove any residual Na^+ current inactivation and ensure a consistent initial state of activation of Na^+ channels within the patch. This was then followed by the depolarising test steps that extended to the end of the 80 ms record length; these were of successively larger amplitudes through the 13 successive sweeps that were applied, and were made to voltages ranging from V_1 = RMP to V_1 = (RMP + 120 mV), in successive +10 mV increments. The observed currents were corrected for residual leakage by the P/4 protocol to give a family of traces reflecting the voltage dependence of Na^+ channel activation, with inward currents shown as downward, negative deflections.

The resulting current traces typically began with a small consistent upward deflection in response to the -40 mV prepulse (A-D). The inward currents obtained in response to the subsequent test voltage steps to level V_1 illustrate the typical Na^+ current activation characteristics expected. The recorded currents initially increased with time to a peak value that became greater with greater voltage excursion and varied nonlinearly with voltage V_1. Each peak was then followed by an inactivation decay whose characteristics were similarly determined by the voltage V_1 (E-H). The records demonstrated that ventricular preparations from young and aged mice showed similar Na^+ current amplitudes. However, *Pgc-1*$\beta^{-/-}$ ventricular preparations showed consistently smaller Na^+ currents than did WT preparations.

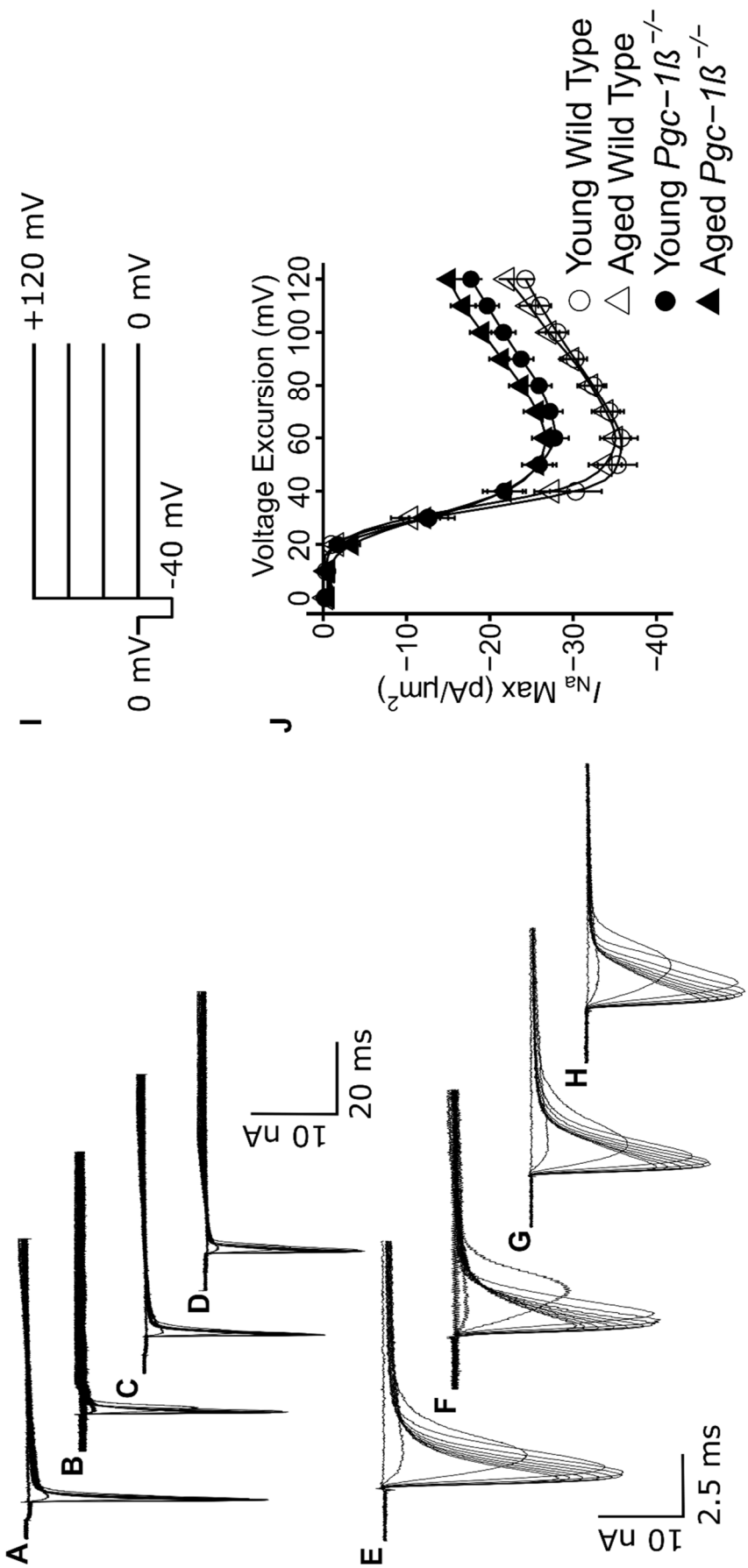

Figure 6-2: Activation properties of voltage-dependent inward Na+ currents of murine ventricular preparations under loose

Typical records are shown for young (A, C, E, G) and aged (B, D, F, H) wild-type (WT; A, B, E, F) and Pgc-1$\beta^{-/-}$ hearts (C, D, G, H), at slow (A-D) and fast (E-G) time bases in response to (I) activation pulse protocols beginning from the resting membrane potential (RMP). This first applied a 5 ms duration prepulse 5 ms into the recording period to (RMP - 40 mV). It then applied successively larger depolarising test voltage steps increased in +10 mV increments up to (RMP + 120 mV). (J) Peak currents, I_{NaMax}, are plotted against the voltage excursion for young (circles) and aged (triangles), wild-type (clear symbols) and Pgc-1$\beta^{-/-}$ ventricular myocytes (filled symbols). Sample sizes for experimental groups were as follows: Young WT (n = 20), aged WT (n = 18), young Pgc-1$\beta^{-/-}$ (n = 23) and aged Pgc-1$\beta^{-/-}$ (n = 20)

6.2.2 *Currents reflecting ventricular Na^+ channel inactivation*

Results from experiments exploring ventricular Na^+ current inactivation properties are illustrated in Figure 6-3. Again, the experimental groups consisted of preparations from young (panels A, C; E, G) and aged (B, D, F, H) wild-type (WT; A, B, E, F) and *Pgc-1β*$^{-/-}$ mice (C, D, G, H). In the pulse protocols (Fig. 6-3I), patches were first held at the RMP for 5 ms. This was followed by a prepulse of 5-ms duration to V_0 = (RMP - 40 mV). Next, depolarising conditioning steps were applied to voltages that were altered in 10 mV increments between V_1 = RMP to (RMP + 120 mV) through the 13 successive sweeps. This conditioning step elicited a Na^+ current reflecting the process of activation followed by inactivation, with the extent of the latter determined by the voltage V_1. The extent of inactivation was assessed by imposition of the test step 5 ms later to a fixed voltage V_2 = (RMP + 100 mV). This voltage was maintained to the end of the record length. The resulting traces (Fig. 6-3A-H) reflect Na^+ currents which would become reduced in amplitude to an extent dependent upon the channel *inactivation* brought about by the prior voltage prepulse to V_1. This combined pulse protocol thus gave families of currents in response to the step to voltage V_2, the peak currents of which vary nonlinearly and decrease in amplitude as voltage V_1 is varied. These also demonstrated that the magnitudes of the observed currents in preparations from young and aged mice were similar, but currents were consistently reduced in *Pgc-1β*$^{-/-}$ relative to WT ventricular preparations.

6.2.3 *Voltage dependence of ventricular Na^+ current activation*

Figure 6-2J plots current-voltage curves quantifying the activation of peak ventricular Na^+ current (means ± standard error of the mean (SEM)) with excursion to the test voltage V_1. It compares results from preparations from young (circles) and aged (triangles), WT (open symbols) and *Pgc-1β*$^{-/-}$ mice (filled symbols). In such activation plots, the peak inward Na^+ current, I_{Na}, increased with the amplitudes of the depolarising steps beyond +10 mV, reaching a maximum value at a voltage excursion at around +80 mV. Their amplitudes then decreased with larger voltage excursions as these reached voltages V_1 successively closer to the Na^+ Nernst potential.

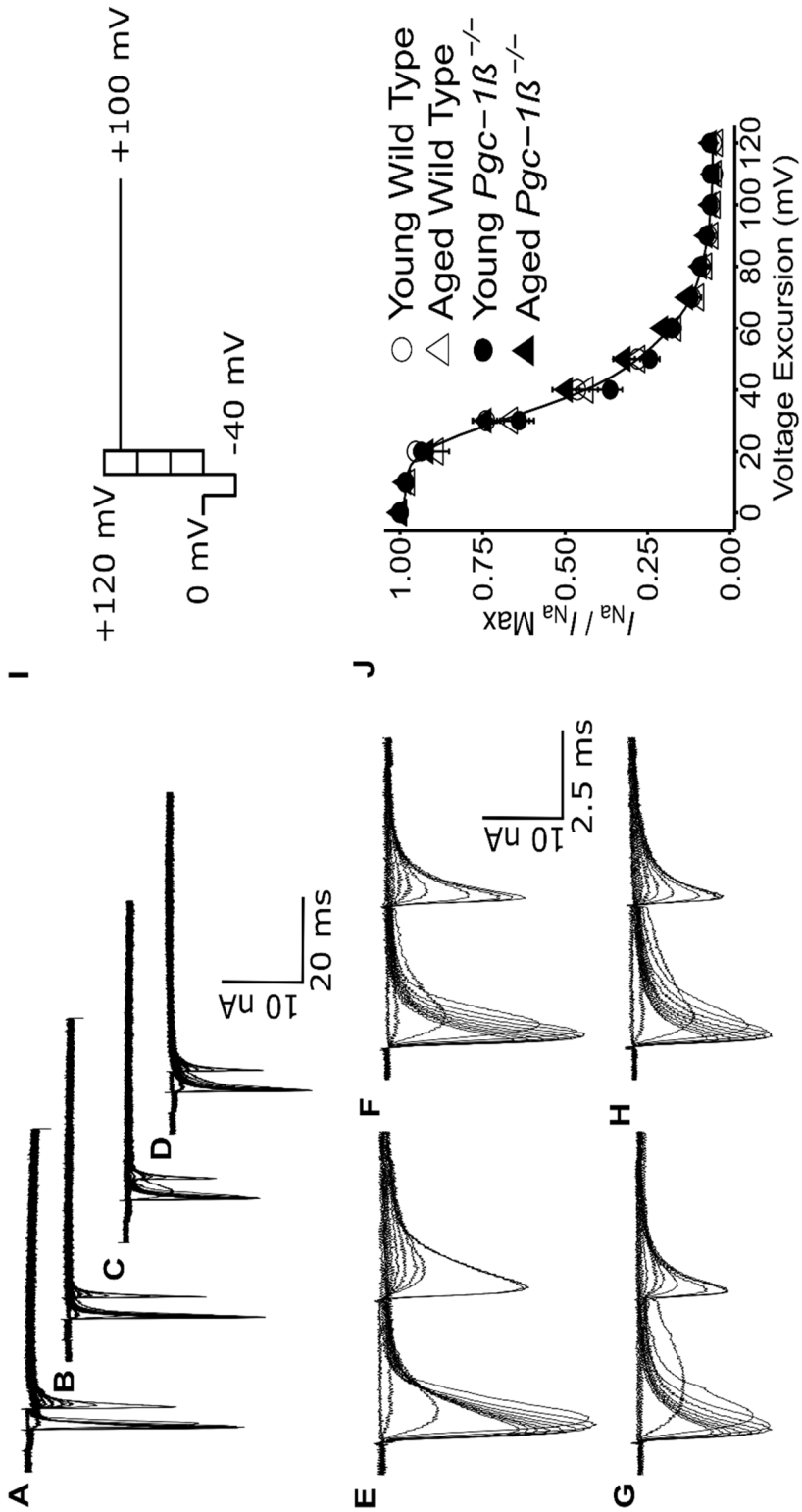

Figure 6-3: Inactivation properties shown by voltage-dependent inward Na+ currents under loose patch clamp of murine ventricular preparations.

Typical records shown for young (A, C, E, G) and aged (B, D, F, H) wild-type (WT; A, B, E, F) and Pgc-1$\beta^{-/-}$ ventricular preparations (C, D, G, H), at slow (A-D) and fast (E-G) time bases in response to inactivation pulse protocols. (I) In the pulse protocol, a prepulse (duration 5 ms) was applied from the resting membrane potential (RMP), 5 ms into the recording period to (RMP - 40 mV). This was followed by successively larger depolarising 5 ms duration conditioning voltage steps increased in +10 mV increments up to (RMP + 120 mV). Finally, in all sweeps, the voltage finally was stepped to a constant test level of (RMP + 100 mV). The resulting peaks of the Na^+ currents were then quantified to characterise the inactivation brought about by the preceding conditioning step. (J) Peak currents I_{NaMax} plotted against voltage excursion for the conditioning voltage step in young (circles) and aged (triangles), wild-type (clear symbols) and Pgc-1$\beta^{-/-}$ ventricular preparations (filled symbols). Sample sizes for experimental groups were as follows: Young WT (n = 20), aged WT (n = 18), young Pgc-1$\beta^{-/-}$ (n = 23) and aged Pgc-1$\beta^{-/-}$ (n = 20)

The activation of such peak Na^+ currents, *I*, was empirically related to the activating voltage $V = V_1$ by a Boltzmann function expressed in terms of the maximum value of the peak current, I_{max}, voltage at half maximal peak current, V^*, and a steepness factor describing the voltage sensitivity of the current, *k*: $I = I_{max}\{1-1/\{1 + \exp[(V - V^*)/k]\}\}$. The maximum values of the peak ventricular inward Na^+ currents were similar in young WT (-36.63 ± 2.14 (n = 20) pA/µm^2) and aged WT (-35.43 ± 1.96 (n = 18) pA/µm^2) mice. They were reduced to similar extents in young (-29.06 ± 1.65 (n = 23) pA/µm^2) and aged *Pgc-1β*$^{-/-}$ mice (-27.93 ± 1.63 (n = 20) pA/µm^2). These changes reflected independent effects of genotype (F= 16.57; p = 0.0001), but not of age (F= 0.40; p = 0.53), or of interacting effects of age and genotype (F< 0.001; p = 0.99) on two-way ANOVA. Post hoc Tukey tests demonstrated pairwise differences between aged WT and aged *Pgc-1β*$^{-/-}$ hearts (p = 0.033), young WT and young *Pgc-1β*$^{-/-}$ hearts (p = 0.019), as well as young WT and aged *Pgc-1β*$^{-/-}$ hearts (p = 0.0075).

In contrast, V^* values were similar amongst ventricular preparations from young (34.28 ± 1.10 (n = 20) mV) and aged WT (34.49 ± 0.85 (n = 18) mV), and young (34.49 ± 1.80 (n = 23) mV) and aged *Pgc-1β*$^{-/-}$ hearts (32.22 ± 1.87 (n = 20) mV). Accordingly, 2-way ANOVA demonstrated that there were no independent effects of either genotype (F = 0.37; p = 0.54) or age (F = 0.52; p = 0.47). Nor were there interacting effects of age and genotype (F = 0.65; p = 0.42). Values of *k* were also similar amongst ventricular preparations from young (3.24 ± 0.25 (n = 20) mV) and aged WT (4.06 ± 0.18 (n = 18) mV), and young (4.04 ± 0.28 (n = 23) mV) and aged *Pgc-1β*$^{-/-}$ hearts (4.11 ± 0.24 (n = 20) mV). 2-way ANOVA indicated no independent effects of either genotype (F = 3.23; p = 0.072) or age (F = 2.96; p = 0.089). Nor were there interacting effects of age and genotype (F = 2.34; p = 0.13).

6.2.4 Voltage dependence of ventricular Na^+ current inactivation

Figure 6-3J plots the voltage dependences of Na^+ current inactivation of preparations from young (circles) and aged (triangles), WT (open symbols) and *Pgc-1β*$^{-/-}$ mice (filled symbols). The peak inward Na^+ currents observed in response to a depolarising step to a constant test voltage decreased as the preceding prepulse voltages, V_1, became progressively positive. This reflects an inactivation process increasing in extent with progressive depolarisation. The peak

currents were related to an inactivation function in the inactivating voltage $V = V_1$ through a Boltzmann function of the form: $I = I_{max} /\{1 + \exp[(V-V^*)/k]\}$.

Values of V^* were similar amongst young (39.33 ± 1.32 (n = 20) mV) and aged WT (37.41 ± 2.20 (n = 18) mV), and young (36.10 ± 1.26 (n = 23) mV) and aged *Pgc-1β*$^{-/-}$ preparations (40.39 ± 1.72 (n = 20) mV) with an absence of independent effects of either genotype (F = 0.040; p = 0.84) or age (F = 0.714; p = 0.401), or interacting effects of age and genotype (F = 3.66; p = 0.059) on two-way ANOVA. Values of k were also similar amongst young (8.11 ± 0.53 (n = 20) mV) and aged WT (7.48 ± 0.68 (n = 18) mV), and young (7.85 ± 0.58 (n = 23) mV) and aged *Pgc-1β*$^{-/-}$ preparations (9.36 ± 0.42 (n = 20) mV), with an absence of independent effects of either genotype (F = 1.75; p = 0.19) or age (F = 0.81; p = 0.37), or interacting effects of age and genotype (F = 3.66; p = 0.060).

Thus, in contrast to the genotype dependant effect upon the maximum peak Na^+ currents I_{max}, neither age or genotype influenced the voltages at half maximal current V^*, or the steepness factors, k, of Boltzmann functions describing current activation or current inactivation.

6.2.5 Time course of Na^+ channel recovery from inactivation

Fig. 6-4 shows typical experimental results of the time course of recovery from inactivation. This was explored by restoration of the baseline voltage after an initial conditioning depolarising step to a fixed voltage. Results are compared for preparations from young (A, C) and aged (B, C), WT (A, B) and *Pgc-1β*$^{-/-}$ hearts (C, D). The pulse protocol (Fig. 6-4F) held the membrane potential at the RMP for 1 ms from the beginning of the recording period. This was followed by a hyperpolarising prepulse to voltage V_0 = (RMP - 40 mV) for 4 ms to establish consistent baseline levels of Na^+ current inactivation as in the previous protocols.

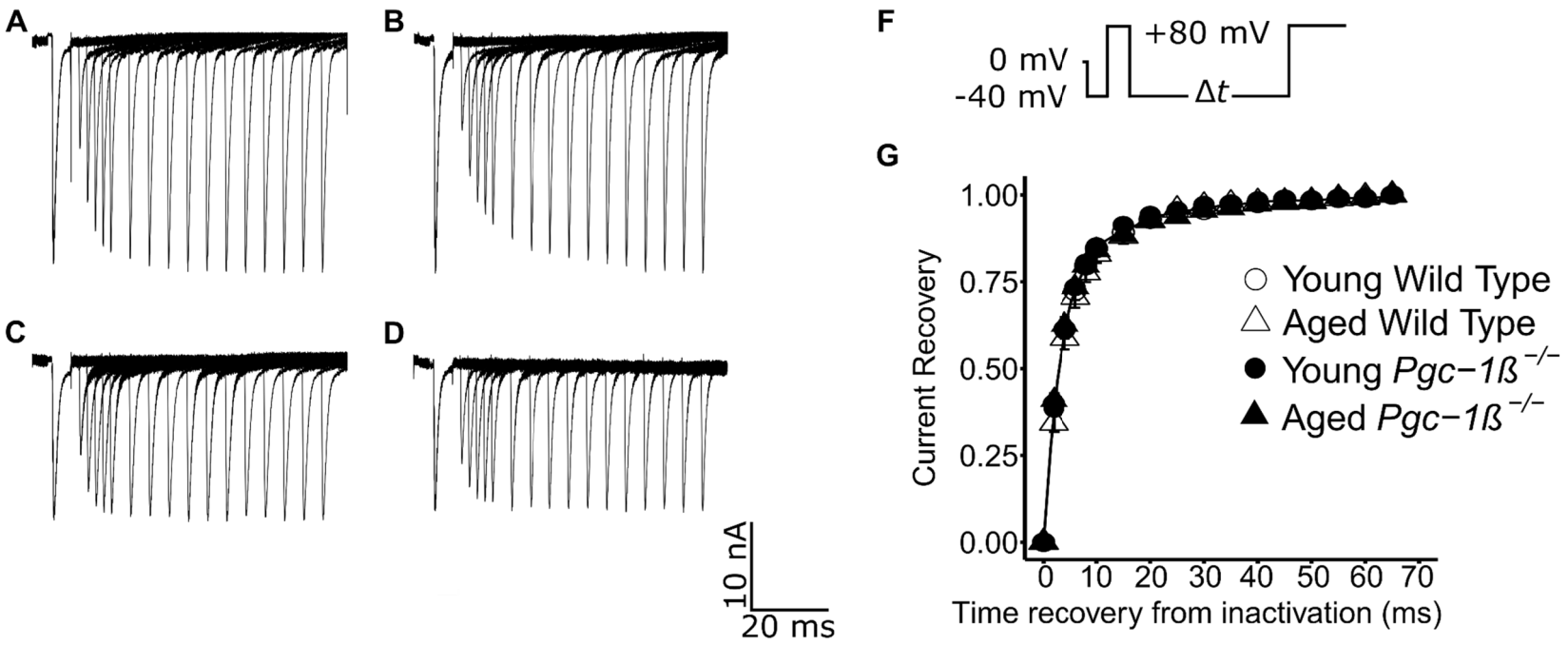

Figure 6-4: Currents illustrating Na+ channel recovery from inactivation following restoration of the membrane potential.

Records are shown for young (A, C) and aged (B, D) wild-type (WT; A, B) and Pgc-$1ß^{-/-}$ ventricular preparations (C, D). In the pulse protocols (F) the membrane voltage was first held at the RMP for 1 ms from the beginning of the recording period. A hyperpolarising prepulse was then imposed to (RMP - 40 mV). This was then followed by a 5 ms duration P1 conditioning step to (RMP + 80 mV). The subsequent 5 ms duration test steps to (RMP + 80 mV) that followed were imposed after different time intervals, ΔT, between 5 ms to 65 ms in 5 ms increments through the 12 successive sweeps making up the protocol. (G) Plots of the recovery of peak I_{Na} against time intervening between termination of the conditioning and imposition of the test pulse. Sample sizes for experimental groups were as follows: Young WT (n = 20), aged WT (n = 18), young Pgc-$1ß^{-/-}$ (n = 23) and aged Pgc-$1ß^{-/-}$ (n = 20)

A 5 ms P1 conditioning step was then imposed between V_0 and V_1 = (RMP + 80 mV). This elicited Na^+ current activation followed by its inactivation decay, before restoration of the baseline voltage V_0. The depolarising 5 ms duration P2 steps to voltage V_3 = (RMP + 80) mV were then imposed after different time intervals, ΔT. This time interval varied between 2 ms to 75 ms, altered in 2 ms increments for the first 5 recordings and 5 ms increments thereafter, through the 16 successive sweeps making up the protocol. These P2 steps elicited a Na^+ current activation whose peak amplitude, normalised to corresponding values in the P1 step, reflected the Na^+ current recovery from inactivation with time ΔT. Time constants, τ, were fitted to the exponential function $I = I_{max}(1 - \exp(-\Delta T/\tau))$ describing this recovery (Fig. 4G). Values of τ were similar amongst young (4.69 ± 0.47 (n = 20) ms) and aged WT (5.31 ± 0.58 (n = 18) ms), and young (4.58 ± 0.27 (n = 23) ms) and aged *Pgc-1β*$^{-/-}$ hearts (4.45 ± 0.29 (n = 20) ms). There was an absence of any effects of genotype (F= 1.31; p = 0.26), age (F=0.30; p = 0.59), or interacting effects of age and genotype (F = 0.88; p = 0.35) on τ with 2-way ANOVA.

6.2.6 *Voltage dependences of ventricular K^+ current activation*

The loose-patch clamp technique was used to investigate voltage-dependent total outward, K^+, currents and their rectification properties in murine ventricular preparations for the first time. They demonstrated that, in contrast to the differences in maximum Na^+ current, these outward current properties were similar amongst groups.

Figure 6-5 illustrates the results of experiments investigating K^+ current activation in preparations from young (Fig. 6-5A, C, E, G) and aged (Fig. 6-5B, D, F, H), WT (A, B, E, F) and *Pgc-1β*$^{-/-}$ (C, D, G, H) mice. The pulse procedure (Fig. 6-5I) initially imposed a voltage step between 1-10 ms from the start of the recording period from RMP to (RMP – 20 mV). It then imposed a 10 ms duration test step to voltages between (RMP – 60 mV) to (RMP + 170 mV), varied in increments of 10 mV through the 24 sweeps that were investigated. The traces shown at slow (A-D) sweep speeds encompassing the entire record demonstrate that such test steps initially elicited Na^+ channel activation, followed by its inactivation. This was succeeded in some traces by a gradual outward current reflecting activation of a rectified voltage-dependent K^+ current. This was followed by a 10 ms hyperpolarising step to a fixed

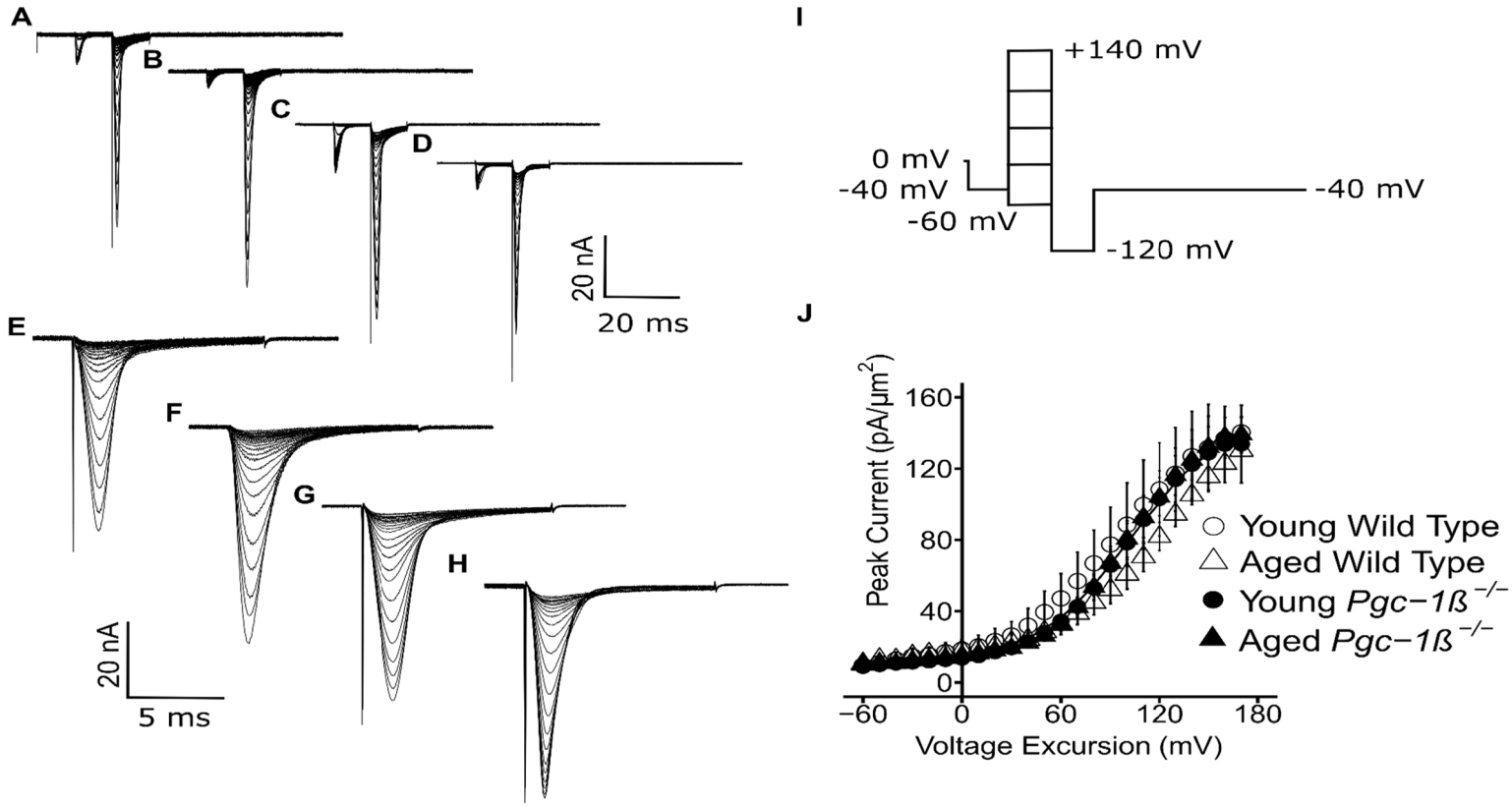

Figure 6-5: Activation properties of K+ currents as reflected in tail currents in ventricular preparations.

This shows records from young (A, C, E, G) and aged (B, D, F, H) wild-type (WT; A, B, E, F) and Pgc-1$\beta^{-/-}$ ventricular preparations (C, D, G, H), at slow (A-D) and fast (E-G) time bases. The pulse procedure (I) first applied a voltage step from RMP to (RMP – 20 mV) between 1-10 ms following commencement of the recording period. This was followed by 10 ms duration test steps to voltages between (RMP – 60 mV) and (RMP + 140 mV) incremented in 10 mV steps through the 21 sweeps investigated. A final 10 ms duration hyperpolarising step to (RMP – 120 mV) was then imposed. This gave tail currents reflecting the preceding K^+ current activation. Finally, the membrane potential was restored to (RMP - 20 mV). (J) Plot of the maximum amplitude of the tail currents against voltage excursion in the young (circles) and aged (triangles) WT (open symbols) and Pgc-1$\beta^{-/-}$ ventricular preparations (filled symbols). Sample sizes for experimental groups were as follows: Young WT (n = 20), aged WT (n = 18), young Pgc-1$\beta^{-/-}$ (n = 23) and aged Pgc-1$\beta^{-/-}$ (n = 20)

voltage of (RMP – 120 mV), before final restoration of the membrane potential to (RMP - 20 mV). The traces shown at the rapid timebases (E-H) demonstrate that this resulted in K^+ tail currents. This reflects the instantaneous conductance resulting from K^+ channel activation induced by and existing at the end of the preceding depolarising step. The amplitudes of these families of tail currents were similar between experimental groups.

Figure 6-5J plots typical activation K^+ current-voltage curves for the young (circles) and aged (triangles) WT (open symbols) and *Pgc-1β*$^{-/-}$ ventricular preparations (filled symbols). The plots were close to superimposable, their areas with the abscissa showing neither independent ($F = 0.02$; $P = 0.89$ and $F = 0.19$; $P = 0.67$ respectively) nor interacting ($F = 0.42$; $P = 0.52$) effects of genotype or age.

6.2.7 Rectification properties of ventricular K^+ currents

Figure 6-6 illustrates results from investigations of K^+ current rectification properties in ventricular preparations from young (Fig. 6-6A, C, E, G) and aged (Fig. 6-6B, D, F, H), WT (A, B, E, F) and *Pgc-1β*$^{-/-}$ (C, D, G, H) hearts. The pulse procedure (Fig. 6-6I) initially imposed a voltage step between 1-10 ms from the start of the recording period from RMP to (RMP – 20 mV). It then imposed a 10 ms test step to a fixed voltage of (RMP + 140) mV. As indicated in the traces displayed at a compressed timebase illustrating the entire record (A-D), such test steps initially elicited an inward, Na^+ current, activation, followed by its inactivation, and this was followed by a specific level of a rectified K^+ current activation. Further test steps to a range of voltages between (RMP - 120 mV) to (RMP + 50 mV) altered in 10 mV increments through successive sweeps then elicited tail currents, shown at low (A-D) and high sweep speeds (E-H), that reflect the instantaneous current-voltage relationship and the rectification properties of the activated channel (Fig. 6-6J). Plots of such currents against voltage (Fig. 6-6J) showed the typical concave downward form of K^+ channel rectification. These were similar amongst the young (circles) and aged (triangles) WT (open symbols) and *Pgc-1β*$^{-/-}$ ventricular preparations (filled symbols), demonstrating close to superimposable plots and enclosing areas with the abscissa in which there were neither independent ($F = 0.18$; $P = 0.67$ and $F = 0.004$; $P = 0.95$ respectively) nor interacting ($F = 0.013$; $P = 0.91$) effects of genotype or age.

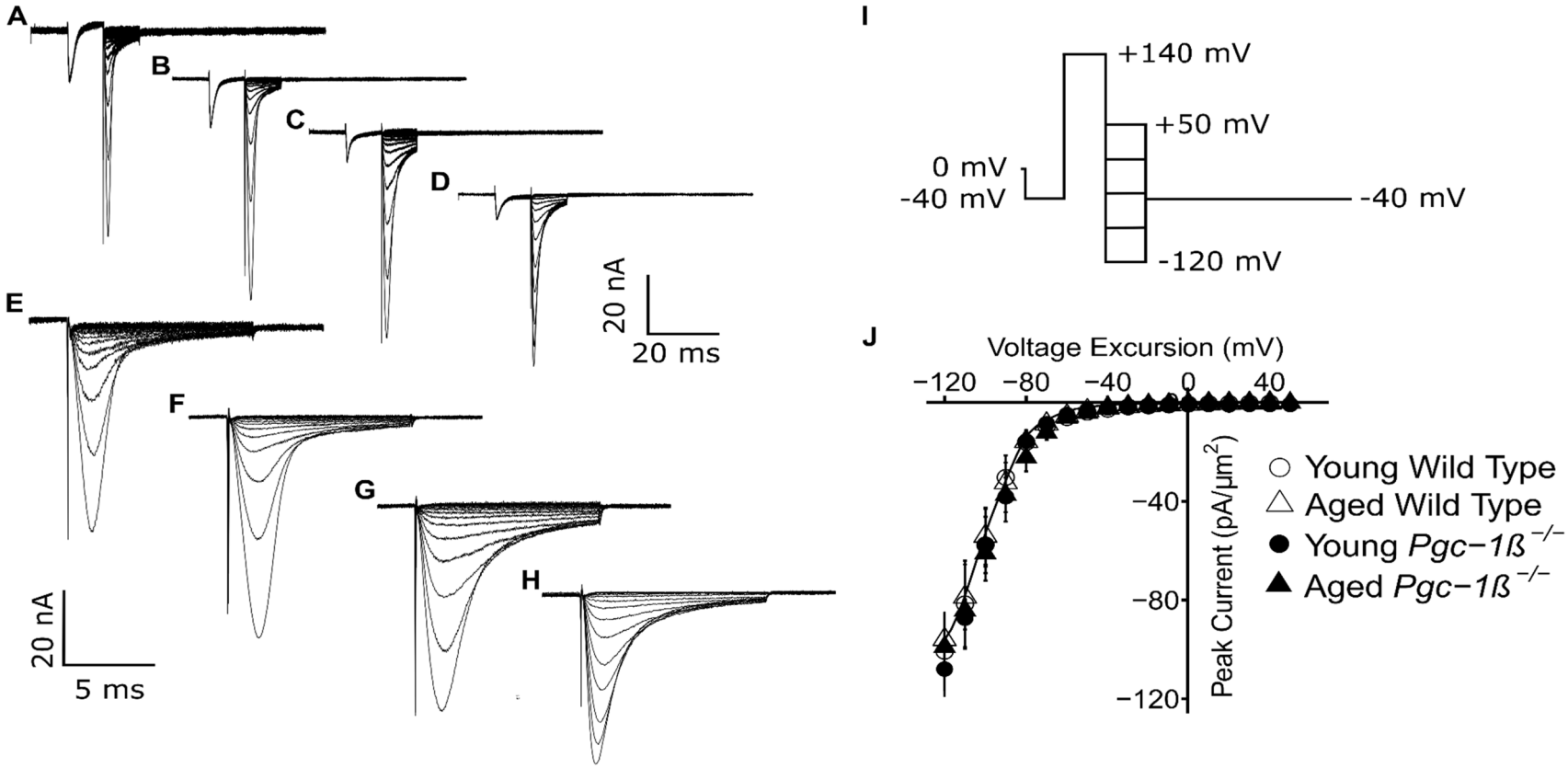

Figure 6-6: K+ current rectification properties reflected in tail currents in ventricular preparations.

Typical records shown from young (A, C, E, G) and aged (B, D, F, H) wild-type (WT; A, B, E, F) and Pgc-1$\beta^{-/-}$ ventricles (C, D, G, H), at slow (A-D) and fast (E-G) time bases. The pulse procedure (I) first applied a voltage step from RMP to (RMP – 20 mV) between 1-10 ms after the beginning of the recording period. This was followed by a 10 ms duration test step to a fixed voltage of (RMP + 140 mV). This was succeeded by a 10 ms duration step to varying voltages between (RMP - 120 mV) and (RMP + 50 mV). The latter resulted in tail currents which could be plotted against voltage to obtain (J) instantaneous current-voltage relationships reflecting the rectification properties of the activated channel in the young (circles) and aged (triangles) WT (open symbols) and Pgc-1$\beta^{-/-}$ ventricles (filled symbols). Finally, the membrane potential was restored to (RMP - 20 mV). Sample sizes for experimental groups were as follows: Young WT (n = 20), aged WT (n = 18), young Pgc-1$\beta^{-/-}$ (n = 23) and aged Pgc-1$\beta^{-/-}$ (n = 20)

6.3 DISCUSSION

Ventricular arrhythmic risk is known to increase with age (Kucharska-Newton et al., 2010; Hookana et al., 2011; Adabag et al., 2015) through accumulation of mitochondrial genomic mutations and impaired autophagy (Michikawa et al., 1999; Pyo et al., 2013). It also increases with clinically common age-related metabolic conditions arising from obesity, metabolic syndrome, diabetes mellitus and heart failure, which constitute independent risk factors for such outcomes. Biochemical effects of the latter conditions were previously replicated in murine *Pgc-1β*$^{-/-}$ hearts which demonstrated deficiencies in key mitochondrial energetic tricarboxylic acid cycle, fatty acid β–oxidative and oxidative phosphorylative processes (Arany et al., 2005; Lin et al., 2005; Finck and Kelly, 2006).

More recent reports on *Pgc-1β*$^{-/-}$ hearts have also demonstrated age-dependent ventricular pro-arrhythmic phenotypes (Gurung et al., 2011 a) accompanying slowed propagation of the action potential (AP) mediating cardiomyocyte excitation (Ahmad et al., 2018 a). This was accompanied by compromised maximum AP depolarization rates, $(dV/dt)_{max}$ and an age-dependent accentuation of fibrotic change accentuated by the *Pgc-1β*$^{-/-}$ genotype (Ahmad et al., 2017, 2018 b). Pro-arrhythmic reductions in conduction velocity have been attributed to compromised cardiac Na^+ channel function in genetically modified *Scn5a*$^{+/-}$ murine models modelling the Brugada Syndrome (Sabir et al., 2008 b; Kalin et al., 2010; Martin et al., 2011 a; b; Huang, 2017 b). They may also arise from fibrotic change altering cardiomyocyte capacitance following cardiomyocyte-fibroblast fusion (Xie et al., 2009; Davies et al., 2014; Mahoney et al., 2016), or increased intercellular gap junction resistance with connexin Cx40 or Cx43 deficiency accompanying or resulting from tissue fibrosis (Jeevaratnam et al., 2011, 2012).

The present experiments accordingly test a hypothesis implicating compromised Na^+ channel function as a contributor to such arrhythmic substrate. Previous reports had suggested that metabolic stress of the kind occurring with the *Pgc-1β*$^{-/-}$ genotype could potentially alter Na^+ channel activity through increased reactive oxygen species (ROS) production (Liu et al., 2010

a), or compromised NAD^+/NADH ratios (Pugh et al., 2013), effects which are reversed by the mitochondrial ROS scavenger mitoTEMPO (Liu et al., 2010 b) and NAD^+ restoration (Gomes et al., 2013) respectively. *Pgc-1β*$^{-/-}$cardiomyocytes also show altered Ca^{2+} homeostasis (Gurung et al., 2011 a) accompanied by increased frequency of pro-arrhythmic delayed afterdepolarisation activity in common with murine *RyR2*-P2328S ventricular cardiomyocytes (Goddard et al., 2008 b).

However, *RyR2*-P2328S ventricles also showed parallel reductions in AP conduction velocity and maximum depolarization rates (Zhang et al., 2013). These were subsequently correlated with reduced Na^+ current (King et al., 2013 b), itself attributed to both chronically downregulated $Na_V1.5$ expression (King et al., 2013 b; Ning et al., 2016 a) and acute (King et al., 2013 b; d; Zhang et al., 2013) but potentially reversible loss of $Na_V1.5$ function (Knollmann et al., 2001 b; Salvage et al., 2015, 2017). Previous studies have reported that increasing or sequestrating intracellular [Ca^{2+}] reduced or restored Na^+ currents and $(dV/dt)_{max}$ respectively in in vitro WT cardiomyocytes (Casini et al., 2009). Altered cellular Ca^{2+} homeostasis could potentially acutely affect Nav1.5 function (Tan et al., 2002; Aiba et al., 2010; Ashpole et al., 2012) through its C-terminal region, either directly at an EF hand motif (Wingo et al., 2004) or indirectly through an IQ domain sensitive to calmodulin/calmodulin kinase II (Mori et al., 2000). Nav1.5 also shows multiple phosphorylatable, serine 516 and 571, and threonine 594 sites in its DI-II linker that are targetable by calmodulin kinase II (CaMKII) action (Mori et al., 2000; Wagner et al., 2011; Grandi and Herren, 2014).

The loose patch clamp method measures transmembrane current flow into an extracellular electrode apposed to the cardiomyocyte surface membrane forming the patch. It further can be applied to intact ventricular tissue preparations (King et al., 2013 b; Salvage et al., 2015; Ning et al., 2016 a). It thereby avoided the tissue disruption, cell isolation and intracellular Ca^{2+} chelation required by conventional whole-cell patch-clamp studies (Lei et al., 2005; Martin et al., 2012 b). The latter may account for differences between some of the present findings and previous observations using conventional patch clamping of isolated cells (Gurung et al., 2011 a). The present studies further employed in vivo rather than reduced

extracellular [Na^+] levels thereby sparing effects on Na^+-Ca^{2+} exchange. Previous reports had identified early inward currents obtained in loose patches with Na^+ currents mediating AP upstroke and its conduction (King et al., 2013 b).

Depolarising test steps elicited inward currents which activated to a peak value then showed an inactivating decline to baseline in a pattern characteristic of voltage-dependent Na^+ currents. These features were observed in all the young and aged, WT and *Pgc-1β*$^{-/-}$ ventricular cardiomyocytes studied. The resulting current-voltage relationships gave values that increased with depolarisation up to voltage excursions of (RMP + 80 mV) beyond which they declined as expected towards the Na^+ reversal potential. In contrast, imposition of voltage steps exploring inactivation characteristics began with prepulse voltages to varying levels of depolarisation which similarly elicited currents rising to a peak followed by an inactivation-mediated decay. These were followed by steps to a fixed depolarised membrane potential. The latter elicited currents whose peaks declined in amplitude with the depolarising prepulse as expected from the voltage dependent inactivation this would produce. Inactivation curves were constructed from plotting such peak currents against the prepulse level. These gave currents that fell with depolarisation. A two-way ANOVA, followed where indicated by post-hoc pairwise testing, then examined for significant independent and interacting effects of the *Pgc-1β*$^{-/-}$ (as opposed to WT) genotype and of age on the quantitative parameters emerging from fitting Boltzmann relationships to both the activation and inactivation data. This demonstrated independent effects of genotype, but not of age, or of interactions between these factors, in reducing maximum values of the peak Na^+ currents. However, there were neither independent nor interacting effects on consequently similar values of voltage at half maximum current, *V**, and the steepness *k* of both activation and inactivation characteristics. Nor were there differences in the time constants describing the timecourses for recovery from inactivation following restoration of the background voltage, which were consequently similar between experimental groups. These findings suggested that the altered availability of functional Na^+ channels accompanied otherwise normal voltage dependences.

These differences specifically in maximum Na^+ current contrasted with indistinguishable outward K^+ current characteristics between groups. Pulse protocols investigating the voltage dependences of K^+ current activation applied voltage steps to a range of test potentials, and followed these with hyperpolarising steps that would elicit a tail current whose amplitude reflected the preceding K^+ channel activation. Conversely K^+ current rectification properties were investigated by first imposing a conditioning step to a fixed membrane voltage step to produce a constant level of activation. This was followed by voltage steps to varying membrane potentials. The latter would result in tail currents flowing through similarly activated channels, in response to different driving forces, which would vary with the voltage dependence of the resulting open channel rectification properties. Both experiments yielded similar ventricular cardiomyocyte currents suggesting similar activation and rectification characteristics in all the four experimental groups explored. These thus yielded closely concordant activation and instantaneous current-voltage curves. Thus, two-way ANOVA demonstrated that there were neither independent nor interacting effects of genotype or age on areas made between observed values representing either plots of K^+ current activation, or of rectification properties and their voltage abscissae.

The loose-patch clamp technique as used in this study does not directly visualize the cells that are patched; it is thus a possibility that some patches are not of cardiomyocytes but of cardiac fibroblasts. Cardiac fibroblasts make up 75% of the total number of cardiac cells (Banerjee et al., 2007) but only around 5-10% of its volume (Shiraishi et al., 1992) and an even smaller percentage of endocardial surface area owing to their spherical shape – this in of itself makes it likely that the majority of the data is derived from cardiomyocytes on a probabilistic basis. It does not eliminate the possibility entirely however. Cardiac fibroblasts were once thought to be electrical bystanders, but more recent data suggests that they are in fact part of a complex electrophysiological milieu in the heart. They have a RMP of -50 to -60mV, slightly less negative than cardiomyocytes (Li et al., 2009). They express voltage gated potassium channels across a number of species (Shibukawa et al., 2005; Li et al., 2009) and human cardiac fibroblasts express TTX sensitive voltage gated sodium channels (Li et al., 2009; Yue et al., 2011); the situation in other species has not yet been determined.

Thus the final electrophysiological effect is determined by the electrophysiological properties of the two cell populations, as well as electrotonic effects between the two. However, there is scant evidence for any active electrical excitability of fibroblasts despite studies looking extensively for them (Kohl and Gourdie, 2014) or heterecellular coupling between them (Kohl and Gourdie, 2014). Ockham's razor would suggest that as cardiac excitability is adequately explained without invoking heterocellular coupling and complex fibroblast-cardiomyocyte interaction, this should be the working hypothesis. In this context, the electrotonic coupling would mean that any patch of mixed patch containing both cardiomyocyte/fibroblast would simply manifest as a reduced charge density per unit area and increased cell membrane capacitance. It may reasonably be questioned whether the lower current density of sodium current in *Pgc-1β*$^{-/-}$ patches thus simply represents the lower current density per unit area due to increased fibrosis (seen in chapter 4) rather than a reduction in cardiomyocyte sodium current density. However, this is not an adequate explanation for the findings – the fibrosis pattern seen in chapter 4 was graded, with differential fibrosis in young vs aged *Pgc-1β*$^{-/-}$ mice and young vs aged WT mice – the same pattern of sodium current density was not seen, with an equal reduction in sodium current density in young and aged *Pgc-1β*$^{-/-}$ mice. This suggest that fibroblasts were not patched to any significant degree as would be expected from their small contribution to cardiac volume and even smaller contribution to cardiac surface area. Any patch that was predominantly fibroblast was unlikely to have yielded experimentally viable patches and data would not have been likely collected from them. It is still however conceivable that small patches of fibroblast were encapsulated in the patch and as such current densities have been expressed as $pA/\mu m^2$ to reflect the measurement of current density per unit area of myocardium. The histology of the patches were not directly examined, but this could be a further avenue for exploration in the future.

The loose patch clamp technique also differs from conventional tight patch clamping in the potential sources of error in its current measurements; while it does not suffer the drawbacks of artificially manipulated ion concentrations (including of the ion currents to be measured)

the loose nature of the seal introduces rim current errors. This is due to the membrane directly under the rim of the pipette being subjected to deformation causing activation (of the ionic channels in the membrane) at an uncontrolled voltage under the rim of the pipette. This results in a graded voltage clamp underneath the rim, with the patch being subjected to the command voltage, the outside of the patch at V_m and the rim underneath displaying an intermediate voltage between the two. Rim current errors can be minimised by increasing pipette size and thus reducing the ratio of the rim area to the patch area. A previous paper has demonstrated that it can be eliminated completely with the construction of concentric, double-barrelled pipettes (Roberts and Almers, 1984).

Despite these limitations, there is robust evidence for the present findings. The present current-voltage analyses of both activation and inactivation properties thus associate the *Pgc-1β*$^{-/-}$ genotype, but not ageing, with alterations in maximum Na^+ conductance. This took place in an absence of alterations in Na^+ channel activation and inactivation properties reflected in their voltages at half maximum current, V^* and the steepnesses k, of their voltage dependences, their timecourses of recovery from inactivation, and in the voltage dependences of K^+ current activation and rectification. The resulting reduction specifically in maximum Na^+ current constitutes a mechanism for the observed pro-arrhythmic reductions in AP conduction velocity accompanied by reduced peak AP upstroke rates $(dV/dt)_{max}$ in the presence of the *Pgc-1β*$^{-/-}$ genotype (Ahmad et al., 2017).

7. SUMMARY, GENERAL DISCUSSION AND FUTURE WORK

7.1 OBJECTIVES AND BACKGROUND OF PRESENT STUDY.

This project sought to design, complete and interpret a robust set of experiments investigating the characteristics and mechanisms of arrhythmogenesis in the setting of mitochondrial dysfunction and the cumulative changes that occur with advancing age. The present findings develop and complement initial reports that were largely preoccupied with properties of isolated *Pgc-1β*$^{-/-}$ cardiomyocytes (Gurung et al., 2011 b). The latter similarly reported arrhythmic phenotypes at the level of whole hearts. Studies in isolated cardiac myocytes associated the peroxisome proliferator-activated receptor-γ coactivator-1β knockout (*Pgc-1β*$^{-/-}$) genotype with alterations in Ca^{2+} homeostasis reflected in diastolic Ca^{2+} transients. Use of conventional (tight) patch clamp recordings suggested alterations in Ca^{2+} channel activation. These findings together implicated altered Ca^{2+} homeostasis, in the form of DADs/EADs and other recovery abnormalities, in the observed increased frequency of diastolic depolarisation events in the arrhythmic phenotype. They also suggested an enhanced Na^{+} channel function in the form of increased maximum rates of action potential upstroke. However, the latter findings were obtained under recording conditions involving intracellular Ca^{2+} chelation. These conditions are unlikely to be replicated in cardiomyocytes in vivo. The effect of such dramatic changes in ionic composition on ionic channel function have only been reported recently. Thus major effects on Na^{+} current densities followed either genetic or pharmacological manipulations of intracellular Ca^{2+}(King et al., 2013 d; Ning et al., 2016 b; Valli et al., 2018). It was therefore important to follow studies performed in isolated cardiomyocyte with explorations of the electrophysiological properties of intact cardiomyocytes in intact working hearts minimizing perturbations in their intracellular homeostasis.

7.2 ELECTROCARDIOGRAPHIC STUDIES AT THE WHOLE HEART LEVEL

The series of experiments outlined here studied electrophysiological characteristics through measurements of cardiomyocyte electrophysiological properties in multiple physiological preparations. Importantly this included experiments on intact working hearts under conditions in which arrhythmia could be observed. These included ECG studies in intact organisms, microelectrode studies of ventricular cardiomyocyte activity in isolated, perfused, hearts, and studies of ion currents using a loose patch clamp technique in a novel ventricular preparation. These studies were performed in groups of young (12-16 week) and aged (>52 week) *Pgc-1β*$^{-/-}$ and WT mice.

First, electrocardiographic (ECG) studies examined overall cardiac electrophysiological phenotypes at the whole animal level. This demonstrated that the mitochondrial dysfunction produced by *Pgc-1β* knockout generates distinct electrocardiographic features that differed between anaesthetised young and aged, WT and *Pgc-1β*$^{-/-}$ mice. Following dobutamine challenge, the *Pgc-1β*$^{-/-}$ hearts displayed compromised sino-atrial node function, and an atrioventricular conduction defect. The latter defect was most frequent in the aged *Pgc-1β*$^{-/-}$ mice. In addition, *Pgc-1β*$^{-/-}$ mice displayed prolonged ventricular activation times consistent with the existence of a ventricular pro-arrhythmic substrate. ECG analysis thus yielded electrophysiological findings bearing on potential arrhythmogenicity in intact *Pgc-1β*$^{-/-}$ mice, and suggested detailed features for subsequent testing. These findings demonstrate that ventricular activation was prolonged in *Pgc-1β*$^{-/-}$ mice consistent with slowed action potential conduction.

7.3 ELECTROPHYSIOLOGICAL STUDIES OF CARDIOMYOCYTES IN INTACT PERFUSED HEARTS

The ECG findings prompted investigations for the importance of slowed ventricular activation in the arrhythmic phenotype. Single cell action potential characteristics in intact Langendorff-perfused hearts were studied using simultaneous microelectrode and ECG recordings. The

first set of these microelectrode experiments studied the effects of programmed electrical stimulation (PES) protocols.

Young and aged *Pgc-1β*$^{-/-}$ mice showed higher frequencies and durations of arrhythmic episodes. These episodes took place over a wider range of S1S2 intervals when compared to WT. Both young and aged, regularly-paced, *Pgc-1β*$^{-/-}$ hearts showed slowed maximum action potential (AP) upstroke rates, $(dV/dt)_{max}$ (~157 vs. 120-130 V s^{-1}), prolonged AP latencies (by ~20%) and shortened refractory periods (~58 vs. 51 ms) but similar AP durations (~50 ms at 90% recovery) compared to WT. However, the *Pgc-1β*$^{-/-}$ genotype and age each influenced extrasystolic AP latencies during PES. Furthermore, young and aged WT ventricles displayed distinct dependences of AP latency upon $(dV/dt)_{max}$, but *Pgc-1β*$^{-/-}$ ventricles displayed a relationship of AP latency upon $(dV/dt)_{max}$ that resembled aged WT mice. They also showed independently increased levels of myocardial fibrotic change. Finally, AP wavelengths combining activation and recovery terms paralleled the contrasting arrhythmic incidences in *Pgc-1β*$^{-/-}$ and WT hearts.

The second set of microelectrode investigations employed an incremental pacing protocol used previously to explore action potential restitution. Hearts were subjected to successive trains of 100 regular stimuli at progressively decremented BCLs. Aged *Pgc-1β*$^{-/-}$ hearts again displayed an increased incidence of arrhythmia compared to other groups. In addition both the young and aged *Pgc-1β*$^{-/-}$ hearts showed higher incidences of alternans, reflecting instabilities known to presage the onset of arrhythmia in both AP activation and recovery characteristics compared to WT hearts. Such differences were particularly apparent at the lower pacing frequencies. They accompanied reduced $(dV/dt)_{max}$ and increased AP latency values in the *Pgc-1β*$^{-/-}$ hearts. In particular, APs observed prior to termination of the protocol showed lower $(dV/dt)_{max}$ and longer AP latencies, but indistinguishable APD_{90} and RMPs in those *Pgc-1β*$^{-/-}$ in which the stimulation protocol culminated in arrhythmia. Restitution curves of AP wavelengths were shorter in *Pgc-1β*$^{-/-}$ than WT hearts, this being particularly the case in aged Pgc-1β$^{-/-}$ hearts. These experiments demonstrated that Pgc-1β$^{-/-}$ hearts show pro-arrhythmic instabilities, and attributed these to altered AP conduction and activation

characteristics. The study confirms the important findings of decreased $(dV/dt)_{max}$ and importantly the unique wavelength characteristics associated with *Pgc-1β*$^{-/-}$ hearts.

7.4 LOOSE PATCH CLAMP STUDIES OF IONIC CURRENTS IN CARDIOMYOCYTES IN SITU

These findings together suggested a hypothesis that associates mitochondrial dysfunction with arrhythmic phenotypes through shortened AP wavelength produced by slowed AP conduction and age-dependent fibrotic change. Such findings parallel earlier reports that implicated a deficiency of Nav1.5 in arrhythmic tendency, similar alterations in action potential characteristics and fibrotic tendency in arrhythmic models (Jeevaratnam et al., 2016).

The final group of experiments accordingly proceeded to test a hypothesis implicating compromised Na^+ channel function. Loose patch-clamp techniques were applied in intact ventricular cardiomyocyte preparations for the first time. This technique permitted studies of cardiomyocytes in situ, conserving their in-vivo extracellular and intracellular conditions. Both young and aged *Pgc-1β*$^{-/-}$ mice showed reductions in the maximum peak Na^+ currents. The remaining Na^+ current activation and inactivation characteristics remained indistinguishable through all experimental groups. These differences were observed despite indistinguishable activation and rectification properties of delayed outward (K^+) currents. These findings directly implicate a reduction in maximum available Na^+ current with unchanged voltage dependences in the pro-arrhythmic reductions in AP conduction velocity in *Pgc-1β*$^{-/-}$ ventricles.

7.5 DISCUSSION OF THE EXPERIMENTAL APPROACH AND FUTURE STUDIES

The work presented here represents a strong experimental approach to describing the electrophysiological characteristics of a model for energetic dysfunction and the changes in

ion channel conductance that may be associated with it. It does not however describe a mechanistic link between the two and the causative biochemical cascade of events that result in the final electrophysiological changes. Such a causative explanation would need evidence from DNA and RNA, transcription factor analyses, intracellular second messenger changes and finally in-depth ionic channel assays. The study does however suggest a number of avenues for future experiments that would be productive in developing this link.

Future studies should therefore aim to further this causative link in a number of ways. Firstly, a direct correlation between energetic dysfunction and the electrophysiological changes such as sodium channel conductance and $(dV/dt)_{max}$ should be made to strengthen the link between the two. This would entail direct measurement of ATP, ADP, AMP concentrations as well as the redox potential of the mitochondria in all experimental hearts. This would clearly establish whether there is a direct relationship and correlation between cellular biochemical markers of energetic sufficiency and the electrophysiological changes in AP characteristics, or whether there is a threshold level below which no changes are induced. Examining the expression of mitochondrial and nuclear gene profiles in genes of interest would also be a useful step in examining the detailed cellular level changes that *Pgc-1β* ablation causes.

Secondly, western blot analysis of ion channel and important mitochondrial proteins would confirm the gene level changes with evidence for functional ion channel expression changes and ascertain whether there are any significant changes in protein expression levels between the experimental groups. With this information, it would then be possible to devise a hypothesis as to what cellular signalling changes may be affecting the biochemical milieu. There is a strong suspicion of altered Ca^{2+} homeostasis which could be an intermediator between the ultimate ion channel level changes seen and the base genetic level changes and this would likely need to be explored regardless – not least because Ca^{2+} homeostasis is known to have a significant impact on arrhythmogenicity in of itself, being important in triggering arrhythmias and being a strong candidate for study from the experiments of this study and allied experiments not presented here.

Finally another promising approach would be to try and integrate the changes in sodium channel properties and AP characteristics to the tissue level fibrosis seen. The relative contribution of fibrotic change to arrhythmias needs to be examined further. Fibrosis alters the structural properties of the tissue and this likely has electrophysiological effects. How this impacts upon tissue resistivity gap junction conductance and the relative importance of this versus changes in sodium channel changes in conduction velocity changes are yet to be determined. A number of different diseases involving the sodium channel seem to have abnormal fibrosis, including the Brugada syndrome. This may lead to investigation as to the importance of Nav1.5 subunit as a macromolecular anchor at the surface membrane that integrates structural as well as signalling components that mediate the normal composition of the extracellular matrix and fibrosis and the cell to cell connections that are important in a syncytium. Experiments to directly measure tissue resistivity and pulldown experiments to isolate the Nav1.5 macromolecular complex would be an initial approach to this question.

The striking SAN and AVN abnormalities seen in the aged *Pgc-1β* deficient mice is a tangential finding that may allow insights into the senile degeneration of the conduction system seen in human populations. It is known that AVN disease is a frequent and important cause of conduction disease in humans, though the age-related mechanism of how nodal tissues are affected by age is mostly unknown. Experimental strategies here would require the ability to isolated the nodal tissue and study their AP characteristics. The small size of the mouse system would make this challenging as cell yield in cardiomyocyte isolation would be low. An initial strategy may instead focus on the structural changes in conduction system with assessment of fibrotic changes and immunohistochemistry allowing further information to be gained as to the likely cellular abnormalities before investing the significant time needed to isolate nodal tissues and cells for in depth electrophysioloical investigation. Pharmacological approaches to target the specific molecules of interests and to reduce free radical burden in mitochondria may also be potential avenues for exploration.

7.8 LIMITATIONS

The main limitations of this study have been discussed previously in the introduction and chapter discussions. The differences in murine and human physiology are a key limitation. Mice are far smaller mammals than humans and have higher basal heart rates. There are clear differences in the cardiac action potential between the two species. Most differences are in the repolarisation and plateau phase of the AP, with the depolarising phase conserved – human APs display rapid K (I_{Kr}) and slow K (I_{Ks}) currents, whilst mice show fast K ($I_{to,f}$) and slow K ($I_{to,s}$) currents. Mouse hearts also use less L-type Ca channel current $I_{Ca\text{-}L}$. This means that the mouse cardiac AP does not have a prolonged plateau phase and has shorter APD values. Thus changes in the depolarising phase of the AP are likely to be more translatable to human findings. This furthers the importance of future Ca^{2+} handling work (which would relate to the plateau phase of the AP) to use human as well as murine tissue as the experimental base.

Secondly, the Langendorff preparation has drawbacks including a non-physiological perfusate and the use of blebbistatin which may have cardio-protective effects and reduce energetic demand of the heart (see chapter 4 and 5 discussion). Finally, the lack of previous normal physiological values for murine ECG data and human work relating to ventricular tissue and PGC-1 (which has invariably looked at the question of heart failure) means there are no studies on the effect of the electrophysiological milieu to compare our findings against. This applies to murine as well as human studies, with no other literature being available to my knowledge on the subject matter of this thesis other than that presented here. The loose patch clamp technique allows measurement of current voltage relationships of important cellular currents, though in the apparatus used here direct visualisation of the patch was not possible and thus there may be additional electrotonic effects of fibroblasts. For this reason, currents were expressed as current densities per unit area. Further, rim current error could not be completely eliminated in the experiments performed here and thus estimated of the Nernst reversal potentials were not made. Despite these caveats, my work offers an important insight into the effect complex energetic and mitochondrial pathologies can have on electrophysiology, though further work is needed to offer mechanistic insight.

8. REFERENCES

Abdurrachim, D., Luiken, J. J. F. P., Nicolay, K., Glatz, J. F. C., Prompers, J. J., Nabben, M., 2015. Good and bad consequences of altered fatty acid metabolism in heart failure: evidence from mouse models. *Cardiovasc Res* 106, 194–205

Adabag, S., Huxley, R. R., Lopez, F. L., Chen, L. Y., Sotoodehnia, N., Siscovick, D., Deo, R., Konety, S., Alonso, A., Folsom, A. R., 2015. Obesity related risk of sudden cardiac death in the atherosclerosis risk in communities study. *Heart* 101, 215–221

Ahmad, S., Valli, H., Edling, C., Grace, A., Jeevaratnam, K., Huang, C., 2017. Effects of ageing on pro-arrhythmic ventricular phenotypes in incrementally paced murine Pgc-1β -/- hearts. *Pflugers Arch* 469, 1579–1590

Ahmad, S., Valli, H., Salvage, S., Grace, A., Jeevaratnam, K., Huang, C. H., 2018a. Age-dependent electrocardiographic changes in Pgc-1β deficient murine hearts. *Clin Exp Pharmacol Physiol* 45, 174–186

Ahmad, S., Valli, H., Chadda, K. R., Cranley, J., Jeevaratnam, K., Huang, C. L. H., 2018b. Ventricular pro-arrhythmic phenotype, arrhythmic substrate, ageing and mitochondrial dysfunction in peroxisome proliferator activated receptor-γ coactivator-1β deficient (Pgc-1β−/−) murine hearts. *Mech Ageing Dev* 173, 92–103

Aiba, T., Hesketh, G. G., Liu, T., Carlisle, R., Villa-Abrille, M. C., O'Rourke, B., Akar, F. G., Tomaselli, G. F., 2010. Na+ channel regulation by Ca(2+)/calmodulin and Ca(2+)/calmodulin-dependent protein kinase II in guinea-pig ventricular myocytes. *Cardiovasc Res* 85, 454–463

Akar, F. G., O'Rourke, B., 2011. Mitochondria are sources of metabolic sink and arrhythmias. *Pharmacol {&} Ther* 131, 287–294

Almers, W., Stanfield, P. R., Stühmer, W., 1983a. Slow changes in currents through sodium channels in frog muscle membrane. *J Physiol* 339, 253–271

Almers, W., Stanfield, P. R., Stühmer, W., 1983b. Lateral distribution of sodium and potassium channels in frog skeletal muscle: measurements with a patch-clamp technique. *J Physiol* 336,

261–284

Amin, A. S., Tan, H. L., Wilde, A. A. M., 2010. Cardiac ion channels in health and disease. *Hear Rhythm* 7, 117–126

Antzelevitch, C., Pollevick, G. D., Cordeiro, J. M., Casis, O., Sanguinetti, M. C., Aizawa, Y., Guerchicoff, A., Pfeiffer, R., Oliva, A., Wollnik, B., Gelber, P., Bonaros, E. P., Burashnikov, E., Wu, Y., Sargent, J. D., Schickel, S. et al., 2007. Loss-of-function mutations in the cardiac calcium channel underlie a new clinical entity characterized by ST-segment elevation, short QT intervals, and sudden cardiac death. *Circulation* 115, 442–449

Antzelevitch, C., Burashnikov, A., 2011. Overview of Basic Mechanisms of Cardiac Arrhythmia. *Card Electrophysiol Clin* 3, 23–45

Arany, Z., He, H., Lin, J., Hoyer, K., Handschin, C., Toka, O., Ahmad, F., Matsui, T., Chin, S., Wu, P. H., Rybkin, I. I., Shelton, J. M., Manieri, M., Cinti, S., Schoen, F. J., Bassel-Duby, R. et al., 2005. Transcriptional coactivator PGC-1 alpha controls the energy state and contractile function of cardiac muscle. *Cell Metab* 1, 259–271

Ashpole, N. M., Herren, A. W., Ginsburg, K. S., Brogan, J. D., Johnson, D. E., Cummins, T. R., Bers, D. M., Hudmon, A., 2012. Ca2+/calmodulin-dependent protein kinase II (CaMKII) regulates cardiac sodium channel NaV1.5 gating by multiple phosphorylation sites. *J Biol Chem* 287, 19856–19869

Balasubramaniam, R., Chawla, S., Mackenzie, L., Schwiening, C. J., Grace, A. A., Huang, C. L. H., 2004. Nifedipine and diltiazem suppress ventricular arrhythmogenesis and calcium release in mouse hearts. *Pflugers Arch* 449, 150–158

Balasubramaniam, R., Chawla, S., Grace, A. A., Huang, C. L. H., 2005. Caffeine-induced arrhythmias in murine hearts parallel changes in cellular Ca(2+) homeostasis. *Am J Physiol Heart Circ Physiol* 289, H1584--93

Banerjee, I., Fuseler, J. W., Price, R. L., Borg, T. K., Baudino, T. A., 2007. Determination of cell types and numbers during cardiac development in the neonatal and adult rat and mouse. *Am J Physiol Circ Physiol* 293, H1883–H1891

Barcellos-Hoff, M. H., Dix, T. A., 1996. Redox-mediated activation of latent transforming

growth factor-beta 1. *Mol Endocrinol* 10, 1077–1083

Bardy, G. H., Lee, K. L., Mark, D. B., Poole, J. E., Packer, D. L., Boineau, R., Domanski, M., Troutman, C., Anderson, J., Johnson, G., McNulty, S. E., Clapp-Channing, N., Davidson-Ray, L. D., Fraulo, E. S., Fishbein, D. P., Luceri, R. M. et al., 2005. Amiodarone or an Implantable Cardioverter–Defibrillator for Congestive Heart Failure. *N Engl J Med* 352, 225–237

Bates, D., Mächler, M., Bolker, B., Walker, S., 2015. Fitting Linear Mixed-Effects Models Using **lme4**. *J Stat Softw* 67

Behr, E., Wood, D. A., Wright, M., Syrris, P., Sheppard, M. N., Casey, A., Davies, M. J., McKenna, W., Group., S. A. D. S. S., 2003. Cardiological assessment of first-degree relatives in sudden arrhythmic death syndrome.[see comment]. *Lancet* 362, 1457–1459

Bers, D. M., 2001. *Excitation–contraction coupling and cardiac contractile force* 2nd edn. Kluwer Academic Publishers, Dordrecht, The Netherlands

Bers, D. M., 2002. Cardiac excitation-contraction coupling. *Nature* 415, 198–205

Bhuiyan, Z. A., van den Berg, M. P., van Tintelen, J. P., Bink-Boelkens, M. T. E., Wiesfeld, A. C. P., Alders, M., Postma, A. V, van Langen, I., Mannens, M. M. A. M., Wilde, A. A. M., 2007. Expanding spectrum of human RYR2-related disease: new electrocardiographic, structural, and genetic features. *Circulation* 116, 1569–1576

Billman, G. E., 2008. The cardiac sarcolemmal ATP-sensitive potassium channel as a novel target for anti-arrhythmic therapy. *Pharmacol Ther* 120, 54–70

Boukens, B. J., Rivaud, M. R., Rentschler, S., Coronel, R., 2014. Misinterpretation of the mouse ECG: 'musing the waves of Mus musculus'. *J Physiol* 21, 4613–4626

Bovo, E., Lipsius, S. L., Zima, A. V, 2012. Reactive oxygen species contribute to the development of arrhythmogenic Ca^{2+} waves during $β$-adrenergic receptor stimulation in rabbit cardiomyocytes. *J Physiol* 590, 3291–3304

Brack, K. E., Narang, R., Winter, J., Ng, G. A., 2013. The mechanical uncoupler blebbistatin is associated with significant electrophysiological effects in the isolated rabbit heart. *Exp Physiol* 98, 1009–1027

Bradshaw, P. J., Stobie, P., Knuiman, M. W., Briffa, T. G., Hobbs, M. S. T., 2014. Trends in the incidence and prevalence of cardiac pacemaker insertions in an ageing population. *Open Hear* 1, e000177

Brooks, W. W., Conrad, C. H., 2000. Myocardial Fibrosis in Transforming Growth Factor β1Heterozygous Mice. *J Mol Cell Cardiol* 32, 187–195

Brown, D. A., O'Rourke, B., 2010. Cardiac mitochondria and arrhythmias. *Cardiovasc Res* 88, 241–249

Brubaker, P. H., Kitzman, D. W., 2011. Chronotropic incompetence: Causes, consequences, and management. *Circulation* 123, 1010–1020

Camelliti, P., Devlin, G. P., Matthews, K. G., Kohl, P., Green, C. R., 2004. Spatially and temporally distinct expression of fibroblast connexins after sheep ventricular infarction. *Cardiovasc Res* 62, 415–425

Casini, S., Verkerk, A. O., van Borren, M. M. G. J., van Ginneken, A. C. G., Veldkamp, M. W., de Bakker, J. M. T., Tan, H. L., 2009. Intracellular calcium modulation of voltage-gated sodium channels in ventricular myocytes. *Cardiovasc Res* 81, 72–81

Chadda, K. R., Ahmad, S., Valli, H., den Uijl, I., Al-Hadithi, A. B., Salvage, S. C., Grace, A. A., Huang, C. L. H., Jeevaratnam, K., 2017. The effects of ageing and adrenergic challenge on electrocardiographic phenotypes in a murine model of long QT syndrome type 3. *Sci Rep* 7, 11070

Chakko, S., de Marchena, E., Kessler, K. M., Myerburg, R. J., 1989. Ventricular arrhythmias in congestive heart failure. *Clin Cardiol* 12, 525–530

Chiamvimonvat, N., Kargacin, M. E., Clark, R. B., Duff, H. J., 1995. Effects of intracellular calcium on sodium current density in cultured neonatal rat cardiac myocytes. *J Physiol* 483, 307–318

Chilton, L., Giles, W. R., Smith, G. L., 2007. Evidence of intercellular coupling between co-cultured adult rabbit ventricular myocytes and myofibroblasts. *J Physiol* 583, 225–236

Cranefield, P. F., Hoffman, B. F., 1968. The electrical activity of the heart and the

electrocardiogram. *J Electrocardiol* 1, 2–4

Dai, D. F., Santana, L. F., Vermulst, M., Tomazela, D. M., Emond, M. J., MacCoss, M. J., Gollahon, K., Martin, G. M., Loeb, L. A., Ladiges, W. C., Rabinovitch, P. S., 2009. Overexpression of Catalase Targeted to Mitochondria Attenuates Murine Cardiac Aging. *Circulation* 119, 2789–2797

Danik, S., Cabo, C., Chiello, C., Kang, S., Wit, A. L., Coromilas, J., 2002. Correlation of repolarization of ventricular monophasic action potential with ECG in the murine heart. *Am J Physiol Heart Circ Physiol* 283, H372-81

Dautova, Y., Zhang, Y., Sabir, I., Grace, A. A., Huang, C. L. H., 2009. Atrial arrhythmogenesis in wild-type and Scn5a+/delta murine hearts modelling LQT3 syndrome. *Pfl{ü}gers Arch Eur J Physiol* 458, 443–457

Davidenko, J. M., Antzelevitch, C., 1986. Electrophysiological mechanisms underlying rate-dependent changes of refractoriness in normal and segmentally depressed canine Purkinje fibers. The characteristics of post-repolarization refractoriness. *Circ Res* 58, 257–268

Davidenko, J. M., Salomonsz, R., Pertsov, A. M., Baxter, W. T., Jalife, J., 1995. Effects of pacing on stationary reentrant activity. Theoretical and experimental study. *Circ Res* 77, 1166–1179

Davies, L., Jin, J., Shen, W., Tsui, H., Shi, Y., Wang, Y., Zhang, Y., Hao, G., Wu, J., Chen, S., Fraser, J. A., Dong, N., Christoffels, V., Ravens, U., Huang, C. L. H., Zhang, H. et al., 2014. Mkk4 is a negative regulator of the transforming growth factor beta 1 signaling associated with atrial remodeling and arrhythmogenesis with age. *J Am Heart Assoc* 3, 1–19

De Mello, W. C., 1983. The role of cAMP and Ca on the modulation of junctional conductance: an integrated hypothesis. *Cell Biol Int Rep* 7, 1033–1040

Deo, R., Albert, C. M., 2012. Epidemiology and Genetics of Sudden Cardiac Death. *Circulation* 125

Dillon, L. M., Rebelo, A. P., Moraes, C. T., 2012. The role of PGC-1 coactivators in aging skeletal muscle and heart. *IUBMB Life* 64, 231–241

Duehmke, R. M., Pearcey, S., Stefaniak, J. D., Guzadhur, L., Jeevaratnam, K., Costopoulos, C.,

Pedersen, T. H., Grace, A. A., Huang, C. L. H., 2012. Altered re-excitation thresholds and conduction of extrasystolic action potentials contribute to arrhythmogenicity in murine models of long QT syndrome. *Acta Physiol* 206, 164–177

Duff, H. J., Offord, J., West, J., Catterall, W. A., 1992. Class I and IV antiarrhythmic drugs and cytosolic calcium regulate mRNA encoding the sodium channel alpha subunit in rat cardiac muscle. *Mol Pharmacol* 42, 570–574

Dyck, J. R. B., Lopaschuk, G. D., 2006. AMPK alterations in cardiac physiology and pathology: enemy or ally? *J Physiol* 574, 95–112

Eghbali, M., Eghbali, M., Robinson, T. F., Seifter, S., Blumenfeld, O. O., 1989. Collagen accumulation in heart ventricles as a function of growth and aging. *Cardiovasc Res* 23, 723–729

Einthoven W, 1903. A new galvanometer. *Ann Phys (N Y)* 12, 1059–1071

Euler, D. E., 1999. Cardiac alternans: Mechanisms and pathophysiological significance. *Cardiovasc Res*

Exil, V. J., Roberts, R. L., Sims, H., McLaughlin, J. E., Malkin, R. A., Gardner, C. D., Ni, G., Rottman, J. N., Strauss, A. W., 2003. Very-Long-Chain Acyl-Coenzyme A Dehydrogenase Deficiency in Mice. *Circ Res* 93, 448–455

Fedorov, V. V., Lozinsky, I. T., Sosunov, E. A., Anyukhovsky, E. P., Rosen, M. R., Balke, C. W., Efimov, I. R., 2007. Application of blebbistatin as an excitation-contraction uncoupler for electrophysiologic study of rat and rabbit hearts. *Hear Rhythm* 4, 619–626

Feridooni, H. A., Dibb, K. M., Howlett, S. E., 2015. How cardiomyocyte excitation, calcium release and contraction become altered with age. *J Mol Cell Cardiol* 83, 62–72

Finck, B. N., Kelly, D. P., 2006. PGC-1 coactivators: Inducible regulators of energy metabolism in health and disease. *J Clin Invest*

Fraser, J. A., Huang, C. L. H., Pedersen, T. H., 2011. Relationships between resting conductances, excitability, and t-system ionic homeostasis in skeletal muscle. *J Gen Physiol* 138, 95–116

Garrey, W. E., 1914. *THE NATURE OF FIBRILLARY CONTRACTION OF THE HEART.-ITS RELATION TO TISSUE MASS AND FORM1*

Gazoti Debessa, C. R., Mesiano Maifrino, L. B., Rodrigues de Souza, R., 2001. Age related changes of the collagen network of the human heart. *Mech Ageing Dev* 122, 1049–1058

Glukhov, A. V, Kalyanasundaram, A., Lou, Q., Hage, L. T., Hansen, B. J., Belevych, A. E., Mohler, P. J., Knollmann, B. C., Periasamy, M., Györke, S., Fedorov, V. V, 2013. Calsequestrin 2 deletion causes sinoatrial node dysfunction and atrial arrhythmias associated with altered sarcoplasmic reticulum calcium cycling and degenerative fibrosis within the mouse atrial pacemaker complex. *Eur Heart J* 1–13

Go, A. S., Hylek, E. M., Phillips, K. A., Chang, Y., Henault, L. E., Selby, J. V, Singer, D. E., 2001. Prevalence of diagnosed atrial fibrillation in adults: national implications for rhythm management and stroke prevention: the AnTicoagulation and Risk Factors in Atrial Fibrillation (ATRIA) Study. *JAMA* 285, 2370–2375

Go, A. S., Mozaffarian, D., Roger, V. L., Benjamin, E. J., Berry, J. D., Borden, W. B., Bravata, D. M., Dai, S., Ford, E. S., Fox, C. S., Franco, S., Fullerton, H. J., Gillespie, C., Hailpern, S. M., Heit, J. A., Howard, V. J. et al., 2013. Executive Summary: Heart Disease and Stroke Statistics--2013 Update: A Report From the American Heart Association. *Circulation* 127, 143–152

Goddard, C. A., Ghais, N. S., Zhang, Y., Williams, A. J., Colledge, W. H., Grace, A. A., Huang, C. L. H., 2008a. Physiological consequences of the *P2328S* mutation in the ryanodine receptor (*RyR2*) gene in genetically modified murine hearts. *Acta Physiol* 194, 123–140

Goddard, C. A., Ghais, N. S., Zhang, Y., Williams, A. J., Colledge, W. H., Grace, A. A., Huang, C. L. H., 2008b. Physiological consequences of the P2328S mutation in the ryanodine receptor (RyR2) gene in genetically modified murine hearts. *Acta Physiol (Oxf)* 194, 123–140

Gold, M. R., Bloomfield, D. M., Anderson, K. P., El-Sherif, N. E., Wilber, D. J., Groh, W. J., Estes, N. a, Kaufman, E. S., Greenberg, M. L., Rosenbaum, D. S., 2000. A comparison of T-wave alternans, signal averaged electrocardiography and programmed ventricular stimulation for arrhythmia risk stratification. *J Am Coll Cardiol* 36, 2247–2253

Goldbarg, A. N., Hellerstein, H. K., Bruell, J. H., Daroczy, A. F., 1968. Electrocardiogram of the

Normal Mouse, Mus Musculus: General Considerations and Genetic Aspects. *Cardiovasc Res* 2, 93–99

Gollob, M. H., Redpath, C. J., Roberts, J. D., 2011. The short QT syndrome: Proposed diagnostic criteria. *J Am Coll Cardiol* 57, 802–812

Gomes, A. P., Price, N. L., Ling, A. J. Y., Moslehi, J. J., Montgomery, M. K., Rajman, L., White, J. P., Teodoro, J. S., Wrann, C. D., Hubbard, B. P., Mercken, E. M., Palmeira, C. M., De Cabo, R., Rolo, A. P., Turner, N., Bell, E. L. et al., 2013. Declining NAD+ induces a pseudohypoxic state disrupting nuclear-mitochondrial communication during aging. *Cell* 155, 1624–1638

Gong, G., Liu, J., Liang, P., Guo, T., Hu, Q., Ochiai, K., Hou, M., Ye, Y., Wu, X., Mansoor, A., From, A. H. L., Ugurbil, K., Bache, R. J., Zhang, J., 2003. Oxidative capacity in failing hearts. *Am J Physiol Circ Physiol* 285, H541–H548

Gourraud, J. B., Barc, J., Thollet, A., Le Marec, H., Probst, V., 2017. Brugada syndrome: Diagnosis, risk stratification and management. *Arch Cardiovasc Dis* 110, 188–195

Grandi, E., Herren, A. W., 2014. CaMKII-dependent regulation of cardiac Na(+) homeostasis. *Front Pharmacol* 5 MAR, 1–10

Grant, A. O., 2009. Cardiac Ion Channels. *Circ Arrhythmia Electrophysiol* 2, 185–194

Gurung, I. S., Medina-Gomez, G., Kis, A., Baker, M., Velagapudi, V., Neogi, S. G., Campbell, M., Rodriguez-Cuenca, S., Lelliott, C., McFarlane, I., Oresic, M., Grace, A. A., Vidal-Puig, A., Huang, C. L. H., 2011a. Deletion of the metabolic transcriptional coactivator PGC1β induces cardiac arrhythmia. *Cardiovasc Res* 92, 29–38

Gurung, I. S., Medina-Gomez, G., Kis, A., Baker, M., Velagapudi, V., Neogi, S. G., Campbell, M., Rodriguez-Cuenca, S., Lelliott, C., McFarlane, I., Oresic, M., Grace, A. A., Vidal-Puig, A., Huang, C. L. H., 2011b. Deletion of the metabolic transcriptional coactivator PGC1beta induces cardiac arrhythmia. *Cardiovasc Res* 92, 29–38

Guzadhur, L., Pearcey, S. M., Duehmke, R. M., Jeevaratnam, K., Hohmann, A. F., Zhang, Y., Grace, A. A., Lei, M., Huang, C. L. H., 2010. Atrial arrhythmogenicity in aged Scn5a+/DeltaKPQ mice modeling long QT type 3 syndrome and its relationship to Na+ channel expression and cardiac conduction. *Pfl{ü}gers Arch Eur J Physiol* 460, 593–601

Hafner, A. V, Dai, J., Gomes, A. P., Xiao, C. Y., Palmeira, C. M., Rosenzweig, A., Sinclair, D. A., 2010. Regulation of the mPTP by SIRT3-mediated deacetylation of CypD at lysine 166 suppresses age-related cardiac hypertrophy. *Aging (Albany NY)* 2, 914–923

Hao, X., Zhang, Y., Zhang, X., Nirmalan, M., Davies, L., Konstantinou, D., Yin, F., Dobrzynski, H., Wang, X., Grace, A., Zhang, H., Boyett, M., Huang, C. L. H., Lei, M., 2011. TGF-β1-mediated fibrosis and ion channel remodeling are key mechanisms in producing the sinus node dysfunction associated with SCN5A deficiency and aging. *Circ Arrhythm Electrophysiol* 4, 397–406

Hart, C. Y. T., Burnett, J. C., Redfield, M. M., 2001. Effects of avertin versus xylazine-ketamine anesthesia on cardiac function in normal mice. *Am J Physiol Circ Physiol* 281, H1938–H1945

Hatch, F., Lancaster, M. K., Jones, S. A., 2011. Aging is a primary risk factor for cardiac arrhythmias: disruption of intracellular Ca $^{2+}$ regulation as a key suspect. *Expert Rev Cardiovasc Ther* 9, 1059–1067

Hayashi, M., Shimizu, W., Albert, C. M., 2015. The spectrum of epidemiology underlying sudden cardiac death. *Circ Res* 116, 1887–1906

Hondeghem, L. M., Katzung, B. G., 1977. Time- and voltage-dependent interactions of antiarrhythmic drugs with cardiac sodium channels. *Biochim Biophys Acta* 472, 373–398

Hookana, E., Junttila, M. J., Puurunen, V. P., Tikkanen, J. T., Kaikkonen, K. S., Kortelainen, M. L., Myerburg, R. J., Huikuri, H. V., 2011. Causes of nonischemic sudden cardiac death in the current era. *Hear Rhythm*

Hothi, S. S., Gurung, I. S., Heathcote, J. C., Zhang, Y., Booth, S. W., Skepper, J. N., Grace, A. A., Huang, C. L. H., 2008. Epac activation, altered calcium homeostasis and ventricular arrhythmogenesis in the murine heart. *Pflugers Arch* 457, 253–270

Huang, C., 2017a. Murine models of cardiac arrhythmogenesis. *Physiol Rev* 97, 283–409

Huang, C., 2017b. Murine electrophysiological models of cardiac arrhythmogenesis. *Physiol Rev* 97, 283–409

Hunter, P. J., McNaughton, P. A., Noble, D., 1975. Analytical models of propagation in excitable

cells. *Prog Biophys Mol Biol* 30, 99–144

Ingwall, J. S., 2009. Energy metabolism in heart failure and remodelling. *Cardiovasc Res* 81, 412–419

Investigators, T. A. versus I. D. (AVID), 1997. A Comparison of Antiarrhythmic-Drug Therapy with Implantable Defibrillators in Patients Resuscitated from Near-Fatal Ventricular Arrhythmias. *N Engl J Med* 337, 1576–1584

Jack, J., Noble, D., Tsien, R., 1983. *Electric Current Flow in Excitable Cells*. Oxford University Press

Jafri, M. S., Dudycha, S. J., O'Rourke, B., 2001. Cardiac Energy Metabolism: Models of Cellular Respiration. *Annu Rev Biomed Eng* 3, 57–81

Janse, M. J., Rosen, M. R., 2006. History of Arrhythmias. *Basis Treat Card Arrhythm*. Springer-Verlag, Berlin/Heidelberg, pp. 1–39

Jarreta, D., Orús, J., Barrientos, A., Miró, O., Roig, E., Heras, M., Moraes, C. T., Cardellach, F., Casademont, J., 2000. Mitochondrial function in heart muscle from patients with idiopathic dilated cardiomyopathy. *Cardiovasc Res* 45, 860–865

Jeevaratnam, K., Zhang, Y., Guzadhur, L., Duehmke, R. M., Lei, M., Grace, A. A., Huang, C. L. H., 2010. Differences in sino-atrial and atrio-ventricular function with age and sex attributable to the Scn5a+/- mutation in a murine cardiac model. *Acta Physiol (Oxf)* 200, 23–33

Jeevaratnam, K., Poh Tee, S., Zhang, Y., Rewbury, R., Guzadhur, L., Duehmke, R., Grace, A. A., Lei, M., Huang, C. L. H., 2011. Delayed conduction and its implications in murine Scn5a+/- hearts: Independent and interacting effects of genotype, age, and sex. *Pflugers Arch Eur J Physiol* 461, 29–44

Jeevaratnam, K., Rewbury, R., Zhang, Y., Guzadhur, L., Grace, A. A., Lei, M., Huang, C. L. H., 2012. Frequency distribution analysis of activation times and regional fibrosis in murine Scn5a+/- hearts: The effects of ageing and sex. *Mech Ageing Dev* 133, 591–599

Jeevaratnam, K., Guzadhur, L., Goh, Y., Grace, A., Huang, C. L. H., 2016. Sodium channel haploinsufficiency and structural change in ventricular arrhythmogenesis. *Acta Physiol* 216,

186–202

Jiang, M. T., Moffat, M. P., Narayanan, N., 1993. Age-related alterations in the phosphorylation of sarcoplasmic reticulum and myofibrillar proteins and diminished contractile response to isoproterenol in intact rat ventricle. *Circ Res* 72, 102–111

Jones, S. A., Lancaster, M. K., Boyett, M. R., 2004. Ageing-related changes of connexins and conduction within the sinoatrial node. *J Physiol* 560, 429–437

Kabunga, P., Lau, A. K., Phan, K., Puranik, R., Liang, C., Davis, R. L., Sue, C. M., Sy, R. W., 2015. Systematic review of cardiac electrical disease in Kearns-Sayre syndrome and mitochondrial cytopathy. *Int J Cardiol*

Kalin, A., Usher-Smith, J., Jones, V. J., Huang, C. L. H., Sabir, I. N., 2010. Cardiac arrhythmia: a simple conceptual framework. *Trends Cardiovasc Med* 20, 103–107

Kanaporis, G., Blatter, L. A., 2015. The mechanisms of calcium cycling and action potential dynamics in cardiac alternans. *Circ Res* 116, 846–856

Killeen, M. J., Gurung, I. S., Thomas, G., Stokoe, K. S., Grace, A. A., Huang, C. L. H., 2007. Separation of early afterdepolarizations from arrhythmogenic substrate in the isolated perfused hypokalaemic murine heart through modifiers of calcium homeostasis. *Acta Physiol (Oxf)* 191, 43–58

Killeen, M. J., Thomas, G., Sabir, I. N., Grace, A. A., Huang, C. L. H., 2008a. Mouse models of human arrhythmia syndromes. *Acta Physiol (Oxf)* 192, 455–469

Killeen, M. J., Thomas, G., Sabir, I. N., Grace, A. A., Huang, C. L. H., 2008b. Mouse models of human arrhythmia syndromes. *Acta Physiol* 192, 455–469

King, J. H., Huang, C. L. H., Fraser, J. A., 2013a. Determinants of myocardial conduction velocity: implications for arrhythmogenesis. *Front Physiol* 4, 154

King, J. H., Wickramarachchi, C., Kua, K., Du, Y., Jeevaratnam, K., Matthews, H. R., Grace, A. A., Huang, C. L. H., Fraser, J. A., 2013b. Loss of Nav1.5 expression and function in murine atria containing the RyR2-P2328S gain-of-function mutation. *Cardiovasc Res* 99, 751–759

King, J. H., Zhang, Y., Lei, M., Grace, A. A., Huang, C. L. H., Fraser, J. A., 2013c. Atrial arrhythmia,

triggering events and conduction abnormalities in isolated murine RyR2-P2328S hearts. *Acta Physiol (Oxf)* 207, 308–323

King, J. H., Zhang, Y., Lei, M., Grace, A. A., Huang, C. L. H., Fraser, J. A., 2013d. Atrial arrhythmia, triggering events and conduction abnormalities in isolated murine RyR2-P2328S hearts. *Acta Physiol* 207, 308–323

Kléber, A. G., Rudy, Y., 2004. Basic mechanisms of cardiac impulse propagation and associated arrhythmias. *Physiol Rev* 84, 431–488

Knollmann, B. C., Katchman, A. N., Franz, M. R., 2001a. Monophasic action potential recordings from intact mouse heart: validation, regional heterogeneity, and relation to refractoriness. *J Cardiovasc Electrophysiol* 12, 1286–1294

Knollmann, B. C., Blatt, S. A., Horton, K., De Freitas, F., Miller, T., Bell, M., Housmans, P. R., Weissman, N. J., Morad, M., Potter, J. D., 2001b. Inotropic stimulation induces cardiac dysfunction in transgenic mice expressing a troponin T (I79N) mutation linked to familial hypertrophic cardiomyopathy. *J Biol Chem* 276, 10039–10048

Kohl, P., Gourdie, R. G., 2014. Fibroblast-myocyte electrotonic coupling: does it occur in native cardiac tissue? *J Mol Cell Cardiol* 70, 37–46

Koplan, B. A., Stevenson, W. G., 2007. Sudden arrhythmic death syndrome. *Heart* 93, 547–548

Kucharska-Newton, A. M., Couper, D. J., Pankow, J. S., Prineas, R. J., Rea, T. D., Sotoodehnia, N., Chakravarti, A., Folsom, A. R., Siscovick, D. S., Rosamond, W. D., 2010. Diabetes and the risk of sudden cardiac death, the Atherosclerosis Risk in Communities study. *Acta Diabetol* 47 Suppl 1, 161–168

Lai, L., Leone, T. C., Zechner, C., Schaeffer, P. J., Kelly, S. M., Flanagan, D. P., Medeiros, D. M., Kovacs, A., Kelly, D. P., 2008. Transcriptional coactivators PGC-1alpha and PGC-lbeta control overlapping programs required for perinatal maturation of the heart. *Genes {&} Dev* 22, 1948–1961

Larsson, N. G., 2010. Somatic Mitochondrial DNA Mutations in Mammalian Aging. *Annu Rev Biochem* 79, 683–706

Lee, R. J., Liem, L. B., Cohen, T. J., Franz, M. R., 1992. Relation between repolarization and refractoriness in the human ventricle: cycle length dependence and effect of procainamide. *J Am Coll Cardiol* 19, 614–618

Lei, B., Lionetti, V., Young, M. E., Chandler, M. P., d'Agostino, C., Kang, E., Altarejos, M., Matsuo, K., Hintze, T. H., Stanley, W. C., 2004. Paradoxical downregulation of the glucose oxidation pathway despite enhanced flux in severe heart failure☆. *J Mol Cell Cardiol* 36, 567–576

Lei, M., Goddard, C., Liu, J., Léoni, A. L., Royer, A., Fung, S. S. M., Xiao, G., Ma, A., Zhang, H., Charpentier, F., Vandenberg, J. I., Colledge, W. H., Grace, A. A., Huang, C. L. H., 2005. Sinus node dysfunction following targeted disruption of the murine cardiac sodium channel gene Scn5a. *J Physiol* 567, 387–400

Lelliott, C. J., Medina-Gomez, G., Petrovic, N., Kis, A., Feldmann, H. M., Bjursell, M., Parker, N., Curtis, K., Campbell, M., Hu, P., Zhang, D., Litwin, S. E., Zaha, V. G., Fountain, K. T., Boudina, S., Jimenez-Linan, M. et al., 2006. Ablation of PGC-1β results in defective mitochondrial activity, thermogenesis, hepatic function, and cardiac performance. *PLoS Biol* 4, 2042–2056

Lenegre, J., 1964. Etiology and Pathology of Bilateral Bundle Branch Block in Relation To Complete Heart Block. *Prog Cardiovasc Dis* 6, 409–444

LEV, M., 1964. ANATOMIC BASIS FOR ATRIOVENTRICULAR BLOCK. *Am J Med* 37, 742–748

Li, G. R., Sun, H. Y., Chen, J. B., Zhou, Y., Tse, H. F., Lau, C. P., 2009. Characterization of Multiple Ion Channels in Cultured Human Cardiac Fibroblasts. (Kowaltowski, A. J., Ed.)*PLoS One* 4, e7307

Li, M., Hothi, S., Salvage, S., Jeevaratnam, K., Grace, A., Huang, C., 2017. Arrhythmic effects of Epac-mediated ryanodine receptor activation in Langendorff-perfused murine hearts are associated with reduced conduction velocity. *Clin Exp Pharmacol Physiol* 2017 Mar 1

Li, N., Chiang, D. Y., Wang, S., Wang, Q., Sun, L., Voigt, N., Respress, J. L., Ather, S., Skapura, D. G., Jordan, V. K., Horrigan, F. T., Schmitz, W., Müller, F. U., Valderrabano, M., Nattel, S., Dobrev, D. et al., 2014. Ryanodine receptor-mediated calcium leak drives progressive development of an atrial fibrillation substrate in a transgenic mouse model. *Circulation* 129,

1276–1285

Lim, C. C., Liao, R., Varma, N., Apstein, C. S., 1999. Impaired lusitropy-frequency in the aging mouse: role of Ca $^{2+}$ -handling proteins and effects of isoproterenol. *Am J Physiol Circ Physiol* 277, H2083–H2090

Lin, J., Handschin, C., Spiegelman, B. M., 2005. Metabolic control through the PGC-1 family of transcription coactivators. *Cell Metab*

Lin, J., Lopez, E. F., Jin, Y., Van Remmen, H., Bauch, T., Han, H. C., Lindsey, M. L., 2008. Age-related cardiac muscle sarcopenia: Combining experimental and mathematical modeling to identify mechanisms. *Exp Gerontol* 43, 296–306

Liu, M., Sanyal, S., Gao, G., Gurung, I. S., Zhu, X., Gaconnet, G., Kerchner, L. J., Shang, L. L., Huang, C. L. H., Grace, A., London, B., Dudley, S. C., Jr., 2009. Cardiac Na+ current regulation by pyridine nucleotides. *Circ Res* 105, 737–745

Liu, M., Liu, H., Dudley, S. C., 2010a. Reactive oxygen species originating from mitochondria regulate the cardiac sodium channel. *Circ Res* 107, 967–974

Liu, M., Liu, H., Dudley, S. C., 2010b. Reactive oxygen species originating from mitochondria regulate the cardiac sodium channel. *Circ Res* 107, 967–974

Loushin, M. K., 2005. The Effects of Anesthetic Agents on Cardiac Function. *Handb Card Anatomy, Physiol Devices*. Humana Press, Totowa, NJ, pp. 171–180

Lukyanenko, V., Chikando, A., Lederer, W. J., 2009. Mitochondria in cardiomyocyte Ca2+ signaling. *Int J Biochem Cell Biol* 41, 1957–1971

Luptak, I., Balschi, J. A., Xing, Y., Leone, T. C., Kelly, D. P., Tian, R., 2005. Decreased Contractile and Metabolic Reserve in Peroxisome Proliferator-Activated Receptor- -Null Hearts Can Be Rescued by Increasing Glucose Transport and Utilization. *Circulation* 112, 2339–2346

Mahoney, V. M., Mezzano, V., Morley, G. E., 2016. A review of the literature on cardiac electrical activity between fibroblasts and myocytes. *Prog Biophys Mol Biol* 120, 128–133

Mangoni, M. E., Nargeot, J., 2008. Genesis and regulation of the heart automaticity. *Physiol Rev* 88, 919–982

Martin, C. a., Matthews, G. D. K., Huang, C. L. H., 2012a. Sudden cardiac death and inherited channelopathy: the basic electrophysiology of the myocyte and myocardium in ion channel disease. *Heart* 98, 536–543

Martin, C. A., Zhang, Y., Grace, A. A., Huang, C. L. H., 2010. In vivo studies of Scn5a+/- mice modeling Brugada syndrome demonstrate both conduction and repolarization abnormalities. *J Electrocardiol* 43, 433–439

Martin, C. A., Grace, A. A., Huang, C. L. H., 2011a. Refractory dispersion promotes conduction disturbance and arrhythmias in a Scn5a (+/-) mouse model. *Pflugers Arch* 462, 495–504.

Martin, C. A., Guzadhur, L., Grace, A. A., Lei, M., Huang, C. L. H., 2011b. Mapping of reentrant spontaneous polymorphic ventricular tachycardia in a Scn5a+/- mouse model. *Am J Physiol Heart Circ Physiol* 300, H1853–H1862

Martin, C. A., Siedlecka, U., Kemmerich, K., Lawrence, J., Cartledge, J., Guzadhur, L., Brice, N., Grace, A. A., Schwiening, C., Terracciano, C. M., Huang, C. L. . H., 2012b. Reduced Na(+) and higher K(+) channel expression and function contribute to right ventricular origin of arrhythmias in Scn5a+/- mice. *Open Biol* 2, 120072

Massumi, R. A., Ali, N., 1970. Accelerated isorhythmic ventricular rhythms. *Am J Cardiol*

Matthews, G. D. K., Martin, C. A., Grace, A. A., Zhang, Y., Huang, C. L. H., 2010. Regional variations in action potential alternans in isolated murine Scn5a (+/-) hearts during dynamic pacing. *Acta Physiol (Oxf)* 200, 129–146

Matthews, G. D. K., Guzadhur, L., Grace, A., Huang, C. L. H., 2012. Nonlinearity between action potential alternans and restitution, which both predict ventricular arrhythmic properties in Scn5a+/- and wild-type murine hearts. *J Appl Physiol*

Matthews, G. D. K., Guzadhur, L., Sabir, I. N., Grace, A. A., Huang, C. L. H., 2013a. Action potential wavelength restitution predicts alternans and arrhythmia in murine *Scn5a* $^{+/-}$ hearts. *J Physiol* 591, 4167–4188

Matthews, G. D. K., Guzadhur, L., Sabir, I. N., Grace, A. A., Huang, C. L. H., 2013b. Action potential wavelength restitution predicts alternans and arrhythmia in murine Scn5a(+/-) hearts. *J Physiol* 591, 4167–4188

Matthews, G. D. K., Guzadhur, L., Sabir, I. N., Grace, A. A., Huang, C. L. H., 2013c. Action potential wavelength restitution predicts alternans and arrhythmia in murine Scn5a+/− hearts. *J Physiol* 591, 4167–4188

Mendis SPP, B, N., 2011. *Global Atlas on Cardiovascular Disease Prevention and Control. Geneva: World Health Organization*

Merchant, F. M., Armoundas, A. A., 2012. Role of substrate and triggers in the genesis of cardiac alternans, from the myocyte to the whole heart: implications for therapy. *Circulation* 125, 539–549

Michikawa, Y., Mazzucchelli, F., Bresolin, N., Scarlato, G., Attardi, G., 1999. Aging-dependent large accumulation of point mutations in the human mtDNA control region for replication. *Science* 286, 774–779

Milton, R. L., Caldwell, J. H., 1990. Na current in membrane blebs: implications for channel mobility and patch clamp recording. *J Neurosci* 10, 885–893

Mitchell, G. F., Jeron, A., Koren, G., 1998. Measurement of heart rate and Q-T interval in the conscious mouse. *Am J Physiol - Hear Circ Physiol* 274

Mootha, V. K., Arai, A. E., Balaban, R. S., 1997. Maximum oxidative phosphorylation capacity of the mammalian heart. *Am J Physiol Circ Physiol* 272, H769–H775

Mori, M., Konno, T., Ozawa, T., Murata, M., Imoto, K., Nagayama, K., 2000. Novel interaction of the voltage-dependent sodium channel (VDSC) with calmodulin: Does VDSC acquire calmodulin-mediated Ca(2+)-sensitivity? *Biochemistry* 39, 1316–1323

Moss, A. J., Zareba, W., Hall, W. J., Klein, H., Wilber, D. J., Cannom, D. S., Daubert, J. P., Higgins, S. L., Brown, M. W., Andrews, M. L., 2002. Prophylactic Implantation of a Defibrillator in Patients with Myocardial Infarction and Reduced Ejection Fraction. *N Engl J Med* 346, 877–883

Murray, A. J., Cole, M. A., Lygate, C. A., Carr, C. A., Stuckey, D. J., Little, S. E., Neubauer, S., Clarke, K., 2008. Increased mitochondrial uncoupling proteins, respiratory uncoupling and decreased efficiency in the chronically infarcted rat heart. *J Mol Cell Cardiol* 44, 694–700

Neglia, D., De Caterina, A., Marraccini, P., Natali, A., Ciardetti, M., Vecoli, C., Gastaldelli, A., Ciociaro, D., Pellegrini, P., Testa, R., Menichetti, L., L'Abbate, A., Stanley, W. C., Recchia, F. A., 2007. Impaired myocardial metabolic reserve and substrate selection flexibility during stress in patients with idiopathic dilated cardiomyopathy. *Am J Physiol Circ Physiol* 293, H3270–H3278

Nerbonne, J. M., Kass, R. S., 2005. Molecular physiology of cardiac repolarization. *Physiol Rev* 85, 1205–1253

Neubauer, S., 2007. The Failing Heart — An Engine Out of Fuel. *N Engl J Med* 356, 1140–1151

NICE, 2014. No Title. *Device Ther*

Ning, F., Luo, L., Ahmad, S., Valli, H., Jeevaratnam, K., Wang, T., Guzadhur, L., Yang, D., Fraser, J. A., Huang, C. L. H., Ma, A., Salvage, S. C., 2016a. The RyR2-P2328S mutation downregulates Nav1.5 producing arrhythmic substrate in murine ventricles. *Pflügers Arch - Eur J Physiol* 468, 655–665

Ning, F., Luo, L., Ahmad, S., Valli, H., Jeevaratnam, K., Wang, T., Guzadhur, L., Yang, D., Fraser, J., Huang, C. H., Ma, A., Salvage, S., 2016b. The RyR2-P2328S mutation downregulates Na(v)1.5 producing arrhythmic substrate in murine ventricles. *Pflugers Arch* PubMed PMI

Ning, X. H., Zhang, J., Liu, J., Ye, Y., Chen, S. H., From, A. H., Bache, R. J., Portman, M. A., 2000. Signaling and expression for mitochondrial membrane proteins during left ventricular remodeling and contractile failure after myocardial infarction. *J Am Coll Cardiol* 36, 282–287

Nisbet, A. M., Camelliti, P., Walker, N. L., Burton, F. L., Cobbe, S. M., Kohl, P., Smith, G. L., 2016. Prolongation of atrio-ventricular node conduction in a rabbit model of ischaemic cardiomyopathy: Role of fibrosis and connexin remodelling. *J Mol Cell Cardiol* 94, 54–64

Nivala, M., Qu, Z., 2012. Calcium alternans in a couplon network model of ventricular myocytes: role of sarcoplasmic reticulum load. *Am J Physiol Heart Circ Physiol* 303, H341-52

Nolasco, J. B., Dahlen, R. W., 1968. A graphic method for the study of alternation in cardiac action potentials. *J Appl Physiol* 25, 191–196

O'Connor, M., McDaniel, N., Brady, W. J., 2008. The pediatric electrocardiogram. *Am J Emerg*

Med 26, 221–228

O'Donnell, J. M., Fields, A. D., Sorokina, N., Lewandowski, E. D., 2008. The absence of endogenous lipid oxidation in early stage heart failure exposes limits in lipid storage and turnover. *J Mol Cell Cardiol* 44, 315–322

Orlandi, A., Francesconi, A., Marcellini, M., Ferlosio, A., Spagnoli, L., 2004. Role of ageing and coronary atherosclerosis in the development of cardiac fibrosis in the rabbit. *Cardiovasc Res* 64, 544–552

Osorio, J. C., Stanley, W. C., Linke, A., Castellari, M., Diep, Q. N., Panchal, A. R., Hintze, T. H., Lopaschuk, G. D., Recchia, F. A., 2002. Impaired myocardial fatty acid oxidation and reduced protein expression of retinoid X receptor-alpha in pacing-induced heart failure. *Circulation* 106, 606–612

Pachon, R. E., Scharf, B. A., Vatner, D. E., Vatner, S. F., 2015. Best anesthetics for assessing left ventricular systolic function by echocardiography in mice. *Am J Physiol Circ Physiol* 308, H1525–H1529

Pandit, S. V., Jalife, J., 2013. Rotors and the dynamics of cardiac fibrillation. *Circ Res*

Physiology, C., Jou, C. J., Spitzer, K. W., Tristani-Firouzi, M., Jerry Jou, C., 2010. *Cellular Physiology Cellular Physiology Cellular Physiology Cellular Physiology Blebbistatin Effectively Uncouples the Excitation-Contraction Process in Zebrafish Embryonic Heart Lake CityOrig Pap Cell Physiol Biochem*, Vol. 25

Priori, S. G., Giuliana Priori, S., Blomströ m-Lundqvist, C., (n.d.) 2015 ESC Guidelines for the management of patients with ventricular arrhythmias and the prevention of sudden cardiac death. *Nikolaos Nikolaou (Greece), Tone M Norekvål (Norway), Christ Spaulding Eur Hear Rhythm Assoc Cardiovasc Pharmacother Cardiovasc Surg*

Pugh, T. D., Conklin, M. W., Evans, T. D., Polewski, M. a., Barbian, H. J., Pass, R., Anderson, B. D., Colman, R. J., Eliceiri, K. W., Keely, P. J., Weindruch, R., Beasley, T. M., Anderson, R. M., 2013. A shift in energy metabolism anticipates the onset of sarcopenia in rhesus monkeys. *Aging Cell* 12, 672–681

Pyo, J. O., Yoo, S. M., Jung, Y. K., 2013. The Interplay between Autophagy and Aging. *Diabetes*

Metab J 37, 333

Rentschler, S., Vaidya, D. M., Tamaddon, H., Degenhardt, K., Sassoon, D., Morley, G. E., Jalife, J., Fishman, G. I., 2001. Visualization and functional characterization of the developing murine cardiac conduction system. *Development* 128, 1785–1792

Riley, G., Syeda, F., Kirchhof, P., Fabritz, L., 2012. An introduction to murine models of atrial fibrillation. *Front Physiol* 3, 296

Roberts, W. M., Almers, W., 1984. An improved loose patch voltage clamp method using concentric pipettes. *Pflugers Arch* 402, 190–196

Rosenbaum, D. S., Jackson, L. E., Smith, J. M., Garan, H., Ruskin, J. N., Cohen, R. J., 1994. Electrical alternans and vulnerability to ventricular arrhythmias. *N Engl J Med* 330, 235–241

Rosenkranz, S., Flesch, M., Amann, K., Haeuseler, C., Kilter, H., Seeland, U., Schlüter, K. D., Böhm, M., 2002. Alterations of β-adrenergic signaling and cardiac hypertrophy in transgenic mice overexpressing TGF-β_1. *Am J Physiol - Hear Circ Physiol* 283, H1253–H1262

Royer, A., Van Veen, T. A. B., Le Bouter, S., Marionneau, C., Griol-Charhbili, V., Léoni, A. L., Steenman, M., Van Rijen, H. V. M., Demolombe, S., Goddard, C. A., Richer, C., Escoubet, B., Jarry-Guichard, T., Colledge, W. H., Gros, D., De Bakker, J. M. T. et al., 2005. Mouse model of SCN5A-linked hereditary Lenègre's: Disease age-related conduction slowing and myocardial fibrosis. *Circulation* 111, 1738–1746

Sabir, I. N., Fraser, J. A., Killeen, M. J., Grace, A. A., Huang, C. L. H., 2007a. The contribution of refractoriness to arrhythmic substrate in hypokalemic Langendorff-perfused murine hearts. *Pflugers Arch Eur J Physiol* 454, 209–222

Sabir, I. N., Fraser, J. A., Cass, T. R., Grace, A. A., Huang, C. L. H., 2007b. A quantitative analysis of the effect of cycle length on arrhythmogenicity in hypokalaemic Langendorff-perfused murine hearts. *Pflugers Arch* 454, 925–936

Sabir, I. N., Killeen, M. J., Goddard, C. A., Thomas, G., Gray, S., Grace, A. A., Huang, C. L. H., 2007c. Transient alterations in transmural repolarization gradients and arrhythmogenicity in hypokalaemic Langendorff-perfused murine hearts. *J Physiol* 581, 277–289

Sabir, I. N., Li, L. M., Grace, A. A., Huang, C. L. H., 2008a. Restitution analysis of alternans and its relationship to arrhythmogenicity in hypokalaemic Langendorff-perfused murine hearts. *Pflugers Arch Eur J Physiol* 455, 653–666

Sabir, I. N., Killeen, M. J., Grace, A. A., Huang, C. L. H., 2008b. Ventricular arrhythmogenesis: insights from murine models. *Prog Biophys Mol Biol* 98, 208–218

Sabir, I. N., Ma, N., Jones, V. J., Goddard, C. A., Zhang, Y., Kalin, A., Grace, A. A., Huang, C. L. H., 2010. Alternans in genetically modified Langendorff-perfused murine hearts modeling catecholaminergic polymorphic ventricular tachycardia. *Front Physiol* 1 OCT, 1–9

Sack, M. N., Rader, T. A., Park, S., Bastin, J., McCune, S. A., Kelly, D. P., 1996. Fatty Acid Oxidation Enzyme Gene Expression Is Downregulated in the Failing Heart. *Circulation* 94, 2837–2842

Salama, G., London, B., 2007. Mouse models of long QT syndrome. *J Physiol* 578, 43–53

Salvage, S., Chandrasekharan, KH Jeevaratnam, K., Dulhunty, A., Thompson, A., Jackson, A., Huang, C., 2017. Multiple targets for flecainide action: implications for cardiac arrhythmogenesis. *Br J Pharmacol* doi: 10.11

Salvage, S. C., King, J. H., Chandrasekharan, K. H., Jafferji, D. I. G., Guzadhur, L., Matthews, H. R., Huang, C. L. H., Fraser, J. A., 2015. Flecainide exerts paradoxical effects on sodium currents and atrial arrhythmia in murine RyR2-P2328S hearts. *Acta Physiol* 214, 361–375

Sato, D., Xie, L. H., Sovari, A. A., Tran, D. X., Morita, N., Xie, F., Karagueuzian, H., Garfinkel, A., Weiss, J. N., Qu, Z., 2009. Synchronization of chaotic early afterdepolarizations in the genesis of cardiac arrhythmias. *Proc Natl Acad Sci U S A* 106, 2983–2988

Scarpulla, R. C., Vega, R. B., Kelly, D. P., 2012. Transcriptional integration of mitochondrial biogenesis. *Trends Endocrinol Metab* 23, 459–466

Sheikh, S. M., Skepper, J. N., Chawla, S., Vandenberg, J. I., Elneil, S., Huang, C. L. H., 2001. Normal conduction of surface action potentials in detubulated amphibian skeletal muscle fibres. *J Physiol* 535, 579–590

Shibukawa, Y., Chilton, E. L., Maccannell, K. A., Clark, R. B., Giles, W. R., 2005. K+ currents

activated by depolarization in cardiac fibroblasts. *Biophys J* 88, 3924–3935

Shiraishi, I., Takamatsu, T., Minamikawa, T., Fujita, S., 1992. 3-D observation of actin filaments during cardiac myofibrinogenesis in chick embryo using a confocal laser scanning microscope. *Anat Embryol (Berl)* 185, 401–408

Simon, A. M., Goodenough, D. A., Paul, D. L., 1998. Mice lacking connexin40 have cardiac conduction abnormalities characteristic of atrioventricular block and bundle branch block. *Curr Biol* 8, 295–298

Singh, S. N., Carson, P. E., Fisher, S. G., 1997. Nonsustained ventricular tachycardia in severe heart failure. *Circulation* 96, 3794–3795

Smyth, J. W., Hong, T. T., Gao, D., Vogan, J. M., Jensen, B. C., Fong, T. S., Simpson, P. C., Stainier, D. Y. R., Chi, N. C., Shaw, R. M., 2010. Limited forward trafficking of connexin 43 reduces cell-cell coupling in stressed human and mouse myocardium. *J Clin Invest* 120, 266–279

Sonoda, J., Mehl, I. R., Chong, L. W., Nofsinger, R. R., Evans, R. M., 2007. PGC-1beta controls mitochondrial metabolism to modulate circadian activity, adaptive thermogenesis, and hepatic steatosis. *Proc Natl Acad Sci U S A* 104, 5223–5228

Sorokina, N., O'Donnell, J. M., McKinney, R. D., Pound, K. M., Woldegiorgis, G., LaNoue, K. F., Ballal, K., Taegtmeyer, H., Buttrick, P. M., Lewandowski, E. D., 2007. Recruitment of Compensatory Pathways to Sustain Oxidative Flux With Reduced Carnitine Palmitoyltransferase I Activity Characterizes Inefficiency in Energy Metabolism in Hypertrophied Hearts. *Circulation* 115, 2033–2041

Sovari, A. A., Rutledge, C. A., Jeong, E. M., Dolmatova, E., Arasu, D., Liu, H., Vahdani, N., Gu, L., Zandieh, S., Xiao, L., Bonini, M. G., Duffy, H. S., Dudley, S. C., 2013. Mitochondria oxidative stress, connexin-43 remodeling, and sudden arrhythmic death. *Circ Arrhythmia Electrophysiol* 6, 623–631

Spector, P., 2013. Principles of cardiac electric propagation and their implications for re-entrant arrhythmias. *Circ Arrhythm Electrophysiol* 6, 655–661

Stanley, W. C., Recchia, F. A., Lopaschuk, G. D., 2005. Myocardial Substrate Metabolism in the Normal and Failing Heart. *Physiol Rev* 85, 1093–1129

Stühmer, W., Roberts, W. M., Almers, W., 1983. The Loose Patch Clamp. In: Sakmann, B. & E. Neher (eds.), *Single-Channel Rec*. Springer US, pp. 123–132

Sullivan, D. E., Ferris, M., Pociask, D., Brody, A. R., 2008a. The latent form of TGFβ 1 is induced by TNFα through an ERK specific pathway and is activated by asbestos-derived reactive oxygen species in vitro and in vivo. *J Immunotoxicol* 5, 145–149

Sullivan, D. E., Ferris, M., Pociask, D., Brody, A. R., 2008b. The Latent Form of TGFβ $_1$ is Induced by TNFα Through an ERK Specific Pathway and is Activated by Asbestos-Derived Reactive Oxygen Species *In Vitro* and *In Vivo*. *J Immunotoxicol* 5, 145–149

Surawicz, B., Knilans, T. K., Chou, T. C., 2008. *Chou's electrocardiography in clinical practice : adult and pediatric*. Saunders/Elsevier

Tan, H. L., Kupershmidt, S., Zhang, R., Stepanovic, S., Roden, D. M., Wilde, A. A. M., Anderson, M. E., Balser, J. R., 2002. A calcium sensor in the sodium channel modulates cardiac excitability. *Nature* 415, 442–447

Taouis, M., Sheldon, R. S., Duff, H. J., 1991. Upregulation of the rat cardiac sodium channel by in vivo treatment with a class I antiarrhythmic drug. *J Clin Invest* 88, 375–378

ter Keurs, H. E. D. J., 2011. Electromechanical coupling in the cardiac myocyte; stretch-arrhythmia feedback. *Pflügers Arch - Eur J Physiol* 462, 165–175

Terentyev, D., Gyorke, I., Belevych, A. E., Terentyeva, R., Sridhar, A., Nishijima, Y., de Blanco, E. C., Khanna, S., Sen, C. K., Cardounel, A. J., Carnes, C. A., Györke, S., 2008. Redox modification of ryanodine receptors contributes to sarcoplasmic reticulum Ca(2+) leak in chronic heart failure. *Circ Res* 103, 1466–1472

Thomas, G., Killeen, M. J., Gurung, I. S., Hakim, P., Balasubramaniam, R., Goddard, C. A., Grace, A. A., Huang, C. L. H., 2007a. Mechanisms of ventricular arrhythmogenesis in mice following targeted disruption of KCNE1 modelling long QT syndrome 5. *J Physiol* 578, 99–114

Thomas, G., Gurung, I. S., Killeen, M. J., Hakim, P., Goddard, C. A., Mahaut-Smith, M. P., Colledge, W. H., Grace, A. A., Huang, C. L. H., 2007b. Effects of L-type Ca(2+) channel antagonism on ventricular arrhythmogenesis in murine hearts containing a modification in the Scn5a gene modelling human long QT syndrome 3. *J Physiol* 578, 85–97

Thomas, G., Killeen, M. J., Grace, A. A. ., Huang, C. L. H., 2008. Pharmacological separation of early afterdepolarizations from arrhythmogenic substrate in deltaKPQ Scn5a murine hearts modelling human long QT 3 syndrome. *Acta Physiol* 192, 505–517

Tipple, M., 1999. Interpretation of electrocardiograms in infants and children. *Images Paediatr Cardiol* 1, 3–13

Tung, R. T., Shen, W. K., Hammill, S. C., Gersh, B. J., 1994. Idiopathic ventricular fibrillation in out-of-hospital cardiac arrest survivors. *Pacing Clin Electrophysiol* 17, 1405–1412

Turakhia, M., Tseng, Z. H., 2007. Sudden Cardiac Death: Epidemiology, Mechanisms, and Therapy. *Curr Probl Cardiol* 32, 501–546

Usher-Smith, J. A., Xu, W., Fraser, J. A., Huang, C. L. H., 2006. Alterations in calcium homeostasis reduce membrane excitability in amphibian skeletal muscle. *Pflügers Arch - Eur J Physiol* 453, 211–221

Vaidya, D., Morley, G. E., Samie, F. H., Jalife, J., 1999. Reentry and fibrillation in the mouse heart. A challenge to the critical mass hypothesis. *Circ Res* 85, 174–181

Valli, H., Ahmad, S., Sriharan, S., Dean, L. D., Grace, A. A., Jeevaratnam, K., Matthews, H. R., Huang, C. L. H., 2018. Epac-induced ryanodine receptor type 2 activation inhibits sodium currents in atrial and ventricular murine cardiomyocytes. *Clin Exp Pharmacol Physiol* 45, 278–292

Van Mieghem, C., Sabbe, M., Knockaert, D., 2004. The clinical value of the ECG in noncardiac conditions. *Chest* 125, 1561–1576

van Veen, T. A. B., Stein, M., Royer, A., Le Quang, K., Charpentier, F., Colledge, W. H., Huang, C. L. H., Wilders, R., Grace, A. A., Escande, D., de Bakker, J. M. T., van Rijen, H. V. M., 2005. Impaired impulse propagation in Scn5a-knockout mice: combined contribution of excitability, connexin expression, and tissue architecture in relation to aging. *Circulation* 112, 1927–1935

Verheule, S., Kaese, S., 2013. Connexin diversity in the heart: insights from transgenic mouse models. *Front Pharmacol* 4, 81

Vianna, C. R., Huntgeburth, M., Coppari, R., Choi, C. S., Lin, J., Krauss, S., Barbatelli, G., Tzameli,

I., Kim, Y. B., Cinti, S., Shulman, G. I., Spiegelman, B. M., Lowell, B. B., 2006. Hypomorphic mutation of PGC-1beta causes mitochondrial dysfunction and liver insulin resistance. *Cell Metab* 4, 453–464

Viskin, S., Belhassen, B., 1990. Idiopathic ventricular fibrillation. *Am Heart J* 120, 661–671

Wagner, S., Ruff, H. M., Weber, S. L., Bellmann, S., Sowa, T., Schulte, T., Anderson, M. E., Grandi, E., Bers, D. M., Backs, J., Belardinelli, L., Maier, L. S., 2011. Reactive oxygen species-activated Ca/calmodulin kinase IIδ is required for late I(Na) augmentation leading to cellular Na and Ca overload. *Circ Res* 108, 555–565

Wall, S. T., Guccione, J. M., Ratcliffe, M. B., Sundnes, J. S., 2012. Electromechanical feedback with reduced cellular connectivity alters electrical activity in an infarct injured left ventricle: a finite element model study. *Am J Physiol Circ Physiol* 302, H206–H214

Wang, J., Wang, H., Zhang, Y., Gao, H., Nattel, S., Wang, Z., 2004. Impairment of HERG K(+) channel function by tumor necrosis factor-alpha: role of reactive oxygen species as a mediator. *J BiolChem* 279, 13289–13292

Weiss, J. N., Lamp, S. T., Shine, K. I., 1989. Cellular K+ loss and anion efflux during myocardial ischemia and metabolic inhibition. *Am J Physiol* 256, H1165-75

Weiss, J. N., Qu, Z., Chen, P. S., Lin, S. F., Karagueuzian, H. S., Hayashi, H., Garfinkel, A., Karma, A., 2005. The dynamics of cardiac fibrillation. *Circulation* 112, 1232–1240

Wessels, A., Sedmera, D., 2003. Developmental anatomy of the heart: a tale of mice and man. *Physiol Genomics* 15, 165–176

Wingo, T. L., Shah, V. N., Anderson, M. E., Lybrand, T. P., Chazin, W. J., Balser, J. R., 2004. An EF-hand in the sodium channel couples intracellular calcium to cardiac excitability. *Nat Struct Mol Biol* 11, 219–225

Wu, J., Zhang, Y., Zhang, X., Cheng, L., Lammers, W. J., Grace, A. A., Fraser, J. A., Zhang, H., Huang, C. L. H., Lei, M., 2012. Altered sinoatrial node function and intra-atrial conduction in murine gain-of-function Scn5a+/ KPQ hearts suggest an overlap syndrome. *AJP Hear Circ Physiol* 302, H1510–H1523

Xie, Y., Garfinkel, A., Camelliti, P., Kohl, P., Weiss, J. N., Qu, Z., 2009. Effects of fibroblast-myocyte coupling on cardiac conduction and vulnerability to reentry: A computational study. *Hear Rhythm* 6, 1641–1649

Yan, X. sheng, Ma, J. hua, Zhang, P. hua, 2009. Modulation of KATP currents in rat ventricular myocytes by hypoxia and a redox reaction. *Acta Pharmacol Sin* 30, 1399–1414

Yang, S., Yang, Z., Wu, C., Li, W., Xu, H., 2015. [Electrophysiological properties and mechanism of aging for the susceptibility of left atrium to arrhythmogenesis in rabbits]. *Zhonghua Yi Xue Za Zhi* 95, 2302–2306

Yeung, C. Y., Lam, K. S. L., Li, S. W., Lam, K. F., Tse, H. F., Siu, C. W., 2012. Sudden cardiac death after myocardial infarction in type 2 diabetic patients with no residual myocardial ischemia. *Diabetes Care* 35, 2564–2569

Yue, L., Xie, J., Nattel, S., 2011. Molecular determinants of cardiac fibroblast electrical function and therapeutic implications for atrial fibrillation. *Cardiovasc Res* 89, 744

Zaitsev, A. V, Berenfeld, O., Mironov, S. F., Jalife, J., Pertsov, A. M., 2000. Distribution of excitation frequencies on the epicardial and endocardial surfaces of fibrillating ventricular wall of the sheep heart. *Circ Res* 86, 408–417

Zamiri, N., Massé, S., Ramadeen, A., Kusha, M., Hu, X., Azam, M. A., Liu, J., Lai, P. F. H., Vigmond, E. J., Boyle, P. M., Behradfar, E., Al-Hesayen, A., Waxman, M. B., Backx, P., Dorian, P., Nanthakumar, K., 2014. Dantrolene improves survival after ventricular fibrillation by mitigating impaired calcium handling in animal models. *Circulation* 129, 875–885

Zhang, Y., Schwiening, C., Killeen, M. J., Zhang, Y., Ma, A., Lei, M., Grace, A. A., Huang, C. L. H., 2009. Pharmacological changes in cellular Ca2+ homeostasis parallel initiation of atrial arrhythmogenesis in murine Langendorff-perfused hearts. *Clin Exp Pharmacol Physiol* 36, 969–980

Zhang, Y., Fraser, J. A., Jeevaratnam, K., Hao, X., Hothi, S. S., Grace, A. A., Lei, M., Huang, C. L. H., 2011. Acute atrial arrhythmogenicity and altered Ca(2+) homeostasis in murine RyR2-P2328S hearts. *Cardiovasc Res* 89, 794–804

Zhang, Y., Wu, J., Jeevaratnam, K., King, J. H., Guzadhur, L., Ren, X., Grace, A. A., Lei, M., Huang,

C. L. H., Fraser, J. A., 2013. Conduction slowing contributes to spontaneous ventricular arrhythmias in intrinsically active murine RyR2-P2328S hearts. *J Cardiovasc Electrophysiol* 24, 210–218

Zhang, Y., Wu, J., King, J. H., Huang, C. L. H., Fraser, J. a, 2014. Measurement and interpretation of electrocardiographic QT intervals in murine hearts. *Am J Physiol Heart Circ Physiol* 306, H1553-7

Zipes, D. P., Camm, A. J., Borggrefe, M., Buxton, A. E., Chaitman, B., Fromer, M., Gregoratos, G., Klein, G., Myerburg, R. J., Quinones, M. A., Roden, D. M., Silka, M. J., Tracy, C., Smith, S. C., Jacobs, A. K., Adams, C. D. et al., 2006. ACC/AHA/ESC 2006 Guidelines for Management of Patients With Ventricular Arrhythmias and the Prevention of Sudden Cardiac Death. *J Am Coll Cardiol* 48, e247–e346

Zoni-Berisso, M., Lercari, F., Carazza, T., Domenicucci, S., 2014. Epidemiology of atrial fibrillation: European perspective. *Clin Epidemiol* 6, 213–220